IAEA-TECDOC-1672

Modelling of Transport of Radioactive Substances in the Primary Circuit of Water-Cooled Reactors

IAEA
International Atomic Energy Agency

Modelling of Transport of Radioactive Substances in the Primary Circuit of Water Cooled Reactors

The following States are Members of the International Atomic Energy Agency:

AFGHANISTAN
ALBANIA
ALGERIA
ANGOLA
ARGENTINA
ARMENIA
AUSTRALIA
AUSTRIA
AZERBAIJAN
BAHRAIN
BANGLADESH
BELARUS
BELGIUM
BELIZE
BENIN
BOLIVIA
BOSNIA AND HERZEGOVINA
BOTSWANA
BRAZIL
BULGARIA
BURKINA FASO
BURUNDI
CAMBODIA
CAMEROON
CANADA
CENTRAL AFRICAN REPUBLIC
CHAD
CHILE
CHINA
COLOMBIA
CONGO
COSTA RICA
CÔTE D'IVOIRE
CROATIA
CUBA
CYPRUS
CZECH REPUBLIC
DEMOCRATIC REPUBLIC OF THE CONGO
DENMARK
DOMINICA
DOMINICAN REPUBLIC
ECUADOR
EGYPT
EL SALVADOR
ERITREA
ESTONIA
ETHIOPIA
FINLAND
FRANCE
GABON
GEORGIA
GERMANY
GHANA
GREECE
GUATEMALA
HAITI
HOLY SEE
HONDURAS
HUNGARY
ICELAND
INDIA
INDONESIA
IRAN, ISLAMIC REPUBLIC OF
IRAQ
IRELAND
ISRAEL
ITALY
JAMAICA
JAPAN
JORDAN
KAZAKHSTAN
KENYA
KOREA, REPUBLIC OF
KUWAIT
KYRGYZSTAN
LAO PEOPLE'S DEMOCRATIC REPUBLIC
LATVIA
LEBANON
LESOTHO
LIBERIA
LIBYA
LIECHTENSTEIN
LITHUANIA
LUXEMBOURG
MADAGASCAR
MALAWI
MALAYSIA
MALI
MALTA
MARSHALL ISLANDS
MAURITANIA
MAURITIUS
MEXICO
MONACO
MONGOLIA
MONTENEGRO
MOROCCO
MOZAMBIQUE
MYANMAR
NAMIBIA
NEPAL
NETHERLANDS
NEW ZEALAND
NICARAGUA
NIGER
NIGERIA
NORWAY
OMAN
PAKISTAN
PALAU
PANAMA
PARAGUAY
PERU
PHILIPPINES
POLAND
PORTUGAL
QATAR
REPUBLIC OF MOLDOVA
ROMANIA
RUSSIAN FEDERATION
SAUDI ARABIA
SENEGAL
SERBIA
SEYCHELLES
SIERRA LEONE
SINGAPORE
SLOVAKIA
SLOVENIA
SOUTH AFRICA
SPAIN
SRI LANKA
SUDAN
SWEDEN
SWITZERLAND
SYRIAN ARAB REPUBLIC
TAJIKISTAN
THAILAND
THE FORMER YUGOSLAV REPUBLIC OF MACEDONIA
TUNISIA
TURKEY
UGANDA
UKRAINE
UNITED ARAB EMIRATES
UNITED KINGDOM OF GREAT BRITAIN AND NORTHERN IRELAND
UNITED REPUBLIC OF TANZANIA
UNITED STATES OF AMERICA
URUGUAY
UZBEKISTAN
VENEZUELA
VIETNAM
YEMEN
ZAMBIA
ZIMBABWE

The Agency's Statute was approved on 23 October 1956 by the Conference on the Statute of the IAEA held at United Nations Headquarters, New York; it entered into force on 29 July 1957. The Headquarters of the Agency are situated in Vienna. Its principal objective is "to accelerate and enlarge the contribution of atomic energy to peace, health and prosperity throughout the world''.

IAEA-TECDOC-1672

MODELLING OF TRANSPORT OF RADIOACTIVE SUBSTANCES IN THE PRIMARY CIRCUIT OF WATER COOLED REACTORS

INTERNATIONAL ATOMIC ENERGY AGENCY
VIENNA, 2012

For further information on this publication, please contact:

Nuclear Fuel Cycle and Materials Section
International Atomic Energy Agency
Vienna International Centre
PO Box 100
1400 Vienna, Austria
email: Official.Mail@iaea.org

Printed by the IAEA in Austria
March 2012

IAEA Library Cataloguing in Publication Data

Modelling of transport of radioactive substances in the primary circuit of water cooled reactors. – Vienna : International Atomic Energy Agency, 2012.
p. ; 30 cm. – (IAEA-TECDOC series, ISSN 1011-4289 ; no. 1672)
ISBN 978-92-0-126010-9
Includes bibliographical references.

1. Water cooled reactors – Corrosion. 2. Water cooled reactors – Safety measures. 3. Radiation – Safety measures. 4. Mathematical models. I. International Atomic Energy Agency. II. Series.

IAEAL 12-00730

FOREWORD

Since the beginning of the development of water cooled nuclear power reactors, it has been known that the materials in contact with the water release some of their corrosion products into the water. As a consequence, some of the corrosion products are neutron-activated while in the reactor core and then create a gamma radiation field when deposited outside the core. These radiation fields are hazardous to the inspection, maintenance and operating staff in the power plant and therefore must be minimized. Many methods have been developed to control these radiation fields, such as the proper selection of materials and surface finishing technologies at the design stage, operating and shutdown water chemistry optimization, and the application of different decontamination methods.

The need to understand the causes of this radioactivity transport has resulted in many mathematical models to describe the transport, irradiation and deposition of the radioactive corrosion products out of the core. Early models were empirical descriptions of the transport, irradiation and deposition steps, and these models allowed analytical solution of the resulting differential equations. As the mechanisms responsible for radioactivity transport gradually became better understood, more precise models of the mechanisms were made. Computer codes to solve the equations describing these models are necessary. Accurate codes are invaluable design tools for carrying out cost–benefit analysis during materials selection, for estimating shielding thicknesses and for evaluating water chemistry specifications, for example. Such codes are also useful in operating plants to predict radiation fields at specific locations where shielding may be required during a maintenance shutdown, for example, when control of radiation dose to staff is essential.

To complement the previous work of the International Atomic Energy Agency (IAEA) to improve the mechanistic understanding of radioactivity transport, a coordinated research project (CRP) was proposed to determine the accuracy of existing computer codes and to identify how they could be improved through application of this body of work. Specifically, the CRP was expected to:

- Build a database for selected pressurized water reactor (PWR) plants that would contain the design information suitable for their description within a computer code, as well as give the operating history of the plant, which would include the water chemistry data over several refuelling cycles;
- Show the contamination of selected out-of-core surfaces such as circulating loops and steam generator channel heads versus operating history and compare the prediction of surface contamination versus time from modern radioactivity transport codes with actual plant data in a blind benchmarking exercise;
- Determine how current codes, as well as new ones, could be improved and encourage the development of accurate new codes in Member States using the recommendations from the present work.

This report uses as its basis the results of this CRP on ‘Modelling of Transport of Radioactive Substances in the Primary Circuit of Water Cooled Reactors’, which was conducted over the period 1996–2001 for PWR type reactors. The report also describes the significant progress demonstrated in this field in the period that followed.

The IAEA would like to thank the four electrical utilities that provided the design and operating data for the four plants selected in this study: EDF (CRUAS-1), KWU Siemens (GKN-2), Imatran Voima Oy (LOVIISA-1), and Slovenske Elektrarne (BOHUNICE-1). The IAEA would also like to thank the experts from the 14 Member States that were involved in the study for their active participation, including: S. Anthoni (CEA), C.B. Lee (KAERI), M. Zmitko (NRI-Rez), K. Kasahara (MHI), L. Horvath (VEIKI), V. Kritsky (VNIPIET), I. Smiesko (Slovenske Elektrarne) and K.A. Burrill (AECL). The IAEA officers responsible for this publication were P. Chantoin, P. Menut, F. Sokolov and J. Killeen.

EDITORIAL NOTE

The use of particular designations of countries or territories does not imply any judgement by the publisher, the IAEA, as to the legal status of such countries or territories, of their authorities and institutions or of the delimitation of their boundaries.

The mention of names of specific companies or products (whether or not indicated as registered) does not imply any intention to infringe proprietary rights, nor should it be construed as an endorsement or recommendation on the part of the IAEA.

CONTENTS

1. INTRODUCTION AND BACKGROUND

The reduction of radiation fields in nuclear power plants (NPPs) is a major goal for vendors and owners all over the world. Economic restraints, such as fuel cycle extension or plant outage reduction, but also technical challenges with next generation reactor design, greatly depend on personal dose reduction. The major contributors to personal dose are activated corrosion products (CP).

The system surfaces exposed to water release corrosion products into the coolant. These are transported through the core where they become activated. The activated corrosion products, especially Co^{58} and Co^{60} are then incorporated in the out-of-core surfaces and generate radiation fields.

The released corrosion products can be divided into three groups:

- particles,
- colloids,
- solubles.

The growth of gamma radiation fields around the surfaces of out-core materials was noted from the beginning of the development of nuclear power reactors. Wohlberg and Kleimola [1] reviewed deposition data both in-core and out-core in the few facilities that existed at that time, e.g. recirculating, high temperature, water cooled loops with an in-core test section, in reactors such as the NRX research reactor at Chalk River Laboratories. Adjustment of the water chemistry with dissolved H_2 and addition of a strong base, e.g. NaOH, were found to reduce the corrosion of the stainless steel (SS) structural materials and to reduce deposition on zirconium surfaces in-core. These conclusions were validated by subsequent work presented at a Tripartite' meeting of workers from the U.K., U.S. and Canada [2]. Due to an inadequate database, hypotheses were advanced for the mechanisms controlling the spread of irradiated corrosion products around the entire system, later to be called 'radioactivity transport'. Mathematical models were made of these hypotheses and two of these models were discussed by Medin [3]. In the model of Steiner, [4], corrosion products were irradiated as they passed through the core, with no allowance for in-core deposition of the particulate material suspended in the coolant, called 'crud'. A second model of Pement considered the production of radionuclides by irradiation of in-core structural materials, and their release by corrosion and subsequent deposition out-core [5].

Over the next forty years, many other models were advanced. The early models were largely empirical and required analytical approaches for their evaluation in pre-computer days so they were limited as predictive tools. Computer codes are used now to evaluate the mass balances where the rate equations in these balances arise from models of mechanisms hypothesized to be important in radioactivity transport. These models generally work well in pressurized water reactors (PWRs) and boiling water reactors (BWRs), and while there are large differences in materials and chemistry, generally the mechanisms can be recognized as also applying to CANDU reactors.

The large number of models for activity transport in PWRs and BWRs resulted in Atomic Energy of Canada Limited (AECL) organizing an international symposium in late 1994 in Ottawa to stimulate discussion among modellers and to review the mechanisms that each model used for possible application in CANDU activity transport codes [6].

One result of this symposium was the start of an IAEA Coordinated Research Program on Activity Transport Modelling with the aim of benchmarking existing model predictions against plant data and then discussion by experts on how the models could be improved.

The CRP included a blind benchmarking exercise and this is described first. Then each of the major models in use is discussed to identify the mechanisms being used and overall assessment of the models

is given to guide further development. Once the comparison of predictions with data is made, the discussion here may help guide code developers in determining how their models in the codes might be altered to improve code accuracy.

There have been many developments in the subject that have occurred since the formal ending of the CRP and these have been discussed at a series of consultants meetings and are also described. The consultants recommended that the detailed reporting of the CRP would be a valuable exercise with the additional material now available.

1.1. Blind-benchmarking exercise

Following the international symposium organised by AECL, intended to stimulate discussion among modellers and to review the mechanisms that each model used for possible application in CANDU activity transport codes [6]. Attendees from the NEA urged the IAEA to initiate an IAEA Coordinated Research Program on Activity Transport Modelling with the aim of benchmarking existing model predictions against plant data and then discussion by experts on how the models could be improved. The end result would be models to be used as design tools for new reactors, and to indicate the important parameters that control the rate of radiation field growth in operating plants, both resulting in minimized radiation exposure to plant operators. The IAEA began this CRP in 1995 and over one dozen countries chose to participate. The first annual meeting of participants was held in Toronto at Ontario Hydro (now called OPG) Headquarters in May 1997, the second meeting was held at the IAEA in Vienna in September 1999, and the third and final meeting was hosted by the Centre Nucleare d'Energie Atomica (CNEA) at their laboratory in Buenos Aires in November 2000.

The International Atomic Energy Agency was coordinating a benchmark on the modelling of radioactive substances in the primary circuit of water cooled reactors. The final goal of this blind exercise, in addition to collecting reactor data, was to perform dose calculations for selected NPPs.

The results of the CRP work are described in this document, with the codes limited to those for non-boiling reactors, i.e. PWRs and CANDU reactors. The CRP began with the collection of data on plant design and operating parameters that are used as input to the codes to predict radiation field growth on primary circuit piping in selected PWRs. A key feature is water chemistry data for each fuel cycle for two 440 MWe WWERs (LOVIISA-1, EBO-1) and two 900–1300 MWe PWRs (CRUAS-1, GKN-2) over 5–10 fuel cycles. The various codes do not use time to make predictions through a fuel cycle, but move through the fuel cycle by altering the water chemistry from time-step to time-step. The codes predict the change in deposition and release rates of corrosion products and radionuclides on various system surfaces. After predictions from each code were made, their predictions were compared with contamination data from the referenced operating power reactors. Finally, recommendations are made to guide code developers in determining how their models in the codes might be altered to improve code accuracy. Activity transport models have not yet been developed from first principles and so they contain empirical coefficients that must be derived from experimental data or from the plants. Different plant designs require models with different emphases on the various physical and chemical processes. Such models can become very elaborate with a number of empirical influence coefficients. Measurement of these parameters under plant conditions is essential for accurate prediction of surface contamination.

During the period after CRP was finished, many of models that participated in the CRP have been further developed, and also new demands from NPP operation linked with corrosion product transport have arisen:

- Injection of zinc into primary coolant
- Shutdown chemistry optimization
- Crud induced power shifts (CIPS) prevention and management

Despite this development, the results of CRP have not lost their value as they represent important reference for the intensive development of NPPs of new generations, and also for handling tasks arising from new environmental restrictions. Therefore, the original CRP results have been supplemented by new information from the further development of activity transport modelling in several countries.

1.2. Models and data used in the CRP

Fifteen countries chose to participate in the CRP. Table 1 lists the countries, the organization that provided the delegate, and the role of the delegate. Full details of the participants are given in Appendix 1. Not all countries had codes for testing in the blind-benchmarking, but some codes were developed in the course of the work. Secondly, the computer codes that were used are described in some detail by their developers. Thirdly, the plant design data to be used in the blind-benchmarking exercise is presented. Fourthly, the operating data for each plant are described. These data were not given to the modellers until their predictions were complete.

TABLE 1. PARTICIPATING COUNTRIES, ORGANIZATION AND DELEGATE ROLE

Country	Organization	'CODE' and role
Argentina	CNEA	Expert (1)
Bulgaria	INRNE	'MIGA-RT'/Expert/Consultant(2)
Canada	AECL	Expert/Consultant
Canada	UNB	Expert
Czech Rep.	NRI	'DISER'/Expert/Consultant
Finland	IVO	Expert/Consultant/Data supplier(3)
France	CEA	'PACTOLE'/Expert/Consultant/Data supplier
Germany	SNP	Water chemistry specialist(4)/Data supplier
Hungary	VEIKI	'RADTRAN'/Expert/Consultant
India	BARC	Expert
Japan	MHI	'ACE'/Expert/Consultant
Norway	Halden	Water chemistry specialist/Consultant
Rep. of Korea	KAERI	'CRUDTRAN'/Expert/Consultant
Russia	VNIPIET	Water chemistry specialist/Consultant
Slovakia	Slovenske Elektrarne	Expert/Consultant/Data supplier
U.S.A.	Penn. State University.	Water chemistry specialist/Consultant

Notes:

(1) 'Expert' means delegate worked actively in the country's organization to understand or control radioactivity transport in his country's NPPs.
(2) 'Consultant' means that the delegate met with the CRP coordinator at an inaugural meeting to define program scope, then attended annual meetings to advise the coordinator on program direction and progress.
(3) 'Data supplier' means delegate supplied plant design and operating data to permit application of each code in the blind benchmarking on that plant.
(4) 'Water chemistry specialist' means delegate had specialist knowledge in reactor chemistry or corrosion that was of value to the CRP.

2. CORROSION PRODUCT CONTAMINATION OF THE PRIMARY CIRCUIT

Before introducing radioactivity transport modelling in Section 3, the overall phenomenon of 'activity transport' is presented in this Section and some of the mechanisms responsible are discussed briefly. Much more detailed discussions can be found in the previous report, [7].

2.1. Introduction to activity transport

Many mechanisms are involved in the process of primary circuit contamination by radioactive corrosion products. A simplified view of the main steps that lead to primary circuit contamination is presented in Fig. 1. The three steps shown are:

(1) The generalized corrosion of primary circuit materials leads to radioactive corrosion product contamination. As far as corrosion is concerned, two separate alloy types have to be distinguished: zirconium alloy and nickel or iron based alloys, such as Inconel, Incoloy or SS. When exposed to the thermal and chemical conditions in the primary circuit, the corrosion of zirconium alloy leads to the formation of a stable oxide, which suppresses mass transport between material and coolant. In contrast, the corrosion of the second alloy type leads to the formation of a double layer oxide (one layer enriched with chromium, the second one mostly composed of nickel ferrite) and to the release of metallic ions of iron, nickel and cobalt, into the primary fluid: so these alloys are mainly responsible for corrosion product contamination. It must be said here that these alloys behave satisfactorily regarding generalized corrosion: only a few mg/dm^2/month can be oxidized.

(2) These metallic species are transported by the coolant to the different parts of the primary circuit and are submitted to various mechanisms: precipitation, particle deposition, erosion, and dissolution, for examples. When passing through the core or deposited on in-core surfaces, some of the corrosion product atoms are made radioactive by activation in the the neutron flux.

(3) The now-radioactive corrosion products are transported to the out-core regions of the primary circuit where they can be deposited.

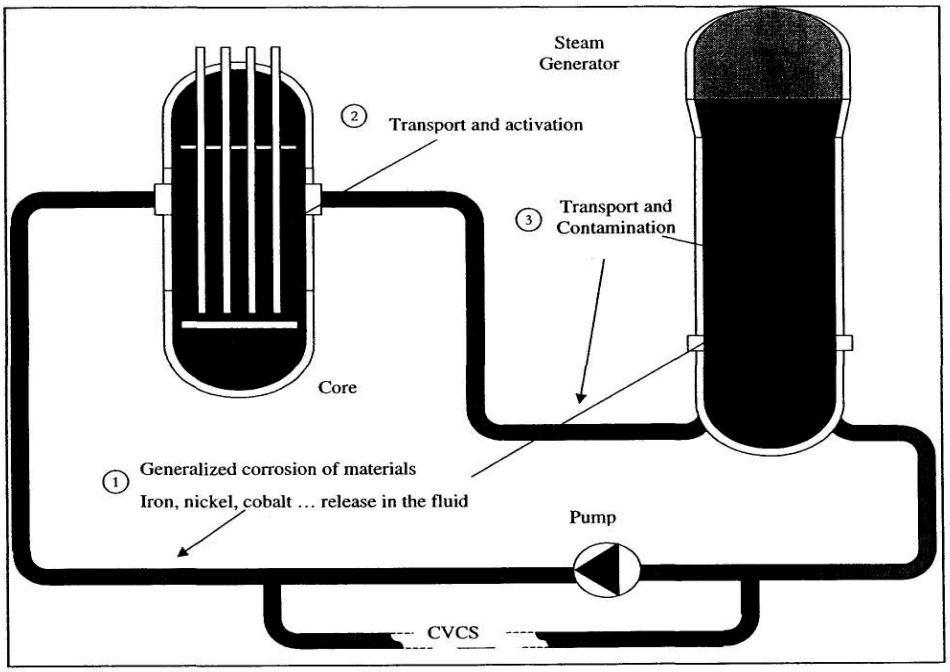

FIG. 1. Schematic description of the processes involved in primary circuit contamination by corrosion products PWRs and WWERs.

2.2. Corrosion and the release of corrosion products

Corrosion is defined as the natural tendency of metals, under the influence of atmospheric or chemical agents, to return to their original state (oxide, sulphate, carbonate...), which is more stable compared to the environment considered, and thus undergo deterioration in their properties [8].

The corrosion of primary circuit materials is process, where the water coolant acts as a reaction agent. All the corrosion processes involved have electrochemical steps. Indeed, on the metal surface, electrochemical batteries are created where anodic and cathodic reactions take place. Thus, between the anodes and the cathodes, a current is established that results in the deterioration of the metallic zones (anodes). Generalized corrosion is characterized by a uniform loss of metal at its surface because a surface site can either be anodic or cathodic over time. In primary circuit conditions, in which metal deterioration is thermodynamically possible, alloys such as SS or Inconel become passivated by the corrosion products growing on their surface. The passive layer, separating the alloy from the coolant, acts as a protective layer. Nevertheless, even though the ion conductivity of the passive layers is very low, mass exchange, through this layer, still exists between the metal alloy and the primary coolant [9].

2.3. The passive oxide layer and corrosion product release

The passive layer that develops on the metal alloy under primary circuit conditions is composed of two different layers, called the inner and the outer oxide layers. Potter [10] was the first author to demonstrate this, during experimental investigations with carbon steel, oxidized in an autoclave at 316°C and in alkaline solution. Later, other experiments on SS [11–13], Inconel [14] and Incoloy 800 [15], revealed these types of oxides.

From a general point of view, these observations show that the inner oxide layer is composed of small grains (less than 0.1 μm according to [16]), and is compact and adherent. On the other hand, the outer oxide layer is not homogeneous and is composed of large and non-homogeneous particulates (1–2 μm according to [14]). Fig. 2 shows the two-layer structure of oxides grown on Inconel, resulting from an 1169 hour test performed at 325°C, in conditions close to those of the primary circuit [17]. The crystals of different sizes compose the outer oxide. An inner oxide layer can be seen between the crystals.

The crystal structure of both the inner and outer oxides is of spinel type $(AB)_3O_4$. The growth of the inner oxide occurs at the metal-oxide interface, whereas the outer oxide develops toward the outside at the oxide-fluid interface as sketched in Fig. 3 [18–19]. The oxidizing compound has to diffuse through the inner oxide up to the metal-oxide interface, to increase the inner oxide growth. At the metal-oxide interface, the ionic species, not participating in the inner oxide formation, diffuse through the inner oxide up to the oxide-fluid interface where they react with the fluid to form the outer oxide. According to different authors, diffusion occurs in water-filled pores, or by solid state diffusion along the grain boundaries.

At the oxide-fluid interface, metallic ions can either grow crystals from solution to form the outer oxide, or diffuse into the bulk water, where they are transported to other parts of the primary circuit [13]. This latest option corresponds to the ionic release of corrosion products. The formation of the outer oxide is an important process, as far as oxide contamination by corrosion products is concerned. Indeed, radioactive ions from the coolant are incorporated in the outer oxide during its growth.

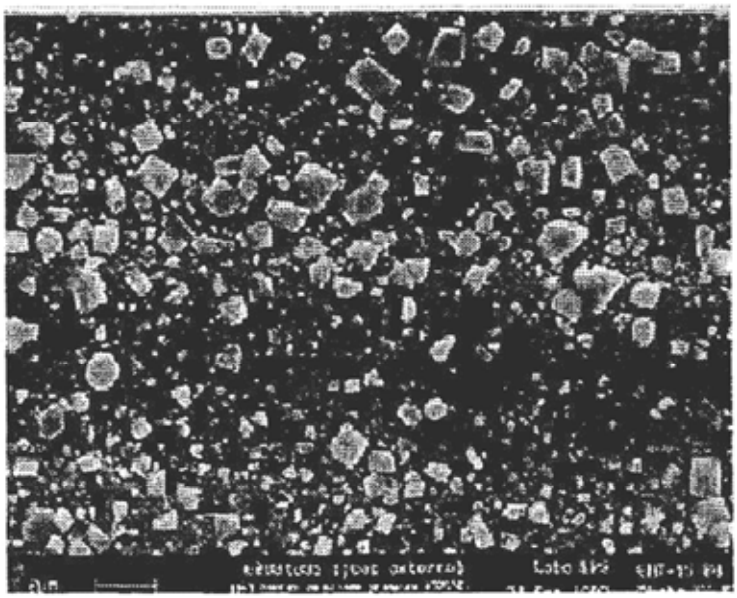

FIG. 2. The inner and outer layer oxide crystals formed on Inconel 600 as viewed by scanning electron microscope (SEM).

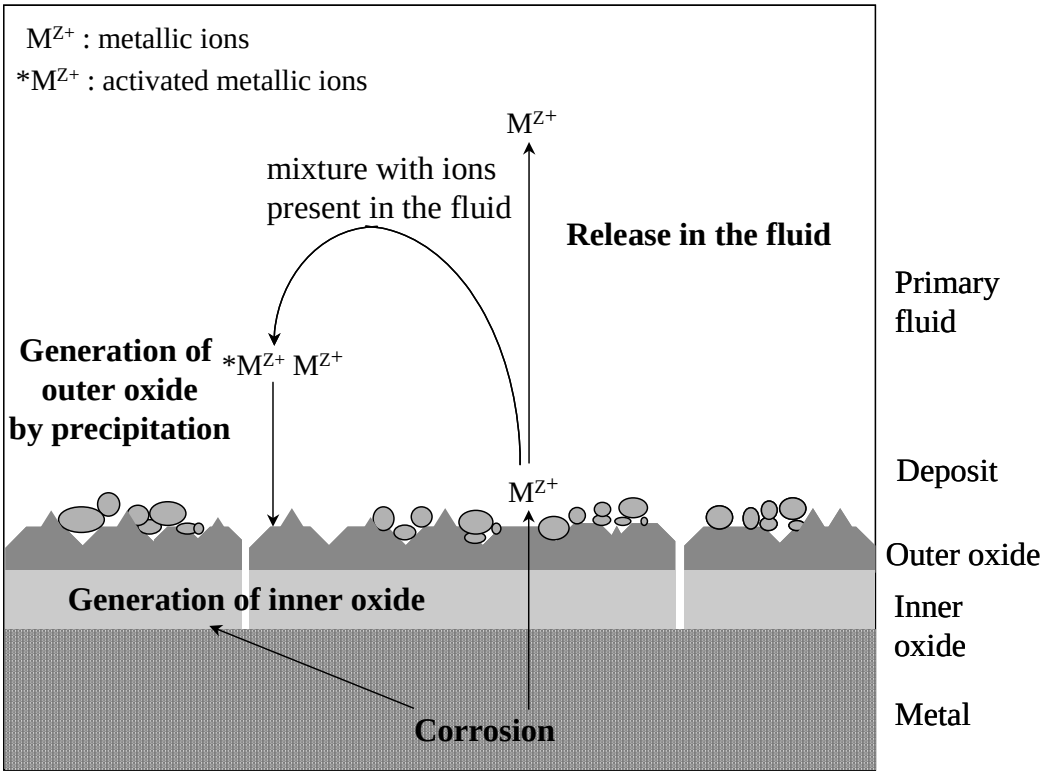

FIG. 3. Growth of the 'double' layer of inner and outer layers of oxide.

2.4. The chemical composition of the oxides in the primary circuit

Experimental investigations were conducted in order to determine the chemical composition of the oxides formed on primary circuit alloys, such as SS [11] and Inconel [14]. From a general point of view, these experiments show that the two oxides have a different chemical composition as shown in Fig. 4. The inner oxide is enriched with chromium and has the composition $Ni_xFe_{1-x}Cr_2O_4$ where $0 < x < 1$. Due to its high chromium content, this oxide is almost insoluble under primary circuit reducing conditions. The outer oxide is enriched with iron and nickel. It either corresponds to a nickel ferrite of type $Ni_xFe_{3-x}O_4$ ($x = 0.6$ according to some experiments [16]) for NPPs equipped with nickel alloy steam generator (SG) tubes, or magnetite Fe_3O_4, for those equipped with SS SG tubes. Some analyses performed on Inconel 600 nuclear reactor SG tubes demonstrate the presence of metallic nickel [20].

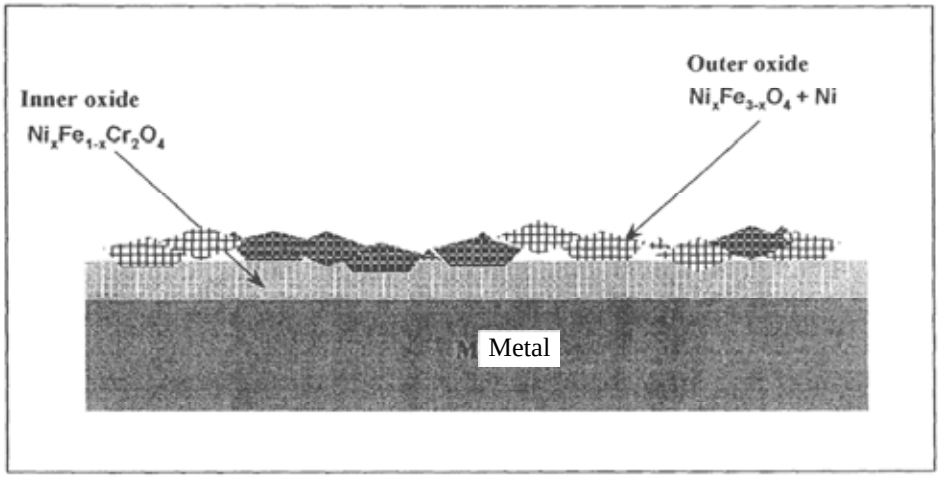

FIG. 4. Composition of oxides formed in the primary circuit on SSs and on Inconel 600.

2.5. Corrosion product transport mechanisms in the primary circuit

Species resulting from metallic corrosion are introduced to the coolant, where they are transported by convection throughout the circuit. These species exist in three states: soluble (ions), non-soluble (particulates) and colloids. These three corrosion product states are involved in different transfer mechanisms between the primary coolant and the circuit wall.

Ions are involved in precipitation/dissolution phenomena that depend on concentrations of the species in equilibrium with the already-formed oxides. Ionic species may be released at one point of the primary circuit, may be transported by the coolant, and may then precipitate in another part of the primary circuit, where the bulk concentration exceeds the equilibrium concentration of the oxides. Indeed, there is an important thermal gradient in the primary circuit – wall temperatures vary from 284°C to 340°C – and the equilibrium concentrations of the ionic species depend on wall temperature as observed in Fig. 5, [21]. Figs 6–7 demonstrate different magnetite solubility vs. pH at different temperatures [22] in the oxidizing and reducing conditions and Fig. 8 shows influence of temperature to the solubility of different cobalt forms [23].

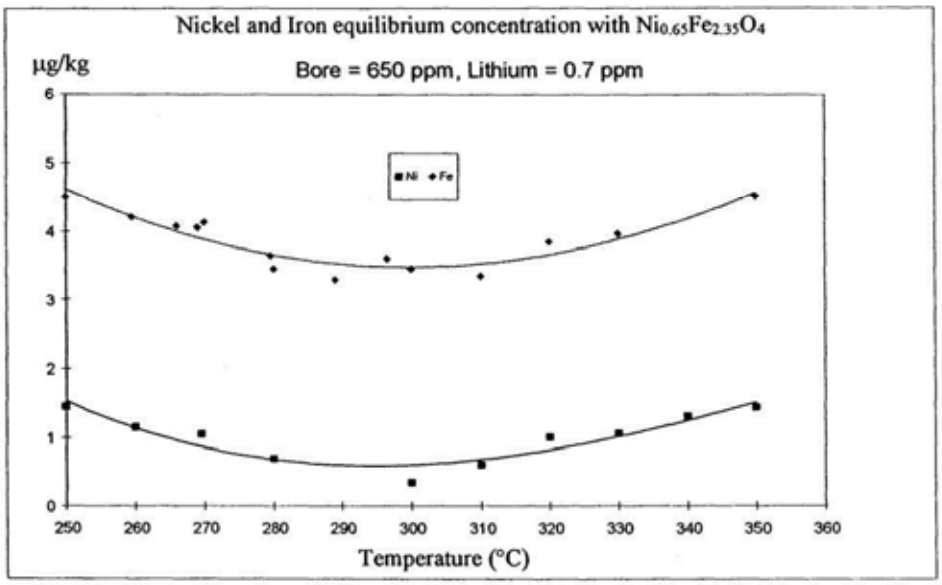

FIG. 5. Concentrations of dissolved nickel and iron in equilibrium with sub-stoichiometric nickel ferrite versus temperature.

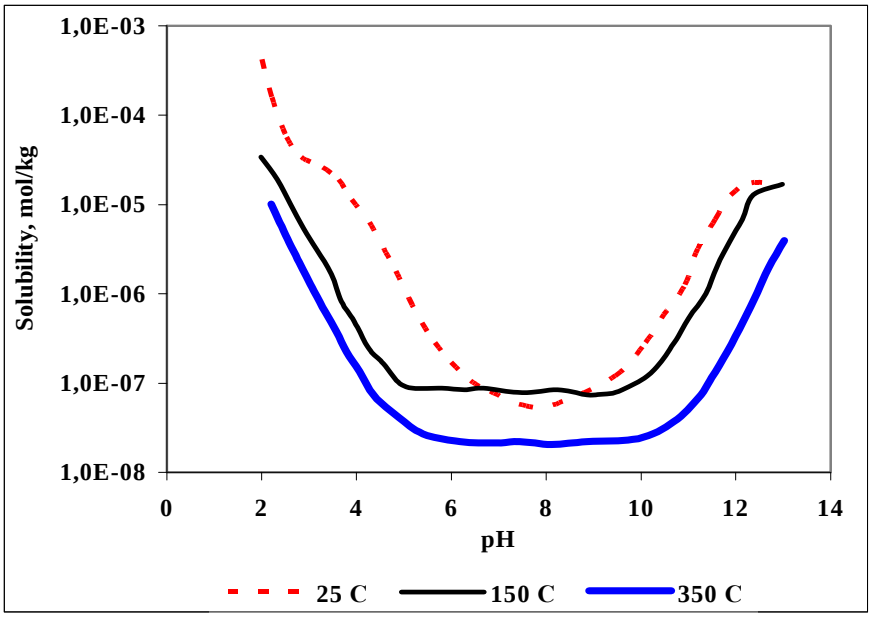

FIG. 6. Influence of pH to solubility of magnetite at different temperatures – oxidizing conditions (oxygen concentration 10^{-6} mol·kg^{-1}).

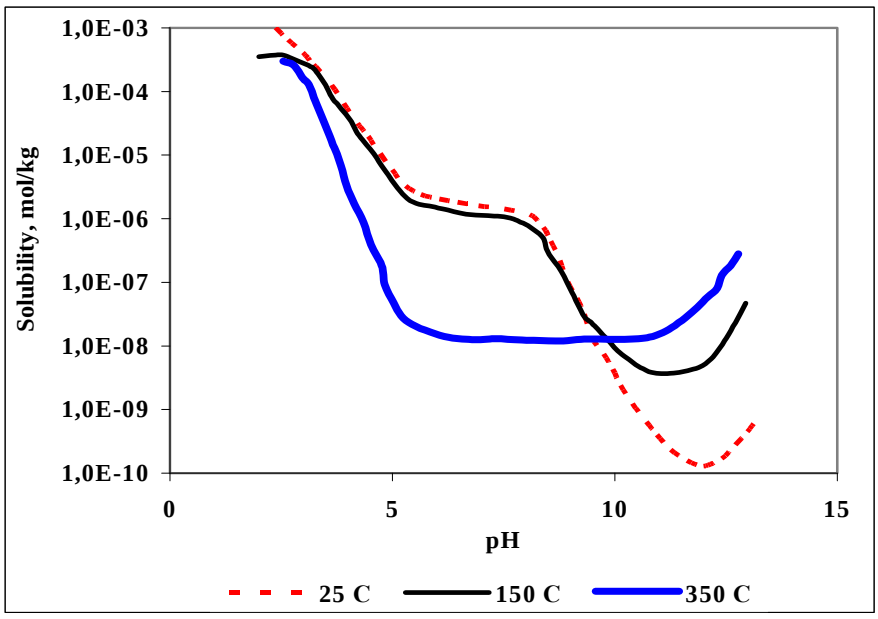

FIG. 7. Influence of pH to solubility of magnetite at different temperatures – reducing conditions (hydrogen concentration 10^{-4} mol·kg^{-1}).

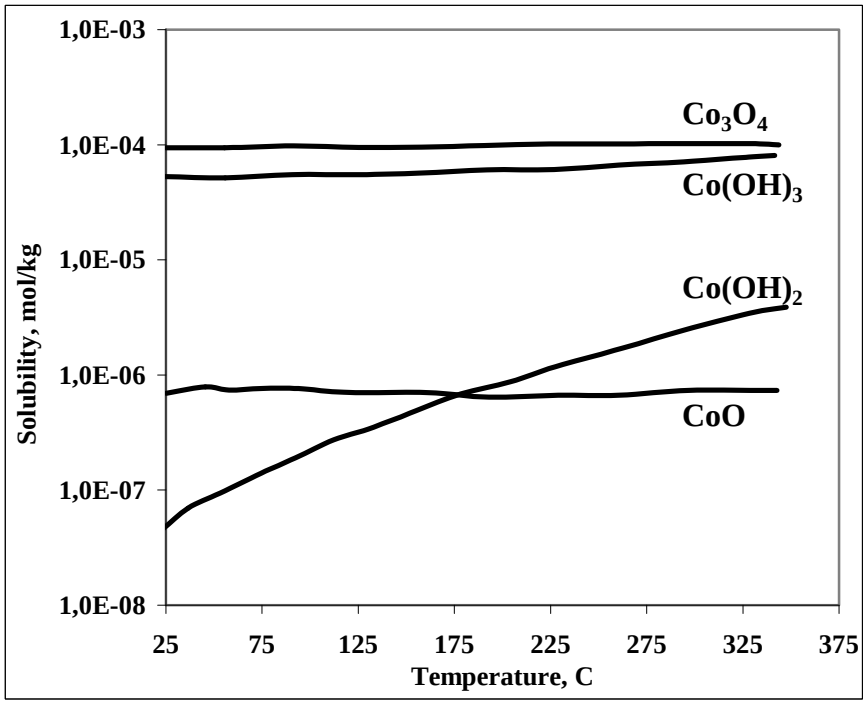

FIG. 8. Solubility of different cobalt forms in co-ordinated chemistry (hydrogen concentration 4×10^{-5} mol·kg^{-1}, pH_{25}=10).

Oxide particulates either created by precipitation in the coolant or by oxide erosion, may be transported from the bulk coolant to wall surfaces to form a deposit. The primary coolant flow is turbulent in most parts of the circuit. The particulate deposition mechanisms are then:

- **Turbulent diffusion**: velocity fluctuations transverse to the flow direction are called eddies, and they are responsible for momentum transfer to the walls. Particulates are entrained by these eddies and are carried toward the walls.

- **Brownian diffusion**: particles are submitted to Brownian agitation, caused by their collision with coolant molecules. Brownian movement of the particles leads to their diffusion, most evident in the laminar layer next to the wall. Rodliffe [24] indicates that only particles < 1 μm will show Brownian diffusion.
- **Inertial impaction**: large particles (>1 μm according to [24]) may have high enough inertia to detach from the coolant eddies and impact the wall, as the velocity of eddies reduce on approaching the wall.
- **Sedimentation**: particulates may settle under gravity to deposit on the walls of horizontal piping.
- **Thermophoresis**: this phenomenon arises from a thermal gradient between bulk coolant and wall surface. The thermal gradient leads to non-symmetry between coolant/particle interaction forces on either side of the particle. Particles therefore diffuse from the hot zones of the coolant to the colder regions (wall).
- **Erosion**: oxide particles present on primary circuit surfaces can be eroded by the coolant turbulence. A particle deposited on a wall surface is submitted to adherent and hydrodynamic forces operating in opposite directions. Oxide particles are eroded when hydrodynamic forces are greater than adherent forces.

Fig. 9 summarizes these mechanisms acting at the metal/oxide interface and the oxide/coolant interface [24]. Mass-transfer coefficients used in equations depend on temperature, $pH_{(T)}$ and redox potential of the particular system.

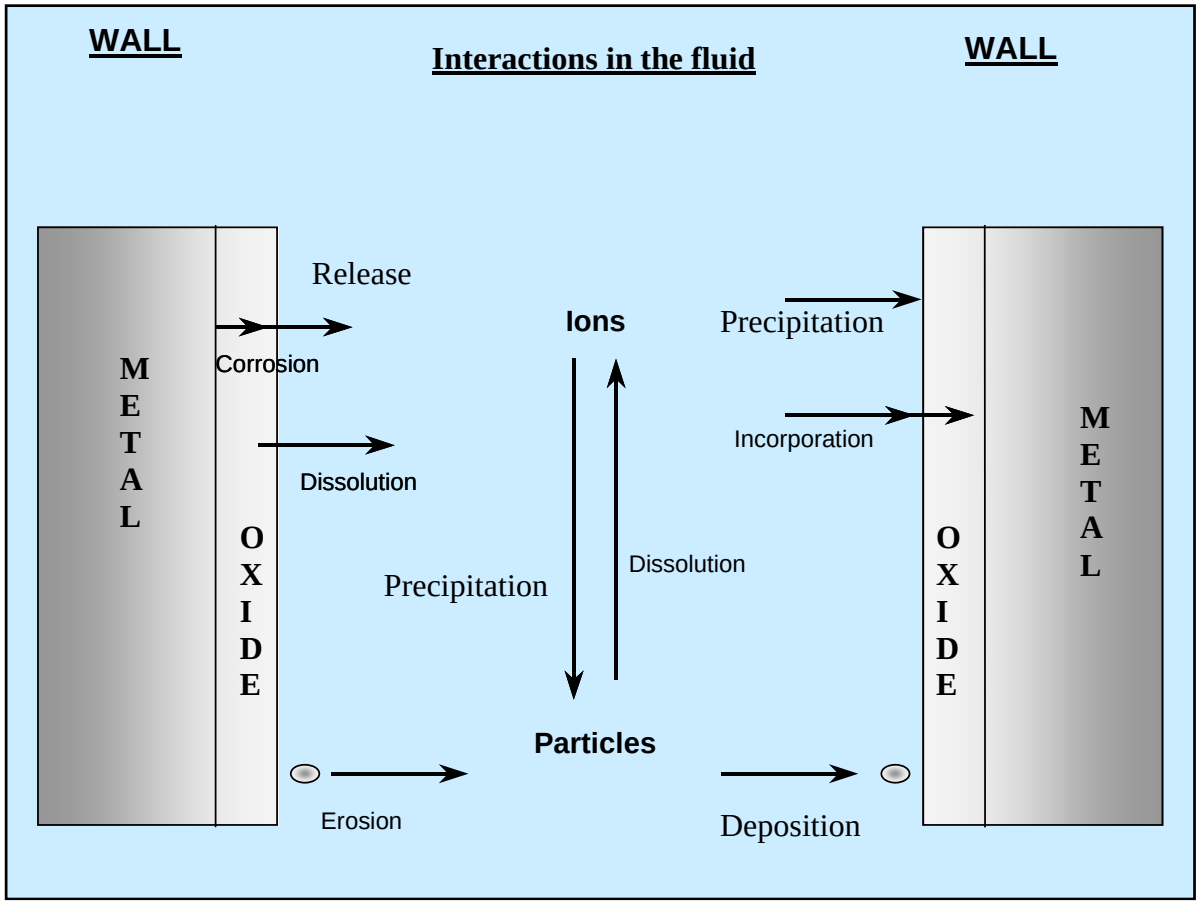

FIG. 9. Mechanisms responsible for activity transport.

2.6. Neutron activation to produce corrosion product radionuclides

Corrosion products can be activated during their exposure to the neutron flux and therefore be transformed into radioactive nuclides. This neutron activation is possible for both ions and particles during their travel in the reactor core region or when they deposit on in-core surfaces. Chemical elements, present in the structural material submitted to a neutron flux, are also made radioactive.

The main radioactive nuclides, which contribute to over 90% of the dose rate around the primary circuit, are ^{58}Co and ^{60}Co.

^{58}Co is the activation product of ^{58}Ni (68% content in natural nickel) created on exposure to fast neutrons and ^{60}Co is the activation product of ^{59}Co (100% in natural cobalt) formed from exposure to thermal neutrons. The activation reactions are:

$$^{58}Ni + n \rightarrow {}^{58}Co + p$$

$$^{59}Co + n \rightarrow {}^{60}Co + \gamma$$

Cobalt can be found as an impurity in primary circuit alloys: from 0.01% up to 0.8%, except in hard-surface materials (stellites) where the cobalt content can be 60%. Stellites only comprise a small part of the primary circuit surface (a few square meters) but provide a significant contribution to the activated cobalt in the coolant, which is the reason that comprehensive stellite replacement programs have been implemented at many plants.

3. REVIEW OF MODELS

The activity transport models developed before 1975 tended to be empirical in nature and generally difficult to evaluate mathematically unless they were very simple. A review of these early models is given in Section 3.1. After twenty-five years of development, the models tend to be mechanistic or, at least, semi-empirical in nature, but still very difficult to solve without fast computers. The mechanisms and models used in the six computer codes used in the blind benchmarking exercise are presented in Section 3.2.

3.1. A comparison of early models for transport of activated corrosion products in water cooled reactors

Some of the theoretical models for predicting the corrosion product activity build-up in the primary heat transport (PHT) circuit of water cooled reactors were studied, with a view to determining the fundamental and significant processes and mechanisms involved in the activity transport. The assumptions made in these models regarding:

- corrosion and corrosion product release,
- deposit, deposition and release,
- coolant crud,

are compared below:

3.1.1. Corrosion and corrosion product release

Out-core radiation field growth due to the activity transport is caused by the corrosion of the structural materials of the heat transport circuit by the action of the hot coolant, and the release of the corrosion products to the coolant that are carried through the reactor core and activated.

Veselkin and Shakh [25] assume an input of corrosion products into the coolant at a constant rate. Yerazunis, et al [26] and Bonalumi and Olivi [27] assume a time-dependant corrosion rate, the composition of the corrosion products being the same as that of the underlying metal. The Yerazunis model uses different corrosion release rates for old and new surfaces, the latter exhibiting a higher corrosion rate. Walton and co-authors [28–30] consider the corrosion film to be preformed, the composition of which is represented by the two limits:

(1) composition of the film is same as that of the underlying metal for each region,
(2) composition of the film is constant throughout the circuit and is an average for all the regions in the circuit.

They assume a first order release of corrosion product from the film to the coolant. Formation of fresh corrosion products is thus neglected.

The need for better estimates for corrosion and release rates is apparent. The oxide films on SS surfaces have been shown to be richer in chromium than the steel itself. This may be due to the lower solubility of chromium oxide in water and/or due to the higher rate of oxidation of chromium in the steel. Thus the assumption that the corrosion film or the material released by corrosion has the same composition as the base metal does not seem to be valid. Values for corrosion release rates, at least for cobalt, have to be ascertained.

3.1.2. Deposit, deposition and release

The Yerazunis model divides the deposits on in-core surfaces as well as out core surfaces into permanent and transient fractions. Only molecular diffusion and recoil processes are allowed for

transport of activity to and from the permanent deposit, except for the particulate transfer from the transient to the permanent layer. In transient deposits particulate transfer is also allowed. The transient layer remains steady in thickness, while the permanent one grows. The particle deposition coefficient is assumed to be the same for all elements and to be controlled by a convective process and is defined in terms of the conventional mass transfer equation, a particulate deposition coefficient typical of 0.1 um particles being used. Release is assumed to be by erosion and the release rate constant is again assumed to be the same for all elements and equal to that for iron. The recoil process has been neglected as unimportant.

According to Yerazunis's model, the molecular transport coefficient for absorption onto the deposits is related to the area of the crud (which is assumed proportional to the amount of the crud) and an assumed mass transfer coefficient. The transport from the deposits to the coolant (desorption) is related to the specific surface area of the crud, the chemical solubility of the element under consideration and the mass transfer coefficient. The molecular transport coefficients describing the release to the coolant are assumed to be the same for all deposits in-core and out of core.

The Walton model describes the deposition and release by ion exchange between the corrosion film on the surfaces and the ions in the coolant. First order kinetics are postulated for these processes. The coefficients of deposition and release, i.e. absorption and emission, are different for different ions and different surfaces.

The model of Veselkin and Shakh [24][25] postulates constant deposition and release rate coefficients throughout the circuit. The model of Bonalumi and Olivi [27] considers the deposition and erosion coefficients as variables in time and space. These coefficients are considered to be different for active and inactive isotopes. The recoil process is also included in the mechanisms for release.

Clearly, a simple mechanism cannot describe deposition and release processes. Both molecular and particulate transport have to be considered. Particulate deposition is possibly determined by diffusion across the boundary layer and by electrophoretic control. Thus the particulate deposition coefficient can be expected to be dependant on the local hydraulics, the depositing species and the deposition surface. Since radiation would affect the species in the coolant, a definite difference in deposition coefficient in-core and out-of-core might be expected. Particulate release, by erosion, would depend on the binding strength of the deposit and hence might be expected to be different for different species and also in a radiation field. It has been observed that the deposit becomes progressively more adherent with increasing depth from the surface of the deposit. Thus erosion should become progressively more difficult and the particulate release rate coefficient should decrease with increasing depth of the deposit. The effect of change in the release rate coefficient would be an increase in the release rate with increasing amount of deposit till it reaches a steady state when the release becomes pseudo-zero order. This would correspond to a first order release rate from a layer of deposit of constant thickness: the transient or erodable layer. The molecular deposition and release process may be due to an ion exchange reaction between the species in the coolant and the deposit on the walls.

3.1.3. Coolant crud

Many of the models do not specify the nature of the coolant crud, i.e., whether it is particulate or dissolved or both. Walton's model considers only dissolved, ionic species. Absorption and desorption processes between the corrosion film and the coolant constitute the removal and input mechanisms for the coolant crud. Yerazunis's model considers both the particulate and the dissolved activities in the coolant. The molecular, diffusion-controlled transport process between these two phases is described in terms of coefficients related to the surface area of the crud, coolant volume and the chemical solubility of the crud. In addition, a 'particulation' coefficient for recent corrosion products is defined in terms of corrosion release rate, purification removal rate and chemical composition of the crud. A description of

the coolant crud should include both suspended and dissolved species. The deposition and release rate coefficient would be different for the two types of species. The deposition and release processes for the dissolved species may be the ion exchange between the coolant phase and the deposit on the walls. There may be a further equilibrium between the dissolved and suspended species, which may be controlled both by the solubility of the species in the coolant and by ion exchange between the two types of species.

3.2. A review of codes and approaches for activity transport in water reactors

Modern digital computers allow complex mathematical descriptions of models for activity transport to be evaluated numerically rather than analytically. The equations describing the mechanisms in the models are solved in computer codes written in a variety of languages such as FORTRAN or C. For purposes of clarity, the words "mechanisms", "models", and "codes" are defined briefly first:

- **Mechanisms** describe the way in which chemical or physical entities interact with each other. Nature's laws for these interactions are the basis of the scientific literature in chemistry, physics, and engineering.
- **Models** are an assembly of one or more mechanisms that the scientist or engineer thinks may account for observations at a particular surface or in a particular volume of fluid. Models may be described in words, or the mechanisms in them may be described mathematically by equations. If some of the mechanisms are not well-known and are described in an empirical way, then the model is called 'empirical'. If the mechanisms are well-understood, then the model is called 'mechanistic'.
- **Codes** are the mathematical descriptions of models that are written in a language suitable for use in a digital computer. The codes allow the equations to be evaluated quickly and permit their predicted observation to be compared with the experimental observation.

3.2.1. ACE-II

The ACE-II model was developed in Japan. Fig. 10 shows the components identified for the improved code ACE-II [6], [31]. The following series of steps is given by the authors:

- The inner and outer oxides are generated by corrosion of component materials.
- Part of the outer oxide is released into the coolant by dissolution or erosion.
- There are two types of corrosion products in the coolant: dissolved and particulate.
- The loose crud grows by precipitation or deposition of corrosion products from the coolant.
- Activity in the loose crud diffuses into the outer and inner oxide by isotopic exchange or 'incorporation with corrosion of material'.
- Materials in the core region are activated directly and the activity is released to the coolant.
- Parent elements are nickel, iron, and cobalt, and radioactive nuclides are ^{58}Co and ^{60}Co.

The rate constants are termed 'deposition coefficient', 'erosion coefficient', and 'mass transfer coefficient' and most have empirical values based on a comparison of prediction with observation in Japanese PWRs. The model uses Beal's theory for particle deposition with 0.68 μm size particles in the loose crud and 3 μm size particles for the outer layer oxide, based on plant data. Solubilities are used for Ni, NiO, and nickel ferrite ($NiO.Fe_2O_3$) determined either theoretically or experimentally. The movement of Co is determined by the behaviour of the nickel ferrite.

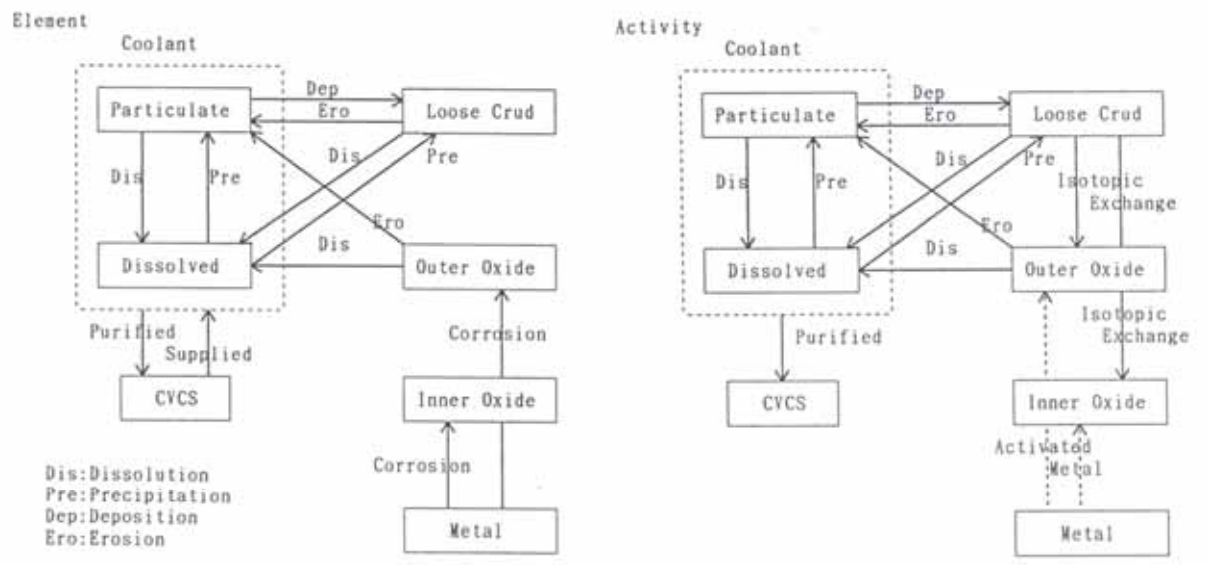

FIG. 10. ACE code transport processes.

Detailed description of the code:

CODE NAME : ACE	*Date* : September 2000
Version : 2	*Development team*
The first version of ACE was composed in 1992. Version 2 was developed in 1999.	Nuclear Chemical Engineering Section *Address* : Omiya R&D Department Nuclear Development Corporation Kitabukuro-cho 1-297, Omiya, Saitama, 330-0835, Japan. Phone: (81)-48-642-4412 Fax : (81)-48-650-2214
OBJECTIVES: ACE is a computer code developed by the Nuclear Development Corporation in cooperation with Mitsubishi Heavy Industries Ltd. for the prediction of radioactivity level and the evaluation of effect of countermeasures in the primary circuit of PWRs. The ACE analyzes the behaviour of corrosion products, activated or not, in order to determine the activity in the fluid and the deposited activity of out-of flux surfaces.	
LANGUAGE : FORTRAN 77	*Running on* : Unix workstation
Number of instructions : Approximately 7000 lines of code (including comments)	

MAIN MODELS :

Corrosion rate

Corrosion rate is thought to follow a cubic law for the first year and to be constant after that. The corrosion rate of the main coolant piping and other SS was determined from the amounts of the inner oxide in the detached piping investigation at Japanese plants and corrosion tests data. The corrosion rate of alloy 600, which was used for the SG tubing, was estimated by simulating nickel inventory from actual plant data. The corrosion rate after the first year was deduced to be constant from the trend of ^{58}Co activity level at the out-of-core surface and amount of Ni removed during plant shutdown. However, the corrosion rate of alloy 690 was set to follow $t^{0.42}$ for all plant life estimated nickel inventories at Japanese actual plants. The cobalt input from the hard-facing alloy, Stellite, was calculated based on the results estimated by EPRI and by using erosion test data.

Deposition, erosion

The deposition and erosion rates were estimated based on S.K.Beal's theory. The particle size was taken to be 0.68 μm for the loose crud and 3 μm for the outer oxide based on actual plant data. The inner oxide is not released by erosion and dissolution. The behaviour of particles depends on many factors other than the fluid condition, temperature, particle size and particle density which can be handled by S.K.Beal's theory, but there is insufficient information to calculate the other factors quantitatively. However, the pH of the coolant is an important factor for water chemistry, and it is known that the pH influences the behaviour of particulate corrosion products due to the surface charge on particles. Therefore, the effect of pH on the deposition and erosion rates has been introduced into this model.

Dissolution, precipitation

The transfer of dissolved species can be expressed as the product of mass transfer coefficient and the difference between the concentrations at the surface and in the coolant. The mass transfer coefficient can be calculated theoretically, but the theoretical value is not consistent with actual plant data, because the gross mass transfer also depends on the condition of the surface. Therefore, the mass transfer coefficient was estimated by using concentration data on the purification rate change at actual plants and inpile loop test data. Also, the solubilities of nickel and cobalt from corrosion products were calculated based on experimental results for $Ni_{0.8}Fe_{2.15}Co_{0.05}O_4$.

Incorporation in oxide film

Radioactivity is incorporated into the outer and inner oxides by isotopic exchange and as a result of corrosion. The isotopic exchange rate depends on the diffusion coefficient, the diffusion distance, the concentration of the dissolved species and the difference in the specific activity. On the other hand, the rate of incorporation as a result of corrosion depends on the specific activity of the loose crud and the rate of oxide growth due to corrosion. There is a clear relationship between the cobalt content and the composition of chromium in the corrosion products. This effect was introduced into the incorporation mechanism by using the composition of chromium in the oxide as input data.

Improved points at version 2

The chemical form evaluated in version 1 is only nickel ferrite. However, metallic nickel was found to have an important role on ^{58}Co generation at Japanese plants. Therefore, ACE version2 was enlarged chemical forms to metallic Ni, NiO and nickel ferrite. NiO is generated by oxidation of metallic Ni. The stability of metallic Ni and NiO will depend on temperature and dissolved hydrogen concentration. The thermodynamic evaluation has been used to estimate stable chemical form at each region and chemistry. It is assumed that there is thermodynamic equilibrium between metallic Ni (or NiO) and nickel ferrite.

DOMAIN OF USE : ACE has been used to predict the effects of reactor design (SGs material, fuel assembly grids…) and the effects of reactor operating conditions (water pH, dissolved hydrogen concentration, fuel cycle duration …) on PWR contamination. At present, ACE is able to treat Fe, Ni, and Co as elements and ^{58}Co, ^{60}Co as activity nuclides, and these are calculated at mass balance condition.
VALIDATION FIELD : The qualification of the ACE code was done by means of comparison of ACE simulated results with actual Japanese plant data.
KEY REFERENCES: [31–41].

3.2.2. CRUDTRAN

The CRUDTRAN code was developed in Republic of Korea. Fig. 11 shows the various crud creation and deposition mechanisms for both dissolved and particulate material [42]. The non-stoichiometric nickel ferrite shows an inverse solubility curve with temperature over most of the pH range considered. Therefore, in the out-of-core region where crud in the coolant is under-saturated, crud is dissolved from the surface into the coolant. In the core where crud in the coolant is super-saturated, crud is precipitated and is deposited on the surface. Radionuclides ^{58}Co and ^{60}Co created in the in-core deposit are transported into the coolant by isotope exchange process in the diffusion and are deposited out-core by the same mechanism. The coolant is at steady state for solute, but the dissolved and particulate radioactivity grows with time. Fig. 12 shows the four node model built on the above mechanisms. The model predicts the dissolved and particulate behaviour of iron, with Ni and Co following the iron in fixed ratios. Only five mass balance equations are needed to describe the iron and radionuclide quantities incore, outcore, and in the coolant. This model was fitted to data from the PWR coolant chemistry loop (PCCL) at MIT to give crud and activity transport factors. These factors combine both mass transfer and crystallization or dissolution kinetic constants. They both show that mass transfer is fast compared to these surface kinetic constants. The CRUDTRAN model considers oxide dissolution from the SG and such dissolution is controlled by surface kinetics, not mass transfer. The transfer of radionuclides from the heavy deposit growing in-core to the corrosion oxide layer out-of-core is controlled by isotope exchange process in the diffusion.

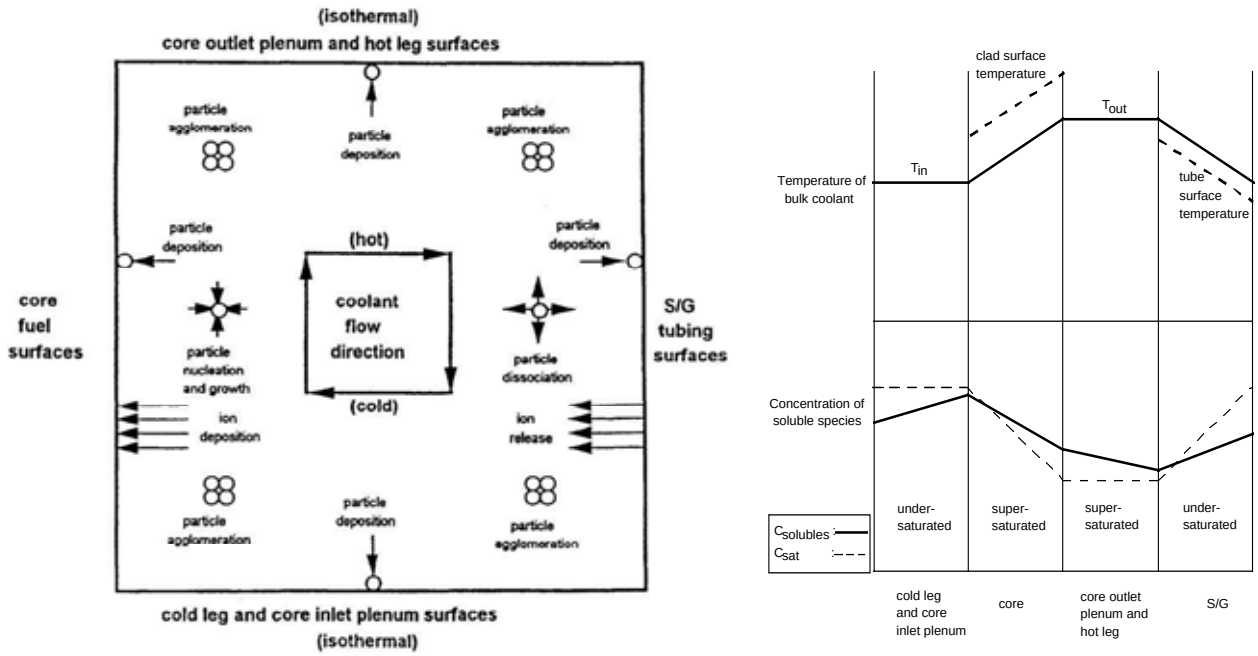

FIG. 11. CRUDTRAN: movement of corrosion products in a PWR primary circuit.

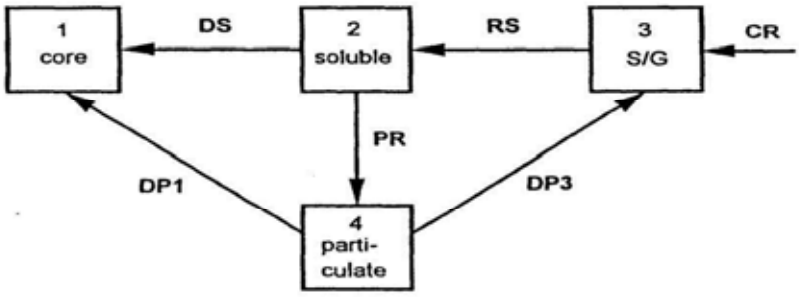

CR	=	corrosion rate in SG
RS	=	crud release rate as soluble species in SG
DS	=	crud deposition rate as soluble species in core
PR	=	crud precipitation rate in the coolant
DP1	=	crud deposition rate as particulate in core
DP2	=	crud deposition rate as a particulate in SG

FIG. 12. CRUDTRAN: four node model for crud transport.

Detailed description of the code:

CODE NAME : CRUDTRAN	*Date*: April. 2002 *Address* : KAERI Yusung P.O. Box 105, Taejon, Korea Phone : +82-42-868-2257 Fax : +82-42-863-0565 E-mail : cblee@kaeri.re.kr

OBJECTIVES

CRUDTRAN is a code to predict the corrosion product and radioactivity transport in the primary coolant system of PWR. The main mechanism of the corrosion product transport is dissolution, mass transfer and crystallization of the crud induced by the difference of the crud solubility in the coolant with temperature and the water chemistry conditions. CRUDTRAN is mainly intended to predict the effects of the coolant chemistry condition on the crud and activity transport.

LANGUAGE : FORTRAN 77	*Running on* : PC
Number of instructions : Approximately 1500 lines of code (including comments)	

MAIN MODELS :

The PWR primary circuit is divided into three principal sections such as the core, the coolant and the SG. The driving force for crud transport in the PWR primary coolant comes from coolant temperature changes throughout the system and the resulting changes in corrosion product solubility. As the coolant temperature changes around the PWR primary circuit, the saturation status of the corrosion products in the coolant also changes. In the core, where the coolant temperature increases, the soluble species exist in a super-saturated state, so that there is a driving force for the soluble species to deposit on the core surface, or precipitate as particulates. On the other hand, in the SG, as the coolant temperature decreases, the soluble species become under-saturated, so that there is a driving force for the corrosion products on the SG surfaces and the particulates in the coolant to dissolve into the coolant to restore a saturation concentration of corrosion products in the coolant.

Water chemistry has a strong effect on the crud and activity transport. The soluble species of the corrosion products are the dominant form in the crud and activity transport while the particulate form of crud in the coolant can also contribute to crud and activity transport.

Soluble Transport

Crud transport processes as soluble species from the SG to the core in the PWR primary circuit are dissolution at the SG tubing surface, mass transfer across the boundary layer in the SG, mass transfer across the boundary layer in the core, and crystallization on the core fuel surface.

Recirculation of the highly turbulent coolant through the PWR primary circuit transfers the corrosion products from the SG to the core without any significant intervening resistance. On the other hand, the activity produced in the core is transported from the core to the SG, driven by its concentration gradients, and its paths are dissolution at the core fuel surface, mass transfer across the boundary layer in the core, mass transfer across the boundary layer in the SG, and crystallization on the SG surface.

Since the crud and activity inventories in the coolant may quickly reach quasi steady-state values the bulk primary coolant can be removed in the nodalization of the primary circuit. The balance equations of crud and activity transport as soluble species which show that crud transport from the SG to the core is proportional to the solubility difference of corrosion products between the SG and core surfaces are:

$$\frac{dI_1}{dt} = \frac{k_1 k_3}{k_1 + k_3} (S_3 - S_1)$$

$$\frac{dI_3}{dt} = CR - \frac{k_1 k_3}{k_1 + k_3} (S_3 - S_1)$$

$$\frac{dA_1}{dt} = -\lambda A_1 + \alpha P I_1 - \frac{k_1^a k_3^a}{k_1^a + k_3^a} \left(\frac{A_1}{I_1} S_1 - \frac{A_3}{I_3} S_3 \right)$$

$$\frac{dA_3}{dt} = -\lambda A_3 + \frac{k_1^a k_3^a}{k_1^a + k_3^a} \left(\frac{A_1}{I_1} S_1 - \frac{A_3}{I_3} S_3 \right)$$

Since the most important corrosion product for which reliable solubility data is available is iron, only iron is considered, and nickel and cobalt are assumed to follow the iron in fixed proportions. Then, crud and activity transport factors, β_c and β_a can be defined as follows.

$$\beta_c = \left(\frac{k_1 k_3}{k_1 + k_3} \right) \frac{\rho_{H_2O}}{F}$$

$$\beta_a = \left(\frac{k_1^a k_3^a}{k_1^a + k_3^a} \right) \frac{\rho_{H_2O}}{F}$$

The crud and activity transport factors, β_c and β_a, control the relative magnitude of the crud and activity transport. Crud transport from the SG to the core is proportional to the difference of the corrosion products solubility at the SG and the core surfaces. The solubility of the corrosion products depends upon the coolant pH, temperature and dissolved hydrogen concentration. Thus, coolant chemistry conditions such as high pH, high temperature and small hydrogen concentrations give smaller solubility differences between the SG and core surfaces, and hence less crud transport from the SG to the core, and less activity build-up in the SG. The corrosion rate of the SG tubing and initial crud inventory in the SG has little effect on the crud and activity transport in this model.

Particulate transport

Dissolved corrosion products in the coolant may precipitate as particles in super-saturated regions of the PWR primary loop. There are four possible paths for such corrosion products as solubles and particles in PWR primary coolant: soluble species deposition on surfaces, solubles diffusion to particles in the coolant, particle deposition on surfaces, and particle agglomeration in the coolant. Activity transport may also be affected by particulate precipitation. When the solubles precipitate in the coolant, the same fraction of radioactive elements is assumed to be incorporated into the particulates along with the iron. Particulates may precipitate in the bulk coolant and agglomerate to form very small particles, and then deposit on the core and SG surfaces before growing into larger particles, due to the much stronger tendency of particulates to deposit on the surfaces than to grow. However, particulate precipitation from the super-saturated soluble species in the coolant does not change the basic dependence of the crud transport from the SG to the core upon the solubility difference. It only decreases the amount of net crud transport from the SG to the core due to re-deposition of the particulates on the SG since particulate can deposit any surfaces regardless of the crud saturation status in the coolant.

Solubility ofiIron The corrosion products formed on the surfaces of the SG Inconel tubing and SS under nominal PWR coolant chemistry – very low oxygen content (< 10 ppb) and high hydrogen partial pressure (~ 25 cc H_2/kg-H_2O) – are measured to be mainly nickel-ferrite ($Ni_xFe_{3-x}O_4$) or nickel-cobalt-ferrite ($Ni_xCo_yFe_{3-x-y}O_4$), with the x value (or x+y in the $Ni_xCo_yFe_{3-x-y}O_4$) ranging from 0.45–0.75. Based upon the composition ratio of nickel-ferrite, the solubility of the iron can be calculated by using chemical dissociation reactions of the nickel-ferrite. The dissolved iron consists of the four dominant ionic forms such as Fe^{++}, $Fe(OH)^-$, $Fe(OH)_2$, and $Fe(OH)_3^+$, and the solubility of the iron(s) is the sum of the saturation (or equilibrium) concentrations of these ions.
TYPE OF NUMERICAL TREATMENTS : CRUDTRAN predict the ^{58}Co and ^{60}Co activities in both the SG and the fuel surfaces. Solubility of iron from the nickel-ferrite under reduction condition is used in the calculation of the corrosion products in the PWR primary circuit.
DOMAIN OF USE : CRUDTRAN can be used for a PWR with Inconel SGs.
VALIDATION FIELD : Validation of CRUDTRAN code was done by comparison with results of in-pile PWR-simulating loop tests in the research reactor (MITR) with different water chemistry conditions.
KEY REFERENCES: [42–44].

3.2.3. DISER

The code DISER was developed in the Czech Republic. Fig. 13 summarizes all the processes described in this code [45–46]. The coolant contains solute, colloids, and particulate corrosion products. Corrosion of the base metal follows parabolic kinetics and creates only an inner layer oxide. Solute is formed by dissolution of the inner oxide layer when the coolant is unsaturated in dissolved iron or nickel, based on magnetite or nickel ferrite solubility. When the coolant is supersaturated in the boundary layer at the local surface temperature, it precipitates to form both an inner and an outer oxide layer. Solute also forms colloidal particles in the coolant when the bulk coolant is supersaturated with respect to a specified iron oxide, e.g. magnetite or nickel ferrite. Similarly, colloids dissolve to form solutes if the bulk coolant is unsaturated. Colloids deposit if Brownian motion provides them enough energy to overcome the energy barrier that may exist at a particular surface due to its composition and the water chemistry at that time, e.g. work against electrostatic repulsion must be done before van der Waals attraction can hold the colloid to the surface. Fig. 14 shows the energy barriers to deposition and to release. Colloids may detach with a change in water chemistry. Colloids >0.8 μm diameter behave as particles with their inertial behaviour important in carrying them across a flow boundary layer at a surface. A sticking probability is calculated from Beal's model to determine if a particle reaching a surface will remain or immediately be carried back into the bulk coolant. Deposits of particles may be eroded in some way not specified. Similar mechanisms operate for corroding surfaces in the reactor core where all three forms of corrosion product may be irradiated and released. Fig. 15 shows in more detail the dissolution of the inner and outer oxide deposit layers that may exist either in the reactor core or in the SG, depending on the water chemistry at that time and its effect on the temperature coefficient of the solubility for that oxide. Fig. 16 shows similar precipitation considerations.

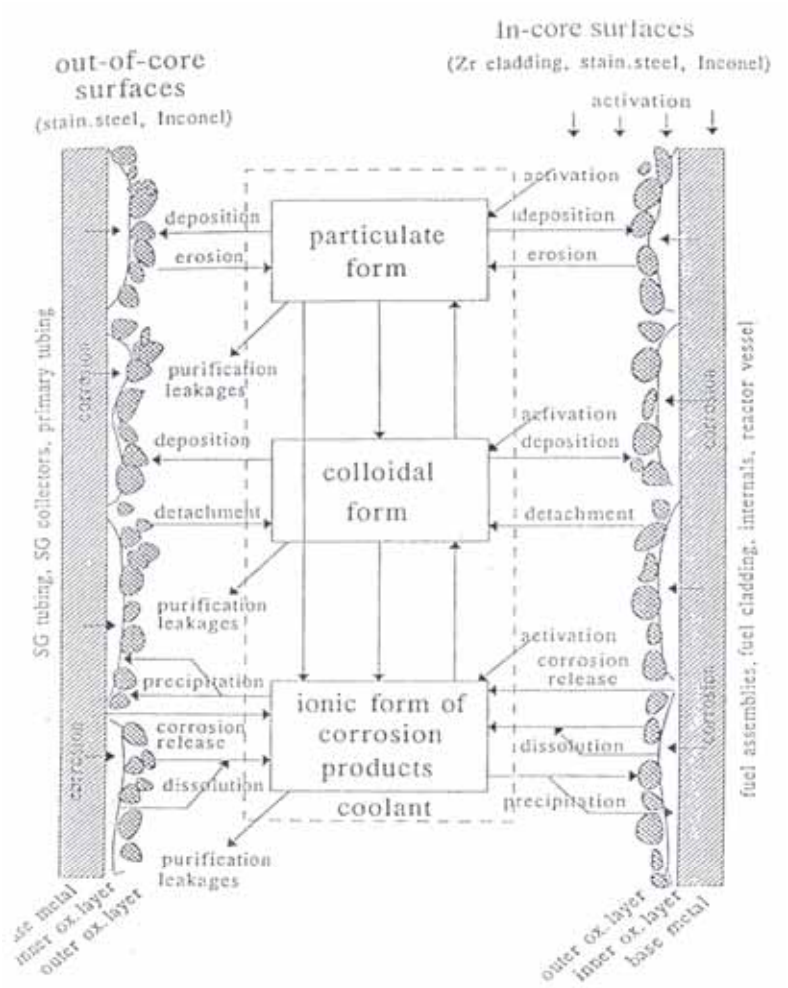

FIG. 13. DISER code: movement of corrosion products in a PWR primary circuit.

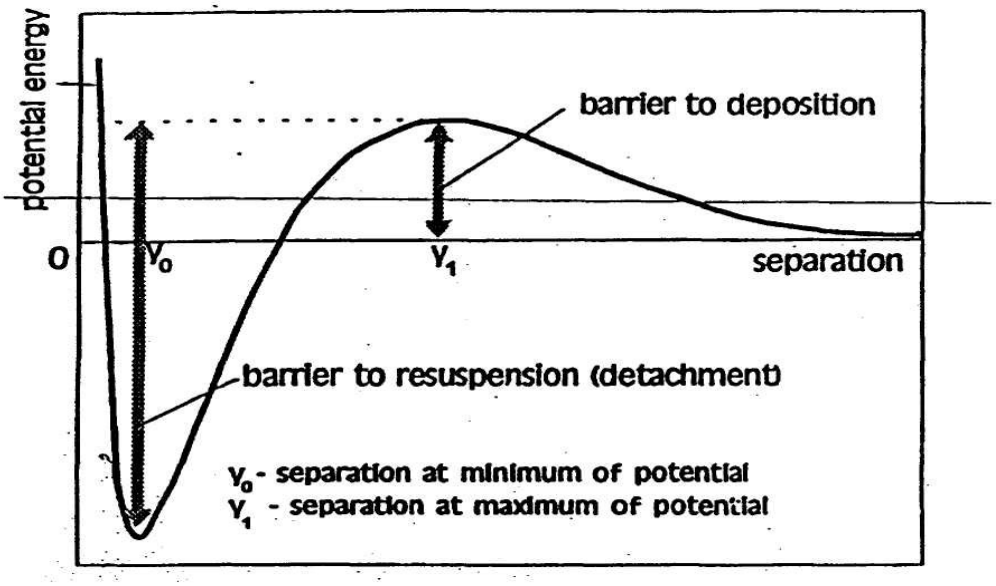

FIG. 14. DISER Code: microscopic model of particle interaction with surface.

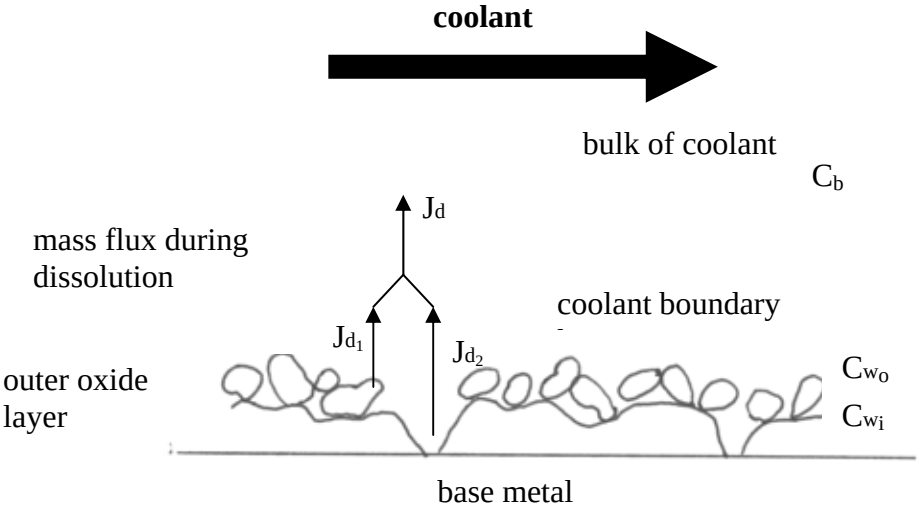

FIG. 15. DISER code: microscopic model of corrosion film dissolution in unsaturated coolant.

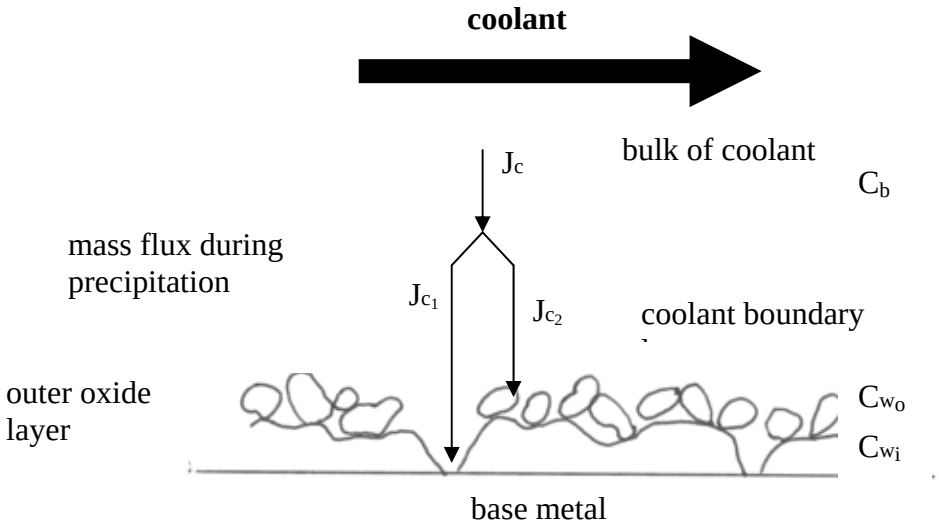

FIG. 16. DISER code: microscopic model of precipitation on corrosion film in saturated coolant.

Detailed description of the code:

CODE NAME : DISER	*Date* : May 2002
Version : 2	*Development team*
The first version of DISER was composed in 1990. Version 2 was developed in 1999.	Irradiation Projects Department, Reactor Services Division
	Address :
	Nuclear Research Institute Rez plc 250 68 Husinec-Rez 130 Czech Republic Phone: (420)-2-6617-2453 Fax : (420)-2-6617-2045 E-mail: zmi@ujv.cz

OBJECTIVES:

DISER is a computer code developed by Nuclear Research Institute Rez plc for prediction of corrosion products behaviour and radioactivity build-up on the WWER and PWR primary system surfaces. The DISER analyzes an effect of various parameters and characteristics (e.g. water chemistry, structure materials) on corrosion products transport and contamination of the out-of-core surfaces.

LANGUAGE : FORTRAN 77	*Running on* : PC
Number of instructions :	
Approximately 2000 lines of code (including comments)	

MAIN MODELS :

The DISER code describes behaviour of corrosion products originating from structure materials (Fe, Ni, Cr) and their major radionuclides (^{58}Co, ^{60}Co, ^{54}Mn, ^{51}Cr, ^{59}Fe). The reactor primary circuit is divided on 15 parts (nodes) characterized by different conditions (thermal-hydraulic, materials, neutronic). Five nodes represents the reactor core (SS and Zr surfaces are considered), five SG tubing, two SG collectors (channel heads), two the primary piping and one a purification system. Simple thermal-hydraulic calculation is performed, and coolant and wall temperature for each part of the primary circuit is determined. Using the primary water chemistry data and calculated temperatures, pH_T values and corrosion products solubilities in the bulk of coolant and in the coolant boundary layer are determined. Various thermodynamic models of solubility can be used (e.g. magnetite, nickel-ferrite, nickel-cobalt-ferrite and nickel oxide).

It is supposed that a double oxide layer is formed on the primary surfaces. The inner oxide layer is formed by corrosion of structure materials that is consider to follow a parabolic kinetics. The outer oxide layer is formed in process of precipitation and deposition of corrosion products circulating in the coolant.

Corrosion products in the coolant exist in three different forms: as a soluble (ionic) species, in colloidal form, and in form of inertial particles. A part of the corroded material is released in process of corrosion into the coolant in ionic (soluble) form. Concentration of non-active ionic species is equal to the solubility under the given thermal and chemistry conditions. The colloids are formed in the coolant by a nucleation process when bulk coolant is supersaturated with respect to specified solubility limit. The inertial particles are formed in agglomeration process. Both, colloids and inertial particles can be dissolved in the bulk of coolant. Also, corrosion product agglomerates break-up is considered if the shear stresses acting on the agglomerate from the side of flowing liquid exceed the attracting forces acting between particles. Colloids and inertial particles are divided into several groups (13) characterized by the certain size (diameter) and

the behaviour of these groups is described depending on their size.

Transport of ionic (soluble) species is described as a diffusion process. Its intensity and direction is determined by a gradient of corrosion products solubility in the coolant boundary layer. Precipitation of corrosion products or dissolution of oxide layer can occur in different part of the circuit.

Corrosion product particles with size in the range of 0.01–0.6 μm carrying an electric charge are described as colloids. Transport processes of colloids are governed by interaction with charged surface and formation of a potential barrier. Probability of its penetration determines colloids deposition and detachment.

Transport processes of the inertial particles are governed by their inertion characteristics in the coolant boundary layer. A sticking probability is calculated from Beal´s model to determine if a particle reaching a surface will remain or immediately be carried back into the bulk coolant. Erosion of the inertial particles from the surface is given from a balance between attractive van der Waals forces and drag forces acting on the surface from the side of flowing liquid.

The following activation mechanisms of corrosion products are considered:

- activation during the passage through the reactor core with the primary coolant,
- activation of corrosion product deposits on the in-core surfaces,
- activation of in-core structural materials, corrosion and release into the primary coolant.

DOMAIN OF USE :

DISER has been used to predict contamination of the primary circuit inner surfaces by corrosion product radionuclides in WWER and PWR units. Also, the effects of reactor design (SG material, fuel assembly grids, purification system parameters, etc.) and the effects of reactor operating conditions (water pH, dissolved hydrogen concentration, fuel cycle duration, coolant flow rate etc.) on WWER and PWR contamination has been analyzed. An accumulation of radioactivity in the WWER unit coolant purification systems (high-temperature Ti filters and ion exchange resins) has been evaluated.

VALIDATION FIELD :

The qualification of DISER code has been performed by means of comparison of the DISER simulated results with actual WWER plant data (data from NPP Dukovany, LOVIISA, Bohunice have been used).

KEY REFERENCES: [47–51].

3.2.4. MIGA-RT

This code was developed in Bulgaria. Fig. 17 shows the four regions plus purification system modelled in this code and Fig. 18 shows the interaction of each region with the coolant [52]. Both particulate and dissolved materials are considered. Corrosion releases only dissolved species with the parabolic rate law being assumed to apply during the first reactor cycle, and thereafter the corrosion rates of the SS and SG alloy are assumed constant. Elements are released in proportion to their content in the corroding material. Only one oxide or deposit layer is considered on each surface. Particles are formed by erosion of these oxide layers. The behaviour of dissolved species is determined by the solubility of the particular oxide phase being considered, e.g. magnetite, nickel ferrite or sub-stoichiometric nickel ferrite, metallic nickel, or nickel oxide. The deposition and release of particles is controlled by the hydrodynamics on each individual surface, with deposition determined by the mass transfer rate for particles of size 0.7–1.0 μm across the flow boundary layer combined with a sticking probability for attachment. Detailed mass balance equations are written for each chemical element in the coolant at a node in a particular region, and for the same element on the surface in that region. Similar equations are written for the radionuclides, e.g. ^{58}Co and ^{60}Co, both particulate and dissolved, in each region in the coolant and on the surface. Each radionuclide behaves as does its parent element, e.g. ^{58}Co will behave in the same manner as nickel.

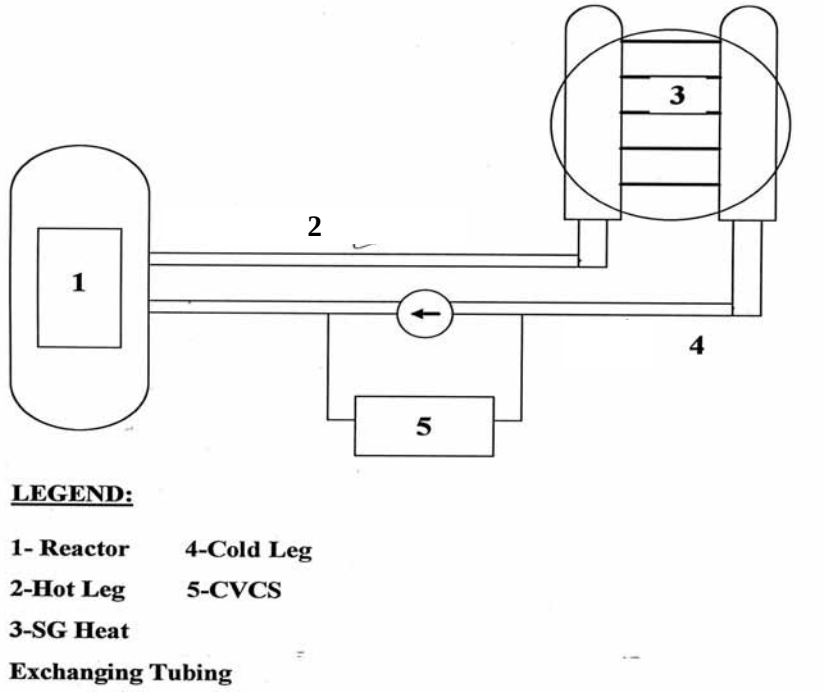

FIG. 17. MIGA-T: description of regions modeled in MIGA code

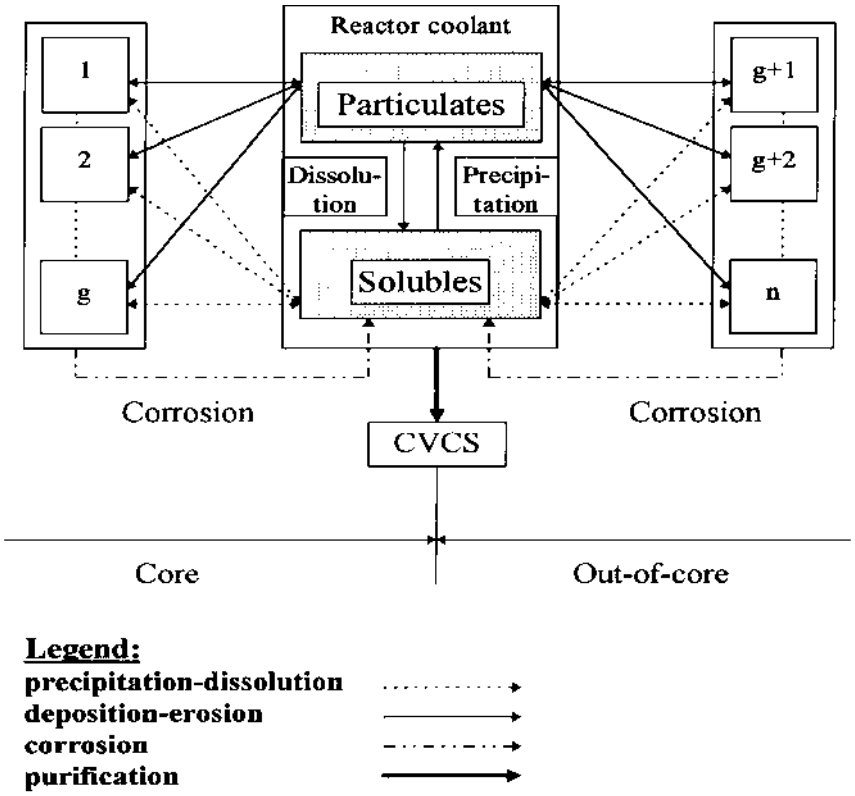

FIG. 18. Transport processes of corrosion products in PWR primary circuit.

Detailed description of the code:

CODE NAME: MIGA Version: MIGA RT	*Date* : November 2000 *Development team:* Department of Nuclear Energy Reactor and System Chemistry Group Institute for Nuclear Research and Nuclear Energy , Bulgarian Academy of Sciences , SOFIA, BULGARIA *Address:* 72 Tzarigradsko Chaussee, Sofia BG-1784 Bulgaria Phone:++359-2-7144576 Fax:++359-2-9753619 e-mail:nely@inrne.bas.bg
OBJECTIVES: The MIGA-RT code was developed for the calculation of time-accumulated activity of the main corrosion products radionuclides ^{60}Co and ^{58}Co on different parts of the primary system of WWER NPPs. This code was developed within the framework of the IAEA CRP "Modelling of Transport of Radioactive Substances in Primary Circuit of Water Cooled Reactors" with the financial support of IAEA. MIGA-RT was applied to the NPPs EBO-1 (Slovakia), LOVIISA-1 and LOVIISA-2 (Finland). MIGA-RT code was used also for calculation of the radioactivity build-up in the primary circuit of French NPP CRUAS-1	
LANGUAGE : FORTRAN 77 *Number of instructions* : Approximately 18508 lines (including the main program, additional subprograms, comments)	*Running on* : PC / DOS
MAIN MODELS: The WWER reactors use specific potassium-ammonia primary water chemistry. The potassium hydroxide is introduced as a pH control agent. Under the core irradiation, ammonia dissociates forming hydrogen and nitrogen. Excess of hydrogen (30–60 $cm^3 \cdot kg^{-1}$) provides for profound suppression of coolant radiolysis. As a result oxygen content in coolant is kept below 5 $\mu g \cdot kg^{-1}$. The specifications of reactor water quality for WWER-440 allows small variations of the pH values (7.2 ± 0.1 at 300°C) though a correlation between the concentration of alkali ions and boric acid in order to maintain the coordinated water-chemistry control. CP transport phenomena, both particulates and solubles, are the cornerstone of the MIGA code. *CP particle transport* The main model involved in description the CP transfer is related mainly to particle/wall interaction and particularly includes deposition and release mechanisms under pressurized water reactors condition. The model itself is based on the updated Beal's deposition model in a turbulent flow [35]. By analogy to the phenomenological models, analytical expressions for both deposition coefficient	

(k_d) and release coefficient (k_e) are defined as follows:

$$k_d = \frac{pK(K + V_{B.} + V_f)}{K + p(V_B + V_f)}$$

$$k_e = \frac{\gamma K}{K + p(V_B + V_f)}$$

Where

K	is the mass transfer coefficient ($m \cdot s^{-1}$);
k_d	is the deposition coefficient ($m \cdot s^{-1}$);
k_e	is the release coefficient (s^{-1});
p	is the sticking probability;
s	is the particle stopping distance (m);
V_B	is the particle velocity in the ***s*** layer due to Brownian diffusion ($m \cdot s^{-1}$);
V_f	is the particle velocity in the ***s*** layer due to momentum ($m \cdot s^{-1}$);
γ	is the release constant (s^{-1}).

For determination of the sticking probability (p) a hypothesis for two-stage particle-wall interaction mechanism was introduced. The first stage is considered removal of the hydrated shells (dehydration) of the particle surface ions while the second stage is related to the adsorption of the dehydrated particles on the metal surfaces. On the other hand, this is a process accounting for both thermal activation in the particular circuit node and the physico-chemical condition on the surface related to the local water chemistry. The above approach has been extended to the ion-wall interaction disregarding all the inertial terms in the equations above and considering the difference in dehydration of CP depending on their size, according to [53].

The application of this approach to the well-known phenomenological models has increased their flexibility for circuits with arbitrary design and operational parameters (geometry, thermohydraulics, and water chemistry). The above described philosophy has been applied in the MIGA computer code, which was created to simulate and predict the crud activity transport in PWR and especially WWER reactors.

The reactor circuit in the MIGA model is generally divided by n-nodes (g-nodes in the reactor core) with well defined design (geometry, construction materials) and thermal-hydraulic condition. Because of the lack of precise plant data the current evaluations for WWER and PWR are limited to the circuit divided by 6 nodes, including that of the CVCS-system.

Activation

Ion and solid particles are transported in different regions of the primary circuit by means of the fluid. When they reach a part of the circuit submitted to neutron flux (mainly in-core regions), they are activated. Classic nuclear reactions are accounted for in the MIGA-RT code. Two radioactive isotopes are of major interest: ^{58}Co and ^{60}Co. They are produced by the following two nuclear reactions:

$$n + {}^{58}Ni \rightarrow {}^{58}Co + p$$

$$n + {}^{59}Co \rightarrow {}^{60}Co + \gamma$$

and have a respective half-life of 72 days and 5.3 years

Ionic transport

The MIGA-RT model version includes an updated thermodynamic approach for calculating the solubility of CP in form of nonstoichiometric Ni-ferrites. Dinov and Kasahara analysis [54] has shown that a high temperature system, containing $Ni_xFe_{3-x}O_4$ in equilibrium with its dissolution products under PWR primary chemistry exhibits a trend to form intermediate (metastable) states, specific to plant conditions, materials and water chemistry. In this relation, the generation of free Ni in metallic state was shown to be important. For such analyses, the introduction of a recently proposed, more integral parameter than $pH_{(T)}$, called thermodynamic stability effect (TSE) indicator, was proposed to be related to the stability of two competing most stable (metastable) states of the system. A program module for evaluation the most stable among the relevant metastable states of the primary aqueous system, containing nonstoichiometric Ni-ferrite ($Ni_xFe_{3-x}O_4$) as a corrosion solid phase of principle interest, together with other decomposition phases, as: magnetite (Fe_3O_4), NiO and metallic Ni – in equilibrium with the corresponding ionic species and hydrolysis products – was developed. This module was included into the computer code version MIGA-RT for further improvement of its capabilities to calculate correctly the yield of solubility in the total mass and activity transport.

TYPE OF NUMERICAL TREATMENTS:

The general equations using by MIGA-RT code are:

- Total concentration of *i*-th parent element in the coolant (m_i)
- Surface concentration in *j*-th node
- Total concentration of *i*-th radionuclide in the coolant (m_i^*)
- Surface concentration of *i*-th radionuclide in *j*-th node

DOMAIN OF USE: WWER, PWR

VALIDATION FIELD:

The qualification of the MIGA-RT code was tested in NPPs EBO-1, LOVIISA-1, LOVIISA-2 and in Beznau PWR NPP

KEY REFERENCES: [53–56].

3.2.5. PACTOLE-2.2

The PACTOLE code has been under development in France for over thirty years. Fig. 19 shows the five regions in each control volume that are modelled by mass balance equations in PACTOLE [57–58]. Metal corrodes to form both an internal oxide layer in contact with the metal and to release ions directly to the coolant. The metal ion solutes may precipitate if the bulk coolant concentration exceeds the solubility of any of the possible ferrites, e.g. nickel ferrite, cobalt ferrite, manganese ferrite, and magnetite. Solute will precipitate either on the inner oxide layer outcore or on incore surfaces, depending on the water chemistry at that point in the fuel cycle, e.g. B and Li concentrations. Precipitation forms a deposit which can be eroded to form particles in the coolant if the deposit is beyond a critical thickness. The particles and the solute may be removed by the purification system. Particles will deposit on all system surfaces, enhancing the radiation field locally if out-of-core, or being irradiated if deposited in-core. Particles deposited in-core are released by erosion and by dissolution. Ions may exchange with the surfaces of the deposit and with the inner oxide layer to contribute to radiation field growth. Fig. 20 shows a case with unsaturated coolant where ions are released to the

coolant by diffusion through the water-filled oxide layer and by grain-boundary diffusion, and by dissolution of the deposit. Fig. 21 shows the more complex case with the saturated coolant precipitating on the inner oxide film, driving radioactive solute into this film for isotopic exchange, with simultaneous release by corrosion. Particles also deposit by various mechanisms, e.g. turbulent diffusion, thermophoresis, gravitational settling. Magnetite is the oxide phase determining the dissolved iron concentration, and the solubilities of all the other dissolved species are used with the appropriate ferrite solubility to determine if they will precipitate, e.g. cobalt ferrite. Solubility versus temperature data are given for cobalt ferrite at a given B and Li concentration, for example and for illustration.

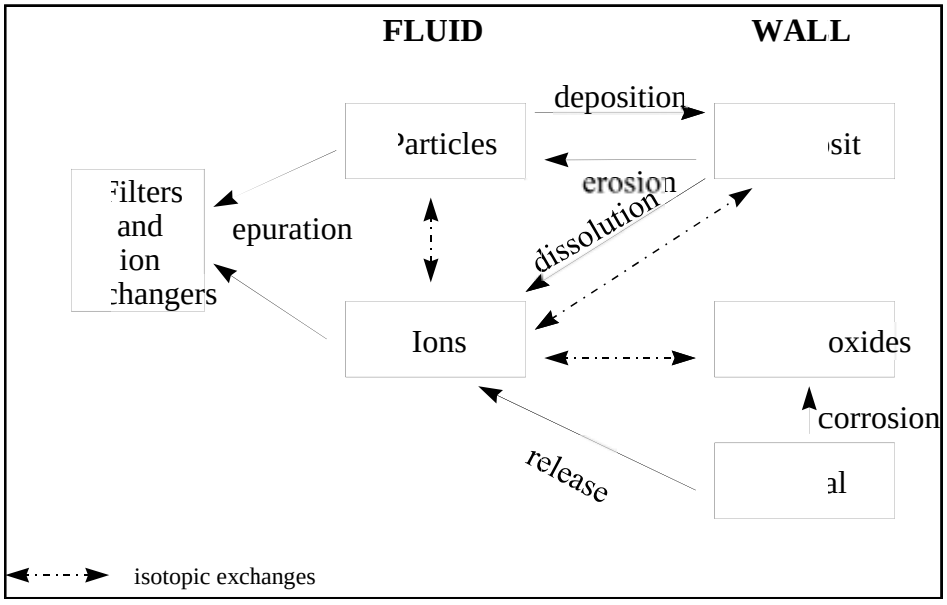

FIG. 19. PACTOLE: movement of corrosion products in PWR primary circuit.

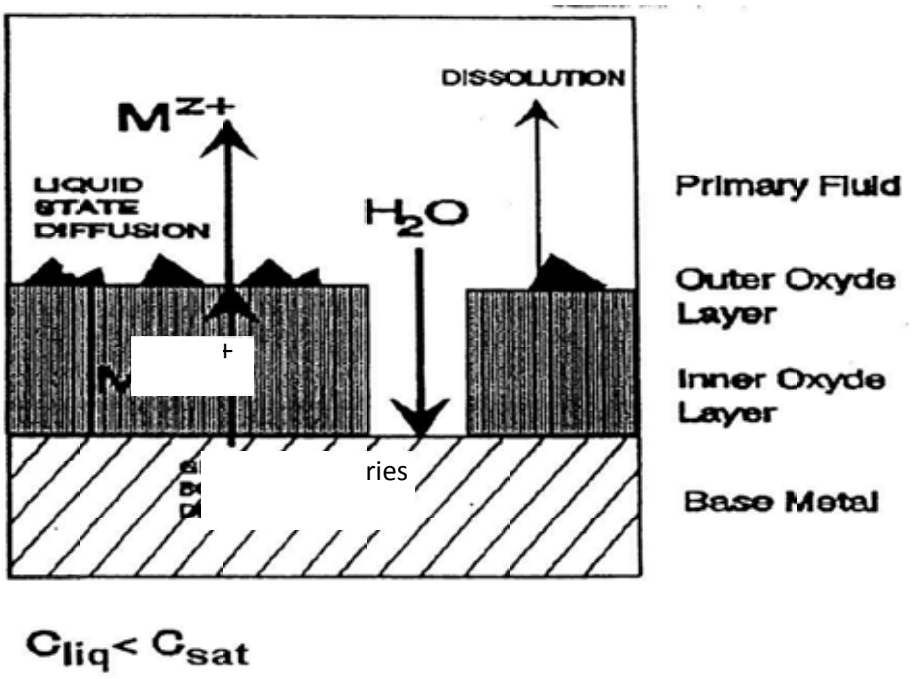

FIG. 20. PACTOLE: microscopic model of corrosion film in unsaturated coolant.

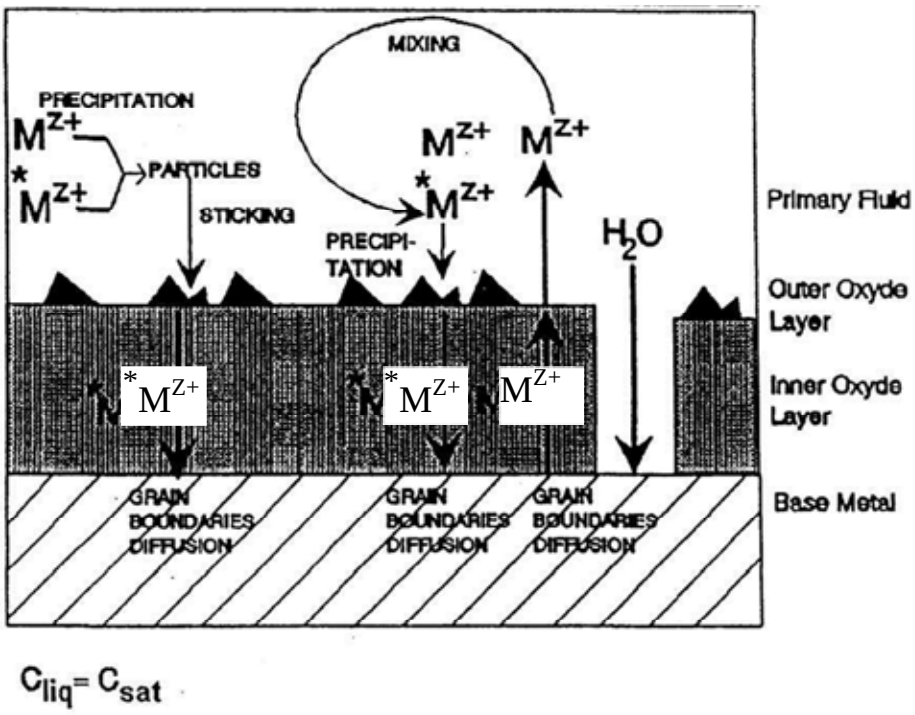

FIG. 21. PACTOLE: microscopic model of corrosion film in saturated coolant.

Detailed description of the code:

CODE NAME: PACTOLE	*Date* : July 1999
Version: V 2.2	*Development team*
The first version of PACTOLE was released in 1973. Subsequent versions have followed since then.	Division of Nuclear Measurement and Transfer Modelling Laboratory for Interactions and Transfers in Reactor Modelling. *Address*: C.E.A. Cadarache Saint Paul lez Durance 13108 cedex France Phone : (33)-4-42-25-78-09 Fax : (33)-4-42-25-77-67
OBJECTIVES: PACTOLE is a computer code developed by the Commissariat à l'Energie Atomique in cooperation with Electricité de France and Framatome for the prediction of contamination in the primary circuit of PWRs. The goal of PACTOLE is to analyze the behaviour of corrosion products, activated or not, in order to determine the activity in the fluid and the deposited activity of out-of flux surfaces.	

LANGUAGE: FORTRAN 77 *Running on* : PC – Unix workstation

Number of instructions :

Approximately 9000 lines of code (including comments)

MAIN MODELS:

Corrosion, ion release and solubility

Corrosion is the initiating process for primary circuit contamination. Metal oxidation leads to the formation of a segregate two-layer oxide. The first layer, in contact with the metal, behaves as a protective layer as far as ion transport from metal and fluid is concerned. Since corrosion occurs, this layer is initially enriched with Cr which promotes the insoluble aspect of this layer. This layer is very thin (less than 1 µm) and is of spinel type (Fe_2NiO_4). The second oxide layer, in contact with the fluid, consists of a more soluble oxide combined with deposit particles.

During the corrosion process of the alloys constituting the primary wall (part of the circuit in contact with the primary coolant), mainly SS and Inconel (nickel-based alloy used for SG tubing) or Incoloy (iron-based metal), metallic ions are released into the fluid.

Even though a small quantity of material is released to the fluid (release rate of some $mg/dm^2/month$), these products travel in the circuit and may be deposited on wall surfaces submitted to neutron flux thus being activated. The radioactive isotopes thus produced are then deposited on different parts of the circuit and are the main contributors to the dose rates.

The main assumption made in PACTOLE is that the concentration gradient, between the wall and the bulk of the fluid, acts as a driving force for the release process. It is also assumed that the concentration for each element at the wall is very close to the equilibrium concentration (solubility) in the same conditions. Release occurs when bulk concentration is lower than solubility at wall temperature condition.

Ion solubility is computed by the PACTOLE code using thermodynamic laws as a function of water chemistry (boron and lithium concentration, H_2 content) for a given temperature.

Ion precipitation, deposition, erosion

Due to ion release from the base metal and to dissolution of deposits, the ion concentration in the fluid increases. In some regions, according to the temperature gradient along the piping, the ion fluid concentration can reach or can exceed equilibrium concentration. Indeed, for given chemical conditions of the fluid, solubility depends on temperature. In other regions of low solubility values, ions will precipitate and will form oxide or metallic particles.

These particles will be submitted to turbulent and Brownian diffusion and will therefore be deposited on the wall surfaces. The gravity effect, for horizontal piping, and the thermophoresis effect are also accounted for.

Fluid turbulence acts as a limit for particle deposition as for particle size. Above a given deposit thickness, the deposited particles are re-entrained by the fluid: this corresponds to the erosion process.

Activation

Ion and solid particles are transported in different regions of the primary circuit by means of the fluid. When they reach a part of the circuit submitted to neutron flux (mainly in-core regions), they are activated. Classic nuclear reactions are accounted for in the PACTOLE code. Two radioactive

isotopes, generating 80% of the dose rate, are of major interest: ^{58}Co and ^{60}Co. They are produced by the following two nuclear reactions :

$$n + {}^{58}Ni \rightarrow {}^{58}Co + p$$

$$n + {}^{59}Co \rightarrow {}^{60}Co + \gamma$$

and have respective half-lives of 72 days and 5.3 years.

DOMAIN OF USE:

PACTOLE has been extensively used to predict the effects of reactor design (SGs material, fuel assembly grids…) and the effects of reactor operating conditions (water pH, Li content, fuel cycle duration …) on PWR contamination.

A peculiar PACTOLE version, namely PACTITER, has been also used to predict the contamination of the various heat transfer circuit of the International Thermonuclear Experimental Reactor (ITER).

VALIDATION FIELD:

The qualification of the PACTOLE code was begun 20 years ago. This qualification is done by means of comparison of PACTOLE simulated results with in-situ measurements.

KEY REFERENCES: [17], [59–63].

3.2.6. Model RADTRAN

This model was developed in Hungary in 1980s. The transport of inactive nuclides is described in Fig. 22. All elements are assumed to follow the behaviour of iron, the major component. The dissolved iron concentration equals the solubility of the metal oxide found on the surface of the piping in contact with the coolant. Several hundred hours after start-up, equilibrium is achieved and maintained throughout the fuel cycle. Once at equilibrium, metal oxide release from the corroding surfaces is solely as particles. Particles deposit on all system surfaces including the fuel cladding in the reactor core. If the coolant pH is sufficiently high, the magnetite solubility increases with temperature so that particles deposited in-core dissolve in the heated coolant and dissolved iron precipitates in the SG tubes. If the coolant pH is relatively low and the magnetite solubility declines with increased temperature, then there is precipitation in-core and dissolution of deposits out-core. There is still creation and release of particles from the corroding surfaces, however. Deposited particles are also eroded as well as dissolved. The code has only two nodes: one in-core and one out-core and they are connected by the coolant. An average dissolution driving force is calculated for one surface, and a precipitation driving force is calculated for the other node, depending on the pH, and using the surface temperatures to determine the magnetite solubility. These wall temperatures are a function of the thermo-hydraulic conditions at each node. The transport processes of radioactive nuclides are described in Fig. 23. These active nuclides are generated by irradiation of inactive elements deposited in-core and then are released by dissolution and by erosion of particles. Dissolved radionuclides are incorporated in the inner oxide layer on the corroding out-core surfaces and incorporated into the outer layer deposits forming by precipitation on either in-core or out-core surfaces, depending on the magnitude of the pH. Alternatively the outer layer gets dissolved radionuclides by incorporation into particles as the concentration of soluble inactive nuclides changes in each cycle of the coolant along the primary circuit. These particles are then carrying activity to outer layer. Allowance is made for irradiation of particles and dissolved elements suspended in the coolant as it passes through the core. In-core SS surfaces are activated and release radionuclides in the particles generated by corrosion and by dissolution of outer layer deposits if present.

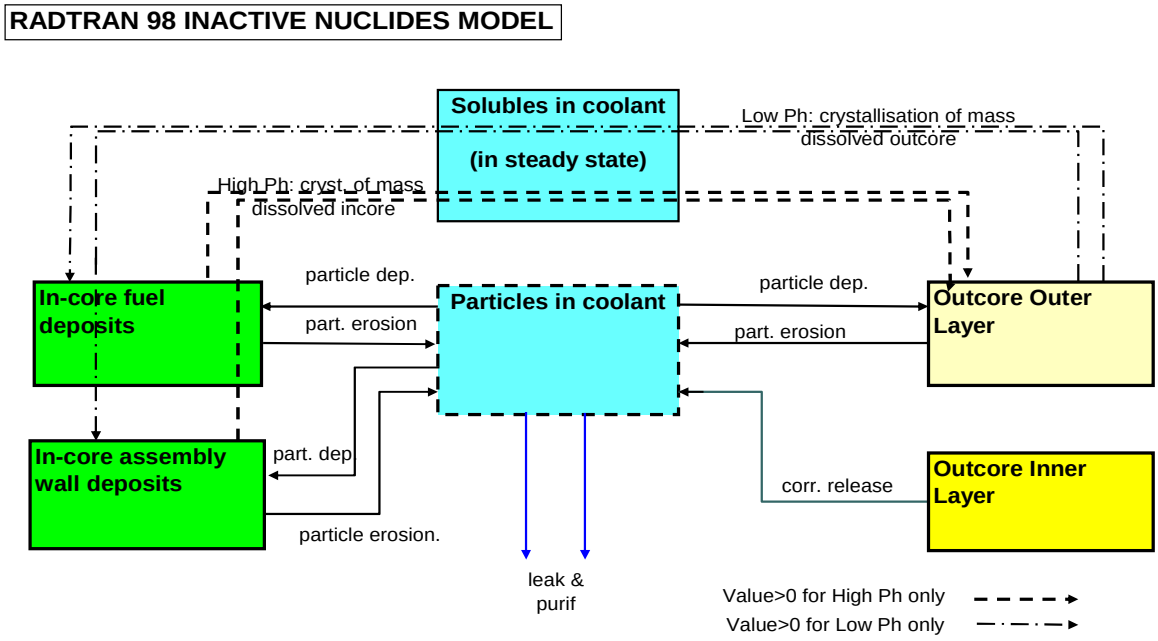

FIG. 22. RADTRAN transport processes of inactive nuclides.

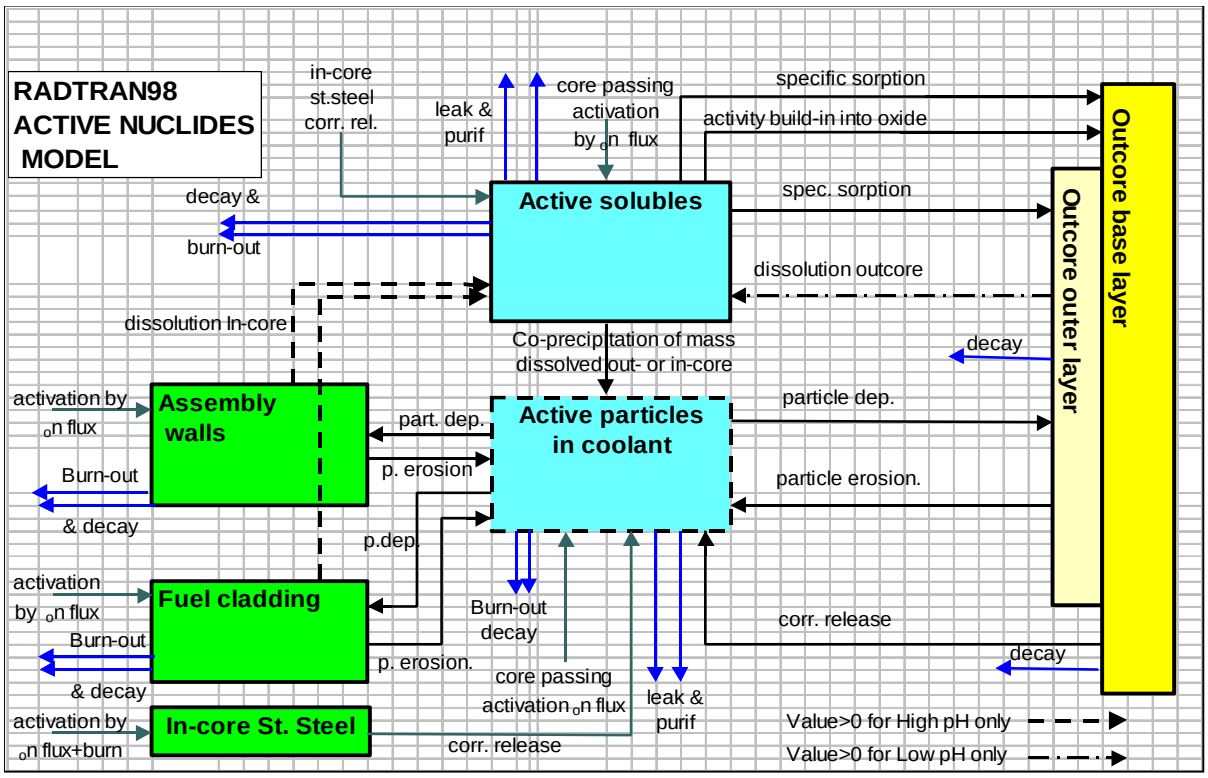

FIG. 23. RADTRAN transport processes of radioactive nuclides

Detailed description of the code:

CODE NAME: RADTRAN 98	*Date* : October 2002
Version : RadUni98 v.004	*Development team*
FIRST RELEASE: 1988.	VEIKI Institute for Electric Power Research Nuclear Power Plant Division Accident Analysis Project H-1251 Budapest Pob 80 Hungary Phone: 361-4578246 Fax:361 4578253 E-mail: h5243hor@ella.hu Contact person: Gábor L. Horváth

OBJECTIVES: Corrosion product activation, and their out-core deposition is one of the major sources of occupational radiation doses of operating and maintenance personal in NPPs. Paks Nuclear Power Plant the Hungarian Electric Utilities with VEIKI initiated research projects to find the main principles of the driving physico-chemical processes. Several years of research and plant data collection resulted in more understanding and controlling the processes. This resulted in a very favourable radiation situation in Paks plant and capability to carry out calculations aimed at predicting radiation fields by computer codes. RADTRAN98 has been designed first of all for the WWER-440 type of reactors (all SS) but using appropriate input data it can be applied to other power plants as well.

LANGUAGE : QUICK BASIC 4.5, PASCAL *Running on* : PC Pentium 300 MHz

Number of instructions :

1700 Lines

MAIN MODELS :

The RADTRAN98 calculates the corrosion product transport and activation in the primary circuits of nuclear reactors. The code treats the generation and transport of the principal isotopes (^{51}Cr, ^{54}Mn, ^{58}Co, ^{59}Fe and ^{60}Co) and gives their concentration in the primary coolant, on primary circuit in-core and out-of-core surfaces and in by-pass filters. The code handles the ^{110m}Ag specific for WWER-440s using the same corrosion driven mechanism as of the other SS corrosion products.

RADTRAN98 assumes that the solubilities in principal locations of the primary circuit are available from other codes.

The following solubilities are required:

- at average surface temperature of fuel cladding (T_4),
- at average surface temperature of assembly walls (T_3) – taken as average bulk liquid temperature in the core),
- at average surface temperature of SG heat exchange tubes (T_2),
- at liquid coolant bulk temperature at core entry (T_1).

These solubilities (based on magnetite (Fe_3O_4)) are dependent on thermo-hydraulic conditions of the primary circuit and of water chemistry conditions (H_3BO_3, $\Sigma L^+ = K^+_{ekv}$, NH_3, N_2H_4, H_2, ... etc.).

The code calculates a single nuclide at a time.

High temperature pH and Fe Solubility

Release of corrosion product nuclides is assumed to be determined by the overwhelming component (Fe) of the SS in the primary circuit. Iron is assumed to be in equilibrium with the oxide layer (assumed as magnetite (Fe_3O_4)) at the bottom of the fluid boundary layer.

The calculation procedure is based on latest works of VEIKI [64–65]. The model can take into account boric acid, ammonia and strong base. The later are considered as equivalent moles of K^+ ion (ΣK^+), and hydrazine is considered as equivalent moles of ammonia. The dissociation constant of boric acid has been calculated according to Messmer which means a set of four dissociation reactions. Ion product of water has been calculated according one of the most frequently used Marshall-Franck expression. The ion strength of the solution has been taken into account by the Debye-Hückel activity coefficients. The fugacity coefficient of hydrogen was assumed to be unity and its partial pressure in normal operating conditions was calculated Henry's law.

Equilibrium constants of Fe solubility were taken into account using Fe(II) and Fe(III) species by an extended version of Tremaine-LeBlanc model. Because of extended model and data base the coefficients in equilibrium constants were re-calculated.

Corrosion product activation

The calculation model and algorithm incorporated in to RADTRAN98 is based on references [64–65].

Actual plant chemistry data can be taken into account for activity build-up calculations. Water chemistry data are pre-calculated and introduced as Fe solubility input data, while reactor power dependent data are data are calculated in the RADTRAN98 module. Instantaneous reactor power is used to calculate the neutron flux [16]. Apart from the instantaneous flux the integrated average flux is also calculated, which is to be used for the activation of in-core SS materials under neutron flux.

Inactive nuclides

Initially clean reactor water corrodes base metal and after forming the initial oxide layer starts to dissolve the base metal and the formed oxide layer. In a few hundred hours the dissolved corrosion product concentration reaches equilibrium conditions and a steady state concentration profile will be created along the path of the coolant in the primary circuit. After this stage, further corrosion product release can be considered to occur as corrosion particles.

On the surfaces (on the boundary layer bottom where the velocity is zero), the solubility conditions are created. In the "high pH" regime the solubility increases with increasing temperature, so on the fuel cladding surface this value is higher than in the bulk of the liquid and on (cold) SG surfaces it is lower than that. In the "low pH" regime the situation is the opposite.

Released particles (mentioned above) are carried away by the high speed coolant and get deposited in the circuit surfaces. In "high pH" regime they get dissolved from the fuel cladding surface and this amount will crystallise on SG surfaces. In "Low pH" mode the opposite will happen. Particles are also subject to erosion.

Active nuclides

Activity transport builds-in into the above cycle. Active nuclides are generated on fuel cladding and assembly wall surface, get released from there by dissolution and erosion. Dissolved active nuclides are incorporated into the inner oxide layer growing on out-core surfaces and get incorporated into particles as the concentration of soluble inactive nuclides changes in each cycle of the coolant along in the primary circuit. Particles are deposited on all the surfaces. The physical processes are illustrated by the included figures below.

Numerical treatment All the differential equations can be written as in a form first order linear (or linearized) differential equations. An analytical solution can be obtained considering the coefficients to be constant. Using these solutions a stepwise analytical solution of the equation system was elaborated. The solution is obtained in a way that the first approximation of the time step end values are obtained taking the other variables constant with a value at the time step start. Than the integral average values during the time step are calculated and the calculation is repeated for all the variables using the time step average for other variables. This iteration is repeated as many times as needed to decrease the difference of the last two iterations below a certain limit (usually 10^{-6}%). In the present case this procedure is suitable because quickly changing the coolant soluble and particulate matter concentrations can be calculated accurately by analytical means, while the slowly changing surface concentrations can be corrected with the changing coolant
DOMAIN OF USE: Previous versions of RADTRAN were applied to WWER-440 at Paks site. New versions are under application to PHWR in India.
VALIDATION FIELD : Paks NPP
KEY REFERENCES: [64–65].

3.2.7. Model CANDU AT

Precipitation fouling is one of the main fouling mechanisms taking place at high temperature whenever precipitating material has inverse solubility curve with temperature. Of particular interest in CANDU plants is the solubility behaviour of magnetite, since it is found to precipitate in water chemistries, which give it both types of curves. A mathematical model to describe precipitation fouling was developed based on detailed deposit data taken from two X-3 reactor loop experiments in the NRX reactor at Chalk River Laboratories where fuel element surfaces with three different surface heat fluxes were fouled with magnetite by operation at low pH either with LiOH or with NH_3.

With this model, precipitation fouling on fuel sheaths in the conditions described above can be predicted quantitatively. Precipitation fouling on the inside of feedwater heater tubes may be described with a simple mass transfer model where supersaturation is generated in the bulk phase. The predicted deposits for the Bruce external preheater compare well with the measured values from chemical cleaning. The film model for precipitation fouling has been applied successfully to predict fouling on the secondary side of the boiling region of SG tubes in Bruce, CANDU-6 and also PWR SGs. Fig. 24 introduces a macroscopic model for dissolved iron transport in the CANDU primary circuit [66–67]. These transport diagrams are essential if models are to be simple yet accurate in describing deposition and release at system surfaces.

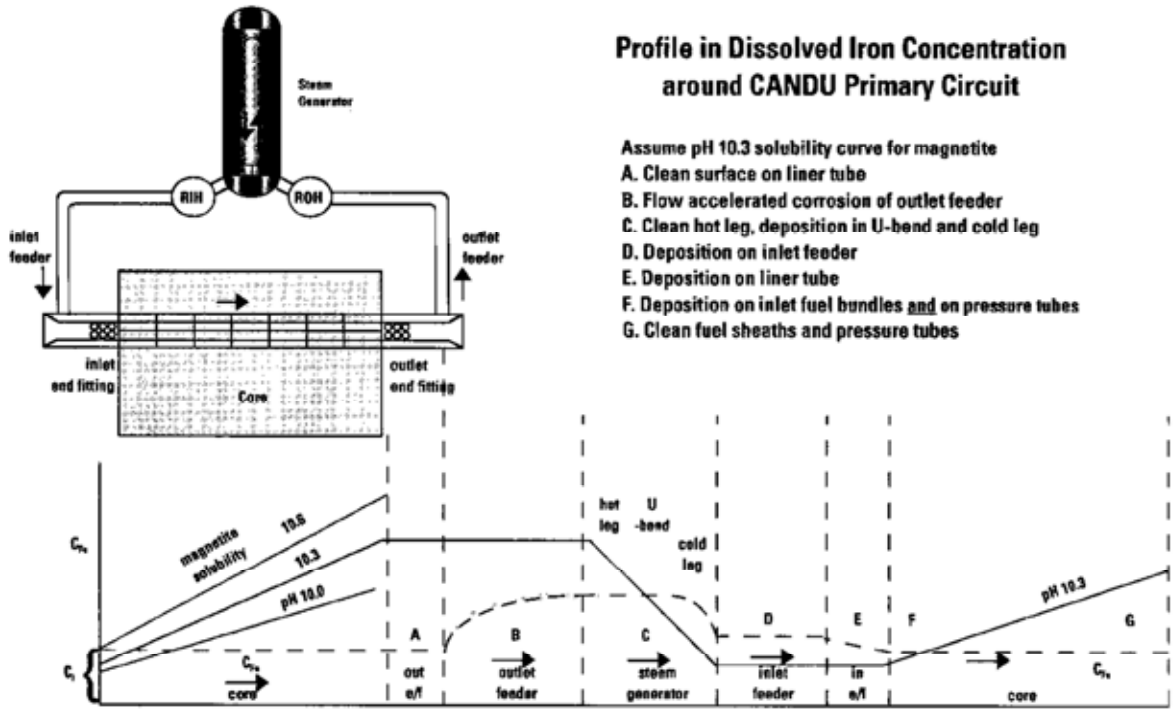

FIG. 24. CANDU macroscopic model for dissolved iron transport.

The driving force for activity transport in CANDU is particle deposition on the fuel sheath and pressure tube surfaces in-core, followed by their simultaneous activation in the neutron flux and their dissolution in the coolant which is made unsaturated in dissolved iron by heating. All chemical elements and therefore their radionuclides are assumed to follow the behaviour of the iron in deposits and in the coolant. Mass balance equations are written for iron in deposits and in the coolant at any time and any axial location in a given region and on any given surface e.g. fuel sheaths in-core. These differential equations must be solved numerically to predict release of dissolved iron from the core and therefore to predict radionuclide release rate from the deposits. Magnetite precipitation on outcore surfaces such as SG tubes, the inlet feeders and inlet end-fittings is assumed to remove radionuclides in proportion to the amount of dissolved iron being precipitated. For example if 90% of dissolved iron precipitates in the SG tubes, then 90% of the radionuclides just released from the core will be deposited there too. The distribution of newly deposited radionuclides in the SG tubes and along inlet feeder pipes and inlet end-fittings will be identical to the distribution of magnetite. Mass balances may be done at any out-core location for each radionuclide with decay taken into account to predict radionuclide surface activity, while the commercial code Microshield can be used then to convert these values to the radiation field on the outside surface.

As described above, the Canadian activity transport program has not focused on creating a single computer code which captures all current knowledge [66–67]. For example, Lister's work [68] on incorporation of radionuclides into oxide films forming on corroding surfaces would be needed to predict the radionuclide content of oxide films where magnetite is not precipitating from solution. Rather, the program has resulted in many different codes which are applied to answer questions at any given time, with simplifying assumptions as needed. For example, the incore equations are currently solved by a code in the commercial software Mathematica, and the outcore equations are described in Fortran codes such as 'FAC' for the outlet feeders, 'RIHT` for the SG tubes, and 'Feedin` for the inlet feeders and inlet endfittings. Most PWR codes assessed here cannot be used for CANDU without particle deposition/dissolution incore and magnetite precipitation out-of-core [69].

3.2.8. Russian model

Development of this model is based on experimental data from long-term corrosion tests. The obtained results allow the establishment of a correlation between the corrosion parameters (rational constant of oxidation, corrosion losses, expressed by mole·dm^{-2}) and equilibrium solubility of the corrosion products phases (C_{eq}) which is stable during the corrosion tests as shown in Fig. 25. This dependence can be expressed by the following form:

$$\Delta m - m_0 = \sqrt{K\tau}\ )$$

where

τ is the time of exposure;
n is a coefficient depending on the water chemistry conditons;
K is the coefficient n times C_{eq}.

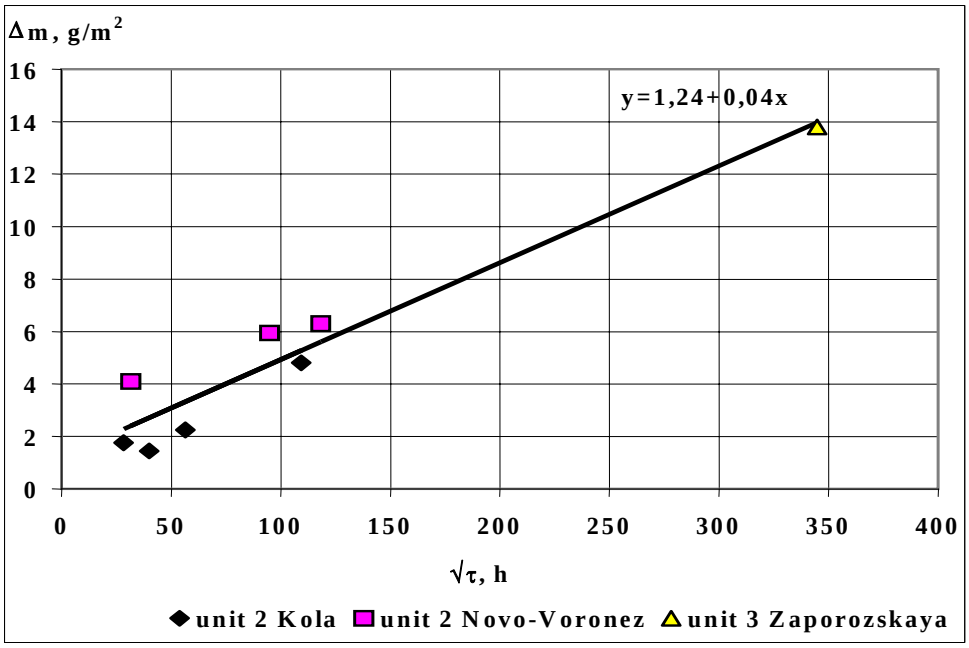

FIG. 25. Correlation between corrosion rate of SS (18Cr10Ni1Ti) under condition of WWER primary circuit (Δm=1,24+0,04√τ). The coefficient of correlation is 0.93.

This relationship generalizes practically all the corrosion and solubility data, regardless of the variety of the conditions for which they were obtained [70]. Corrosion variation in time is often described by a parabolic equation, which could be explained by the presence of surface films. The parabolic character of the corrosion dependence on time demonstrates that corrosion product diffusion through the growing oxide (for example, oxygen delivery to the reaction area or, by the analogy with steels corrosion, removal of dissolved corrosion products which are in equilibrium with the water environment) is the controlling stage of the corrosion process.

For constant corrosion product concentration in the volume and on the surface layers, and with continuous solution stirring or flowing, the corrosion process is defined by the diffusion of dissolved corrosion products, i.e. by the solubility of metal alloys forming the surface films.

$$\Delta m = \rho_{Me}\sqrt{2C_{eq}DV_o t}$$

Where
Δm is the corrosion, g·m^{-2};

ρ_{Me} is the Me density;
C_{eq} is the solubility of corrosion products of a metal alloy, mole·cm^{-3} [71];
D is the diffusion coefficient, m^2·s^{-1};
Vo is the specific mole volume of corrosion products forming the surface layer, mole·cm^{-3};
t is time in seconds.

Under WWER condition e.g. T~320°C, pH_T ~7, [H_2]~2–4 ppm and in agreement with the results of [72] the following data can be used for calculations by expressions above:

C_{eq} (Fe_3O_4) = 10^{-12} mole·cm^{-3}

D_{H2O} = ~10^{-4} cm^2·s^{-1}

V_{Fe3O4} = 10 cm^3·mole^{-1}

In the calculations, the assumption was made that the actual test time for points with t_{exp}>10000 h is about 0.7 of the calendar period (hours). Fig. 26 illustrates correlation of calculation and experimental data. The coefficient of correlation, R_m > 0.93, shows the acceptable quality of the calculation.

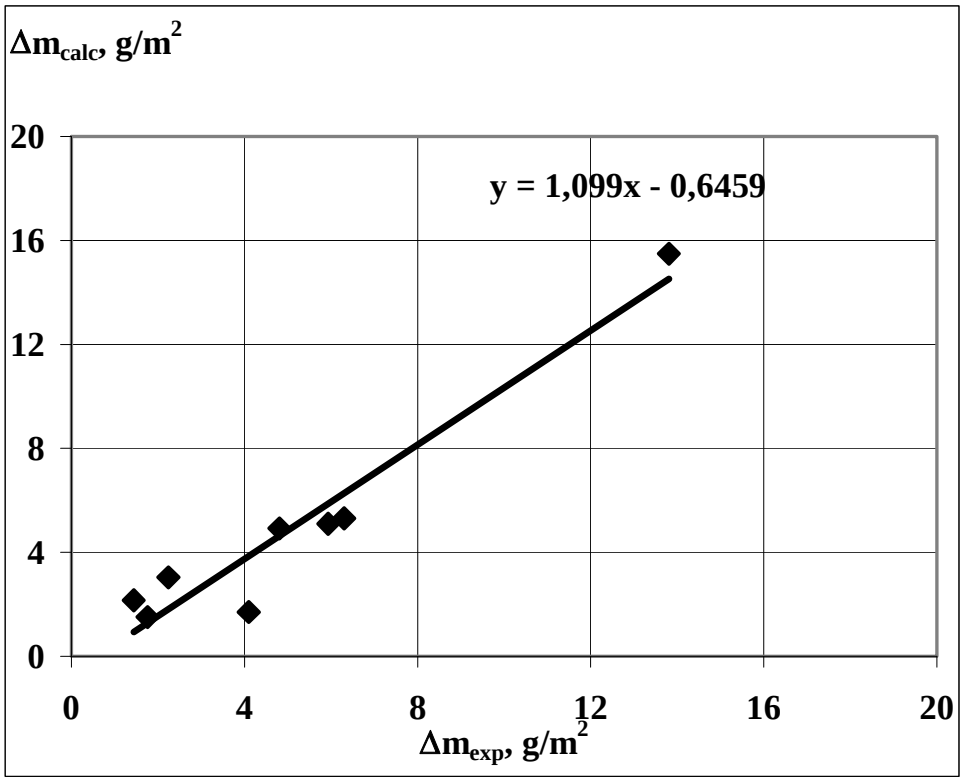

FIG. 26. Correlation between Δm_{exp} and Δm_{calc}.

In the context of a simple model of oxidation, in the case of gas-phase oxidation the form of the equation defining the amount of the metal ionized during a certain period of time turns out to be identical to that derived on the basis of the experimental dependence of the industrial metal alloys corrosion on water chemistry conditions. The term C_{eq} has a physical meaning of a thermodynamically balanced gross concentration of metal corrosion products that form the outer layer of the oxide film. The corrosion process is limited by the removal of the dissolved corrosion products through the pores of the formed film. This process is essentially the unique mechanism for industrial metal alloys under condition of water chemistry on NPPs.

3.2.8.1. Release of corrosion products

The specific weight of corrosion products passing into the water and specific weight of total products of steel corrosion formed during the same time period under the same conditions (R and K, respectively) were used as the criteria of corrosion product transfer from steel surfaces to the water. The values R and K were defined as:

$$K = \Delta m_c / S$$

$$R = \Delta m / S$$

where S is specimen surface area and Δm_c is the weight loss of the specimen due to formation of corrosion products, some of which form an oxide film and others pass into the water in the insoluble form or dissolve in it. (The value Δm_c is defined as a difference between the specimen weight in the initial conditions and one after removal of all corrosion products from the surface). The value Δm is weight loss of the specimen due to formation of corrosion products which pass into the water and is defined as a difference of Δm_c and oxide film weight (in terms of pure metal).

Calculation of the R/K ratio allows determination of the direction of processes on the metal-coolant interface. To form an absolutely stable corrosion products layer, strongly bound to the metal surface, the R/K value may be equal to zero. If the corrosion products do not form protective film and are able to pass completely into the water, then R/K = 1. If only a part of the steel corrosion products pass to the water, then $0 < R/K < 1$. And the process of corrosion products deposition from the coolant flow takes place, then $R/K < 0$. The amount of corrosion product transport changes smoothly in time and depends on the chromium content.

For the set of specimens, the relationship between corrosion and release (non-linearly dependent on time and alloying degree) may be described by linear equation:

$$R = A \cdot (K - K_0)$$

Where

R is the release during the test period ($g \cdot m^{-2}$);
K is the corrosion (ionisation of metal) during the same time period ($g \cdot m^{-2}$);
K_0 is the constant of metal content in the minimum protective film in test conditions ($g \cdot (ml)^{-1}$);
A is the constant dependent only on the type of water chemistry conditions.

The data from [15], [73], [74] and [75] on the correlation of corrosion and corrosion product release for typical values of R and K, type of water chemistry, pH, temperature, flow velocity, test duration, treatment of steel surface and steel composition (chromium) are presented in Figs 27–28.

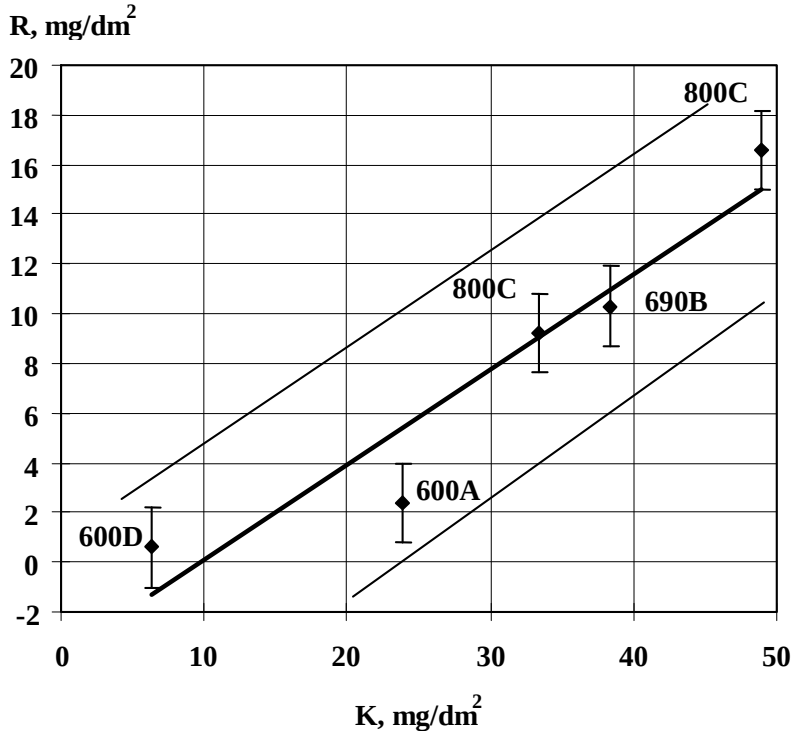

FIG. 27. Correlation between R and K for nickel base alloys 600, 690, 800. Condition of test: recirculating autoclave t_{test}~2000 h; T - 325°C; 2 ppm l, 1035 ppm B, 10–30 Cc/Vq H_2, O_2 ~ 1 ppb, pH_{300}=6.5–6.8. [15]

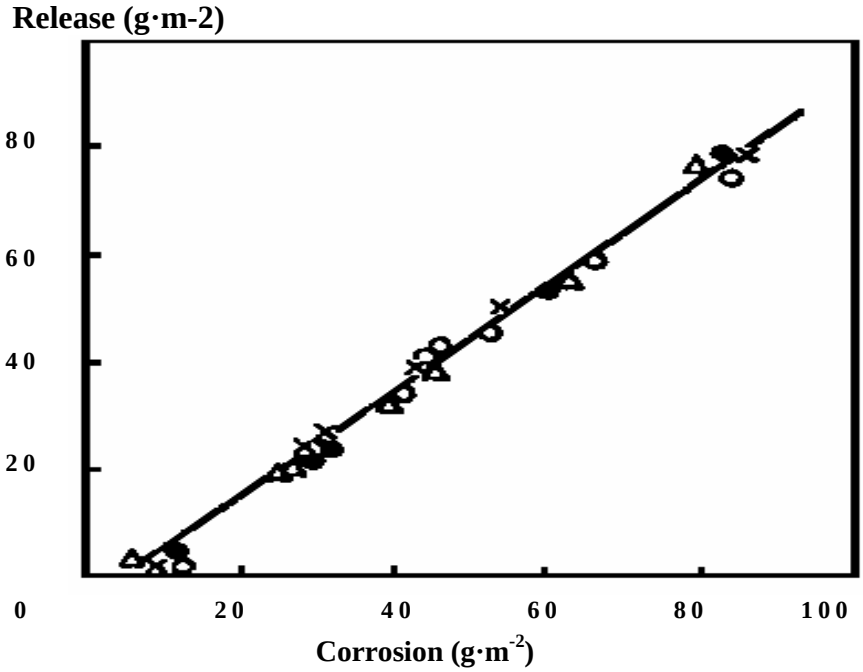

FIG. 28. Dependence of corrosion product transport on corrosion at different surface treatment: x–polishing; ○ – milling; △ – machining; ● - electropolishing. [74], [75], [76]

The presented data support the existence of a functional dependence, described above, with the coefficient, A, dependent only on the type of water chemistry conditions. This experimentally established fact was confirmed by the analysis of the data on steels corrosion under all water chemistry

conditions which can be of interest for nuclear power engineering. Values of the coefficient A are usually the following:

1. primary circuit of PWR and WWER reactors A~ 0.7±0.1
2. A << 1 corresponds to elevated oxygen levels in the primary water BWR A~ 0.2

Under the same water chemistry conditions, steels with different chromium content usually possess similar values of the coefficient, A, as shown in Fig. 29.

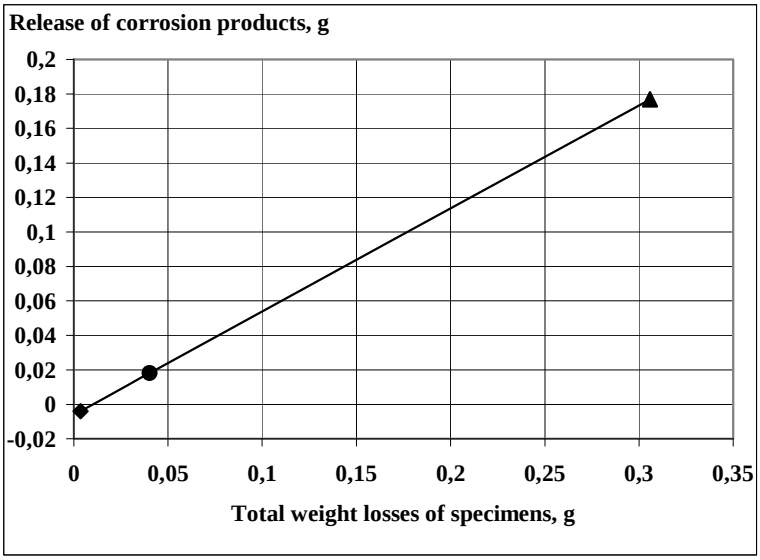

FIG. 29. Correlation between (Y) and (X) under conditions of WWER-1000. Test $\tau=1.19\times10^5$ h ♦ - SS Ch18N10T, ● - steel – 15Ch2NMFA, ▲ - steel – 10GN2MFA, $Y=A(X-X_0)$, A=0.7 X - total weight losses of specimens, g X_0 - total content of corrosion products in compact films, g. [76]

In fact, the coefficient, A, may be considered as a parameter that integrally characterizes the quality of water chemistry. This factor takes into account the set of water chemistry parameters determining the direction and rate of the processes of corrosion, mass transfer and deposition [76].

3.2.9. German approach to modelling

In Germany, a purely thermodynamic approach for modelling of corrosion product transport in water cooled reactors was applied in model development [77]. In Fig. 30 the relevant thermodynamic equilibrium between different components and phases are illustrated.

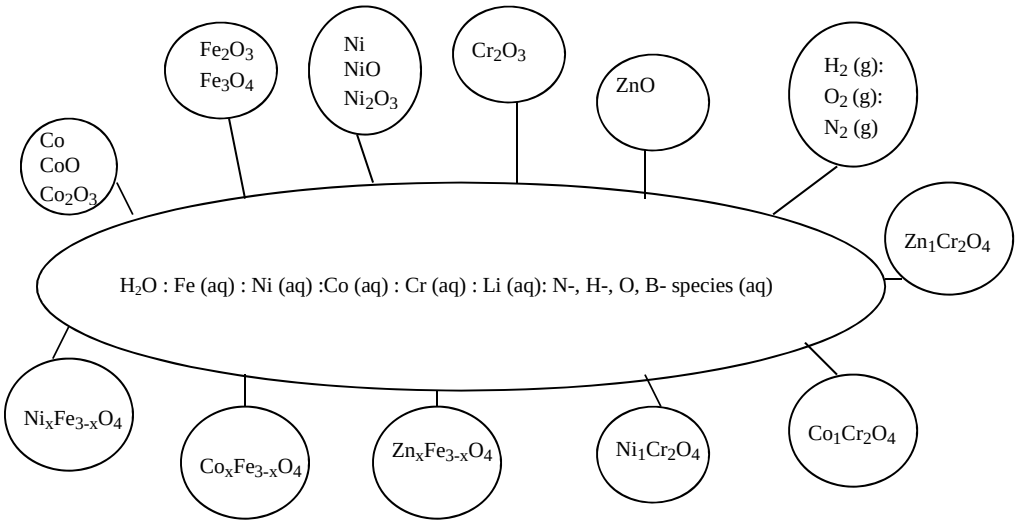

FIG. 30. Relevant multicomponent-multiphase thermodynamic equilibrium.

The aqueous phase consists of metal ions, hydrolysis species as well as the dissociated components of additives adjusting the pH and the redox potential. The model calculates equilibrium between one or more components and phases corresponding to the Gibbs phase rule. A characteristic feature of the code is the consideration of a complex spinel mixed phase. For this purpose the metal cations are arranged in separate sublattices. As a consequence only divalent or trivalent cations can be mixed amongst each other. The calculation routine is based on a Gibbs energy minimisation which can be expressed by one fundamental equation:

$$G_{sys} = \sum_i n_i \cdot G_i \rightarrow \min$$

The minimization procedure is performed with the commercial Gibbs-Energy minimizer, ChemSage [78]. In all mixed phases the mixing free energy is considered. Additionally, in the spinel mixed phase an excess term was included based on the approach by Redlich and Kister [79].

$$G_{spinel}^{excess} = Y_{C_b} \cdot Y_{C_i} \cdot \sum_{i=1}^{n} (Y_{C_i} - Y_{C_C})^{n-1} \cdot L_n(T)$$

The excess energy coefficients $L_n[T]$ were derived from solubilities of various non-stoichiometric nickel ferrites measured in high temperature water by Kunig and Sandler [80–81].

The primary circuit has been nodalised in four nodes corresponding to the core area and one node representing the SG as is shown in Fig. 31.

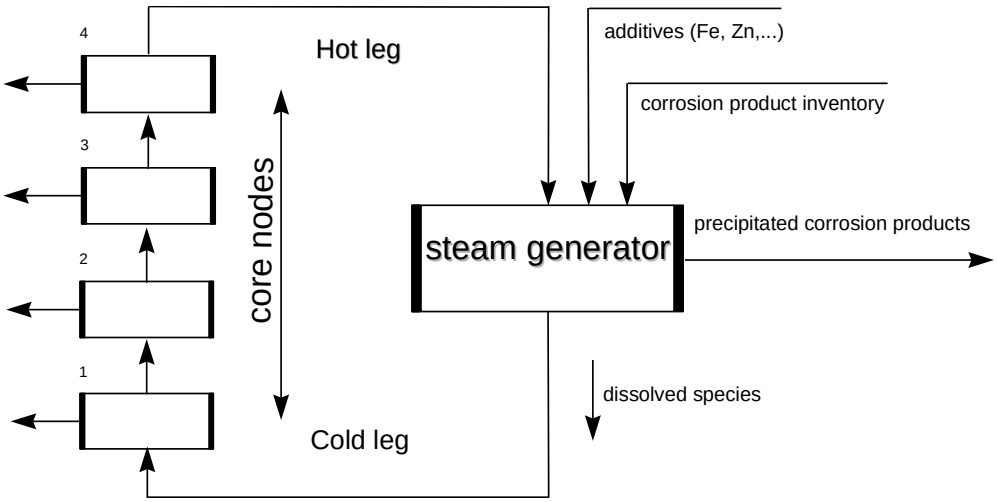

FIG. 31. Nodalisation of the primary circuit of a PWR.

The corrosion product inventories as well as the chemicals adjusting the pH and the redox potential value are used as input in the SG node. After calculation of the thermodynamic equilibrium the dissolved corrosion product species are fed into the next node. The calculation is performed until the deviations become small.

The output results of such a calculation are:

- concentration profile of dissolved corrosion products in the primary circuit.
- structure and composition of deposits at thermodynamic equilibrium.
- prediction of corrosion product transport in dependence of cycle chemistry.
- assessment of the influence of additives (Fe, Zn) on the activity build-up.

The model was used for the calculation of solubility of various oxide layer compositions measured in a Siemens designed PWR are outlined and compared with Siemens plant data [82]. Results are shown in Fig. 32. The best agreement to plant data is obtained with the solubility calculated from chromium rich spinel oxides. This characteristic spinel oxide was taken for further calculations.

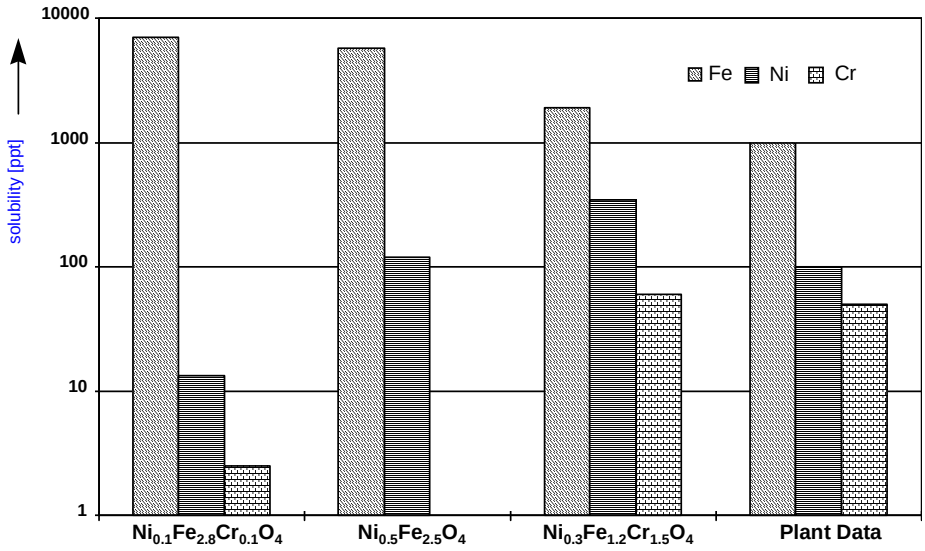

FIG. 32. Calculated solubility of various oxide layer compositions.

In Fig. 33 the concentration profile of dissolved corrosion products over the core height is shown. As is can be seen all the solubilities decrease over the core height. It seems that the core acts as a filter for dissolved corrosion products.

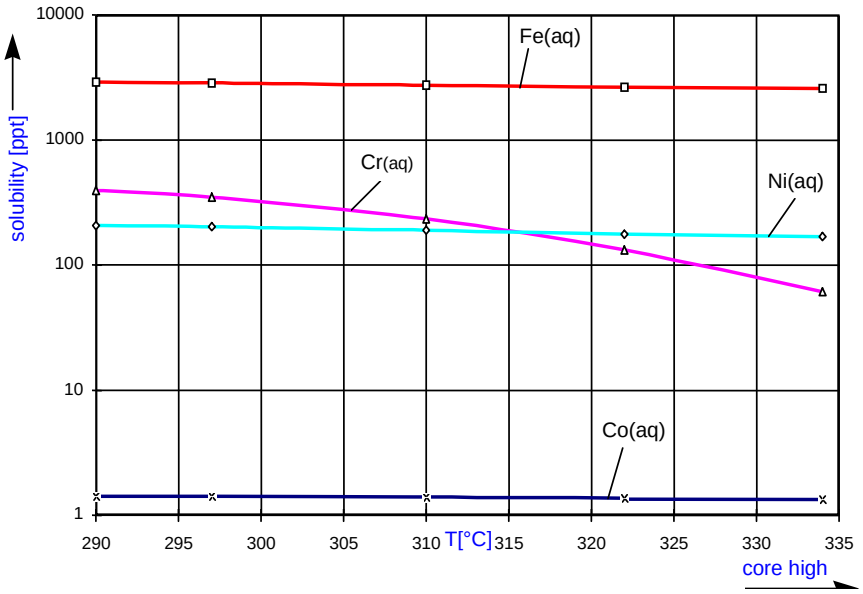

FIG. 33. Calculated concentration of corrosion products over the core at the end of cycle.

This fact could be a key factor for the precipitation-dissolution behaviour of corrosion products out-of-core. It can be supposed that the coolant is under-saturated after passing the core. As a result, the probability of dissolution processes at the hot leg (HL) is small. Whilst the coolant is streaming through the SGs it will become saturated or over-saturated. The affinity is raised for precipitation of corrosion products at the cold leg (CL).

In Fig. 34, the solubility of the characteristic oxide is illustrated as a function of $pH_{(300)}$. The plot for iron concentration is distinguished by a minimum at $pH_{(300)}$ = 7.0 whereas the nickel and the cobalt concentration decrease with increasing $pH_{(300)}$. The chromium concentration increases in the pH-range from 6.9–7.4. These values of calculated solubilities are in good agreement with measured dissolved corrosion product concentrations.

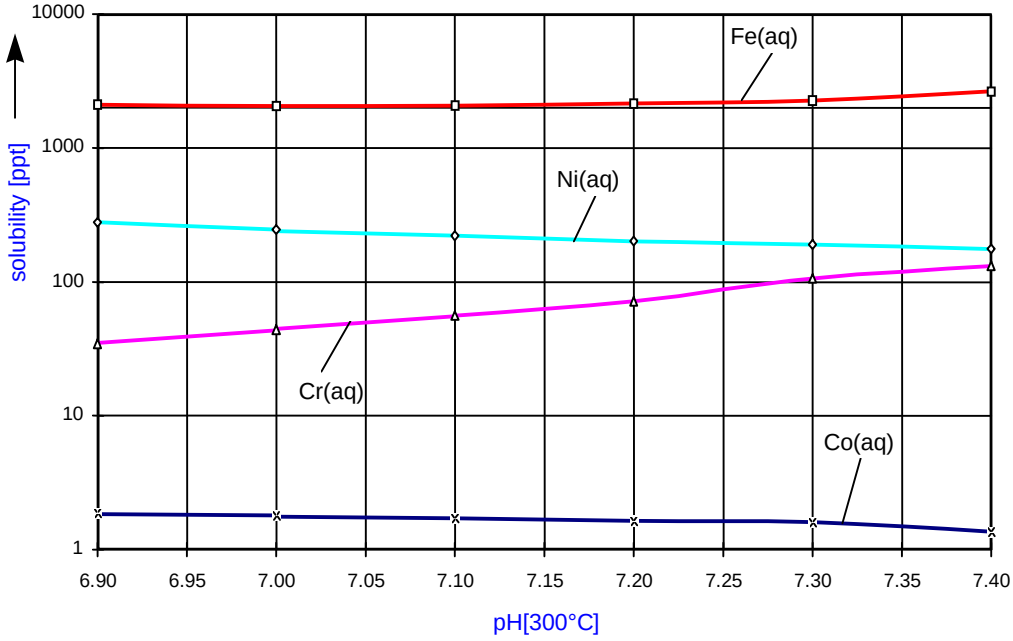

FIG. 34. Calculated solubility of corrosion products in dependence of $pH_{(300)}$.

In Fig. 35, trends of measured and calculated values of crud distribution over the core are shown. The calculated values are based on the assumption of a constant oxide layer thickness over the core height.

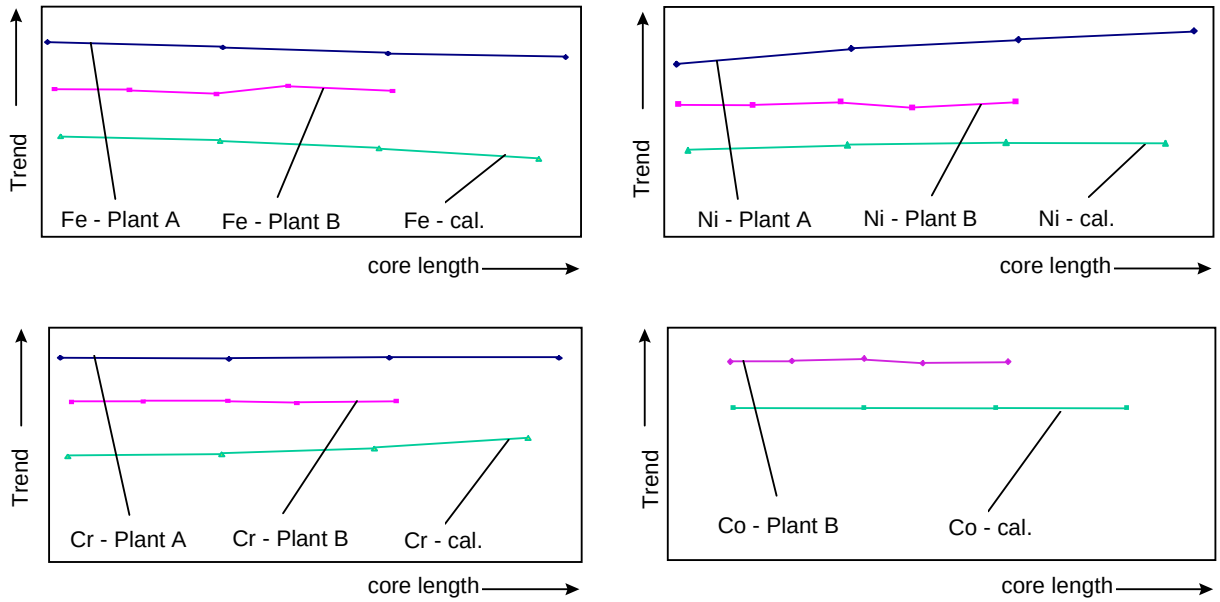

FIG. 35. Comparison between measured and calculated values of crud distribution over the core.

As can be seen, a good agreement between the measured and calculated data for the trends in iron and nickel was achieved. A clear trend for cobalt and chromium distributions cannot be seen because the very small values of measured deposits in the fuel crud.

Fig. 36 displays comparison of the measured and calculated crud composition.

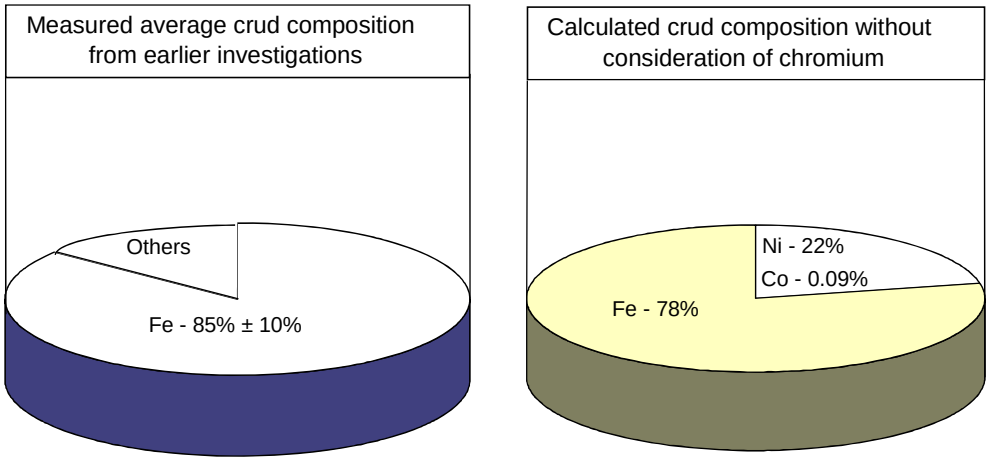

FIG. 36. Comparison between measured and calculated crud composition.

Earlier investigations of fuel deposits resulted in about 85% of iron in the form of magnetite. In model calculations also, chromium was transported into the core area. If this fact is neglected, the agreement to measured crud composition is quite good.

Possible reasons explaining the behaviour of chromium transport include:

- the kinetic restriction of chromium dissolution and transport.
- the chromium dissolution during shut down.
- the quality of thermodynamic data of chromium species.

Future work will be devoted to a better understanding of corrosion product transport through the inclusion of plant start-up and shut-down procedures and the validation of the dissolved chromium species.

3.2.10. American approach of combined use of deterministic model and neural networks.

A model has been developed for predicting mass and activity transport in the primary coolant circuits of PWRs and WWERs with the objective of demonstrating and quantifying the importance of the electrochemical corrosion potential (ECP) in determining the impact of both processes on reactor operation [83]. The model initially employs a radiolysis/mixed potential code to calculate the ECP at four locations (core, HL, SG, CL) and the ECP is then used to estimate the local magnetite solubility. The solubility is then averaged around the loop to yield the "background" solubility. Comparison of the background solubility with the local solubility determines whether precipitation or dissolution will occur at any given point in the circuit under any given set of conditions. It is further assumed that the concentration of ^{59}Co in the coolant is given by the isotopic fraction of this species compared with iron averaged over all materials and weighted by the respective wetted areas. Activation of ^{59}Co to ^{60}Co is assumed to occur in the coolant phase by fast, epithermal, and thermal neutron capture. The calculated activity is then used to train an artificial neural network (ANN) to establish relationships between activity at any given location and the operating properties of the reactor, including coolant pH, ECP, temperature, power level, etc. The model predicts that during shut down, magnetite (and hence ^{59}Co) migrates to the core, where it is irradiated and activated, particularly during subsequent start-up. During start-up, the magnetite (and hence ^{60}Co) migrates from the core to out-of-core surfaces where it establishes the radiation fields.

The goal of work was to develop a model for mass and activity transport that is *electrochemically* realistic, noting that previous models have emphasized mass transport and thermal hydraulic factors. While these factors are obviously important, there is a thesis assumed that no model can successfully account for activity transport in PWR primary circuits without recognizing the important (and possibly dominant) role played by electrochemistry. The importance of electrochemical factors was demonstrated many years ago by Lister and co-workers, [84–87], in loop experiments and at the fundamental level by Macdonald and Owen [88] in their work on the electrochemistry of iron in high temperature aqueous solutions. For example, Lister et al demonstrated that the rate of pickup of radioactive species on a carbon steel surface depended upon the potential of the metal with respect to a reference electrode. Importantly, the rate of incorporation of ^{60}Co into the surface was enhanced by shifting the potential in the negative or positive direction from the open circuit value. Enhancement by negative polarization was attributed to the plating of cobalt onto the surface while that by positive polarization can be attributed to the formation of the magnetite carrier. This latter postulate is consistent with the work of Macdonald and Owen [88], who demonstrated that the formation of the outer layer of the passive film on iron in contact with alkaline solution was an anodic electro crystallization process. Since the initial work, [88–93], electrochemical factors have been incorporated into models in an ad hoc fashion, which is never satisfactory from a modelling viewpoint. It is the *ad hoc* nature of inclusion of electrochemical effects that the present model seeks to overcome.

3.2.10.1. Activity transport model

Because the incorporation and release of ^{60}Co into/out of the outer layer is an electrochemical process, the electrochemical potential is postulated to play an important role in the dynamics of distribution of

radioactive cobalt around the primary circuit. Noting that the ECP depends strongly upon the temperature, the relative concentrations of hydrogen and of oxidizing species produced by the radiolysis of water, which in turn depend on the power level of the reactor and water chemistry of the coolant, it is evident that the operating conditions for the reactor can (and do) have a major impact on the build-up of radiation fields in out-of-core components. In the present work, we have used a radiolysis model coupled with a mixed potential model and an equilibrium chemistry model to calculate the ECP and pH at four points in the primary coolant [89–90]. These points are in the core, the HL, the SG, and the cold leg. Average properties were employed for each region in this study, simply because we were interested in exploring only the gross activity transport phenomena. The radiolysis/ECP model employed has the capability of performing calculations at closely spaced points (centimetres apart) around the entire circuit, in order to estimate the ECP and pH, so that detailed ECP maps of the coolant circuit may be generated with the present software. In any event, once the ECP is calculated, and since the temperature and pH are known (sometime only the water chemistry and not the pH is known, in this case the model can be used to calculate the pH), we calculate the local concentrations of dissolved iron species by assuming that the dissolution and precipitation of magnetite occurs under quasi-equilibrium control. Noting that the iron species are transported by convection around the circuit, and that the fluid is highly turbulent, the concentrations of the Fe(II) and Fe(III) species, and hence the solubility of magnetite, become "homogenized" to produce values that are averaged over the four locations. If the average solubility is found to be greater than the local solubility of magnetite then precipitation is deemed to occur at a rate that is proportional to the difference. On the other hand, if the coolant iron concentration is calculated to be less than that dictated by the local magnetite solubility, dissolution occurs at a rate that is again proportional to the difference. ^{59}Co is assumed to be released upon dissolution of magnetite at the magnetite dissolution rate, but weighted by the fraction of this species in the steels (including SSs, nickel-base alloys, and hard facing alloys, such as Stellite) and the wetted area for each alloy. Data for these factors were supplied in the frame of this IAEA CRP.

3.2.10.2. Reaction model

The radiolysis/ECP model (PWR_ECP) that was used to calculate the concentrations of water radiolysis species, and hence used to estimate the ECP, is similar in form to the models (e.g., RADIOCHEM) that was previously developed for modelling the electrochemistry of the primary circuits of BWRs, [90–96]. Values for the pH at the operating temperature or/and room temperature, water chemistry, temperature, power, water conductivity, and hydrogen level over several operating cycles of the reactor, along with the reactor hydrodynamic characteristics, wet surface areas for each alloy, and alloy composition data for both PWR and WWER reactors were supplied within this IAEA CRP.

3.2.10.3. Use of ANN

As noted above, an ANN was developed to establish relationships between the concentration of magnetite at the four points of interest and various properties of the reactor primary coolant, using the calculated concentration of magnetite as the target function. The inputs to the ANN were daily data for the time, reactor power level, pH_T, temperature, hydrogen concentration, water conductivity, and ECP at four points in the primary coolant circuit (core, HL, SG, and CL) of a WWER. Once the net had been trained to imitate the magnetite concentration (solubility) in the coolant, the net was then used to predict magnetite solubility for a different reactor type (PWR), and hence to predict the local excess solubility. The specific radiation activity is then calculated following the procedures outlined above. It is important to notice that the ANN was not a necessary tool, because there were the means of deterministically calculating the solubility of magnetite in the primary coolant (reaction model above). However, the ANN is used as a means greatly enhancing the speed of the magnetite dissolution/precipitation calculations, particularly when a large number of locations are considered. It must be noted also that if measured activities versus location data are available, the activity data could be used to train the net.

An ANN is a pattern recognition technique that mimics the brain of a living organism by simulating the neurons and dendrites (interconnections) and their physiological operations. As in the case of a brain, an ANN is first trained to perform a task and is then used to make predictions (testing phase). There are two types of learning: with supervision and without supervision. When an ANN learns in a supervised manner, both inputs and outputs are shown to the net and the weights of the dendrites are adjusted, so as to minimize the difference between the predicted answer and the known result. However, during the "testing" phase, only the input is provided to the net with the "answer" providing the desired prediction. The ANN employed in the present work was designed to be trained in a supervised manner, i.e., the ANN "learned" the relevant relationships between magnetite solubility (and hence extents of sub saturation and super saturation) and the important chemistry parameters (pH, hydrogen concentration, water conductivity, temperature, and ECP), and reactor operation mode (power, time). As noted above, the net was trained using calculated magnetite solubility in a WWER, and tested using the input parameters of a PWR. Thus, once the net was trained, the day-to-day operational and water chemistry parameters of an actual plant were used as input to the ANN, and the ANN estimated the concentrations of the different iron species considered as well as the total solubility, the extent of sub saturation or super saturation, and the direction of transport. The latter was estimated by comparing the calculated solubility of magnetite for the reactor core and the SG.

It is important to emphasize that the ANN was used only to demonstrate the concept that if input (plant data) and outputs (calculated ^{60}Co activity, in our example) are available, the ANN can effectively mimic and generalize the response on the activity to changes in plant operating conditions. No restrictions exist in extending the model to other radioactive atoms, nor to using measured activity instead to calculated activity to train the net. Also, the net should be readily adaptable to other reactor types (e.g., BWRs).

3.2.11. Indian model

The computer code ANUCRUD was developed for the purpose of predicting the time dependent concentration of active as well as non-active forms of the corrosion products in the coolant and on the walls [97]. The control volume approach is adopted for which the code needs the PHT system to be adequately discretized into a number of sequentially connected volume segments in a closed loop. The discretization of the PHT circuit into several segments will be done by the user depending upon the variations in respect of materials of construction and the steady state operational parameters such as coolant flow velocity and temperature, neutron flux (for activation of deposited corrosion products), etc. The thermal-hydraulic module of the code ANUCRUD performs the calculations for the various segments of the PHT circuit for steady state as well as transient reactor operation to arrive at various parameters such as coolant mass flow rate through a segment, coolant velocity, coolant temperature, wall temperature etc.

The multiple species' mass conservation equations are built so as to include the rates of various processes which contribute to the transport mechanisms of corrosion products and the activity products. These are:

- corrosion rates of different construction materials used for the PHT system components,
- release of corrosion product species from wall to the coolant both in particulate and soluble form,
- redeposition of the species from the coolant on the in-core surface and their activation,
- re-release of the activated species from the in-core surfaces to the coolant and their further transport into the PHT circuit and re-deposition on the out-of-core surfaces.

Some simplifying assumptions in the model are as follows:

- The concentration of particular parent nuclide in the pipe and other component materials is input to the code and is based on the knowledge of its abundance in given materials. This value is assumed to be the same for the corrosion products formed.
- The purification circuit is not modelled in the code. Instead, only the values of time dependent purification flow rate and efficiency are input to the code to calculate the species concentration in the coolant returning back from the purification loop.
- The influence of particle sizes and/or size distribution on deposition and other particulate mechanisms is not accounted in the code.

To start with, the empirical rate equations for corrosion and release rates for different materials in the code are used. For considering solubility effects, the temperature versus solubility can be fed into the code in tabular form. The modular approach adopted in the code allows further improvements from the present empirical to semi-empirical or mechanistic approach in the future.

The method was tested by performing the calculations to obtain oxide thickness growth as function of time. Based on the results obtained, the code in general appears to under-predict deposit thickness by a factor between 2 and 3 for isothermal carbon steel surfaces and by a factor 1.5–2.0 for Monel-400 surfaces. Individual models have been tested and full integration is underway.

4. DATA DESCRIPTION

4.1. Description of the input data

Models benchmarking has been done as a blind exercise on real operating units. The following reactor units provided set of input data for models benchmarking (Table 2):

TABLE 2. SOURCES OF DATA FOR BENCHMARKING

Unit name	Country	Reactor type	Thermal power
CRUAS-1	France	PWR	2775 MW
GKN-2	Germany	PWR	3850 MW
LOVIISA-1	Finland	WWER	1375 MW
EBO-1	Slovakia	WWER	1375 MW
Pickering A	Canada	CANDU	1744 MW
Darlington-2	Canada	CANDU	2064 MW

Each unit provided input data according to following specification:

- General and construction parameters (layout, surfaces, materials composition) for
    - Pressure vessel and internals
    - Primary circulating circuit
    - SGs
    - Core
    - Fuel assembly
- Operating parameters
    - Temperature
    - Pressure
    - Flow-rate
    - Neutron flux distribution in the core
- Operating cycles information
    - Effective full power days
    - Power and temperature
    - Water chemistry
    - Purification rate
    - Fraction of fuel reloaded
    - Shutdown chemistry

Using these input data, modellers have calculated surface activities to be compared with real measurements results.

The first unit of CRUAS NPP, (CRUAS 1), was selected for this benchmark on corrosion product behaviour. CRUAS is a French PWR with nominal power of 900 MWe. Its primary circuit is composed of three individual loops with SG tube bundles made of Inconel 600 (71 wt% of nickel) with thermal

treatment. The shutdown of the first cycle of CRUAS 1 was operated in April 1985. The main characteristics of the CRUAS 1 history were: a changing mode of operation for water chemistry, and a replacement of Inconel core grids by zircoloy grids. In cycles 1, 2 and 3 CRUAS-1 operated with water chemical conditions leading to a $pH_{(300)}$ of 7.0. Actually, the $pH_{(300)}$ was equal to 7.0 during the first part of these cycles, and increased to a value of 7.5 by the end of each cycle due to the fact that lithium content was specified to be equal to 0.6 ppm. After the 4th cycle, CRUAS-1 operated with chemical conditions which were aimed to reduce the contamination caused by corrosion products. These chemical conditions led to a $pH_{(300)}$ of 7.2. Nevertheless, the lithium concentration cannot exceed 2.2 ppm which gives a $pH_{(300)}$ lower than 7.2 in the earlier phase of the cycle. From cycle 1 to cycle 5 the fuel grids were made of Inconel 718 (70.5 wt% of nickel). In order to reduce the contamination due to the presence of nickel (activated to ^{58}Co), the Inconel core grids were replaced by zircoloy grids. For the 7th cycle, 77 grids were Inconel while 80 grids were manufactured from zircoloy (Zr4).

Units LOVIISA-1 and EBO-1 were selected as two units with WWER primary chemistry based on ammonia/potassium. These units differ slightly in structural materials and in the operating chemistry. Also here, fuel grids originally made of SS were replaced by ZrNb alloy during later operational periods. A special case to be considered is the operation of EBO-1 in the 20th cycle with long criticality standby at the beginning of cycle with relatively low $pH_{(300)}$ through this period.

4.2. Description of the output data

As output data following categories were provided by participating plants:

CRUAS-1

- Deposited activity average values for Fe and Mn isotopes
- Deposited activity for ^{58}Co and ^{60}Co
- Dose rates in SGs and primary piping

GKN-II

- Activity measurement of deposit and dose rates
- Water elemental analysis including shutdown period

LOVIISA-1

- Database of dose rates measurements in SG collectors of LOVIISA-1
- SG surface activities for all isotopes:
- SG collector surface activities ^{58}Co and ^{60}Co (hot & CL)
- Dose rates level in primary circuit loop hot and CLs

EBO-l

- SG collector dose rates
- Corrosion product activities in primary coolant
- Primary piping hot and CL dose rates
- Primary piping hot and CL surface activities of Co, Mn, Fe isotopes

PICKERING A

- Elemental analysis of deposits
- Activity measurement of deposit

These output data were used to verify results of surface activity calculation made by CRP participants.

5. RESULTS OF CALCULATON

The sequence of work in the blind bench-marking exercise is first described. The participants provided design data on various PWRs and the modellers set up their codes with these design data. Plant operating data for water chemistry and fuel cycle times were also inputs to the code. Then the codes were run to mimic the plant operation and predict the radioactive contamination of the coolant and various system surfaces. The results are summarized in Table 3. Subsections of this Section compare the predictions with ^{58}Co and ^{60}Co contamination data for the hot and CLs at the end of selected fuel cycles. These data were withheld from the modellers and the comparisons given here were first made at the third participants meeting in Buenos Aires. Reasons for any obvious deviations of the individual codes from plant contamination data should then be sought by the modellers to improve the accuracy of their codes.

5.1. Comparison of predicted with observed plant contamination data for each code

Most of the modelling results have been provided in the agreed protocol devised by the consultants group. A graphical presentation showing predicted versus measured contamination for all the cycles of a particular plant, e.g. CRUAS-1, was prepared by most of the modellers. These graphs show at a glance the degree of agreement between data and prediction. Further work could be done to summarize the results of the various codes, for example, some measure of the correlation coefficient between the data and predictions for each plant for each code would allow a single number to take the place of the whole graph. However, trends in prediction are important and these would be lost in a single number and the full data are presented.

Each of the code predictions are presented and discussed in the same order as they were described in Section 3.

TABLE 3. SUMMARIZED RESULTS OF MODELING

Plant	Region	Nuclide	Time	Unit	PACTOLE	CRUDTRAN	RADTRAN	DISER	MIGA RT	ACE
CRUAS 1	HL	^{58}Co	1st outage	GBq·m^{-2}	10					3.5
			7th outage	GBq·m^{-2}	7			2		4.2
		^{60}Co	1st outage	GBq·m^{-2}	1					0.16
			7th outage	GBq·m^{-2}	5			0.3		1.1
	CL	^{58}Co	1st outage	GBq·m^{-2}	14					7.3
			7th outage	GBq·m^{-2}	6			2		8.7
		^{60}Co	1st outage	GBq·m^{-2}	2					0.5
			7th outage	GBq·m^{-2}	4			0.3		2.6
	SG	^{58}Co	1st outage	GBq·m^{-2}	3.5	1.25				0.87
			7th outage	GBq·m^{-2}	3.5	1.5		2		0.97
		^{60}Co	1st outage	GBq·m^{-2}	0.4	0.2				0.073
			7th outage	GBq·m^{-2}	2.5	1.5		0.3		0.4
	SG	crud	7th outage	g·m^{-2}		11				
	Fuel	crud	7th outage	g·m^{-2}		1.5				
	Activity	^{58}Co	1st to 7th	Bq·g^{-1}				1–6		0.5
		^{60}Co	1st to 7th	Bq·g^{-1}				0.01–0.05		0.04
GKN 2	HL	^{58}Co	1st outage	GBq·m^{-2}	1					1.7
			4th outage	GBq·m^{-2}	1.6			1		2.4
		^{60}Co	1st outage	GBq·m^{-2}	0.2					0.19
			4th outage	GBq·m^{-2}	0.9			0.3		0.93
	CL	^{58}Co	1st outage	GBq·m^{-2}	2.7					3.6
			4th outage	GBq·m^{-2}	2.3			1		5
		^{60}Co	1st outage	GBq·m^{-2}	0.8					0.55
			4th outage	GBq·m^{-2}	2.7			0.3		2.5
	SG	^{58}Co	1st outage	GBq·m^{-2}		1.1				0.48
			4th outage	GBq·m^{-2}		2.3		1		0.63
		^{60}Co	1st outage	GBq·m^{-2}		0.35				0.11
			4th outage	GBq·m^{-2}		2.5	4.5	0.3		0.49
	Activity	^{58}Co	1st to 4th	Bq·g^{-1}				0.7–4		0.2
		^{60}Co	1st to 4th	Bq·g^{-1}				0.01–0.05		0.08
	SG	crud	4th outage	g·m^{-2}		7				
	Fuel	crud	4th outage	g·m^{-2}		1.5				
	Activity	^{58}Co	1st to 4th	Bq·g^{-1}						
		^{60}Co	1st to 4th	Bq·g^{-1}						

TABLE 3. SUMMARIZED RESULTS OF MODELING (cont.)

Plant	Region	Nuclide	Time	Unit	PACTOLE	CRUDTRAN	RADTRAN	DISER	MIGA RT	ACE
EBO 1	HL	^{58}Co	1st outage	GBq·m^{-2}						0.4
			16th outage	GBq·m^{-2}				0.7	0.78	0.71
		^{60}Co	1st outage	GBq·m^{-2}						0.1
			16th outage	GBq·m^{-2}				0.3	0.35	1.4
	CL	^{58}Co	1st outage	GBq·m^{-2}						0.54
			16th outage	GBq·m^{-2}				0.7	0.41	0.96
		^{60}Co	1st outage	GBq·m^{-2}						0.14
			16th outage	GBq·m^{-2}				0.3	0.15	2
	SG	^{58}Co	1st outage	GBq·m^{-2}						0.048
			16th outage	GBq·m^{-2}				0.7	0.34	0.085
		^{60}Co	1st outage	GBq·m^{-2}						0.013
			16th outage	GBq·m^{-2}				0.3	0.075	0.18
	Activity	^{58}Co	1st to 16th	Bq·g^{-1}				0.2–3		0.2
		^{60}Co	1st to 16th	Bq·g^{-1}				0.005–0.05		0.05
Loviisa 1	HL	^{58}Co	1st outage	GBq·m^{-2}	1.1					
			17th outage	GBq·m^{-2}	1.5			0.5		
		^{60}Co	1st outage	GBq·m^{-2}	0.1					
			17th outage	GBq·m^{-2}	0.2			0.3		
	CL	^{58}Co	1st outage	GBq·m^{-2}						
			17th outage	GBq·m^{-2}				0.5		
		^{60}Co	1st outage	GBq·m^{-2}						
			17th outage	GBq·m^{-2}				0.3		
	SG	^{58}Co	1st outage	GBq·m^{-2}	0.13					
			16th outage	GBq·m^{-2}	0.24			0.5		
		^{60}Co	1st outage	GBq·m^{-2}	0.015					
			16th outage	GBq·m^{-2}	0.025			0.3		
	Activity	^{58}Co	1st to 17th	Bq·g^{-1}				0.3–3		
		^{60}Co	1st to 17th	Bq·g^{-1}				0.01–0.06		

5.1.1. ACE

With the ACE code, calculation was done for three units: CRUAS-1, GKN-1 and EBO-1. Results are shown in Figs 37–42 and can be summarized as follows:

At CRUAS-1, ^{58}Co activities on the hot-leg and cold-leg are in relatively good correspondence, while ^{60}Co activities on all points are underestimated by about one order. It is considered that there are two reasons for this disagreement. First is an unsuitable parameter in the code, and second is the calculation method. Some of parameters used by ACE code, for example corrosion rate, deposition rate, dissolution and precipitation rates may not be set properly, but it is difficult to identify which is incorrect. Further evaluation to find such incorrect parameters requires a lot of information about (radioactive) corrosion products behaviour in the water and on the surfaces. The power operation pattern of CRUAS-1 had many variations, but the average power value during each cycle was used in the calculation. Power changes sometimes increase the release rate of crud on the fuel, and the amount of crud may be decreased by such crud bursts. The ACE code is not capable of calculating the influence of crud burst through power changes.

For GKN-2 case, ^{58}Co activities on the hot-leg matched well the measured results, whilst for the CL calculation the results were slightly overestimated. ^{60}Co activities are underestimated by factor 2–8. The reasons for these differences are expected to be the same as noted above.

For EBO-1, calculations were done for cycles 1 to16, while output data were only available for cycles 17–20. Just observing trends it can be concluded that for both the ^{58}Co and ^{60}Co activities, the calculation results were overestimated by factor 3–10. The reasons for these differences are expected to be the same as noted above.

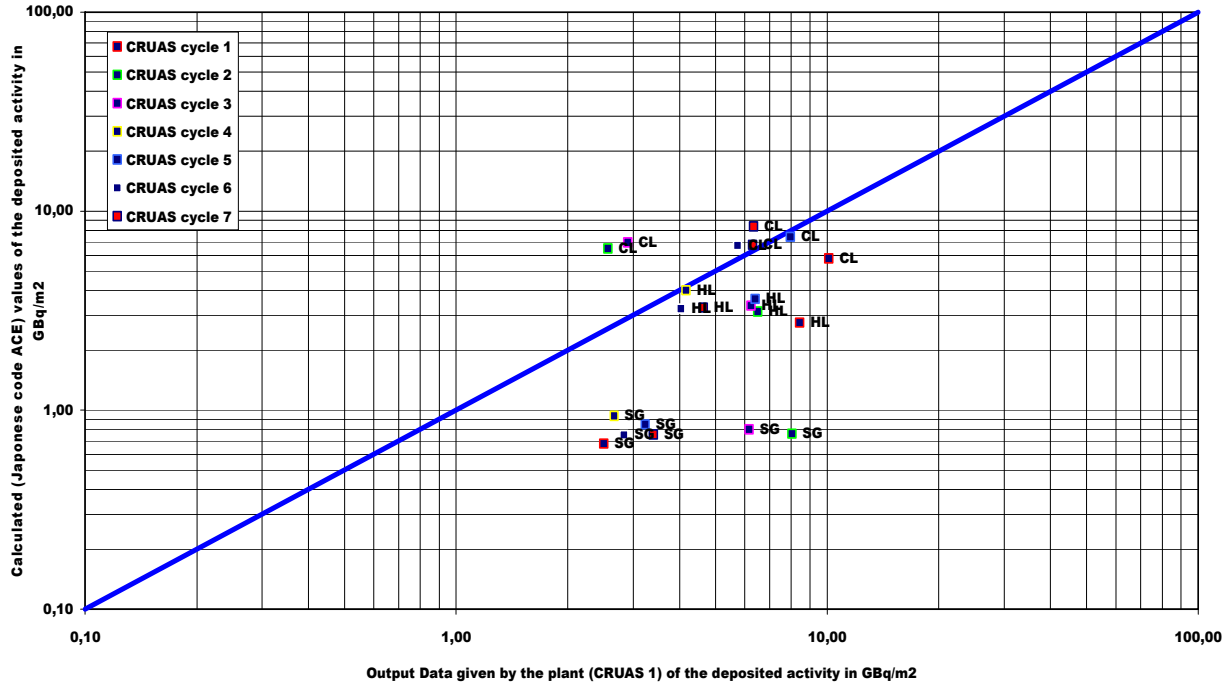

FIG. 37. Comparison of calculated and measured values for ^{58}Co activity deposited for 7 cycles of CRUAS-1.

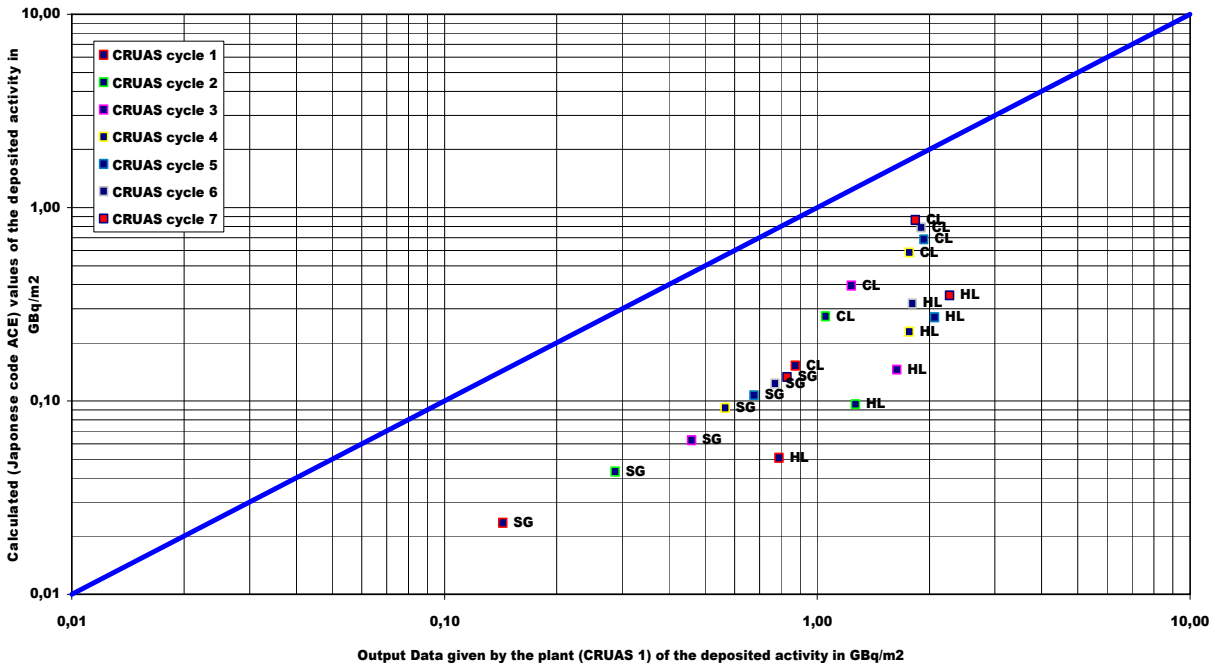

FIG. 38. Comparison of calculated and measured values for ^{60}Co activity deposited for 7 cycles of CRUAS-1.

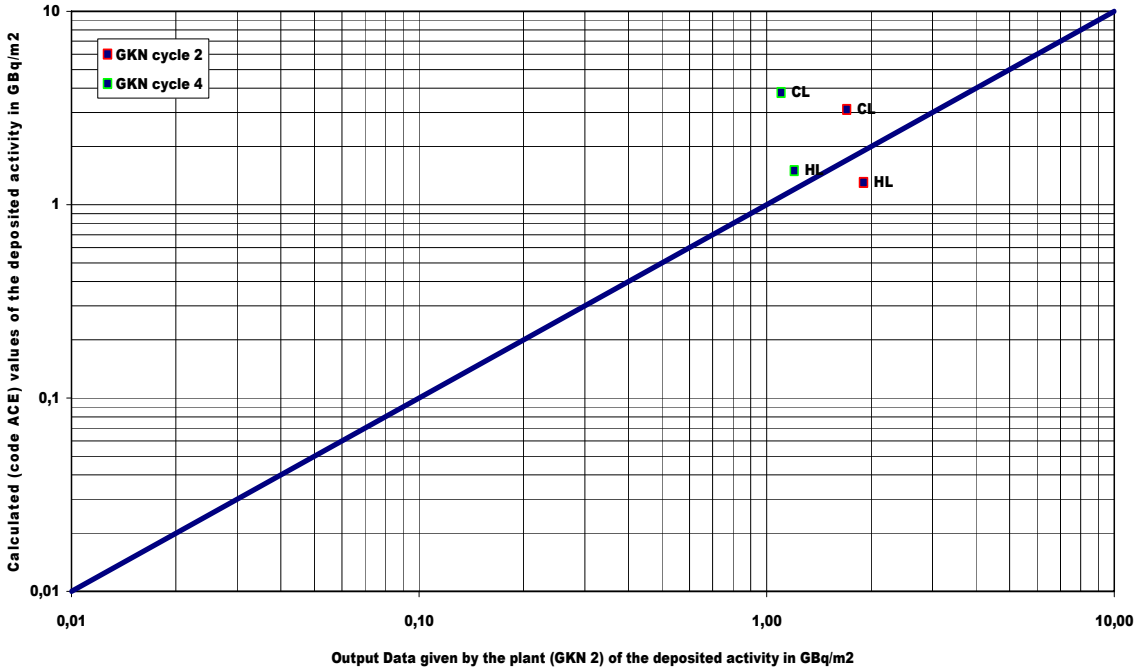

FIG. 39. Comparison of calculated and measured values for ^{58}Co activity deposited for 2 cycles of GKN-2.

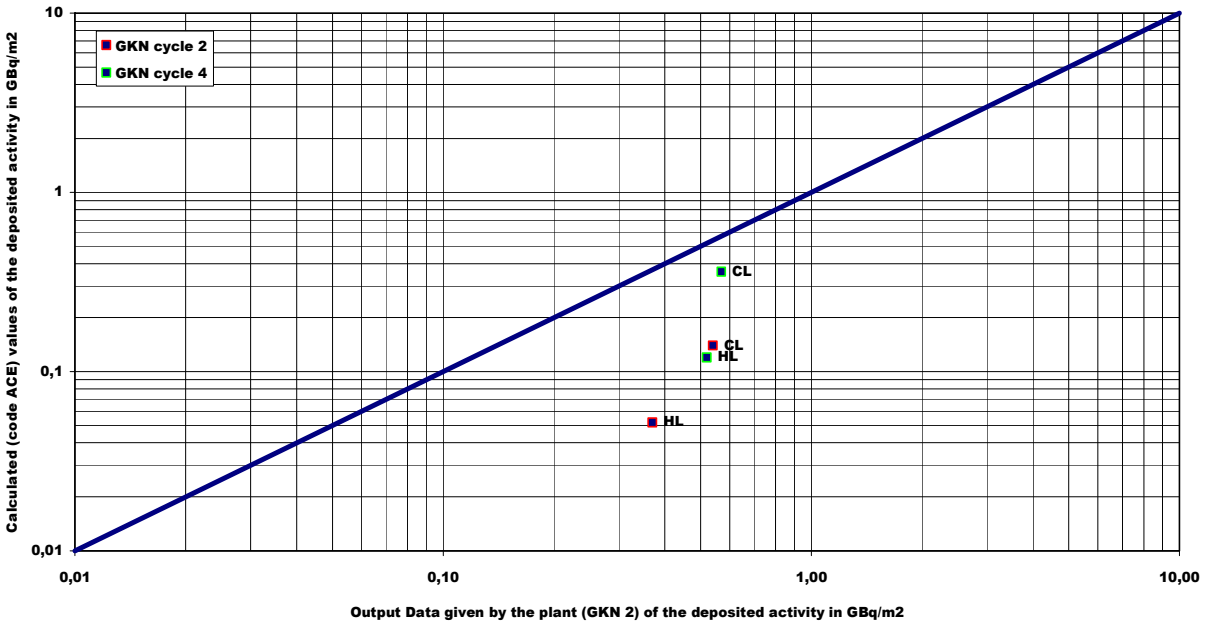

FIG. 40. Comparison of calculated and measured values for ^{60}Co activity deposited for 2 cycles of GKN-2.

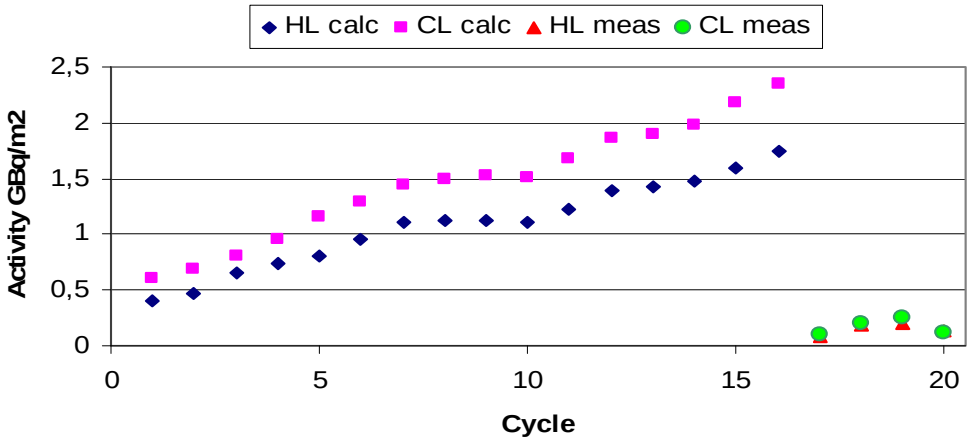

FIG. 41. Comparison of calculated and measured values for ^{58}Co activity deposited for 20 cycles of EBO-1.

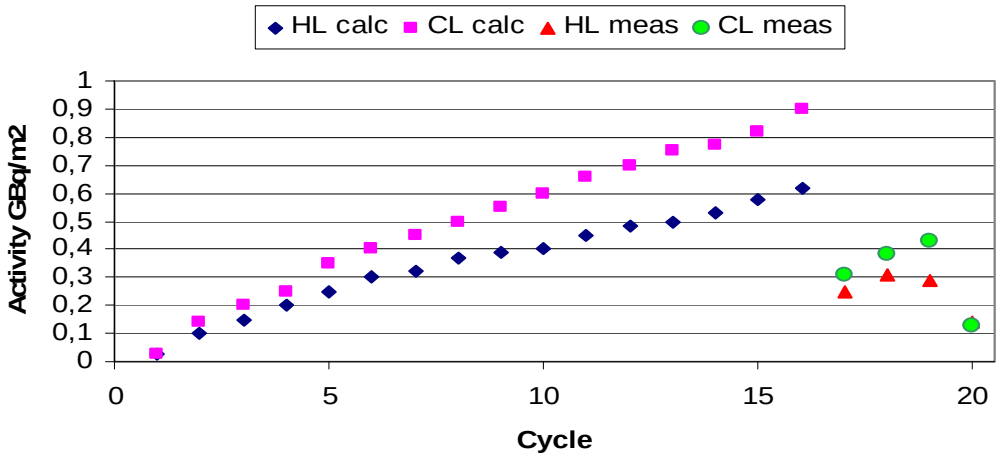

FIG. 42. Comparison of calculated and measured values for ^{60}Co activity deposited for 20 cycles of EBO-1.

5.1.2. CRUDTRAN

The CRUDTRAN code prediction was compared with the CRUAS-1 PWR operational data. CRUDTRAN code predicts the ^{58}Co and ^{60}Co activities only in the SG tubes. However, it could be assumed that the activities in the other areas, such as hot and CLs, have a linear relationship with those in the SG. For the GKN-2 plant, comparison could not be done since the measured data for the SG were not available. Predicted results of the SG activity of GKN-2 are given in Table 4. Those of CRUAS-1 are shown in Figs 43–44.

In the prediction for the CRUAS-1 plant, the crud and activity transport factors derived from the test results of MIT in-reactor simulation loop PCCL are used, while all other parameters were derived from the CRUAS-1 plant data provided through this CRP. It showed that CRUDTRAN over-predicted the ^{60}Co activity in the SG and under-predicted the ^{58}Co activity with consistency in both cases. Therefore, adjustment factors of 1.5 and 0.56 were applied to ^{58}Co and ^{60}Co activation factors, respectively. Neutron activation factors of ^{58}Co and ^{60}Co depend upon both the neutron reaction rates in the core and the ratios of ^{58}Ni and ^{59}Co to iron in the crud deposited in the core, which also depend upon the chemical compositions of construction materials in the PWR primary system and dissolution characteristics of different elements into the coolant. Fig. 45 compares the CRUDTRAN prediction with the measured plant data after correction. It shows that CRUDTAN code can predict the variation of ^{58}Co and ^{60}Co activities in SG tubes from cycle 1 to cycle 7 quite well. It is also notable that for the ^{58}Co activity, variations of the measured data from cycle 1 to cycle 7 due to the variations of reactor power and coolant chemistry histories in each cycle can be successfully predicted by the CRUDTRAN code.

Therefore, it can be said that after determining activation factors for ^{58}Co and ^{60}Co, which are the plant-specific parameters and could be derived from the previous plant operation data, CRUDTAN could predict the variation of radioactivity in the subsequent cycles. Validation of CRUDTRAN models also indicates that primary driving force for crud transport is the solubility change around the PWR primary coolant system, and dissolution and crystallization processes are rate controlling steps in the crud transport.

TABLE 4. PREDICTED SG ACTIVITY OF GKN-2 PLANT

Cycle	SG activity ($GBq \cdot m^{-2}$)	
	^{58}Co	^{60}Co
1	1.14	0.32
2	1.74	0.87
3	2.19	1.72
4	2.0	2.46

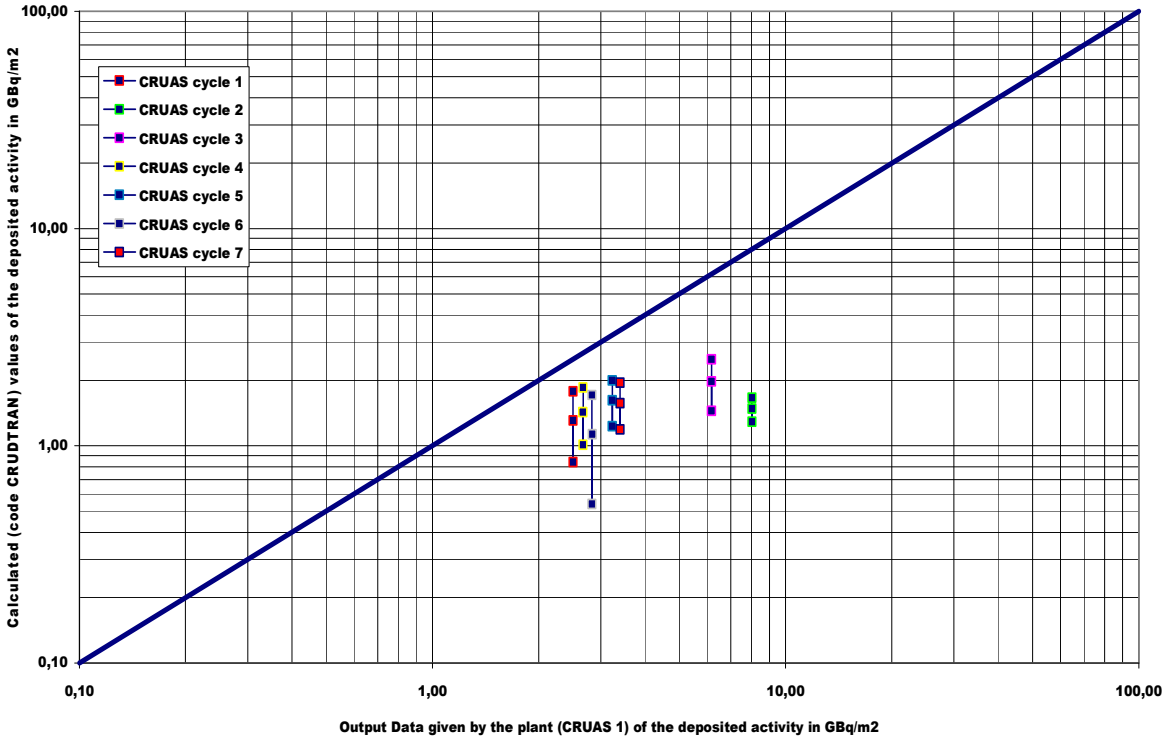

FIG. 43. Comparison of calculated and measured values for ^{58}Co activity deposited for 7 cycles of CRUAS-1.

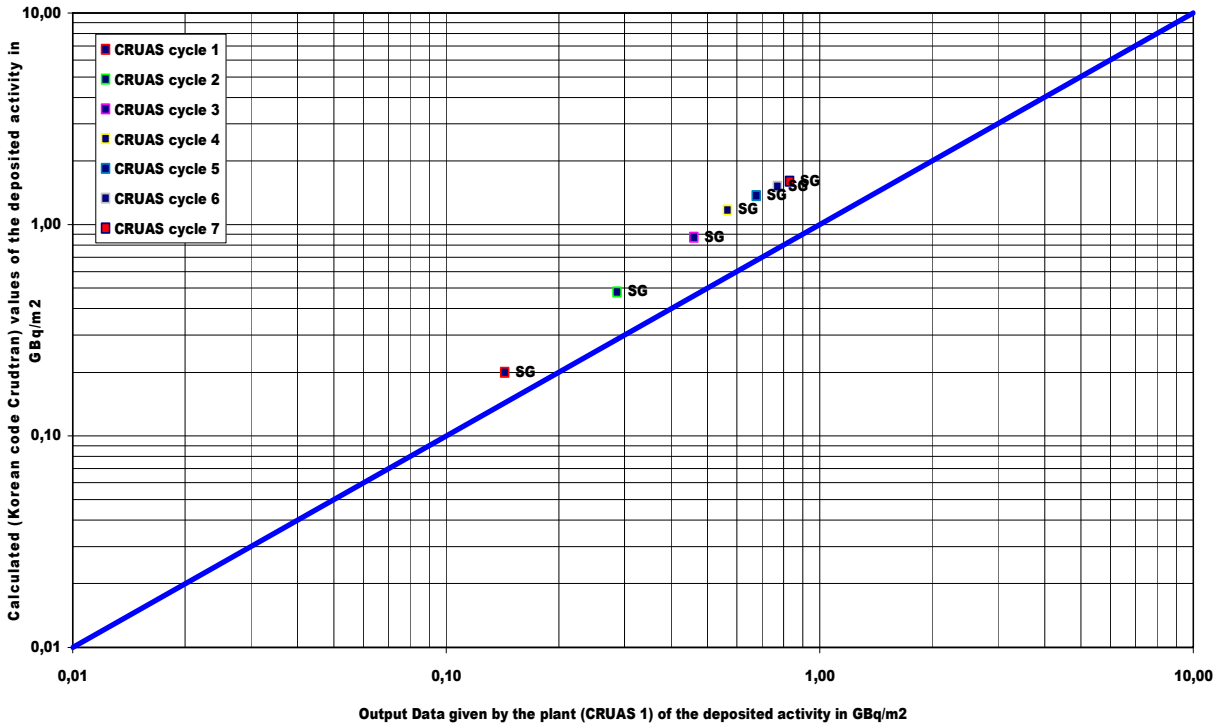

FIG. 44. Comparison of calculated and measured values for ^{60}Co activity deposited for 7 cycles of CRUAS-1.

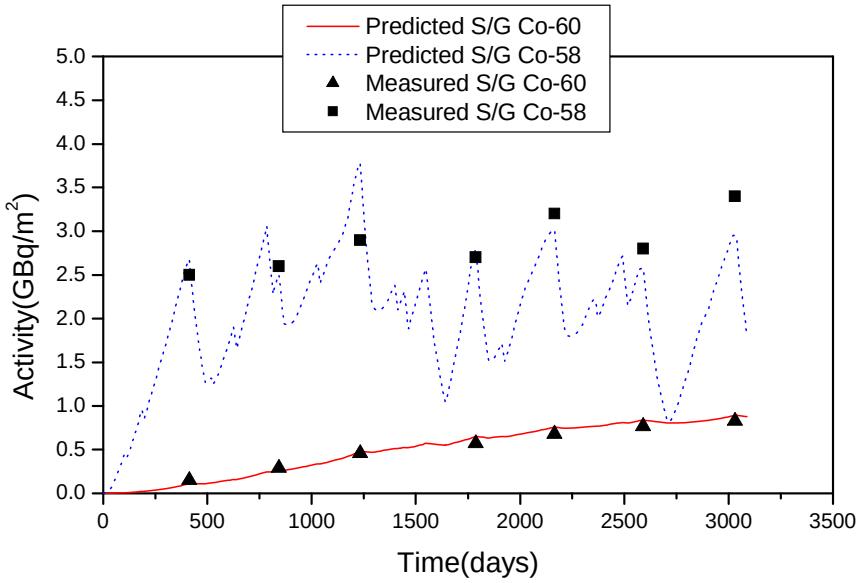

FIG. 45. Comparison of calculated and measured values for ^{60}Co activity deposited for 7 cycles of CRUAS-1 after correction of activation factors.

5.1.3. DISER

DISER code was used for modelling of all four PWRs. The results can be summarized as follows:

For CRUAS-1, see Figs 46–47 for ^{58}Co activities, the DISER code gave underestimated results for both hot and CL for the first two cycles. This observation can be explained by the calculation of lower corrosion product release at the beginning of the unit operation in comparison with the real situation. The modelling results for the following operation cycles are in good agreement with the measured data. For ^{60}Co modelling results for SG are in good agreement with the plant data. The results for the CL and HL are underestimated for the beginning of the unit operation (cycles 1–3), however the results from the following operation show good agreement with the plant data. Also in this case, the observed discrepancy can be explained by a difference in corrosion products release rate.

For GKN-2, results are shown in Figs 48–49. For ^{58}Co activities, modelling results are in good agreement with the plant data. In fact, only a small amount of measured data is available for the comparison (the plant data available only after 2nd and 4th cycle). For ^{60}Co, calculation results show an underestimation for the beginning of the unit operation. The remaining results are in good agreement with the plant measurement. As in the case of CRUAS-1 unit, the discrepancy can be explained by a difference in corrosion products release rate at the beginning of the unit operation. The comparison of the calculation and measurement is difficult because of lack of the plant data.

At LOVIISA-1, as shown in Figs 50–51, almost all ^{58}Co activity calculation results for the compared cycles (the plant data available from cycle 10 to cycle 16) are overestimated. There is no clear explanation for the observed situation. The plant data themselves exhibit fluctuations from cycle to cycle and do not show any clear trend in the deposited radioactivity. For ^{60}Co, most of the calculation results are in good agreement with the compared plant data, except some particular points for the CL.

Results for EBO-1 are shown in Figs 52–53. Calculation results of ^{58}Co activity for the compared cycles (the plant data on surface activities are available for cycles 17–20) are overestimated for both HL and CL. There is no clear explanation for this observation. Unfortunately, the plant data are not available from the beginning of the unit operation. The available plant data themselves exhibit fluctuations from a cycle to cycle. These fluctuations can not be reproduced by the code modelling or easily explained, for example, by water chemistry changes. For ^{60}Co, calculation results for the HL are in a good agreement with the plant data. The results for the CL, cycles 17–19, are slightly underestimated. The comment made for EBO-1 unit, radionuclide ^{58}Co is valid also for ^{60}Co.

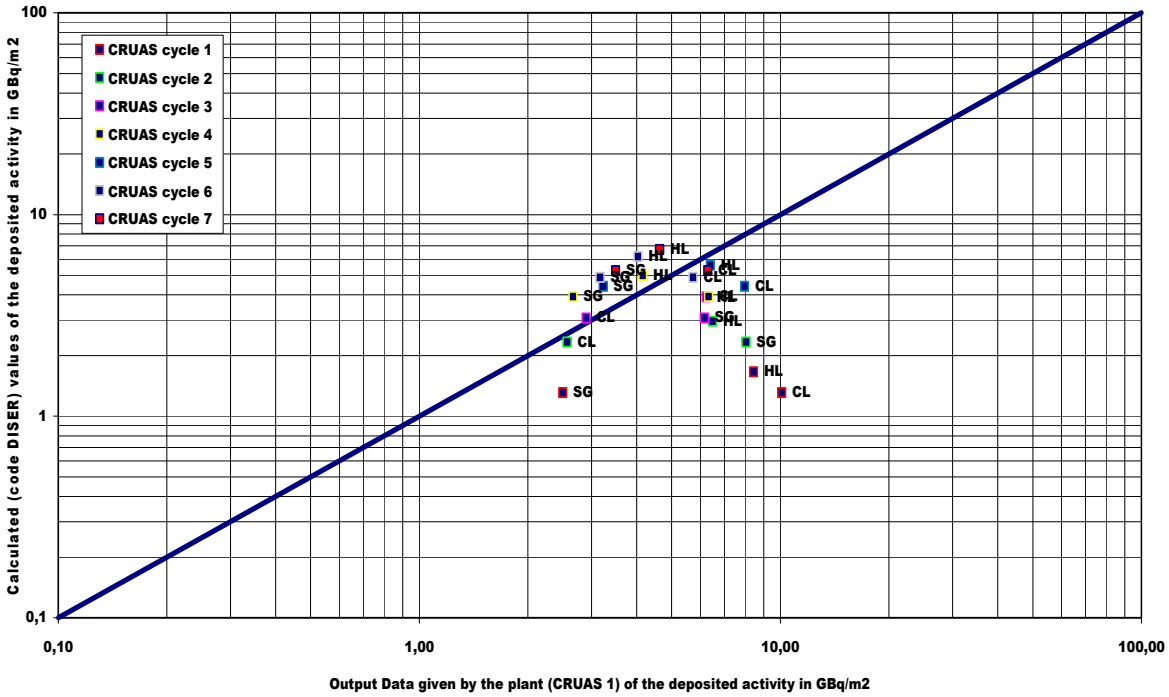

FIG. 46. Comparison of calculated and measured values for ^{58}Co activity deposited for 7 cycles of CRUAS-1.

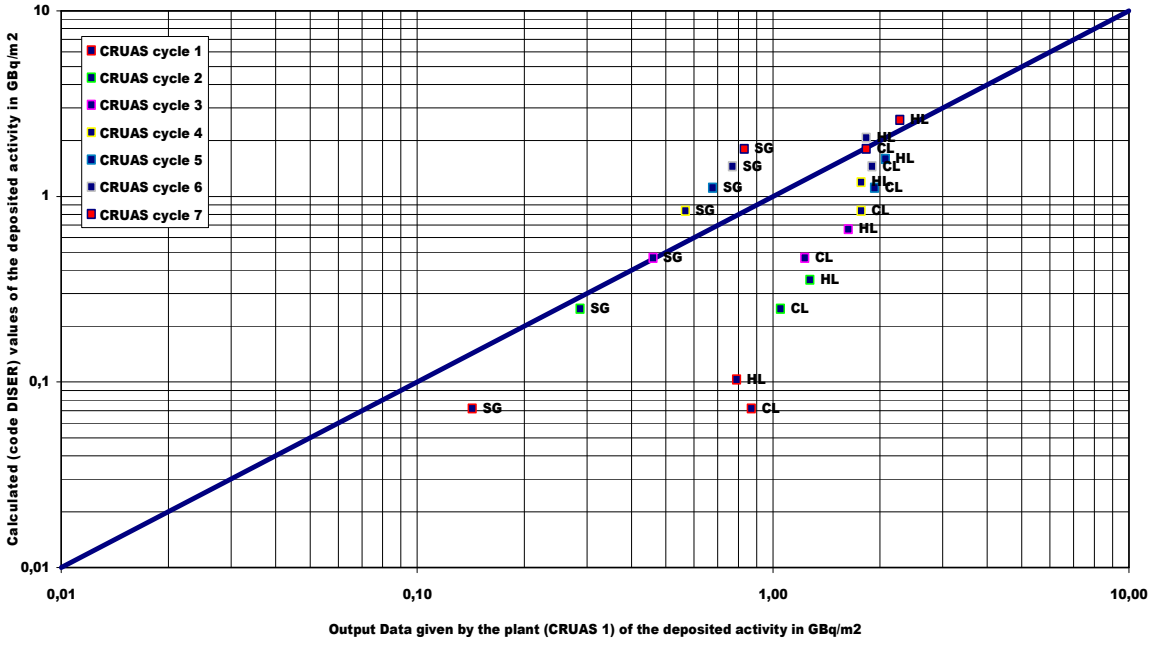

FIG. 47. Comparison of calculated and measured values for ^{60}Co activity deposited for 7 cycles of CRUAS-1.

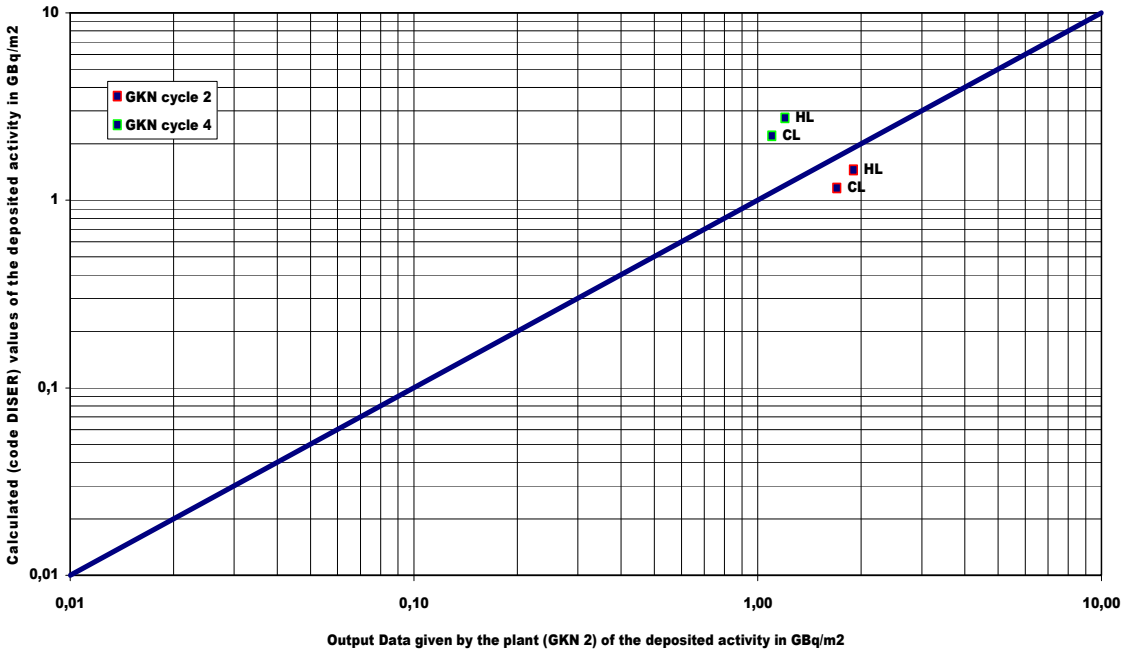

FIG. 48. Comparison of calculated and measured values for ^{58}Co activity deposited for 2 cycles of GKN-2.

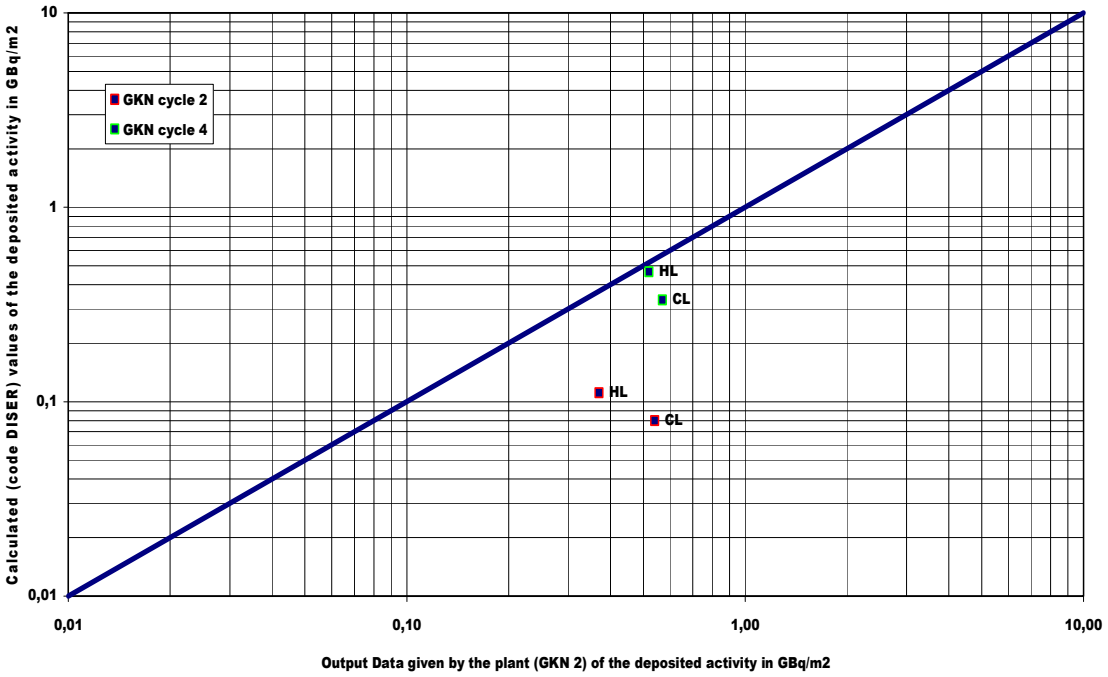

FIG. 49. Comparison of calculated and measured values for ^{60}Co activity deposited for 2 cycles of GKN-2.

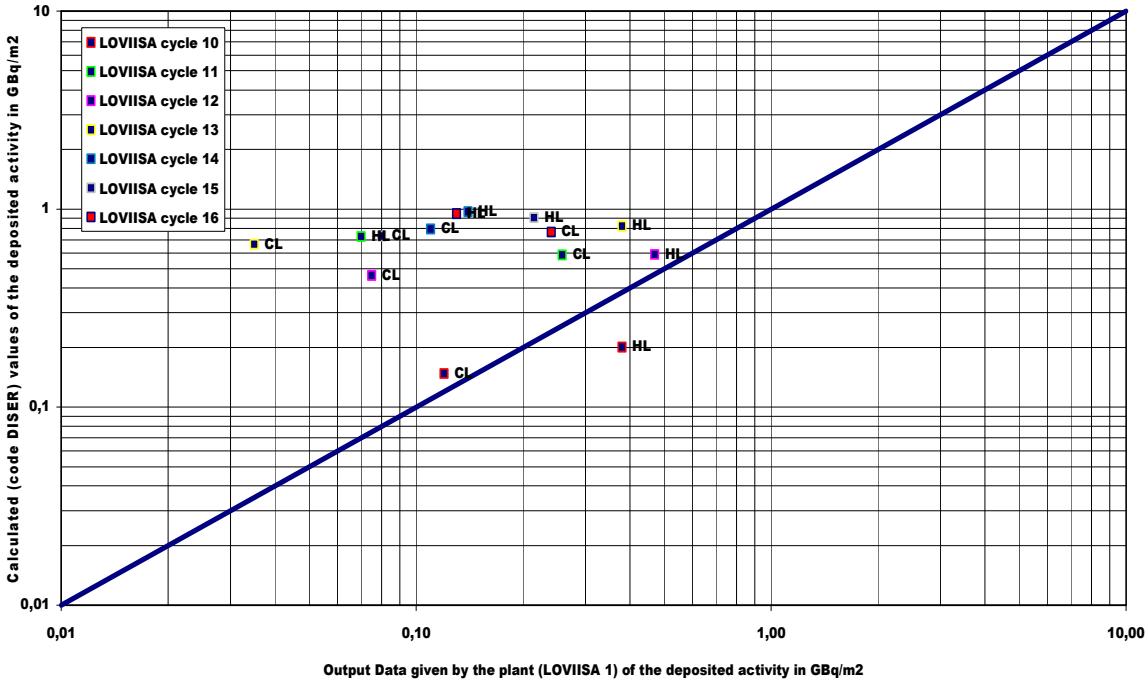

FIG. 50. Comparison of calculated and measured values for ^{58}Co activity deposited for 7 cycles of LOVIISA-1.

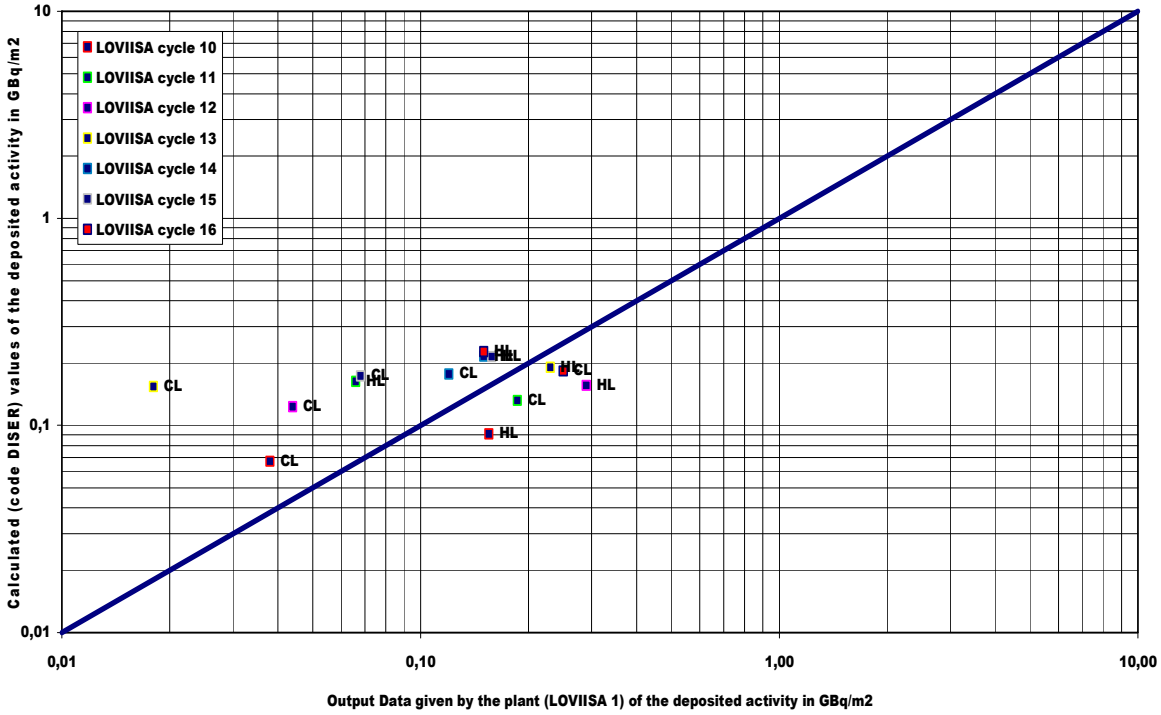

FIG. 51. Comparison of calculated and measured values for ^{60}Co activity deposited for 7 cycles of LOVIISA-1.

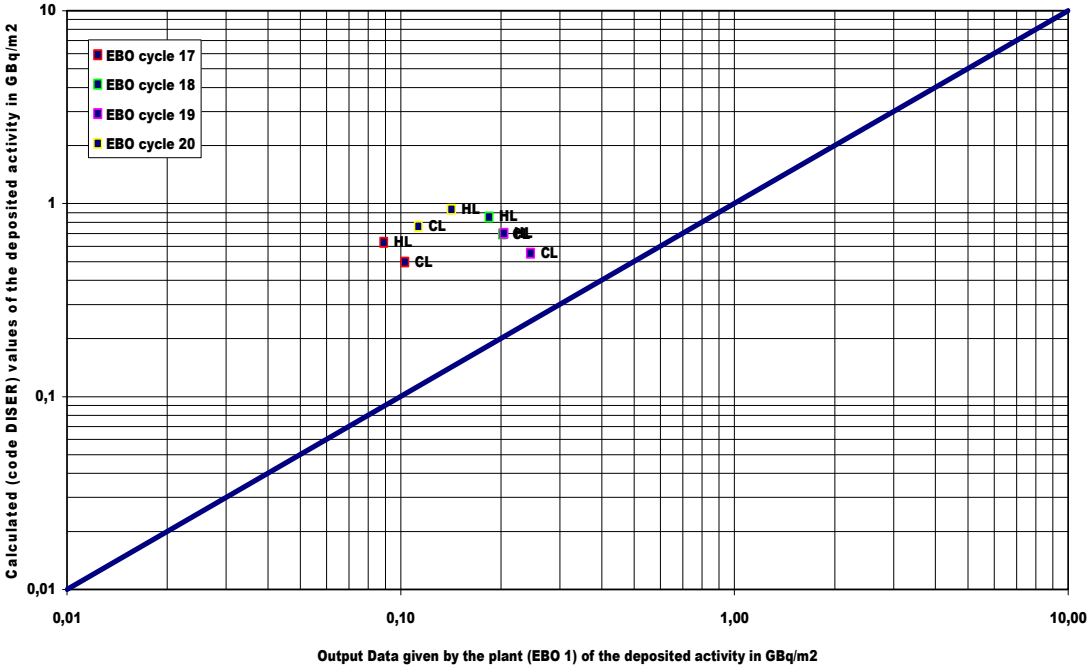

FIG. 52. Comparison of calculated and measured values for ^{58}Co activity deposited for 4 cycles of EBO-1.

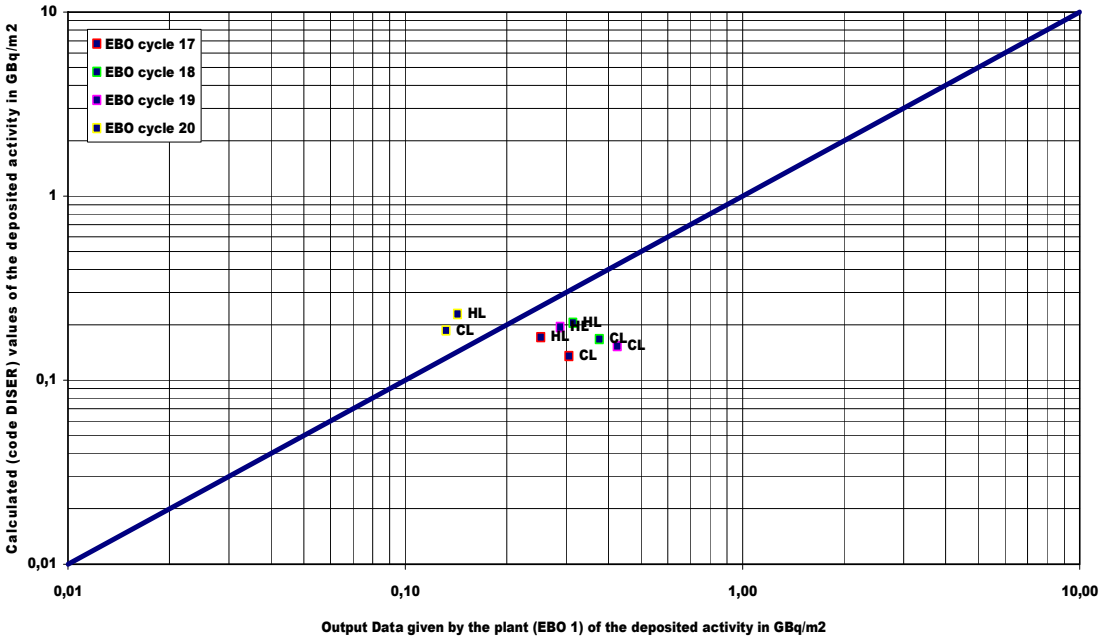

FIG. 53. Comparison of calculated and measured values for ^{60}Co activity deposited for 4 cycles of EBO-1.

5.1.4. MIGA RT

With MIGA RT code, three units: CRUAS-1, LOVIISA-1 and EBO-1 were modelled and the results are shown in Figs 54–59. The results can be described as follows:

For CRUAS-1, the ^{58}Co activities matched the measured data well, for ^{60}Co the calculation results were underestimated by factor 5–10.

For the LOVIISA-1 case, the calculated ^{58}Co activities were slightly overestimated, while ^{60}Co calculation results matched measured data very well.

For EBO-1, the calculation was done for cycles 1–16, while output data were available for cycles 17–20. By observing trends it can be concluded that the calculated ^{58}Co activities were overestimated, for ^{60}Co activity, calculation results matched the measured data well for HL and were underestimated for CL.

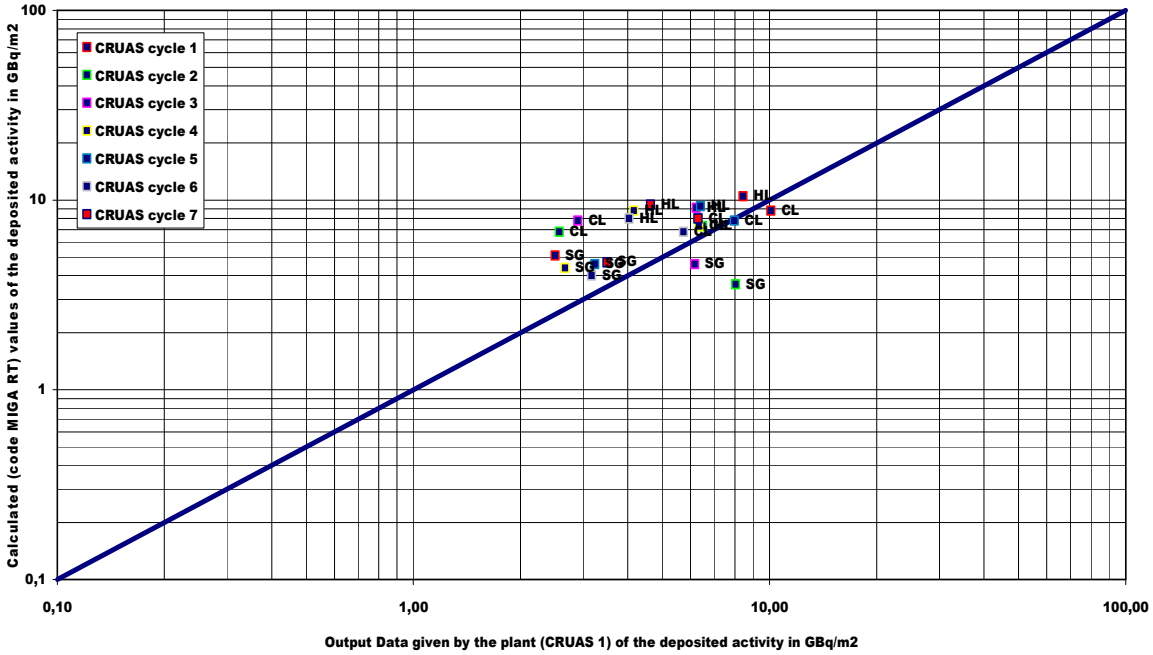

FIG. 54. Comparison of calculated and measured values for ^{58}Co activity deposited for 7 cycles of CRUAS-1.

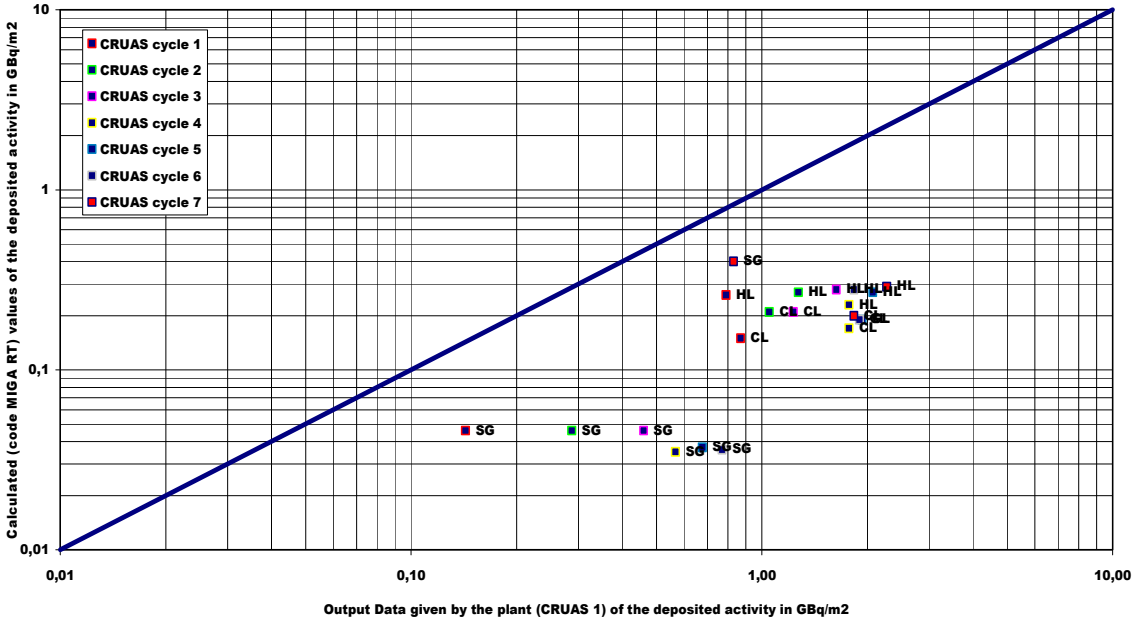

FIG. 55. Comparison of calculated and measured values for ^{60}Co activity deposited for 7 cycles of CRUAS-1.

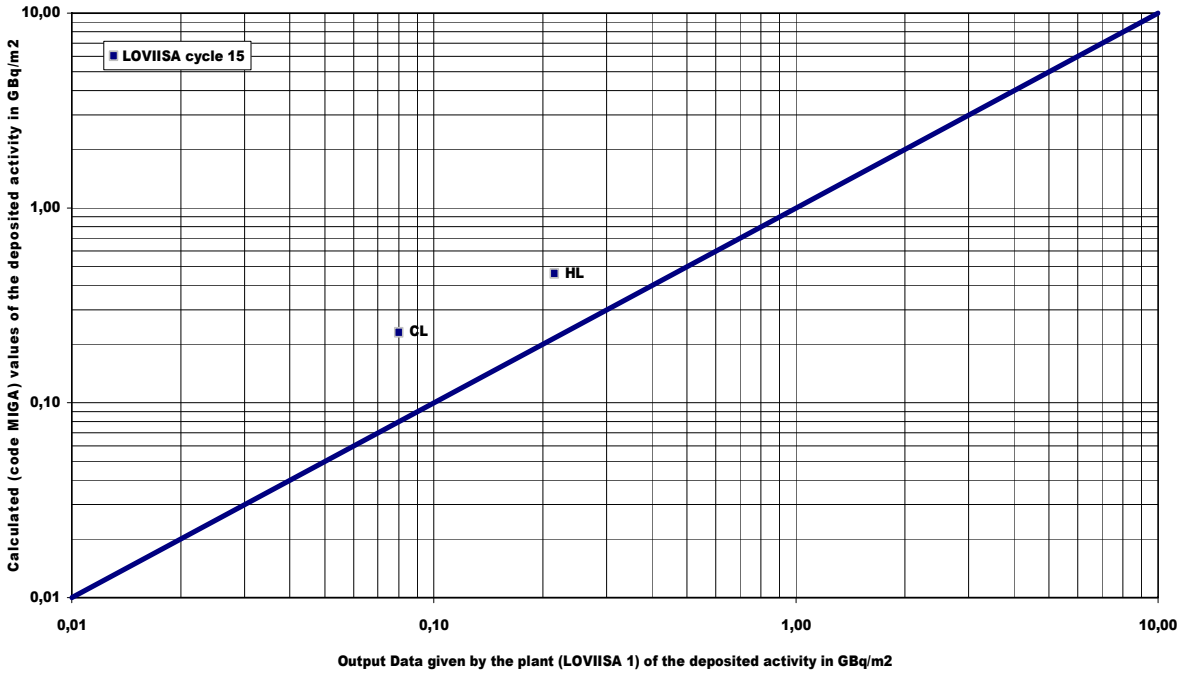

FIG. 56. Comparison of calculated and measured values for ^{58}Co activity deposited for 1 cycle of LOVIISA-1.

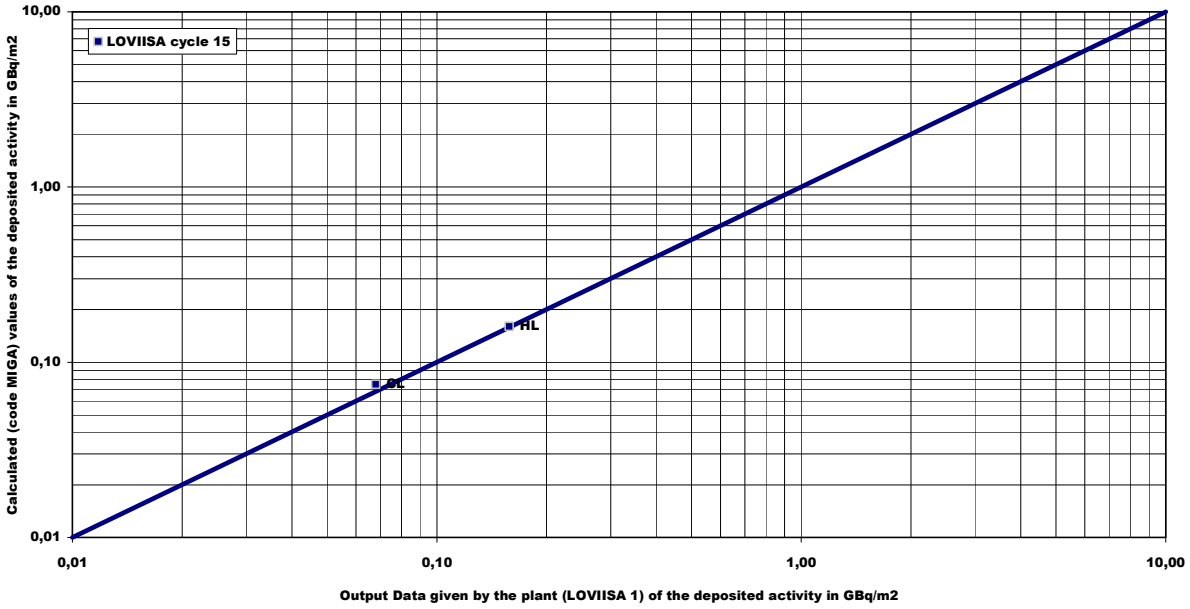

FIG. 57. Comparison of calculated and measured values for ^{60}Co activity deposited for 1 cycle of LOVIISA-1.

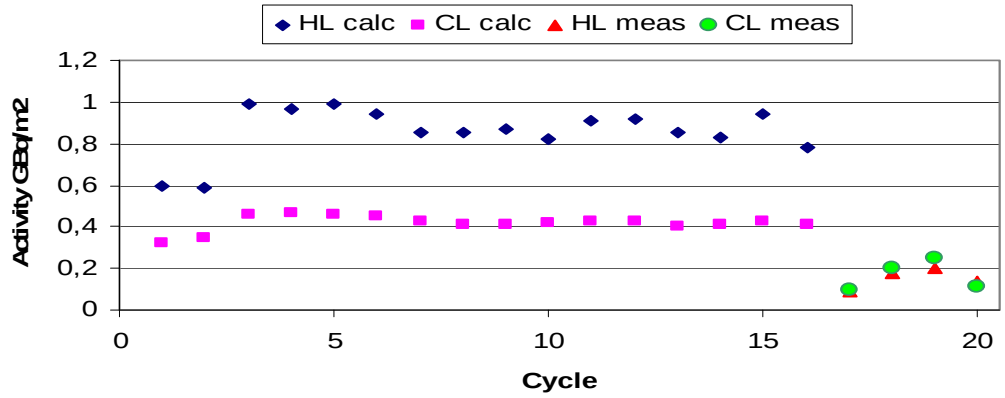

FIG. 58. Comparison of calculated and measured values for ^{58}Co activity for 19 cycles of EBO-1.

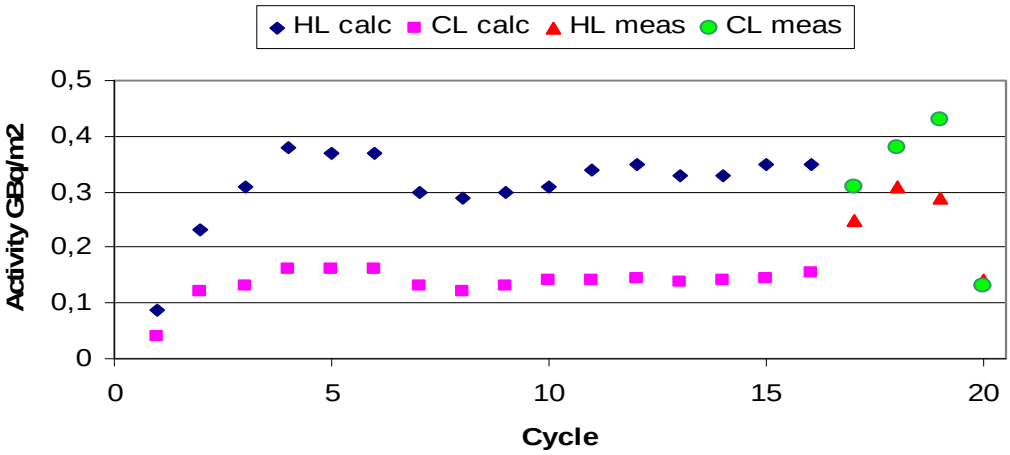

FIG. 59. Comparison of calculated and measured values for ^{60}Co activity for 19 cycles of EBO-1.

5.1.5. PACTOLE

With PACTOLE code Version 2.2, calculation was done for three units: CRUAS-1, GKN-1 and LOVIISA-1. Results are shown in Figs 60–65 and can be summarized as follows:

At CRUAS-1, ^{58}Co activities on the hot-leg and cold-leg are well corresponding to measured values, while ^{60}Co activities on majority of points are overestimated by a factor 2–5.

Although the trends are quite different – ^{58}Co activity globally decreases and ^{60}Co increases – it can be seen that the deposited activity is higher for ^{58}Co than for ^{60}Co. Indeed, if one focuses on the HL the activity of ^{58}Co is equal to 6 GBq·m^{-2} at fuel cycle number 7 while ^{60}Co activity is only 3 Gbq·m^{-2}. This difference is reduced for the CL (7.5 GBq·m^{-2} for ^{58}Co and 5.5 GBq·m^{-2} for ^{60}Co at cycle number 7).It is quite important to notice that deposited activity for ^{58}Co is higher for the early cycles on CL compared to the HL (23 GBq·m^{-2} and 10 GBq·m^{-2}) but the level of deposited activity is relatively homogeneous for both legs for the last cycles.

The global trends for ^{58}Co and ^{60}Co can be reproduced if one plots the deposited activity on SG tubes. Nevertheless, the level of activity is much lower: 1.5 GBq·m^{-2} for ^{58}Co and 1 GBq·m^{-2} for ^{60}Co for the 7th cycle.

For the GKN-2 case, ^{58}Co activities matched well measured results better agreement was found in 4th cycle than in the 2nd one. ^{60}Co activities for the CL are overestimated by factor about 6.

It is quite obvious, compared to the CRUAS 1 simulation, that the contamination level is much lower in GKN 2 than in CRUAS 1. Indeed, the maximum deposited activity obtained for GKN 2 is only 3.5 GBq·m^{-2} for ^{58}Co on the CL compared to almost 25 GBq·m^{-2} for CRUAS 1.

As previously observed for CRUAS 1, the trend for ^{58}Co is decreasing while it is more or less increasing for ^{60}Co. Deposited activity for ^{58}Co sharply decreases and can be lower than ^{60}Co (which was not observed for CRUAS 1). This is mainly obvious on Figs 62–63 (deposited activity on CL) where activity for ^{58}Co is 1.5 GBq·m^{-2} at the end of fuel cycle number 5 and 3 GBq·m^{-2} for ^{60}Co.

For LOVIISA-1, calculation was done for cycles 8–16, it can be concluded that for ^{58}Co results corresponded well to measured values while for ^{60}Co activities, calculation results were underestimated by factor 5–10. The reasons for such a difference could be the incomplete set of input data, and a need for approximation of some values (axial power distribution, wall and fluid temperatures).

One result that can be drawn from these Figures is that, comparing the results of CRUAS 1 and GKN 2, the contamination level for LOVIISA predicted by PACTOLE is really the lowest.

As was observed for CRUAS and GKN, the ^{58}Co deposited activity globally decreases for the first fuel cycles (6 in the LOVIISA's case) but it tends to stabilize for higher fuel cycles. This stabilization is quite obvious for ^{60}Co deposited activity which remains constant from cycle 4 to cycle 9.

What is also remarkable, comparing CRUAS and GKN behaviour is that the level of activity is higher on the HL than on the CL. The maximum of deposited activity is obtained on the HL for ^{58}Co was 1.5 GBq·m^{-2}.

If the iron release rate is approximately the same for GKN, CRUAS and LOVIISA, the nickel release rate is actually really different for the three studied reactors: it is the lowest for LOVIISA. This can be explained, at first glance, by the lower content of nickel in the SG tube bundles of LOVIISA.

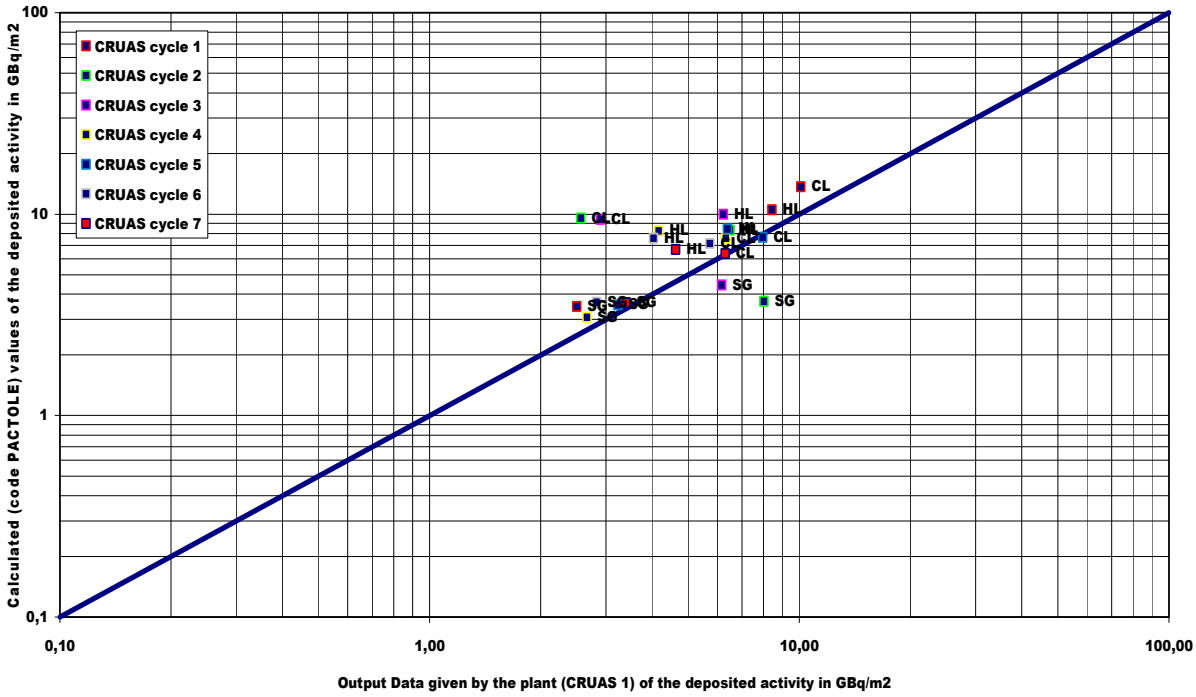

FIG. 60. Comparison of calculated and measured values for ^{58}Co activity deposited for 7 cycles of CRUAS-1.

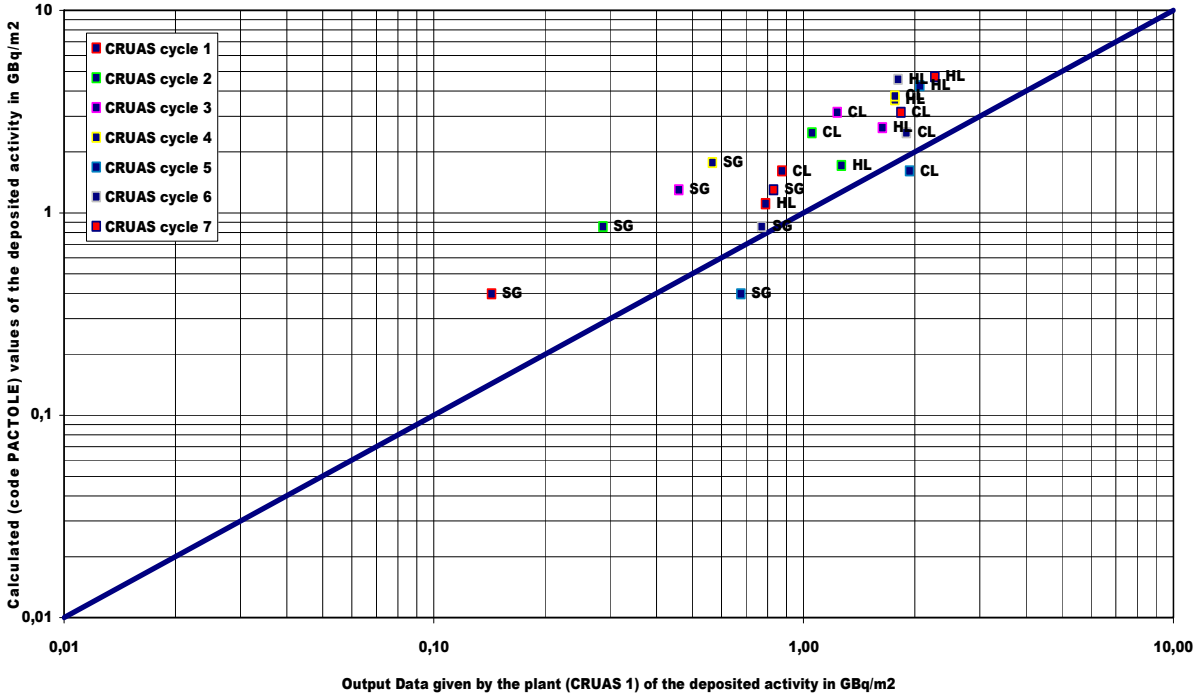

FIG. 61. Comparison of calculated and measured values for ^{60}Co activity deposited for 7 cycles of CRUAS-1.

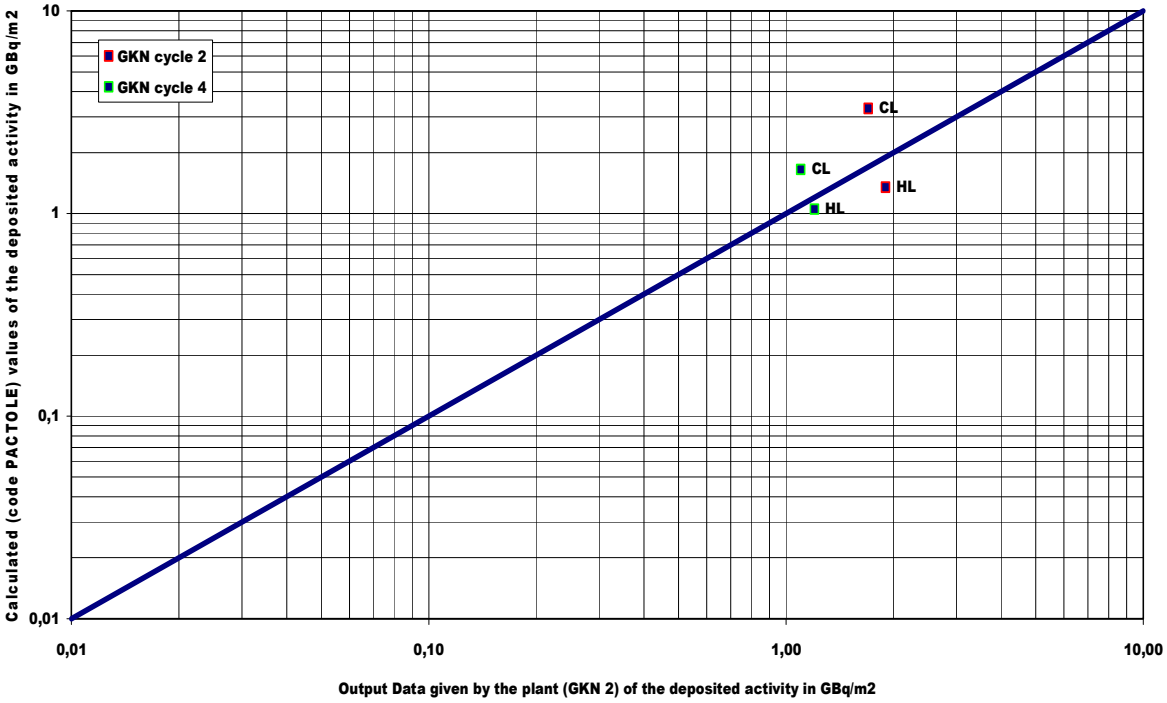

FIG. 62. Comparison of calculated and measured values for ^{58}Co activity deposited for 2 cycles of GKN-2.

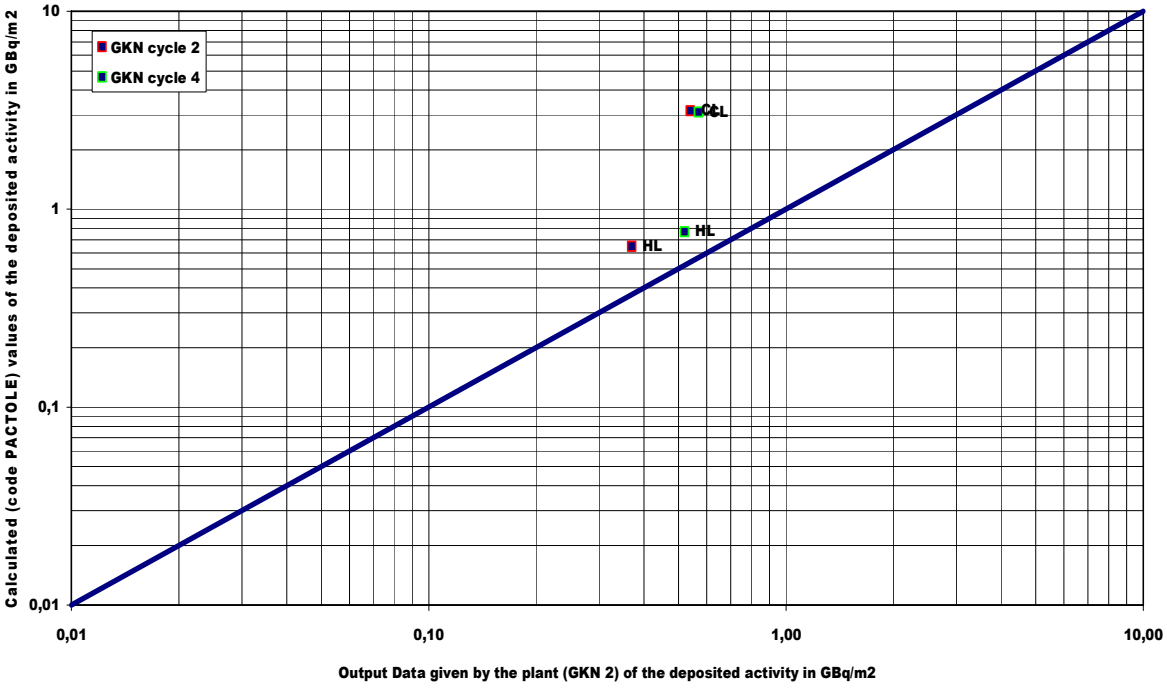

FIG. 63. Comparison of calculated and measured values for ^{60}Co activity deposited for 2 cycles of GKN-2

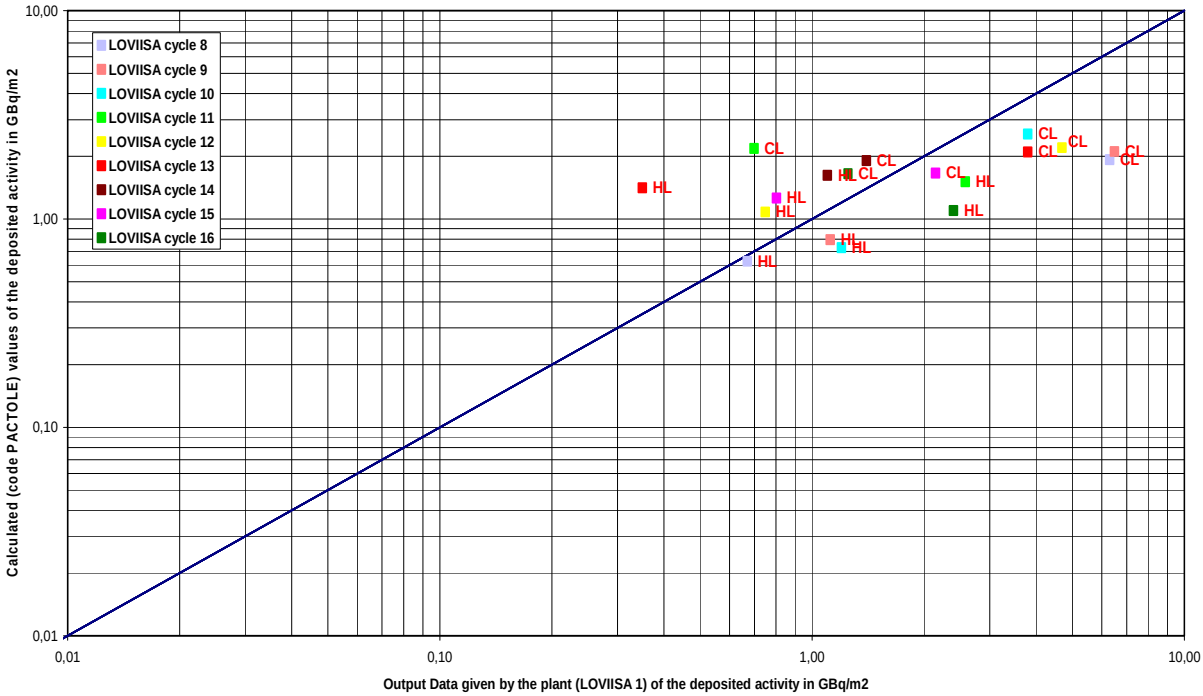

FIG. 64. Comparison of calculated and measured values for ^{58}Co activity deposited for 9 cycles of Loviisa-1.

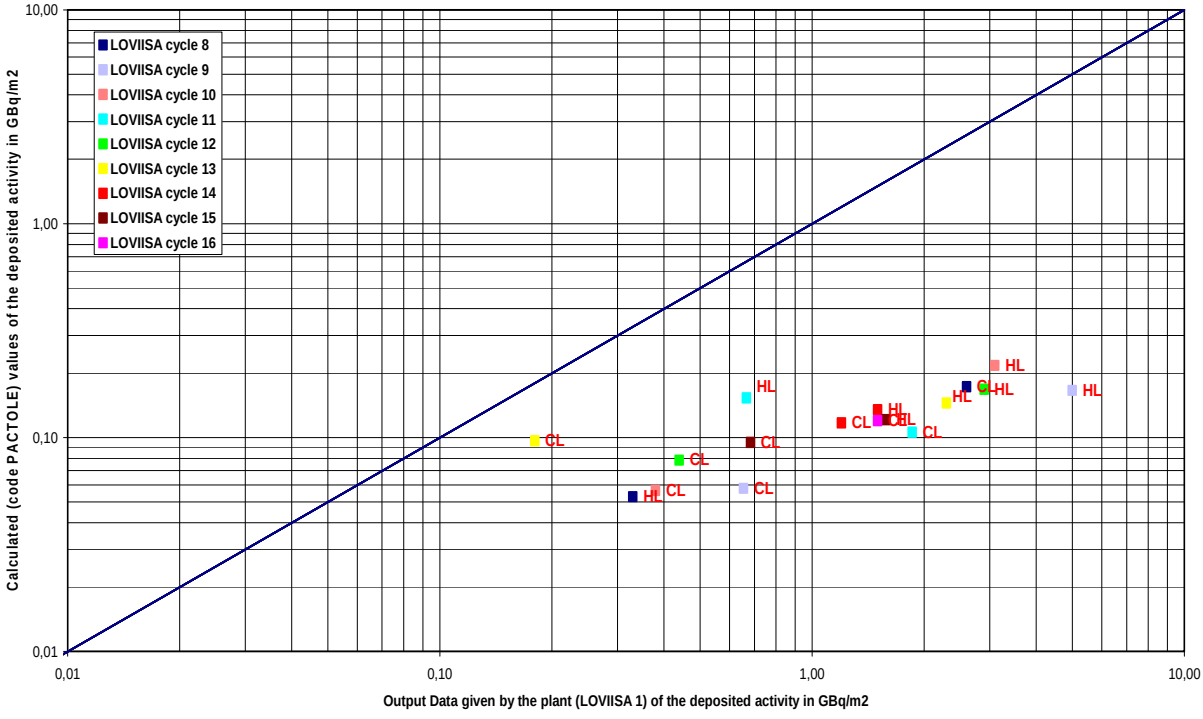

FIG. 65. Comparison of calculated and measured values for ^{60}Co activity deposited for 9 cycles of Loviisa-1.

5.1.6. RADTRAN

With the RADTRAN code, calculations were done for the 1st and 7nd cycle of CRUAS-1 Results are shown in Figs 66–67 and can be summarized as follows:

For ^{58}Co best agreement is found for SG activities, for HL results are less (factor 2–3) and for CL more (factor of ×5) underestimated.

For ^{60}Co results are underestimated, for 1st cycle by a factor about 100, for 7th cycle by a factor 7–10.

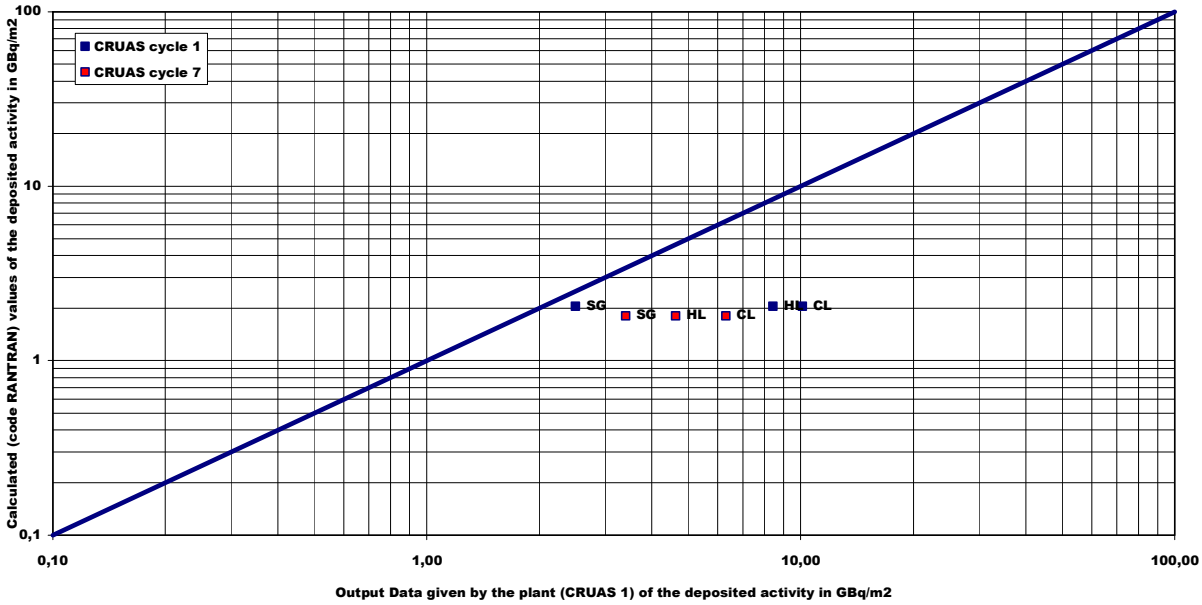

FIG. 66. Comparison of calculated and measured values for ^{58}Co activity deposited for 2 cycles of CRUAS-1.

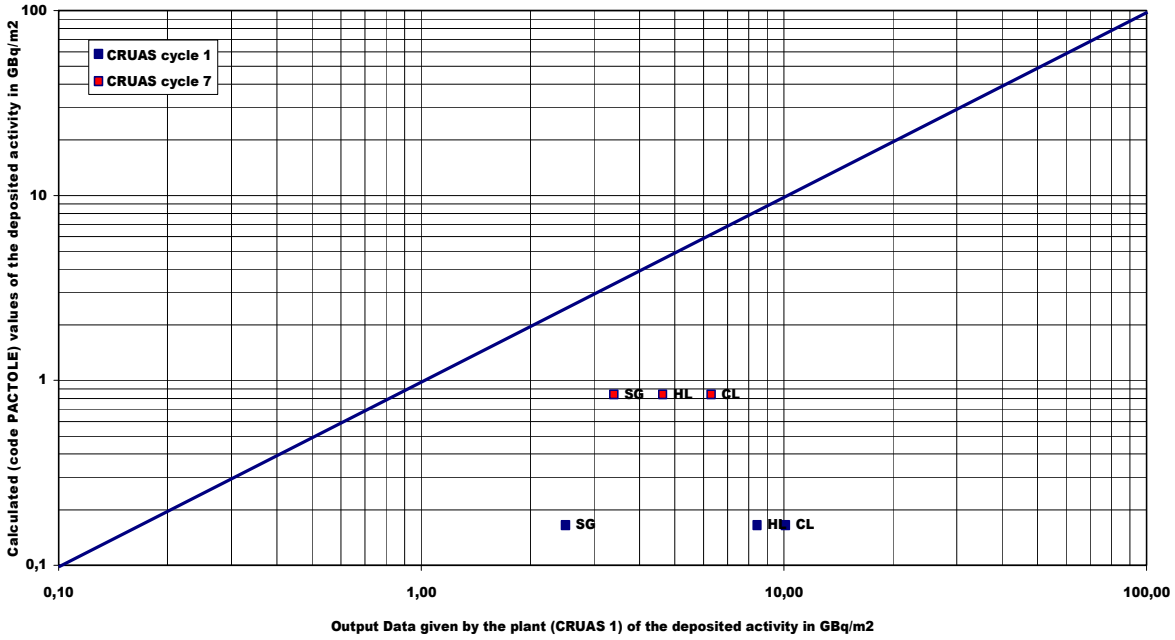

FIG. 67. Comparison of calculated and measured values for ^{60}Co activity deposited for 2 cycles of CRUAS-1.

5.1.7. American model calculation results

The dissolution/precipitation deterministic model as described above was used to calculate the accumulated specific activity of ^{60}Co in the core, HL, SG, and CL, as shown in Fig. 68. The accumulated specific activity is expressed in GBq·m^{-2} as a function of real time for plant operation over 4 cycles. As noted above, the data used in training the model correspond to a WWER and it is assumed that the filter efficiency for the removal of ^{60}Co in the primary circuits of both reactors is 96.6%. Parenthetically, it must be noted that the radiolysis/mixed potential model predict that, for the WWER used to train the ANN, the ECP in the core, HL, SG, and CL were predicted to be (typically) -0.35, -0.72, -0.75, and -0.60 V_{she} under full power conditions, corresponding to an outlet temperature of 295°C, pH_{300} = 6.3–9.3, [H_2] = 2.7–5.1 m^3·t^{-1}, with the values for the pH and hydrogen concentration varying on a day-to-day basis (the actual day-to-day values used in the simulations are given in [83]). Under cold shut down conditions, where the reactor power is zero (but the dose rate of ionizing radiation was assumed to be 1% of the full power value) and the temperature is 35°C, the ECP is estimated to be 0.42 V_{she} at all locations. Calculated specific and accumulated activity due to ^{60}Co at the four locations for a WWER over four operating cycles are shown in Figs 68–69. During initial, steady state, full power operation, the specific activity in the core is predicted to increase monotonically with time. Simultaneously, ^{60}Co in the out-of-core regions is predicted to monotonically decrease with time as magnetite moves to the reactor core and/or because of day-to-day changes in the pH (typically increases from 6.3–9.3 at 300°C) and hydrogen concentration (typically varies over the range of 2.7–5.1 m^3·t^{-1}) during a cycle. Note, again, that actual plant data were employed in the present analysis. Toward the end of each cycle, the in-core activity is predicted to reach a constant value.

Shut down and start-ups produce significant transients in the coolant chemistry and those transients are reflected in the activity transport as seen most clearly by examining the temporal variations in both the specific activity (Fig. 68) and the accumulated activity (Fig. 69). Thus, a sudden increase in the specific activity in all locations during shut down occurs because of the transport of magnetite (and hence ^{60}Co) into the core from the external locations as the temperature of the coolant decreases. During start up, as the temperature of the coolant increases, the core temporarily releases ^{60}Co to the external surfaces at a rapid rate, but during subsequent normal operation, the activity at the external locations slowly decreases, as noted previously, while that in the core increases due to the continued irradiation of ^{59}Co and the slow transport of magnetite to the core. The total activity in the system is predicted to increase with cycle number, as shown by the accumulated activity calculation shown in Fig. 69.

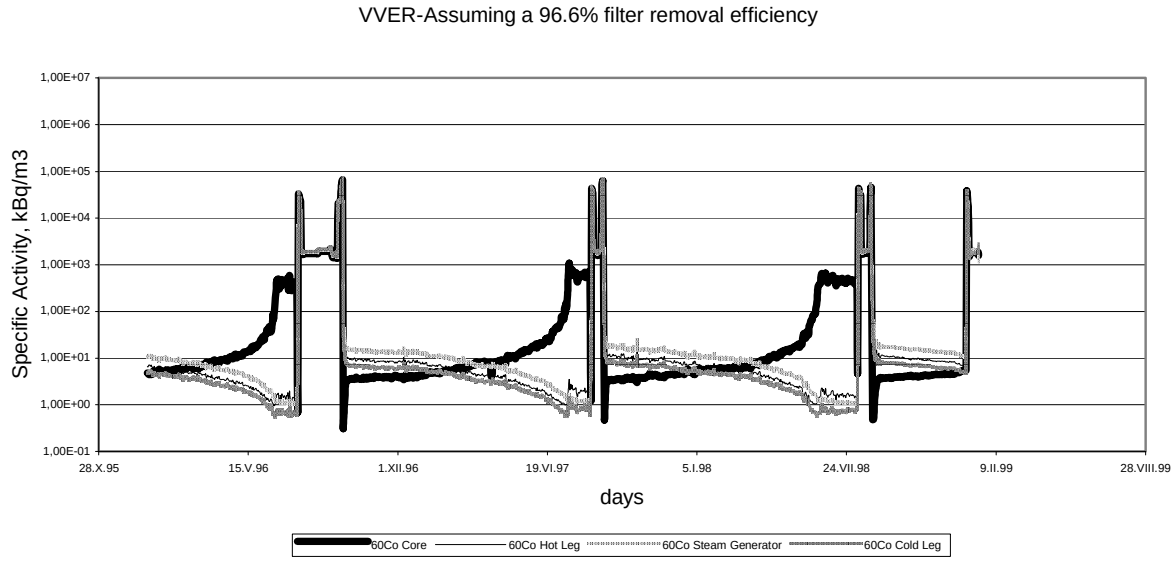

FIG. 68. Specific activity for ^{60}Co versus real time (cycles).

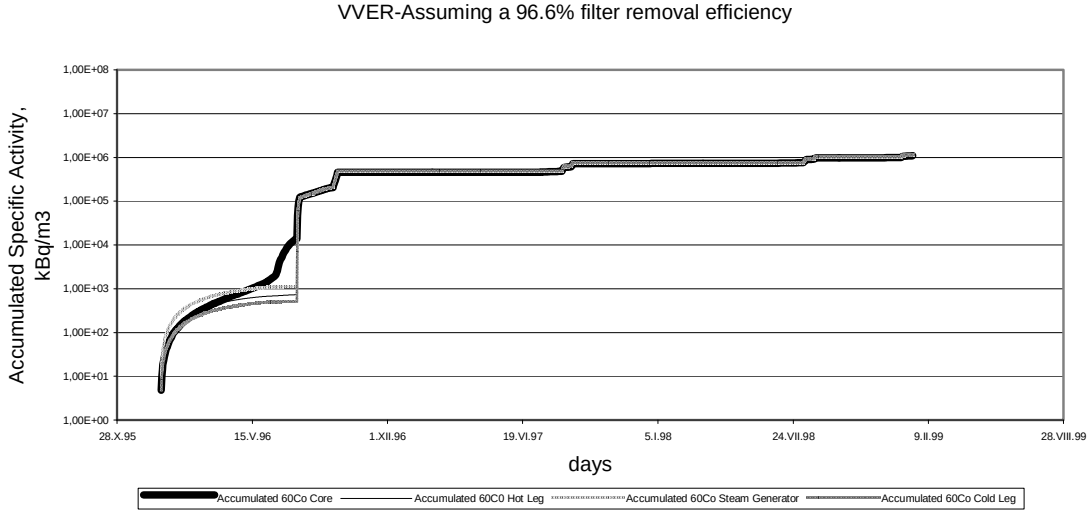

FIG. 69. Accumulated specific activity for ^{60}Co versus real time (cycles).

The data generated with the deterministic model (Figs 68–69) were used to train the ANN. Then the net was used to predict the specific activity in the same WWER, except that the ECP was arbitrarily increased during the shut down periods to 0.57 V_{she} (i.e., 0.15 V more positive than the normal shut down condition), as might be achieved by injecting an oxidizing agent into the primary coolant (Figs 70–71). Those two figures clearly demonstrate the importance of the ECP, which to certain extent can be controlled with water chemistry. Thus, Fig. 70 predicts that the day-to-day, ANN-simulated specific activity for ^{60}Co during shut down is reduced by a factor of 10–100, when the ECP during the same period is increased by a modest 0.15 V. Likewise, as shown by comparing Fig. 69 and Fig. 71, model predicts that the accumulated activity after four cycles will be reduced by a factor of about ten, which is a significant amount. If this prediction can be confirmed by additional modelling and field testing, control of the ECP during shut down and also perhaps during operation may prove to be an effective means of mitigating activity transport and the development of radiation fields external to the cores of water cooled nuclear reactors. However, this conclusion is based upon meagre modelling work to date and hence it must remain tentative.

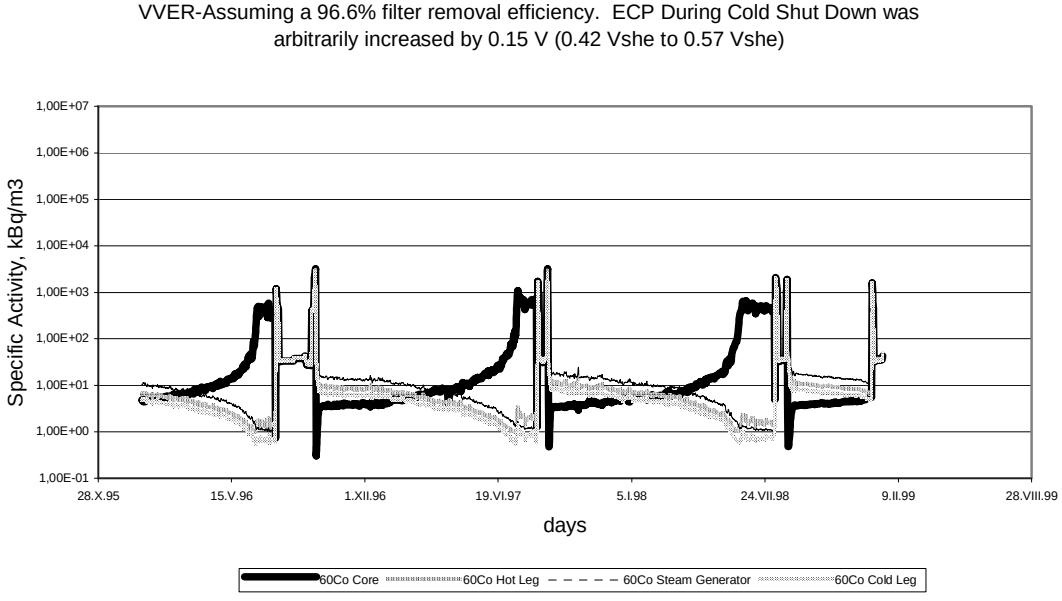

FIG. 70. Simulated specific activity for ^{60}Co versus real time (cycles) in a WWER in which the ECP during shut down was increased by 0.15 V.

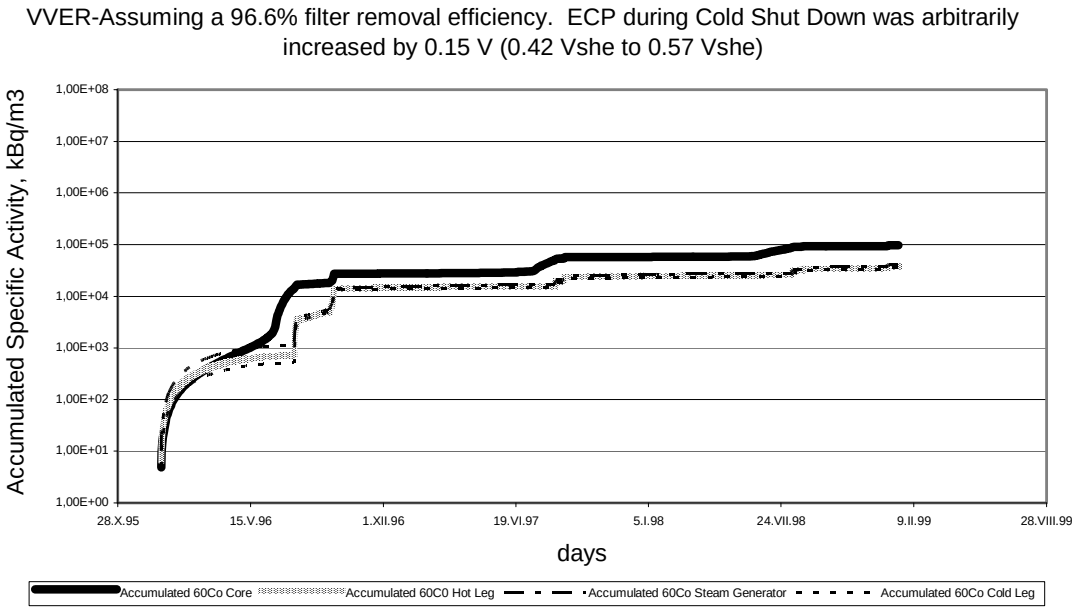

FIG. 71. Simulated accumulated specific activity for ^{60}Co versus real time (cycles) in a WWER in which the ECP during shut down was increased by 0.15 V.

Figs 72–73 show the specific activity and the accumulated activity for ^{60}Co as predicted by the ANN-simulation of a German PWR. The specific activity is predicted to be considerably lower than that calculated for the WWER. Experimental data not shown in this paper confirm our findings. Notice that the same filter clean up system efficiency for ^{60}Co was adopted in both types of reactor. However the main difference in the results reflects the different water chemistry employed in the two reactors, given that the wet area and the initial ^{59}Co in both reactors are comparable (differ by no more than 10–20%, which is not sufficient to explain the results).

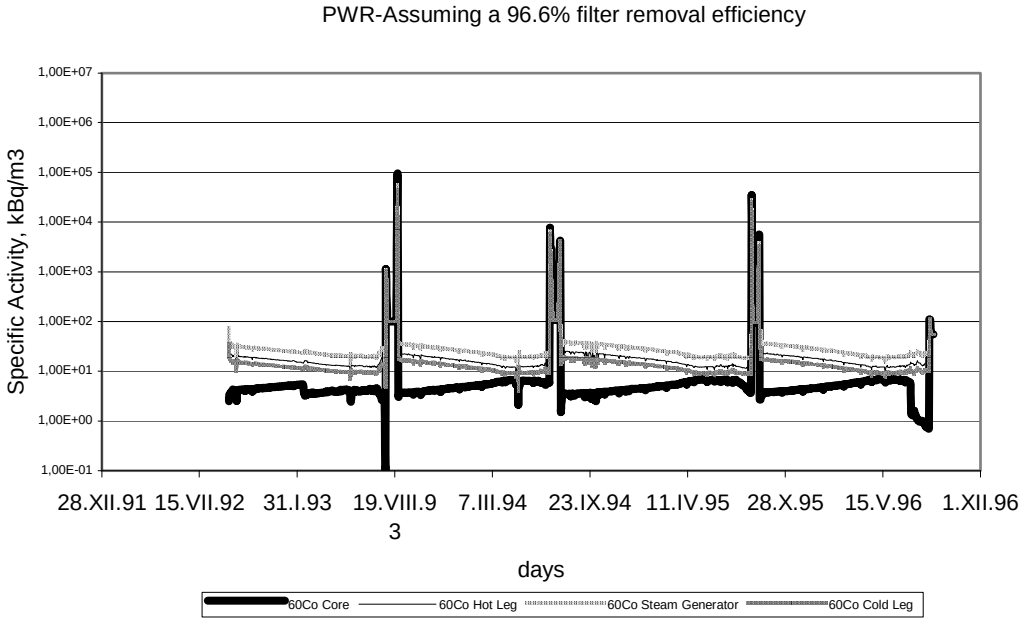

FIG. 72. ANN Simulated specific activity in a PWR for ^{60}Co versus real time (cycles).

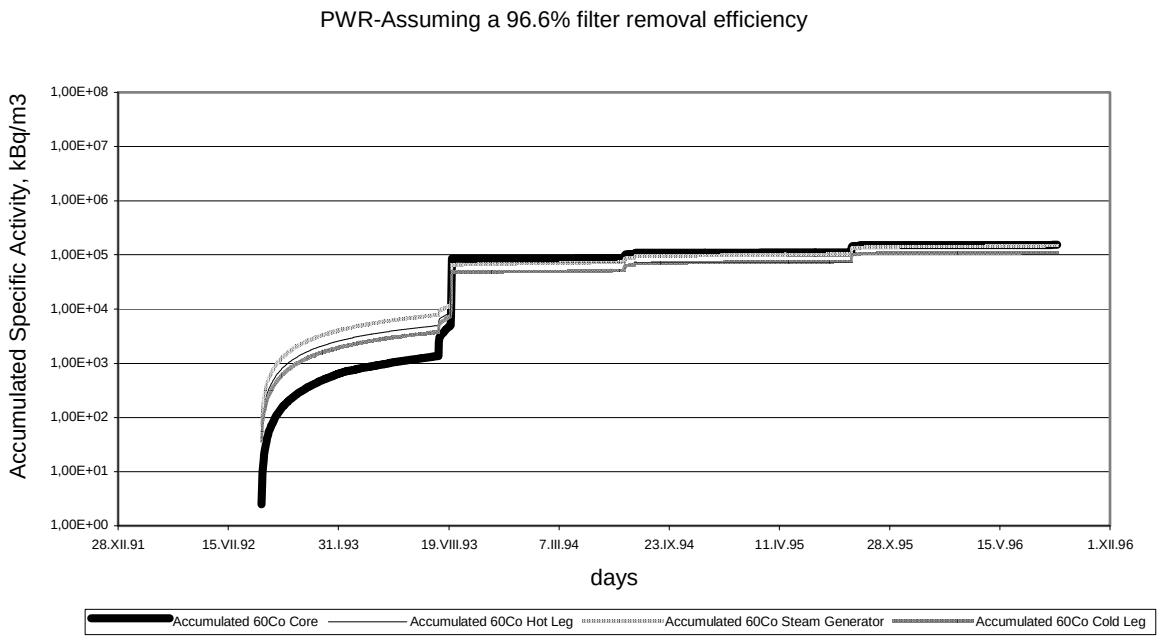

FIG. 73. Simulated accumulated specific activity in a PWR for ^{60}Co versus real time (cycles).

5.2. Assessment of model calculation results

While the results of the blind benchmarking are encouraging, clearly, the French PACTOLE code should work well for French PWRs such as CRUAS. The Japanese code ACE should work less well for CRUAS-1 since the latter uses rate constants in its models based on Japanese PWR operating data. Neither code should work well for Russian-designed WWER reactors. Similarly, DISER, MIGA-RT and RADTRAN should work well for WWER plants.

As noted in the above presentations, it is tempting to provide some figure-of-merit for how well each code has fitted the plant contamination data. A statistical analysis using the method of least squares to fit a polynomial to the predicted versus measured contaminations is possible with considerable work since each case is different, e.g. CRUAS-1 ^{58}Co comparison for PACTOLE is different than for ACE, and so forth. Given the complexity of the codes and the large number of variables in them, it is not helpful to the code developers to be given a correlation coefficient since it does not tell them what variable they might consider to improve the fit.

Many discussions with the codes' authors indicate that further improvement is unlikely unless sufficient funding can be found in either national nuclear power programs or from international sources, e.g. the IAEA. Such funding has become increasingly difficult to obtain and it may be that the codes as used here are unlikely to improve significantly in their present form. The discussion of codes in an earlier Section has suggested simpler codes with purely mechanistic models as the way forward. Realistically, no code author is willing to abandon his code for this approach because of the large investment in resources that has gone into code development.

A large database was built in this CRP to support the code calculations. The database required that the code authors be given design data to input into their code and that operating chemistry and reactor power data be provided so the codes could be run. The codes were run for short operating times with fixed chemistry, and then the chemistry was changed as given in the chemistry database. The chemistry and power data all had to be digitized before they could be used.

Many of the participants in the CRP were developing codes or were encouraged to develop codes in their national programs during the course of the work shown here. Some interesting aspects of the work from other participants are noted here.

(1) The Indian participant (an R&D engineer) was encouraged to contact other organizations in his country that apparently had a large database on chemistry and contamination data from their operating CANDU plants.

(2) The Argentine participant had an activity transport code specific to the Atucha power plant that was being used to predict the effect of a change in materials on plant radiation fields. This code was too specific to be used for other PWRs.

(3) The Canadian participant had developed a purely mechanistic activity transport code 25 years previously. However, his more recent work had shown how important the presence of carbon steel and its magnetite corrosion product were to radiation field control in CANDU plants. This understanding was of little value when applied to PWRs with their large SS and high-nickel boiler alloys and no attempt was made to run the old code for them. Published design data for CANDU plants were provided for future code development work.

(4) The RADTRAN code for WWERs is mechanistically-based and similar to the old Canadian code. Its successful application to WWERs is encouraging for the development of such purely mechanistic codes. This code was used in contract work with the Indian power plant program to describe their CANDU plants and results are published.

(5) The Westinghouse CORA-II code developed in the 1980s was well-documented from EPRI-sponsored contract work, and was of great interest to the CRP, but no participant could obtain it.

(6) Many of the codes in the present CRP were not run for all cases due to competing demands on the participants from their employing organisations.

(7) The American participant is a physicist and mathematician who came to the CRP with no initial background in activity transport. However, by the end of the CRP she had published an extremely important paper, which took into account the change in redox potential between the in-core and out-of-core regions and its effect on iron oxide solubility.

(8) The Russian participant in the CRP had a strong practical background in materials corrosion in high temperature water in power plants and had finished a monograph on this topic by the time the CRP work was completed [76]. This work is a good source of corrosion rate data for various materials for code developers to draw upon in future work for WWER plants.

6. SENSITIVITY STUDY

6.1. Description of sensitivity analysis principles

A sensitivity study was proposed to be performed within the frame of the CRP in order to demonstrate the reaction of code calculation to pre-defined changes in the input data sets. It was proposed to use only the total out-core value of the activity calculated after 7 cycles for the CRUAS-1 reactor. The following scenarios were proposed and tested:

Surfaces (8 cases)

- to change the value for the surface in pile for ± 10% of the normal value;
- to change the value for the surface in pile for ± 50% of the normal value;
- to change the value for the surface out of pile for ± 10% of the normal value;
- to change the value for the surface out of pile for ± 50% of the normal value.

Materials (2 cases)

- Inconel space grids to be changed into zircoloy;
- with the value 0 for the SS under the neutron flux.

Purification rate (2 cases)

- to change the value for ± 100% of the normal value.

Cobalt content (5 cases)

- to change the value for the in core SS surface for ± 50% of the normal value;
- to change the value for the out of core SS surface for ± 50% of the normal value;
- to change the value for the stellite surface out of the flux as the nominal value +5 m^2.

Reaction rate (2 cases)

- to change from a data set that will be provided by France for CRUAS 1 to ± 50%.

Corrosion rate or Release rate (depending on the codes) (2 cases)

- to change the value for the rate for ± 50% of the normal value.

Role of the pH (2 × 4 cases)

- for CRUAS-1 (change in lithium concentration) from pH=6.8–7.4 (0.2);
- for EBO/Loviisa (change in potassium concentration) from pH=6.8–7.4 (0.2).

Particle deposition rate (2 cases)

- to change the value for rate for ± 50% of the normal value.

6.2. Sensitivity analysis results

6.2.1. ACE code

Sensitivity analysis of ACE code was performed for selected parameters of the CRUAS-1 and EBO-1 plants. Results are shown in Fig. 74. They can be summarized as follows:

- Response was proportional for changes of surfaces, corrosion and reaction rates and stellites.
- There was very weak response for change of SS grids to zircoloy and for zero SS incore surface.
- Effect of increasing $pH_{(300)}$ is monotonous decrease of activities, more pronounced for CRUAS case and for ^{58}Co.

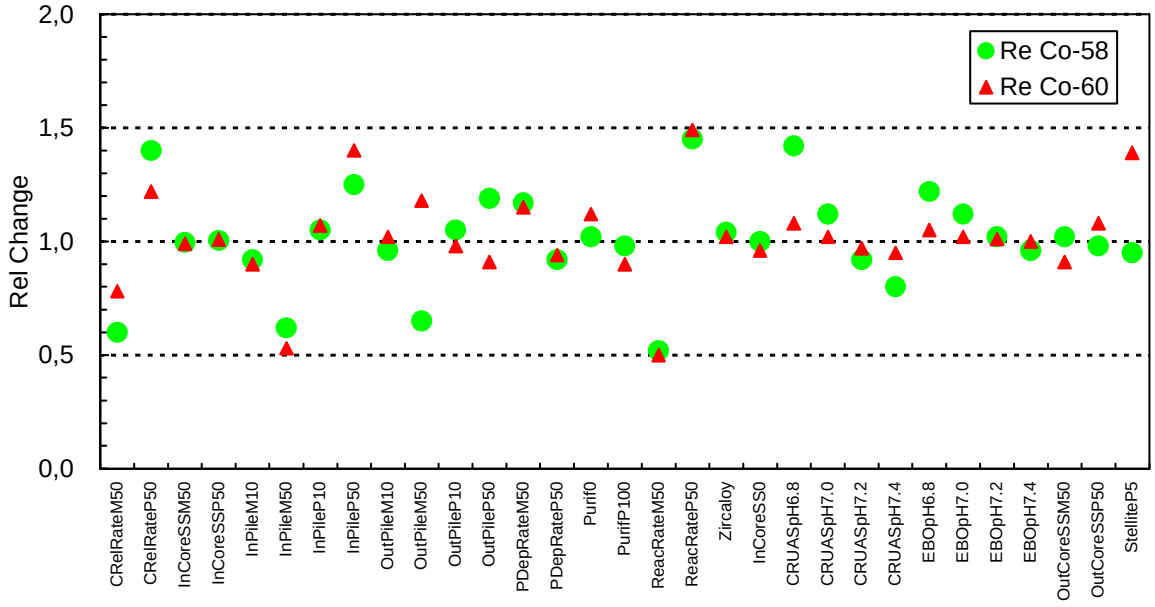

FIG. 74. Total ^{58}Co and ^{60}Co out of core activity behavior.

6.2.2. CRUDTRAN code

The CRUDTRAN code was applied to the sensitivity analysis of the selected parameters for the CRUAS-1 Plant. Results are shown in Fig. 75. These can be summarized as follows:

- For the surface area, ^{58}Co and ^{60}Co activities of the SG decreased with the core surface area. Reduction of out-of-pile surface area also decreased the SG activity, but it gave smaller effect than the core surface area.
- For the purification rate changes, the effect of purification rates on the SG activities was very small.
- For the cobalt content of the construction materials in primary system, cobalt content in the materials rather than the surface areas of the materials were changed. Change in the cobalt content in SG tubes had the biggest effect on the activity since the fractional surface area of SG is highest. Stellite also has very significant effect on the ^{60}Co activity.
- For the reaction rate, the surface activity has an exact linear relation with the reaction rate.
- For the corrosion or release rate, dissolution rate of corrosion product into the coolant was changed. 50% decrease of dissolution rate decreased the activity by 24–27%.
- For the pH, low pH resulted in higher activity. Operation at pH 7.2 decreased ^{60}Co activity by 16% while operation at pH 6.8 increased ^{58}Co activities by 30%. The dependence of ^{58}Co and ^{60}Co activities on pH are different, due to the difference in their decay constants. For the pH 7.4 case, CRUDTRAN predicted the extreme reduction of the activity due to the reversal of the iron solubility variation with the temperature. That is, at pH 7.4, iron solubility increases with the temperature, so that a primary driving force for the crud transport from out-of-core to in-core does not exist.

Particle deposition rate does not influence the activity since the primary type in the crud and activity transport is the soluble. For the effect of spacer grid, CRUDTRAN does not have specific models for the spacer grid.

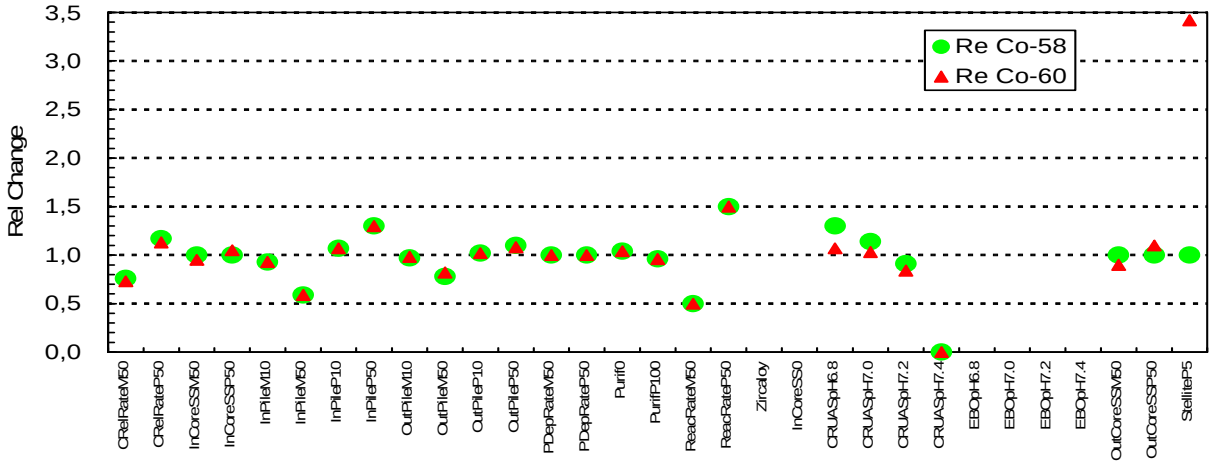

FIG. 75. Total ^{58}Co and ^{60}Co out of core activity behavior.

6.2.3. DISER code

Sensitivity study results for set of variables are given in Fig. 76. The main conclusions are following:

Most of the changes were proportional in response

Response was very small for:

- change of filtration rate in moderate range;
- change of out of core cobalt.

Response was strong for:

- reduction of out core surface by 50%.

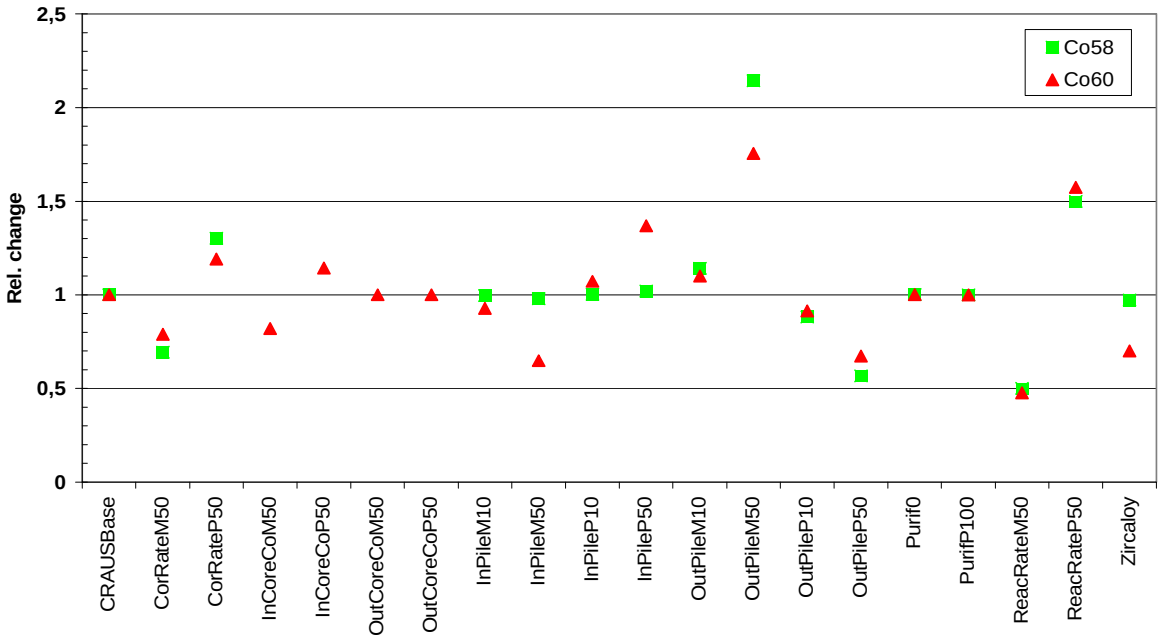

FIG. 76. Total ^{58}Co and ^{60}Co HL activity behavior.

6.2.4. *MIGA RT code*

A sensitivity study was performed for two data sets – EBO-1 after first cycle and EBO-1 after 16th cycle. For the study of $pH_{(300)}$ deviation, a value of 7,1 was taken as a base level. Calculations were performed separately for HL and CL surfaces. Results are shown in Figs 77–78. These results can be summarized as follows:

- There is no significant difference between hot and CL surfaces
- Response was proportional for release and reaction rate changes
- There was no response for in-pile and out of pile surface changes
- Response was strong for purification rate changes
- Surface activities are monotonously decreasing with increasing $pH_{(300)}$

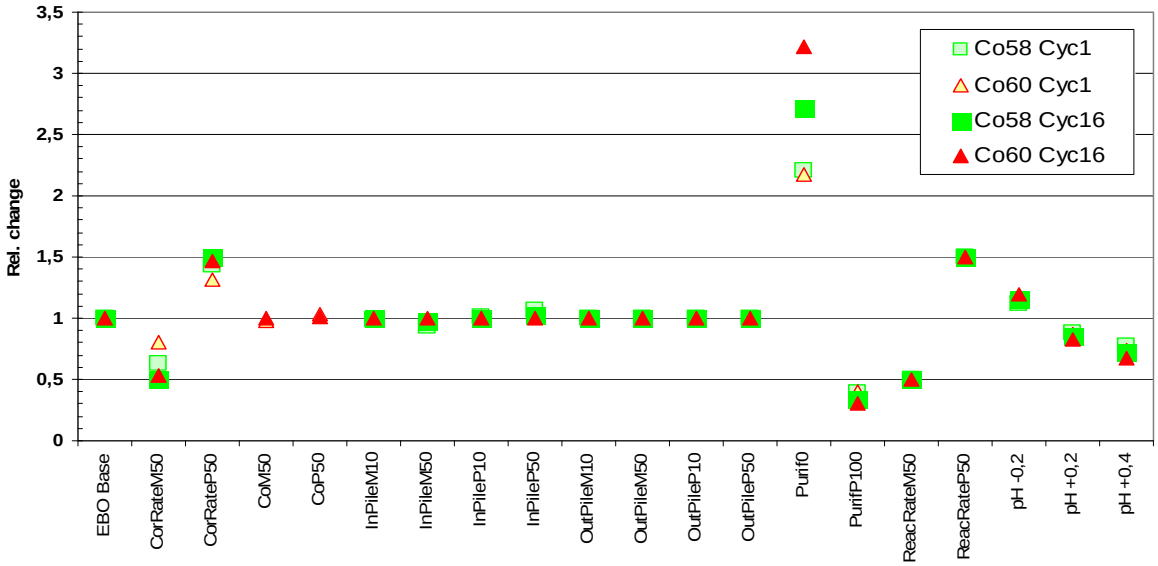

FIG. 77. *^{58}Co and ^{60}Co HL activity behavior.*

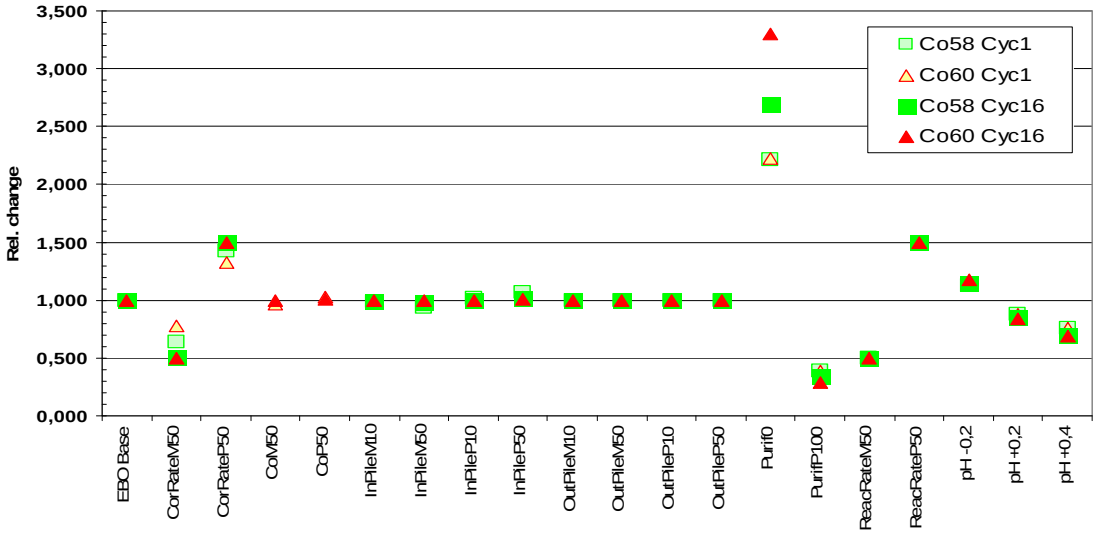

FIG. 78. *^{58}Co and ^{60}Co CL activity behavior.*

6.2.5. PACTOLE code

Results of the sensitivity study are shown in Figs 79–80. Analysis of results obtained is divided into two parts, the first one taking into account design parameters (surface, materials) and the second one the chemical conditioning of the primary coolant.

6.2.5.1. Design parameters:

The activities deposited in ^{58}Co and ^{60}Co out of pile are directly proportional to the reaction rates. The variation of 50% of the SS surface under neutron flux has no effect on contamination out of pile in ^{58}Co and is low for that in ^{60}Co (10%). This can be explained by the low initial surface under neutron flux in SS, as indeed the fuel grids are made of zircaloy and the springs are made of Inconel 718.

The activities deposited in ^{58}Co and ^{60}Co out of pile are directly proportional to the variations of the surface under flux since the mass of corrosion product deposits likely to be activated is proportional to the surface of the deposits in-pile. This is the same for the activity under neutron flux and eventually of out-of-pile contamination.

The activity deposited out-of-pile per surface unit in ^{58}Co and ^{60}Co only slightly changes with the surface variation out of pile, which means that the total activity deposited out-of-pile is proportional to this surface. The largest source of corrosion products comes from the release of these surfaces out-of-pile, the mass of corrosion product released in the primary circuit water is nearly proportional to this surface and thus eventually the total activity in ^{58}Co and ^{60}Co which will be re-deposited out-of-pile.

The out-of-pile contamination is nearly proportional to the release rate of the parent isotope. The variation of the purification rate has a lower effect on ^{58}Co than on ^{60}Co. This is due to the fact that the cobalt concentration in most of the primary circuit regions is lower than its concentration at equilibrium, and thus a non-negligible fraction is eliminated by the purification circuit, which is not the case for nickel.

6.2.5.2. Chemical conditioning:

The parametric study carried out for CRUAS-1 shows that the simulation with operation at a constant pH 7.2 at 300°C gives the lowest contamination in ^{58}Co and ^{60}Co. This is the best chemical conditioning, as it corresponds to the minimum of solubility for iron and nickel at core entry. These values are very close to those obtained by simulating the chemical conditioning actually applied, which is normal as this is the one recommended and applied at best to the operating restrictions imposed by EDF on its reactors.

The conditioning at pH 6.8 and 7.4 gives the highest contamination values for ^{58}Co; the concentrations at equilibrium of iron and nickel at core entry are the highest. This leads to the greatest deposition of corrosion products and highest in pile activities.

Within the framework of the LOVIISA parametric study, the activities deposited out of pile greatly increase (especially for ^{60}Co) for simulations at pH 7.0 and 6.8. This increase is explained by a significant increase in the concentrations at equilibrium calculated by the PACTOLE code for these pH values at operating temperatures of this reactor, which are much lower that those of CRUAS. These concentrations at equilibrium calculated by the code have not been experimentally validated in this temperature range.

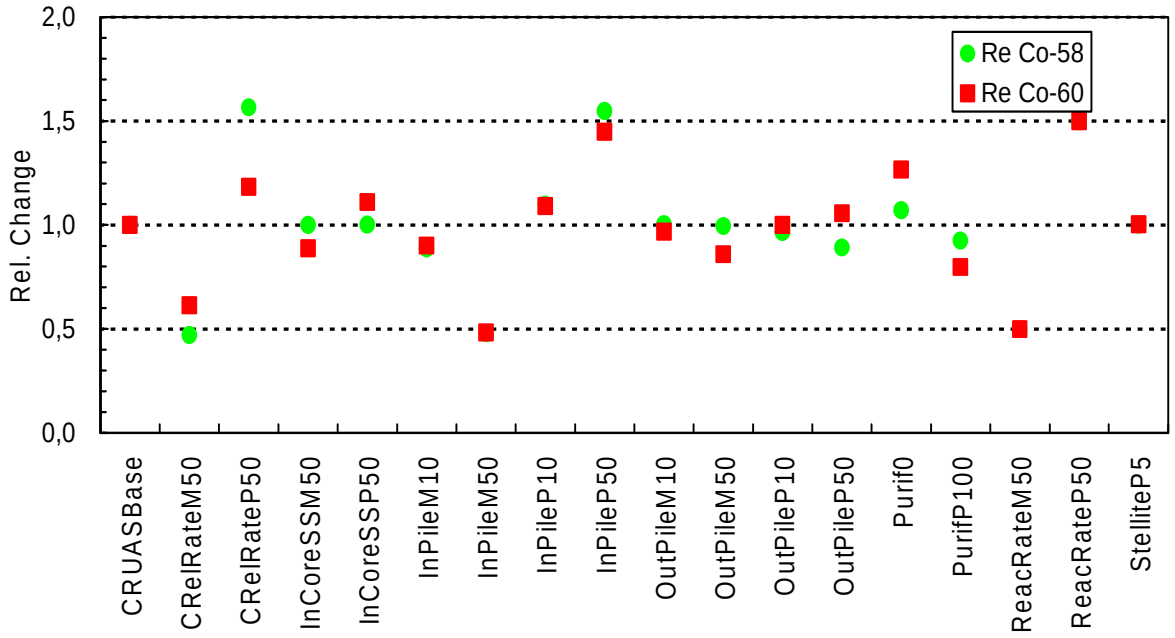

FIG. 79. Total ^{58}Co and ^{60}Co out of core activity behavior.

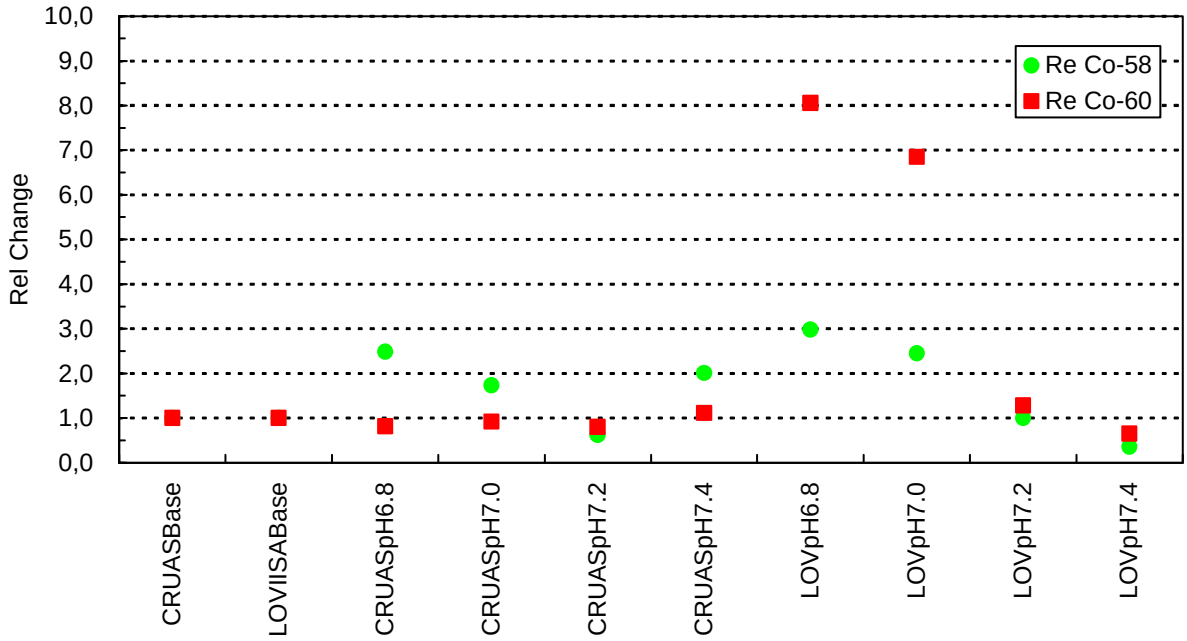

FIG. 80. Total ^{58}Co and ^{60}Co out of core activity behavior.

6.2.6. RADTRAN code

Sensitivity analysis was performed on the CRUAS-1 and EBO-1 cases. Results of the sensitivity analysis are shown in Figs 81–82. These can be summarized as follows:

For ^{60}Co:

- Most of the changes were proportional in responses
- Response was very small for increase of filtration rate in moderate range
- Response was small for change of particle deposition rate and in-core SS surface
- Response was strong for
- filtration rate (no filtration case) – activity increase more than 100 × (out of picture scale)
- for in-core dissolution driving force (pH(T) effect)
- Different responses for CRUAS-1 and EBO-1 were obtained for
- In core SS surfaces (CRUAS proportional, EBO-1 -no response)
- In-pile surfaces - outer layer for EBO weak positive.

For ^{58}Co:

- Results were similar except for in-pile surfaces, where outer layer for EBO response was weak negative.

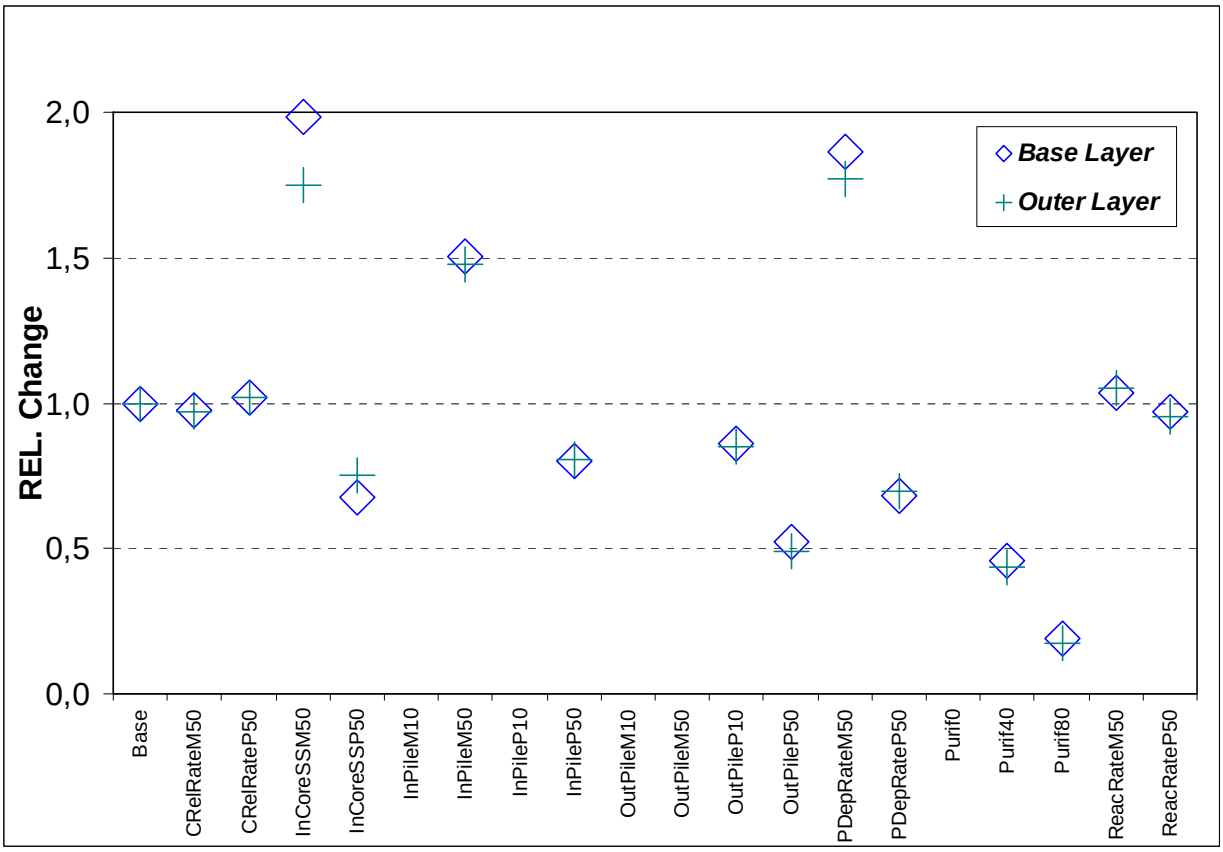

FIG. 81. Total ^{58}Co out of core activity behavior.

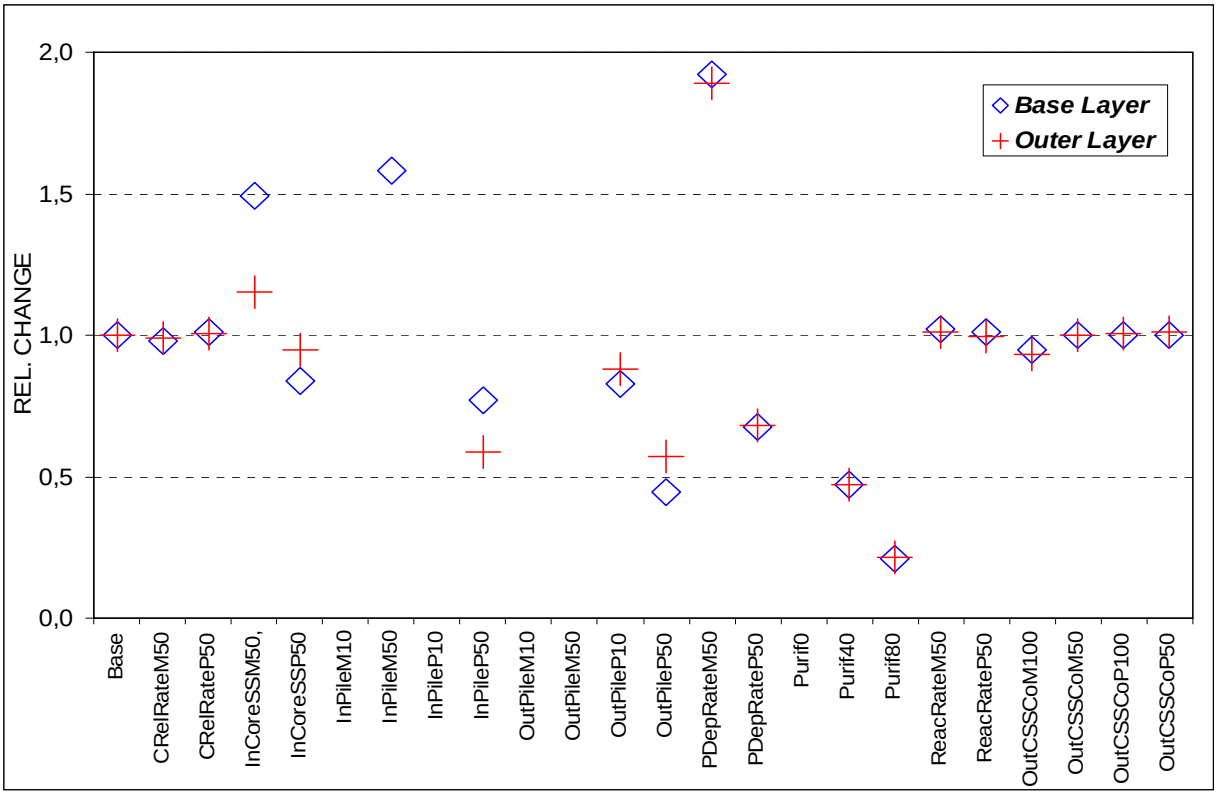

FIG. 82. Total ^{60}Co out of core activity behavior.

6.3. Summary evaluation of sensitivity study

Based on these results the following conclusions can be made:

Agreement between the various codes and the plant contamination data was generally good, e.g. with +/- 50%, but some codes agreed better with one dataset than another, illustrating the large effect of the different models within each code on its predictions.

Material corrosion rate and release rate are among the most important parameters in the models since they determine the source of the corrosion products that enter the coolant. Selection of materials with the lowest possible corrosion rates and release rates combined with material compositions that provide the smallest source of neutron-activatable material will minimize activity transport and radiation field growth on out-core surfaces.

In many models, purification flow rate to either a filter or to an ion-exchange bed has a negligible effect on the rate of radiation field growth during plant operation. However, high purification flow during surface prefilming before initial start-up is essential to limit the amount of crud available for driving activity transport.

All codes show the strong effect of water pH on activity transport. The importance of pH arises from its determination of metal oxide solubility and the change in solubility with temperature.

The change in SG material from Inconel 600 to Incaloy 800 and its effect on activity transport is not well-predicted by the codes when compared with plant contamination data.

Predictions from the simplest code compared as well with plant data as did the most complex codes. The simplest code is built around the transport of dissolved species created by metal oxide dissolution around the heat transport circuit and their removal by precipitation.

7. FURTHER DEVELOPMENT OF MODELS AND CODES FOLLOWING THE COMPLETION OF THE CRP

7.1. Development of existing models

7.1.1. PACTOLE model

Significant development of the PACTOLE code has been undertaken in recent years. The latest PACTOLE code version, namely V3.0.f takes into account developments in the modelling of corrosion product behaviour, and was released in 2003 [98]. The V3 version of the PACTOLE code was completely reengineered and is intended to evolve as soon as new developments are available. Written in a fully object-oriented design, the PACTOLE V3 code is modular and easily evolving. The consequence on the PACTOLE V3 development was the implementation of a numerical solution for the corrosion product transport equations.

Combined with a fully object programming language (C++), the PACTOLE V3 code has been written and designed using the Unified Method Language. Thanks to its code architecture, and confirmed by the development of a mock-up, the latest PACTOLE version is an easy evolving computer tool in which new media can be added and in which new models can be tested. Moreover, the class management process, introduced in the PACTOLE code, allows a non-limited number of control volumes, isotopes and fuel cycles. The only restriction comes from the memory of the computer on which the code runs.

Based on a control volume approach, the primary circuit is represented by an arrangement of several volumes in which mass balance equations are solved. As shown in Fig. 83 which shows a typical nodalization of a primary circuit, the loops are gathered into one because a homogeneous contamination is assumed for the loops. Nevertheless, the loops can be individually computed in order to study, for instance, the effect of SG composition or surface treatment on contamination repartition between loops. The primary circuit is composed of one mainstream line to which derived circuits (like the CVCS) are connected. The reactor core can be multifold (e.g. threefold or fourfold), depending on the fuel management.

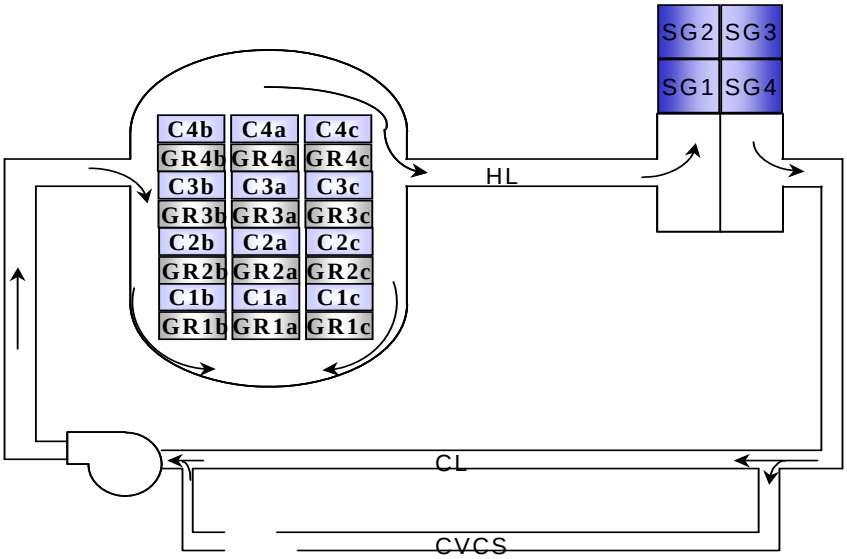

FIG. 83. Typical representation of a PWR primary circuit.

For each control volume, representing a part of the primary circuit, input parameters are relevant to geometrical aspects, thermohydraulics considerations and material properties. Since the PACTOLE code is based on control volume approach, the only requested geometrical parameters are hydraulics diameter and wet surface. The later is defined as the surface that can be oxidized and on which corrosion products can be deposited. Concerning thermohydraulics data, classical parameters such as fluid velocity, flow rate and fluid temperature have to be provided. Furthermore, wall temperature is of major concern, since corrosion product equilibrium concentrations depend on the wall temperature gradient along the primary circuit. For material properties, the metal composition of each part of the primary circuit has to be given. In addition, surface roughness and surface treatments that appear to have a large influence are provided in term of release and corrosion rates. Obviously, corrosion product activation in reactor core is directly proportional to the neutron flux. Thus the power fraction, relative to the nominal power, has to be specified with care in every part of the core. Reactor operating conditions, which may impact primary circuit contamination, are also provided in the PACTOLE input data. These data can be summarized as follows: power history, water chemistry (Li, B(pH), dissolved hydrogen) and reactor shutdown.

7.1.1.1. Form of corrosion products in a control volume

Although the PACTOLE code is based on a control volume approach, different physical states can be found in one control volume, also called region. These states, called media in what follows, have different behaviours and corrosion products concentrations and can interact. Fig. 84 displays the different media that can exist in a control volume.

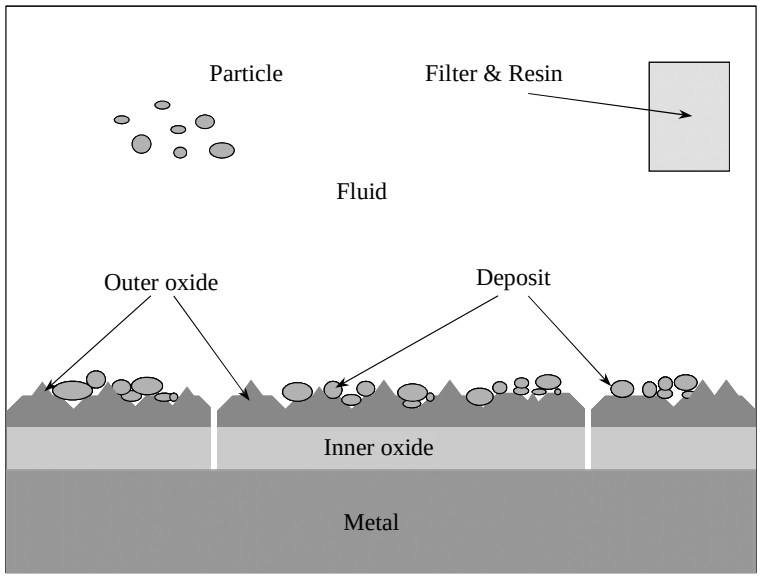

FIG. 84. Media in a control volume for a PACTOLE representation (fluid means ions).

Directly produced by metal oxidation, the inner oxide is an enriched chromium layer. Dense and relatively thin, it is a low soluble oxide and acts as a protective barrier against metal oxidation. The outer oxide, more soluble in reactor operating conditions than the inner oxide, is mainly composed of nickel ferrite. As a result of metal oxidation combined with ion precipitation, the outer oxide becomes contaminated by the incorporation of activated corrosion products. (Corrosion of zirconium base metal is not accounted for in the PACTOLE code).

Released from base metal, ions are carried by the fluid in the different part of the primary circuit where they can precipitate in bulk, producing particles, which form another medium. Both particles and ions, which can be activated when crossing a core region, can respectively deposit on piping walls or precipitate on either the deposit or the outer oxide. Finally, a peculiar medium, which aims at cleaning the primary circuit, can be represented: the filter and ion exchanger resin devices.

7.1.1.2. Main models

Major phenomena, which are involved in corrosion product transport, are accounted for in the PACTOLE code. The transfer mechanisms between all considered media are summarized in Fig. 85.

.

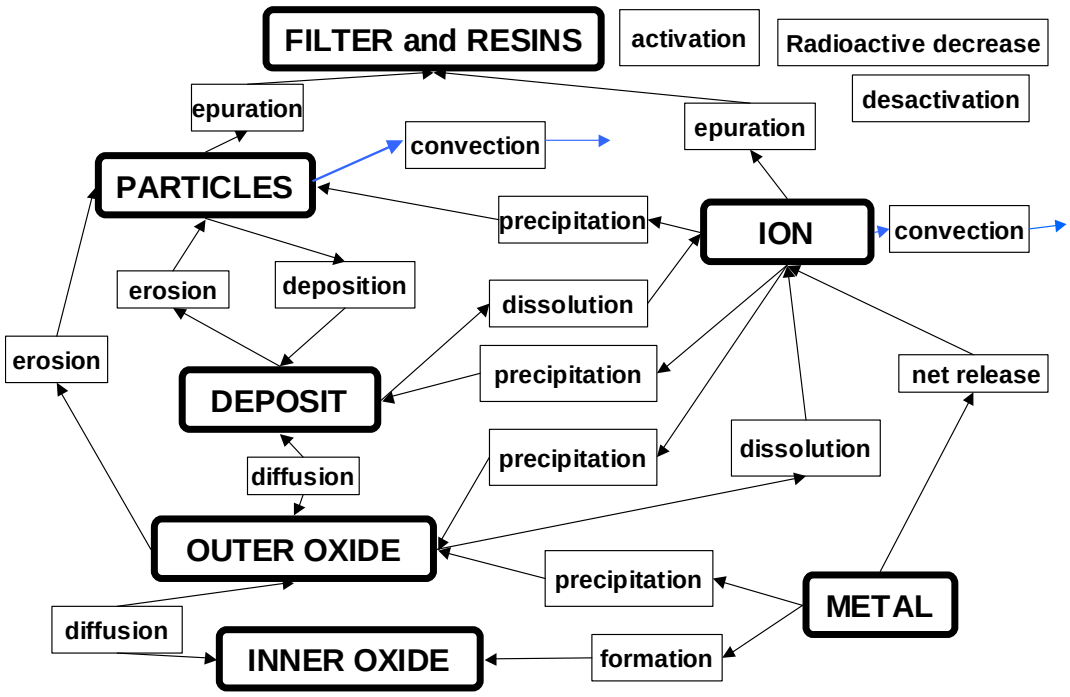

FIG. 85. Main mass transfer processes in the PACTOLE code.

7.1.1.3. Corrosion, ion release and ion incorporation in oxides

In the proposed modelling, corrosion is the process by which the base metal becomes oxidized. This oxidation leads to several mass transfers which are: generation of an inner oxide, generation of an outer oxide and release of metallic ions directly in the fluid. These transfers are shown in Fig. 86. In the PACTOLE V3 code, corrosion and release mass transfers are, respectively, directly dependent on a corrosion and release velocity, which are defined by the user. The experimental background results from a common work between EDF, Framatome-ANP and CEA. For the outer oxide, the incorporation mechanism of ions is described as a function of the release velocity. This modelling allows accounting for the impact of the material surface treatment on the oxide contamination.

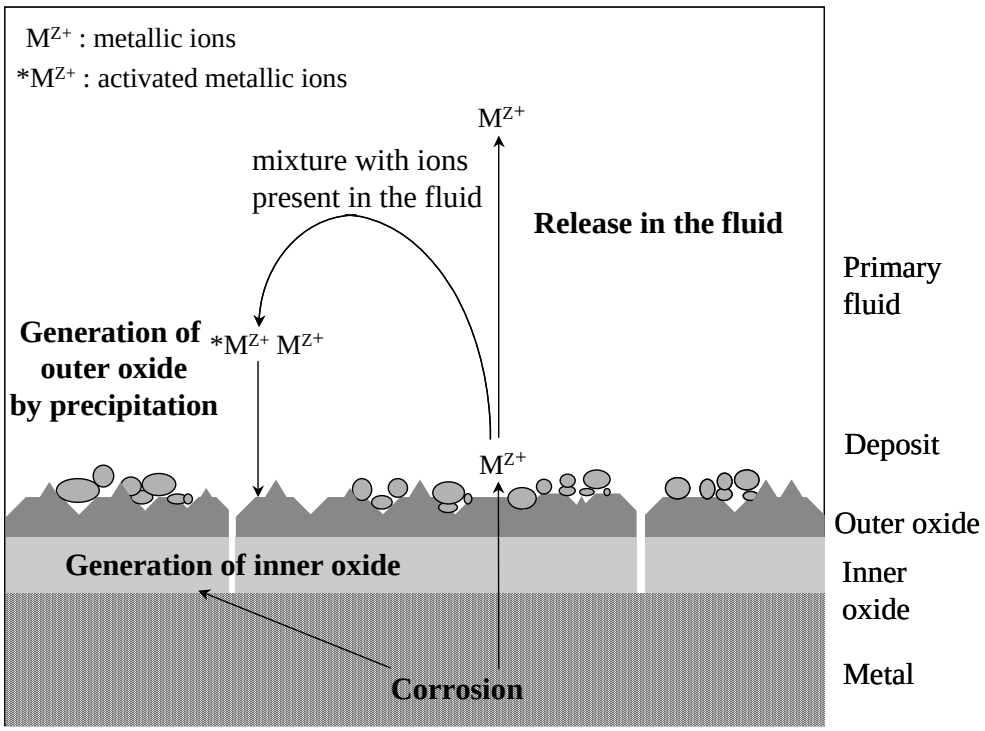

FIG. 86. PACTOLE local modeling for inner and outer oxide generations and ion release.

7.1.1.4. Ion and particle transport

After being released from the base metal, metallic ions are transported in the primary circuit. Since solubility depends on temperature and water chemistry, metallic ions can reach regions where their concentrations exceed the local saturation and therefore precipitate on wall surfaces or in bulk, forming particles. When the ion concentration is below saturation, dissolution of the oxide and deposit occurs. Corrosion products, transported by the fluid in particulate form, deposit on wall surfaces when they are submitted to Brownian and turbulent diffusion and to thermophoresis effects. This last effect is important in SG tubes where the thermal gradient between the fluid and the wall is high and positive. Moreover, particles are assumed to follow a log-normal probability function in PACTOLE modelling. Both deposited particles and oxides can be eroded when hydrodynamics forces become higher than those from adhesion. Erosion produces new particles in the bulk fluid, which can be transported by convection to the other regions of the primary circuit. Concerning the erosion process, PACTOLE modelling assumes that above a threshold deposit thickness, deposits and oxides may be eroded. The key point of these interactions, between the wall surfaces and the fluid, occurs when the deposit/oxides are submitted to a neutron flux (in-core regions). Indeed, deposited corrosion products become activated and therefore can be again transported in out-of flux regions of the primary circuit where they contribute to the dose rate.

This model has been already tested on data sets from different French PWRs. The comparison of the simulations made with the PACTOLE code with on-site measurements of deposited activities demonstrates a reasonable agreement between numerical simulations and experimental data. Nevertheless, further calculations have to be performed with other reactors and with experimental loop results to get a good picture of the code capabilities. Further code developments are already ongoing. These include improvement of physical models for corrosion release mechanism, oxide composition, shutdown process modelling with their rigorous validation using set of validation cases.

The model continues to be upgraded and the current version, PACTOLE V3.2 [99], is based on the arrangement of control volumes as shown in Fig. 87. Therefore, the PWR primary system is discretized into several volumes or regions defined according to the geometric, thermohydraulic, neutron, material property, and operating characteristics. The primary system is composed of a main line (blue volumes in Fig. 87) to which various lines and circuits are connected, e.g. the chemical and volume control system (CVCS). The loops of a PWR primary system are generally considered as one main loop (see Fig. 87) but it is possible to differentiate between them to take into account, for example, the state of a different surface of the SG tubes.

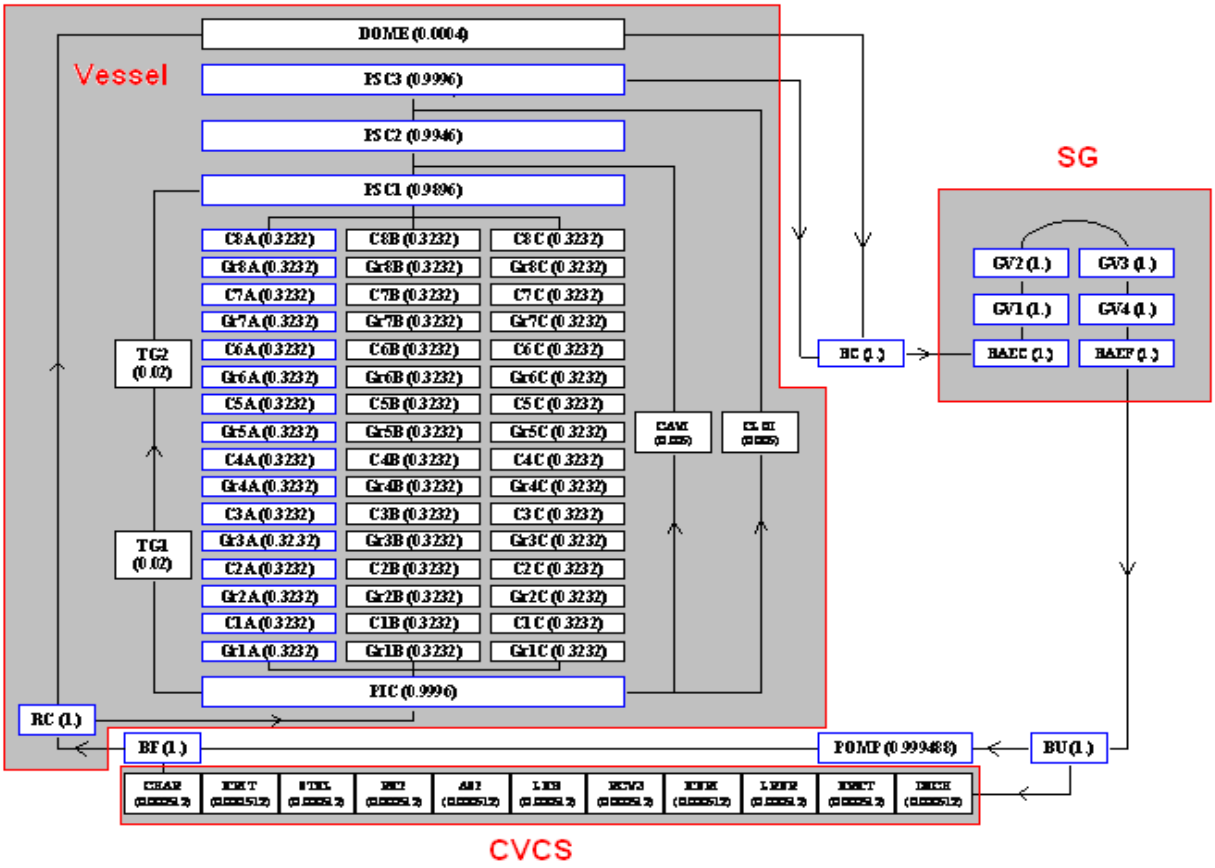

FIG. 87. Representation of a PWR primary system and a CVCS in terms of control volumes.

The behaviour of the corrosion products in each control volume is modelled by the mass balance equation for each isotope in each medium

$$\frac{\partial m_i}{\partial t} + \left(\dot{m}_{out} - \dot{m}_{in}\right) = \sum_{Source} J_m - \sum_{Sink} J_m$$

With m_i representing the mass of the isotope (i) in a given medium, and t representing the time, m_{out} -m_{in} the convection term and J_m representing the material flux between 2 media (except for nuclear reactions that represent a mass transfer inside the same medium). The different transfer mechanisms taken into account in the PACTOLE V3.2 mass balance equations are indicated in Fig. 85.

Corrosion of the base metal leads to the formation of an inner oxide layer on the one hand, and to the supply of ions in the primary coolant (net releases) and the formation of the outer oxide layer on the

other hand. The formation of this outer layer is partially due to the ions coming from the base metal that precipitate after mixing with the ions in the boundary layer. Therefore, radioactive ions in the coolant can be incorporated into the outer oxide layer even in a saturated medium. This modelling is based on a pragmatic approach [99] for which the parameters – especially corrosion and release rates – are determined on the basis of test loop experiments.

The dissolution of the deposit or the outer oxide layer can occur when the concentration of ions in the coolant is below the equilibrium concentration. The dissolution phenomenon is controlled by the transport kinetics of ions on the wall into the bulk of the coolant (mass transfer coefficient), by the oxide transformation kinetics, and by the concentration gradient.

Ions precipitate when their concentration in the coolant is greater than the equilibrium concentration. This occurs near a precipitation site, i.e. near already-existing oxide, and thus near particles but especially near the wall. Ions therefore need to be transported to near the wall or other particles before precipitating.

The equilibrium concentration of each chemical element is calculated with the PHREEQC code [100] in combination with a thermodynamic database developed by the CEA and coupled with PACTOLE.

This chemical module determines the composition of the ideal solid solution to model 1) a mixed oxide, 2) any pure solid phases possibly in excess (mainly metal nickel), and 3) the molar quantities of each element in equilibrium, for each control volume and in relation to the chemical conditions, the coolant temperature, and the masses of the metallic elements.

The particle deposit term is a deposit rate that takes into account:

- Turbulent diffusion and the effects of inertia [101],
- Sedimentation for horizontal ducts [102],
- Thermophoresis for temperature gradients between the coolant and the wall [103].

The erosion term involves the erosion of particles composing the deposit resulting from the coolant friction forces. The PACTOLE code model assumes that the deposit can be eroded above the laminar sub-layer.

The diffusion mechanism occurs between the inner oxide layer and the outer oxide layer, as well as between the outer oxide layer and the deposit. This mechanism follows Fick’s law.

The activation or decay term describes the production or disappearance of an isotope through nuclear reactions or by radioactive cooling. Nuclear reactions occur in areas of the primary system subjected to neutron flux and are a function of the microscopic rates of these reactions.

The convection term describes the transport of particles or ions in the primary coolant through the different primary system control volumes. More specifically, this term is a function of the coolant flow rate.

Finally, the purification term takes into account the trapping of particles and ions during their passage through the filters and demineralizers of the CVCS. This term is a function of the flow rate and the filtration efficiency

To run the PACTOLE V3.2 code, it is necessary to provide a set of input data containing the following main data:

- The geometric parameters of a control volume are the hydraulic diameter and its wet surface.
- The thermohydraulic data such as the velocity, flow and temperature of the coolant must be indicated, as well as the wall temperature.

- The materials are defined by their density, their chemical composition and their roughness. Any possible surface treatment is taken into account via the experimental corrosion and release rates.
- As the activation of the corrosion products is directly proportional to the neutron flux, the power fraction is specified in each part of the core.

In terms of the operating data, a cycle is defined by its duration, its power history and its concentration levels in boron, lithium, hydrogen and oxygen

PACTOLE V3.2 was tested by the simulation of CRUAS-1 unit. The 900 MWe PWR, CRUAS-1 (CPY standardized plant series), is equipped with three SGs whose tube bundle is made of the 600 TT alloy. Simulation of CRUAS-1 includes 196 regions, 168 of which are for the core. The core is divided into 12 sections to take into account 1/3 reloading, and then ¼ reloading from the 4th cycle (see Fig. 87). Fig. 88 and Fig. 89 compare the deposited activities for the two main radioelements (^{58}Co and ^{60}Co) calculated using PACTOLE V.3.2 with the deposited activities of the EMECC measurements [104] for the HLs and the SG tubes (coldside).

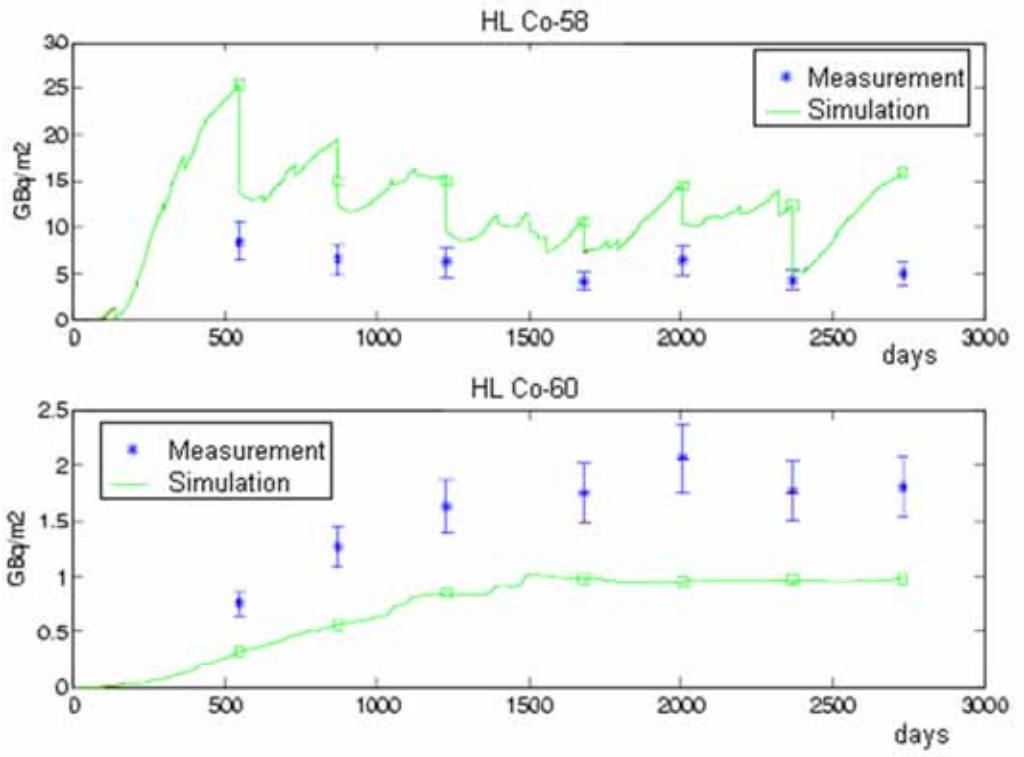

FIG. 88. CRUAS-1 – Activity deposited in the HLs.

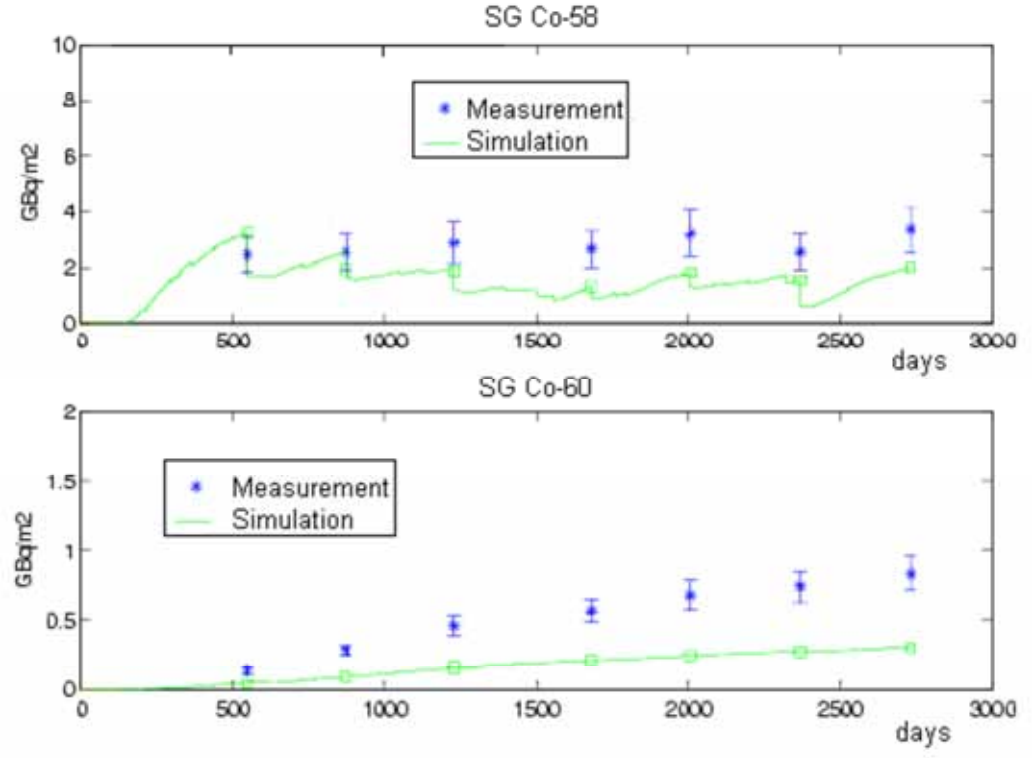

FIG. 89. CRUAS-1 – Activity deposited in the in the steamgenerator tubes (cold side).

In relation to the ^{58}Co activity measurements, the CRUAS-1 simulation overestimates the contamination in the HLs by a factor of 2–3 and in the SGs by a factor less than 1.7.

The CRUAS-1 simulation underestimates the ^{60}Co activities deposited in the HLs by a factor of 2 and in the SGs by a factor below 1.7.

Comparisons between simulations performed with the PACTOLE code and measurements taken in PWRs show that variations in the activities deposited in the primary system are generally consistent with experimental feedback. The activity levels deposited for ^{58}Co and ^{60}Co – the two main contributors to dose rates around the primary system – are about the same order of magnitude as the EMECC site measurements (ratio generally below 5). In relation to the experimental values, the volume activities calculated for ^{58}Co and ^{60}Co are underestimated by a factor of 10 or less.

Simulations of the impact of certain design or operating parameters demonstrated that the code behaves consistently with experimental observations. They therefore confirm or explain the results of studies focusing on feedback.

The difference between the calculated figures and the experimental measurements can therefore be significant but is greatly reduced in relation to previous versions of the code, and new improvements are expected for the future versions. In order to validate the code and improve the modelling of activated corrosion products behaviour, comparisons between experimental results obtained with the CIRENE loop and simulations with the PACTOLE V3.2 code were also carried out [104].

CEA, in collaboration with EDF and AREVA NP, has carried out an R&D program for many years involving specific experiments related to the development and validation of the PACTOLE code. Among them, the CIRENE out-of-pile loop is dedicated to the study of activated CP deposits on fuel rods and on SG tubes. This pressurised water circulation loop corresponds to a PWR coolant system at a scale of 1/7000. The outlines of the CIRENE facility required for the test are presented on Fig. 90.

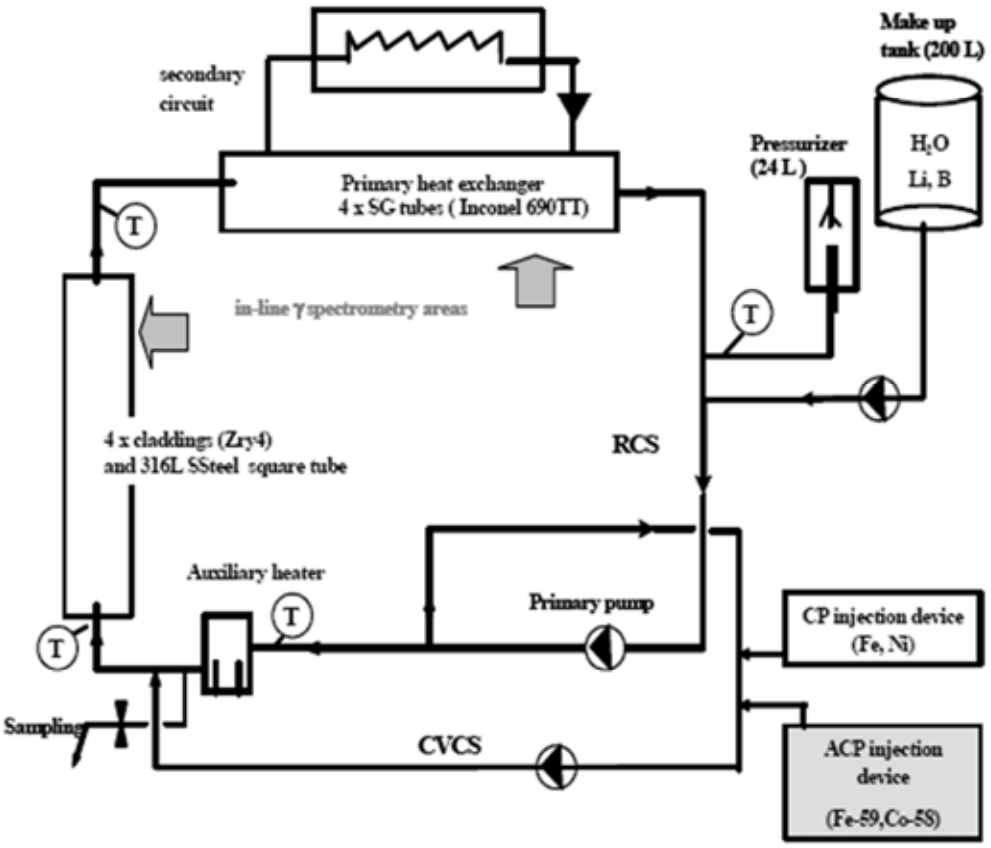

FIG. 90. CIRENE loop outlines required for the test.

A 30 day test has been performed at this loop to compare the experimental results from CIRENE loop with numerical simulations obtained with the PACTOLE V3.2 code. This test has been carried out with thermal-hydraulic parameters corresponding to a subcooled boiling regime at the outlet of the core section, and chemical conditions representative of a French PWR primary circuit. A radioactive tracing methodology have been applied, using gamma spectrometry measurements with the injection of specific radiotracers, ^{58}Co and ^{59}Fe: in-situ gamma spectrometry measurements were performed at the outlet of the core section and the SG tubes, while frequent radiochemical analyses of the primary fluid were carried out for checking the instantaneous mass balances. Assuming that the rapid shutdown with dT=197°C /10 min without any oxidation led to a weak dissolution of the deposits in the upper part of the core section, then for this area, the calculated activities at 30.45 days could be compared with those measured after shutdown. The values to be compared are shown in Table 5.

TABLE 5. DEPOSITED ACTIVITIES CALCULATED AT T=30.5 DAYS AND MEASURED AFTER RAPID SHUTDOWN FOR THE CIRENE TEST

	PACTOLE V3.2 calculation	Experimental measurements after shutdown on claddings and square tube
	CONTROL VOLUME [SE4_I] : CORE OUTLET	
^{58}Co	75	82 +/- 27%
^{59}Fe	40	50 +/- 15%
	CONTROL VOLUME [ECF] : SG TUBES OUTLET	
^{58}Co	13	12 +/- 3%
^{59}Fe	1.7	1.5 +/- 9%

Note: Activities are given in Bq·cm^{-2} (1×10^{-5} GBq·m^{-2}).

A good agreement was observed between the “calculation" and “measurement" values, and more especially on the SG tube section, which had already been demonstrated by direct comparison of the activity profiles as shown in Fig. 91.

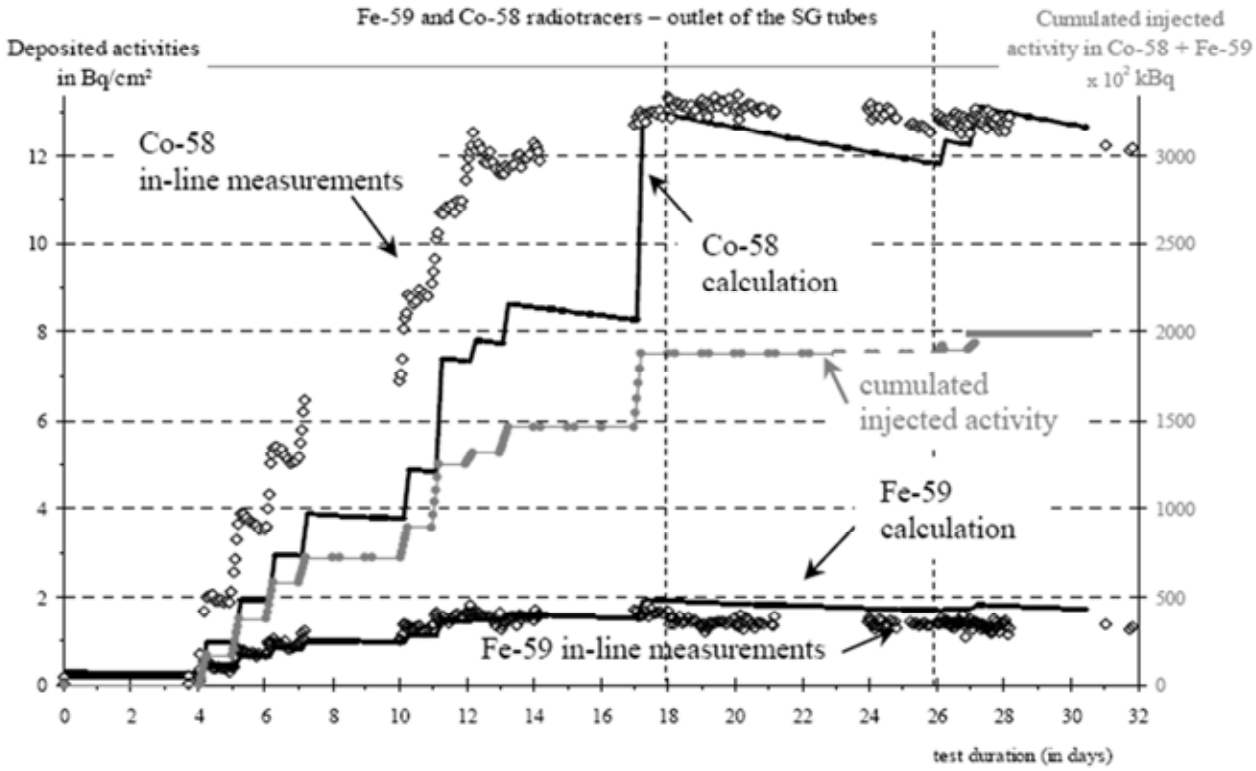

FIG. 91. ^{59}Fe and ^{58}Co deposited activities at the outlet of the SG tubes section for calculated (PACTOLE V3.2/4h-time step) and in-line measurements.

In Table 6, the masses of deposited corrosion products on the "core" section calculated at 30.5 operation days are compared with those measured after shutdown using characterizations of the cladding and

square tube scrapings. It should b4 noted that this relates to the characterization of a labile remained deposit resulting from a rapid shutdown without oxygenation. The relevant control volumes are [SE2], [SE3] and [SE4], corresponding to the under-flux area as depicted on Fig. 92. As a result, the same order of magnitude of surface density in the upper part of the claddings was obtained, whereas a difference can be observed as soon as we examine the control volumes corresponding to the beginning of the under-flux area: it can be reasonably assumed that the rapid shutdown has led to a partial CRUD dissolution in the lower part of the core section where oxides of ferrite nickel type are preferentially formed, whereas it has preserved the Ni-enriched CRUD deposited in the upper part of the core section [104].

TABLE 6. SURFACE DENSITIES CALCULATED AT T=30.5DAYS (AS DEPOSITED CRUD) AND MEASURED AFTER RAPID SHUTDOWN (REMAINED CRUD) FOR THE CIRENE TEST

Axial elevation (cm)	Relevant control volumes	Surface densities (in 10^{-4} kg·m^2 equivalent to mg·dm^{-2})	
		PACTOLE V3.2 calculation t=30.5 days	Experimental measurements after shutdown on claddings and square tube
315	SE4_h	28	23 +/- 3.5
265	SE4_c	26.7	11 +/- 1.7
205	SE4_a	24.5	1.35 +/- 0.2
165	SE2_a	20.5	(0.8–1.5) +/- 0.2

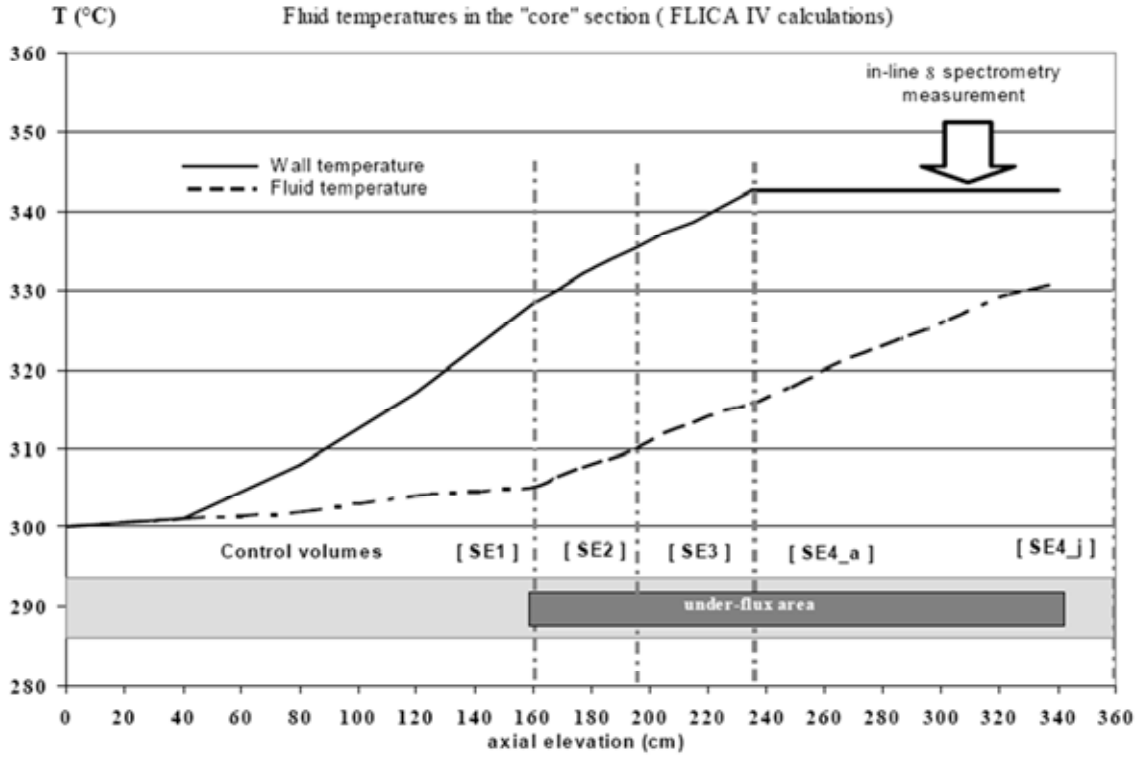

FIG. 92. Temperature profiles integrated in the input data set for the "core" section of the CIRENE test.

The CIRENE test calculations gave the following results:

Deposited activity profiles: it should be noted that, for both the core section and the SG tube section, the "calculation" profiles displayed good agreement with the "measurement" profiles. The "calculation" profiles effectively retranscribe the 11 radioactive tracer injection sequences, although sometimes the kinetics and amplitudes are different.

Deposited activity at 30.5 days: good agreement was observed between the “calculation" and “measurement" values, especially on the SG tube section.

Deposited masses at 30.5 days: the same order of magnitude was obtained between “calculation" and “measurement" (i.e. the surface density of the labile remained deposit) in the upper part of the "core" section, whereas a difference was observed as soon as the control volumes at lower axial elevations of the under-flux area were examined.

Composition of the primary coolant in activated CP and non-activated CP elements: for the non-radioactive as well as for the radioactive elements, the experimental values and the calculation agree, but only to a certain extent since the detection limits of the required analysis methods are often reached.

It is important to note that gamma spectrometry measurements combined with injection of radiotracers provide access to numerous experimental data and profiles which give added value in the comparison with code simulations.

This CIRENE test and the relevant simulations have revealed new directions in the understanding of contamination transfer phenomena and ways of improving their modelling in the PACTOLE code (contamination kinetics, temperature effects, chemical conditioning effects…).

The PACTOLE code has been developed over the past thirty years and continues to be upgraded. However, mutual interaction and relation of fission and corrosion products takes place in the real plant conditions and was not considered by any model. Therefore next major upgrade focused to the merging of the PACTOLE code with the PROFIP [105] code to create the new, advanced code. In cooperation with EDF and AREVA NP, CEA has developed the OSCAR code (French acronym for *Simulation tool of the nuclear reactor contamination*), a unique tool for simulating PWR contamination [106]. The OSCAR package results from the merging of two codes, which simulate PWR contamination by fission products and actinides (PROFIP code) and by activated corrosion products (PACTOLE code).

Development of OSCAR code package, combining the features of the two above mentioned codes was motivated by the fact that, wherever they originate from, the contamination products are subject to the same severe conditions (300°C, 150 bar, neutron flux, water velocity up to 15 $m \cdot s^{-1}$) and follow the same transport mechanisms in the primary circuit. The main processes involved are erosion/deposition, dissolution/precipitation, adsorption/desorption, convection, purification, neutron activation and radioactive decay.

The V1.1 version of the OSCAR package is qualified for fission products (Xe, Kr, I, Sr), actinides (U, Np, Pu, Am, Cm) and corrosion products (Ni, Fe, Co, Cr).

Particular focus was put on the main upgrades in the OSCAR simulations compared to the PROFIP and PACTOLE codes: adaptation of the MARGARET module to assess fission product release out of fuel pellets in a defective rod, adsorption/desorption model development for strontium behaviour, multi-criteria calibration of input data which are not well known for corrosion product simulation.

The source terms taken into account in the OSCAR V1.1 code are presented for the different types of contamination products : fission products and actinides released from defective fuel rods, fission products emitted by recoil from actinides deposited on surfaces under neutron flux (see Fig. 93), and corrosion products released from the base metal.

In case of rod cladding defect, fission products are released in the primary circuit from the fuel rod. Three stages can be distinguished in this process: release out of the rod pellets, transfer through the fuel-cladding gap and release through the defect.

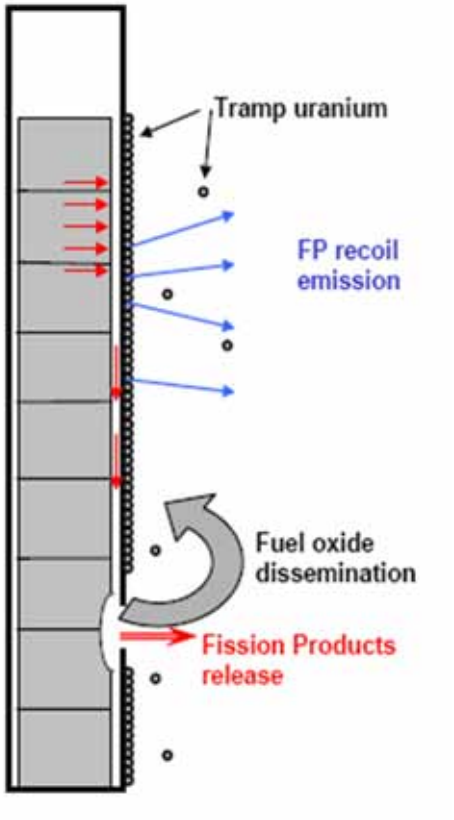

FIG. 93. Fission products and actinides release.

Considering the defective fuel rod situation, experimental data show that the fuel burnup has no impact on the radioactive fission products release from the fuel pellet. Hence the mechanisms which induce an enhancement of the release of stable gas with the burnup are not considered for defective fuel.

For defective rods, oxidation of the fuel matrix leads to released fractions much higher (by a factor of roughly 30) than for non defective fuel rods. This impact from oxidation is taken into account in the simulation by the following adjustments:

- Fraction of free surface F_{free}: it is fixed to 100%, which prevents percolation from playing any role.
- Diffusion coefficient inside the grain D: a correction factor is applied to the intrinsic stable gas diffusion coefficient used for tight fuel.
- Fuel temperature: besides the fact that for a defective configuration, water vapour replaces helium in free volumes of the rod and that the internal pressure of the rod is balanced with external pressure (no further clad creeping), a degradation of the thermal conductivity of the fuel is taken into account.

Fig. 94 gives a comparison between measurements and OSCAR calculations after calibration, concerning the released fractions from defective UO2 fuel rods of the database (including EDITH 02 and EDITH 06 analytical irradiations, respectively for low and high burnup UO2 rods). The validation domain is up to 50 $GWd \cdot t^{-1}$. Relatively good agreement between experimental and calculated released fractions was observed.

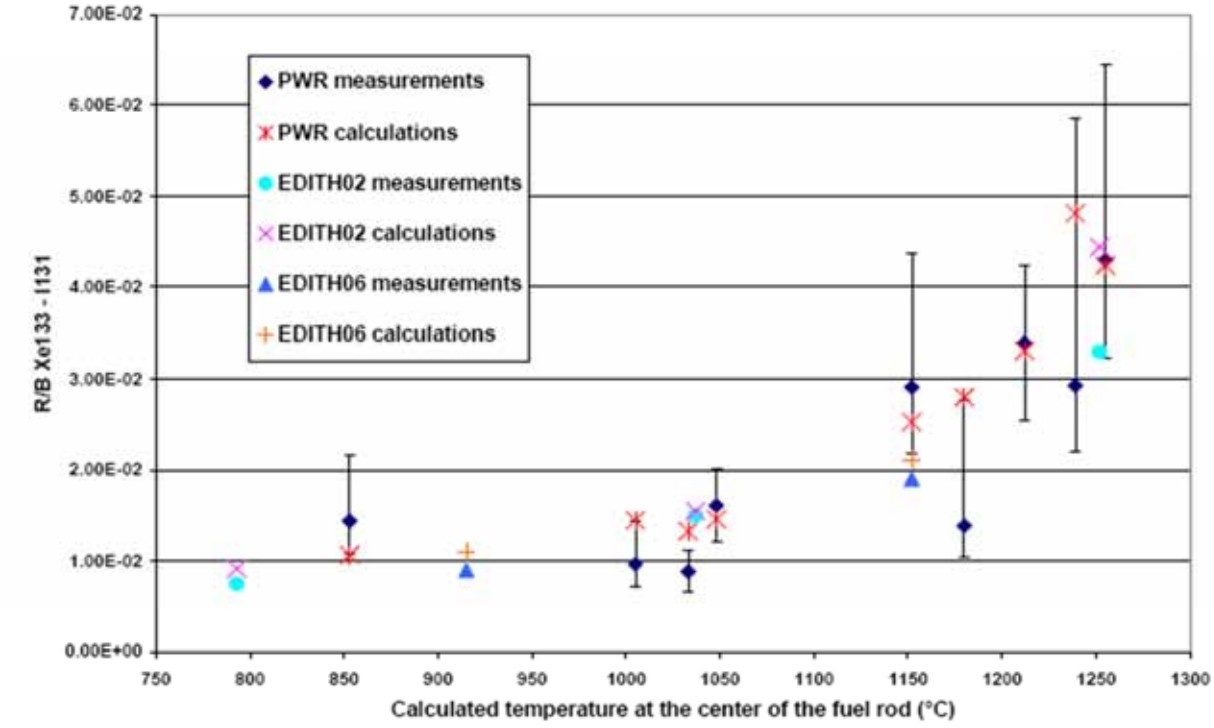

FIG. 94. Comparison between experimental and calculated released fractions for UO_2 defective fuel.

The OSCAR code can be used to assess the iodine amount which is trapped in free volumes and released during a power transient. However, it can not reproduce the kinetic of the iodine release which is observed during the transient.

For corrosion products modelling, an empirical approach for corrosion and ion release processes has been chosen, as for the PACTOLE code modelling. The main mechanisms involved in corrosion product transfer are dissolution/precipitation and erosion/deposition. As already mentioned, the modelling is the same as for PACTOLE V3, except that the thermodynamical database has been improved. Moreover, a multicriteria calibration has been performed to calibrate the parameters which are not well known. The parameters to be calibrated have been chosen as most influential. They are the following: erosion rate, dissolution kinetic, metal release (within the range fixed by the experimental results), initial deposit mass (thought to be due to the hot functional tests prior to the first cycle). Besides, an experimental program is under progress to determine the oxide dissolution kinetic [107]. Once calibrated, the OSCAR calculations are compared for the main radioisotopes (^{58}Co, ^{60}Co) to the deposited activities on HLs, CLs, SG tubes, as well as to the volume activities. As illustrated in figure 95 for ^{58}Co and ^{60}Co deposited on SG tubes, the OSCAR code provides a reasonable estimation of PWR corrosion products contamination

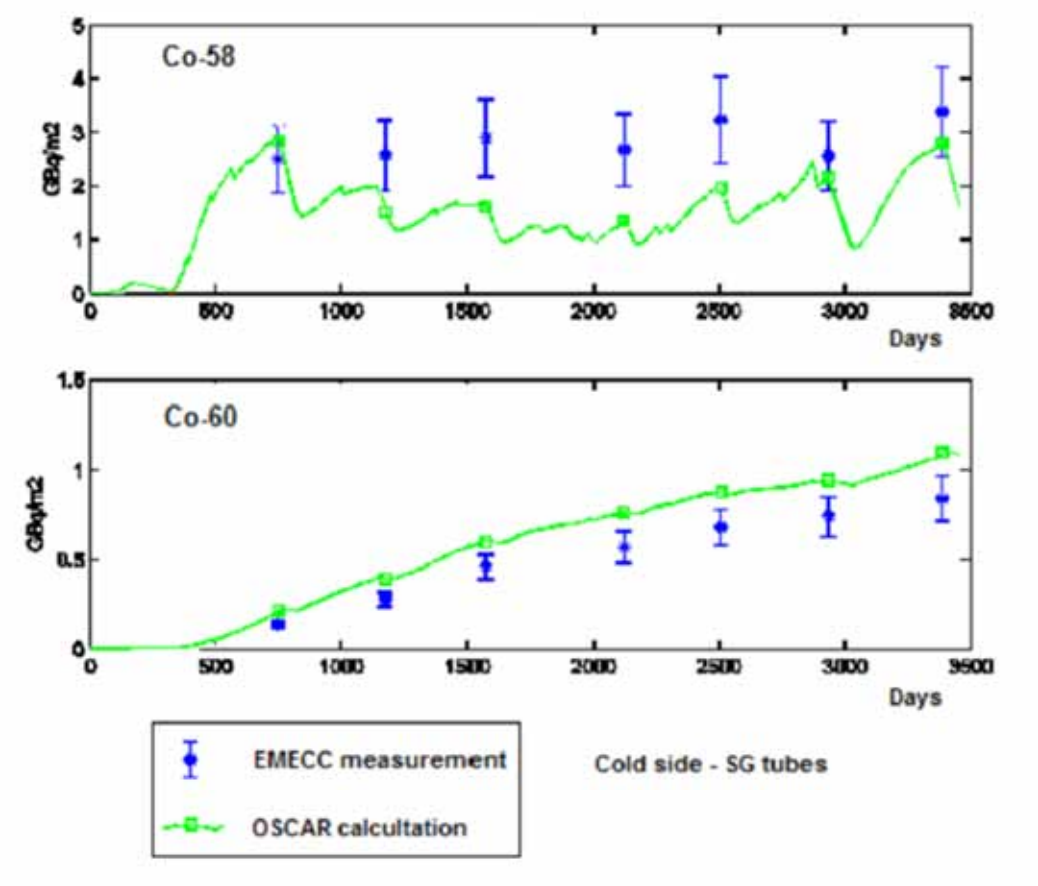

FIG. 95. Activity deposited inside the SG tubes.

In the model, the release of corrosion products in the primary circuit corresponds to several kilograms of iron and nickel, which determine the behaviour of the deposited contamination, including actinides (a few grams) and insoluble fission products (a few milligrams). The released corrosion products are transported by the coolant to the core where they can deposit on fuel assemblies. Such corrosion product deposits can be activated and subsequently set back into the coolant where they can redeposit on out-of-core surfaces and raise radiation fields. Moreover, in the case of surfaces under neutron flux, the activation mechanism (see Section 3.2.5) generates radioactive corrosion products in the base metal, which are directly released in the primary circuit through the release process

Considering the source terms and mechanisms described above, OSCAR is able to simulate the behaviour of four groups of contaminant species: actinides, gaseous and volatiles fission products, ^{90}Sr and lastly corrosion products. In the case of the presence of tramp uranium consecutive to fuel oxide dissemination, actinide contamination is a source term for fission products and must be calculated prior to fission product contamination.

Fig. 96 shows a comparison between measurements and OSCAR code calculations for ^{133}Xe primary volume activity during a PWR cycle with occurrence of a cladding defect on a first cycle rod. A fair agreement between measurements and calculations was found.

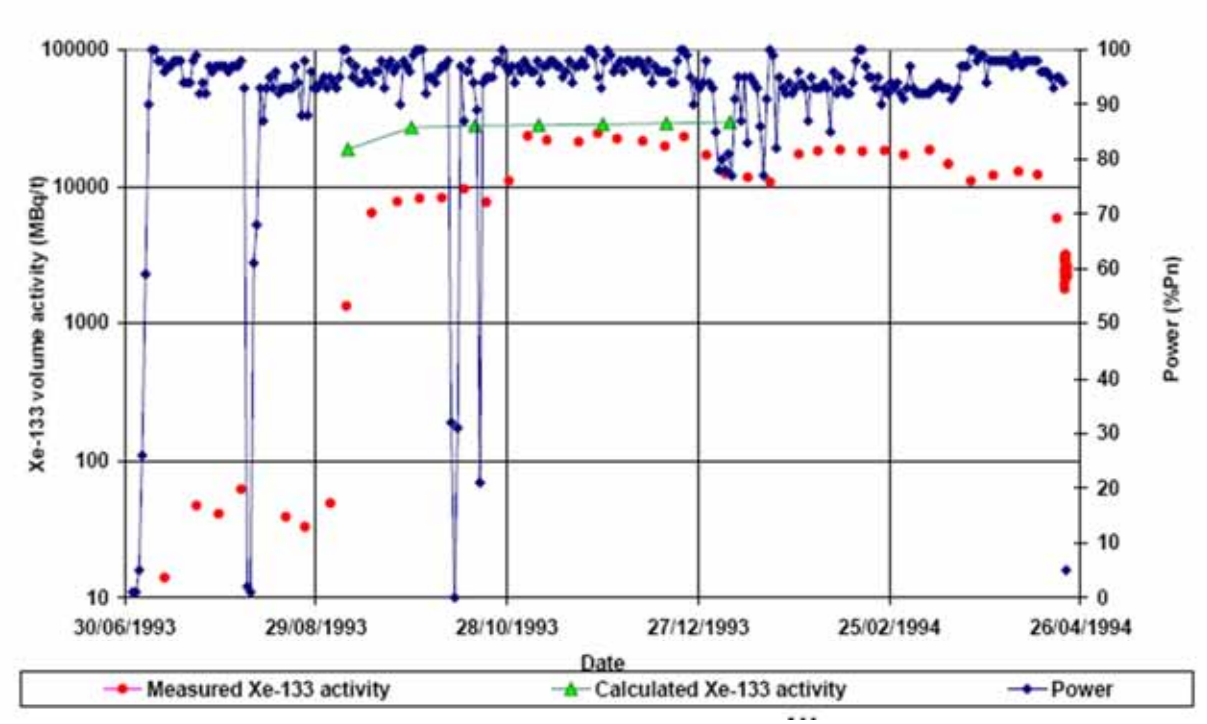

FIG. 96. Calculation/measurement comparison for ^{133}Xe primary volume activity after cladding defect occurrence.

However, in this first version of OSCAR, the fission products and actinides calculations are still independent from corrosion products calculations. In the next version, common transport of actinides and other non soluble fission products by the corrosion products will be considered, so that the erosion and deposition mechanisms will be determined by the corrosion products, even for actinides and fission products. This will allow describing simultaneously in a consistent framework the coupled behaviour of corrosion products and fission products/actinides. Further, a soluble form of actinides will be considered, especially after the primary fluid oxygenation at the end of the cycle, and the return of actinides to the water due the corrosion product dissolution. These new models will allow the simulation of alpha activity behaviour in the primary fluid during a refuelling shutdown.

7.1.2. CANDU model

While aspects of iron and radionuclide transport in the CANDU heat transport system (HTS) have previously been modelled, a single system model was never developed. Therefore development of a robust, semi-empirical system model of iron and radionuclide transport that can reproduce available plant measurements with a minimum of fitting parameters was initiated. A principal requirement was that the model should predict radiation fields at the reactor face and SGs. A semi-empirical model has been developed that can predict magnetite and radionuclide distributions around the CANDU HTS, and radiation fields around CANDU plants [108].

A principle conclusion of the model is that the magnetite deposits on CANDU HTS surfaces largely determine the spatial and temporal distributions of radionuclides on out-core surfaces, and hence the radiation fields. Magnetite deposition is the major process responsible for the observed continuous increase in the radiation fields on SGs and at the reactor face in CANDU plants. The large inventory of magnetite in the SGs mean that the SGs act a “full-flow” purification system, removing most of the circulating radionuclides, and their inactive parents, from the HTS coolant. The iron transport model reproduces both the magnitude of the observed magnetite deposit loadings and their distribution around

the out-core surfaces of the CANDU HTS. The model developed is successful in predicting plant data on radionuclide surface activities and radiation fields, especially for the SGs. While the iron transport model is based on a detailed theory of corrosion and magnetite solubility, the radionuclide deposition rates are derived empirically from station data. At least two measurements of radionuclide specific activities (Bq ^{60}Co/g oxide) are necessary to predict the future radionuclide behaviour: one from a magnetite-covered surface, and the other from a "bare" surface.

The model accurately predicts the deposit loadings and distributions for plant ages from 4.5–20 EFPY, see for example Fig. 97.

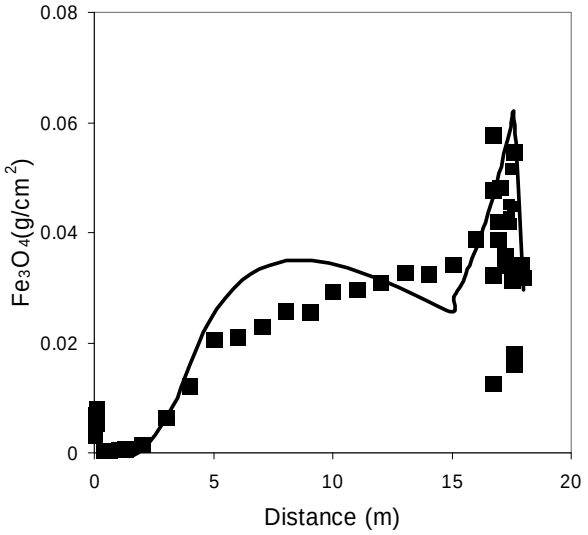

FIG. 97. Predicted (solid curve) and measured (squares) Fe_3O_4 deposition in the SG tubes from Gentilly-2 after 10.4 EFPY at pH_a = 10.7 and c_{in} = 7.36 μg Fe/kg D_2O entering SG. (The distance scale starts at the inlet of the HL and ends at the thermal plate of the SG).

No data were available against which to check the predictions for plant operating times less than 4 years. It is expected that the model might not be suitable for use during the first 1–2 years of plant operation, when steady-state corrosion and deposition had not been achieved. The good agreement with the station data shows that small variations in operating parameters such as pH_a do not need to be considered to obtain the level of agreement required by the model. (The pH_a - pH apparent - is defined to be the pH reading displayed on a pH meter, calibrated in light water buffers, for the heavy water coolant at room temperature at 25ºC). However, operation at pH_a values less than 10.2 may not be adequately modelled, as these low pH_a values are close to the region where the magnetite solubility changes from normal to retrograde. In this pH_a regime, the uncertainties in solubility data and choice of auxiliary parameters such as K_w result in large uncertainties in the model predictions. The deposit distribution around the SG is shown to be sensitive to the pH_a of HTS coolant and the initial concentration of iron entering the SG, whereas the overall magnitude of the deposition in the SG is relatively insensitive to these parameters.

While the model predicts the SG ^{60}Co fields well, it is less successful in predicting the fields at the reactor face. This is at least in part due to the changes in deposition behaviour with operating time as the magnetite deposits in the SGs grow, and to changes in the ^{60}Co concentration in the coolant as the coolant passes through the SGs. Further work is required to resolve this.

7.1.3. Modelling CIPS in PWRs

CIPS was first described as Axial Offset Anomaly, (AOA) and many papers and references refer to it as such. For most purposes the terms are used interchangeably, but CIPS is used throughout this document, except in original figures and references. CIPS has only been observed in high duty PWR cores with sub-cooled nucleate boiling when sufficient corrosion products are available for on-fuel deposition. Many plants have experienced this phenomenon, either mild or severe for one or more fuel cycles. However, other plants that have operated with aggressive thermal conditions have been free of the effect. The most severe occurrences of CIPS have been at the Callaway PWR. A schematic of the modelling logic is presented in Fig. 98 [109]. The neutronics calculated from the core map are used to derive the thermal hydraulics for the clean core. The thermal hydraulics defines the steaming profile of the core, and these data are coupled with the bulk and near-clad chemistry to develop the axial corrosion product deposition for a given channel for each burn-up step. The model considers deposition based on thermodynamic concentration, mass-transfer driven deposition, and steaming concentration processes. The result is a quantitative mechanism for deposition onto the fuel surfaces. The sources of corrosion products include not only soluble material released from the SG and other primary surfaces, but also the release and redistribution of deposits from re-load fuel, in either soluble or particulate form. Subsequent refinement of the model included feedback effects on steaming of deposited corrosion products and on neutronics from residual ^{10}B in deposited boron. In developing the model, estimates of experimental input values, such as corrosion product release from SGs, were determined from the Callaway plant. Thermal hydraulics was calculated from input data for Callaway cycles 6 and 9, two fuel cycles that experienced significant CIPS.

This EPRI fuel deposit chemistry approach (FDCA) model has been successful by itself to calculate boron deposit mass for Callaway fuel cycles 6 and 9. However, it was not possible to include the effect of neutronics feedback in the Callaway calculations. The presence of crud deposits with adsorbed boron at the surface of fuel assemblies could have an influence on the neutronics calculation and then on the local thermal-hydraulics parameters of the core because of the Doppler effect and the neutron absorbing properties of the boron.

The FDCA model was then combined with two EDF reactor core models: THYC, a thermal hydraulic model; and COCCINELLE, a model that calculates the internal neutron fluxes as a function of burnup [110]. These three models were used together to estimate the build-up of corrosion products on the core, the inclusion of boron (as undissociated boric acid) in these deposits, and the impact of these deposits and included boron on the neutronics of the core. The final output of the calculation is an estimate of the CIPS profile for the core. Using the calculation method described above, the observed axial offset of a 12-month cycle has been successfully modelled for CHINON-2 plant as shown in Fig. 99.

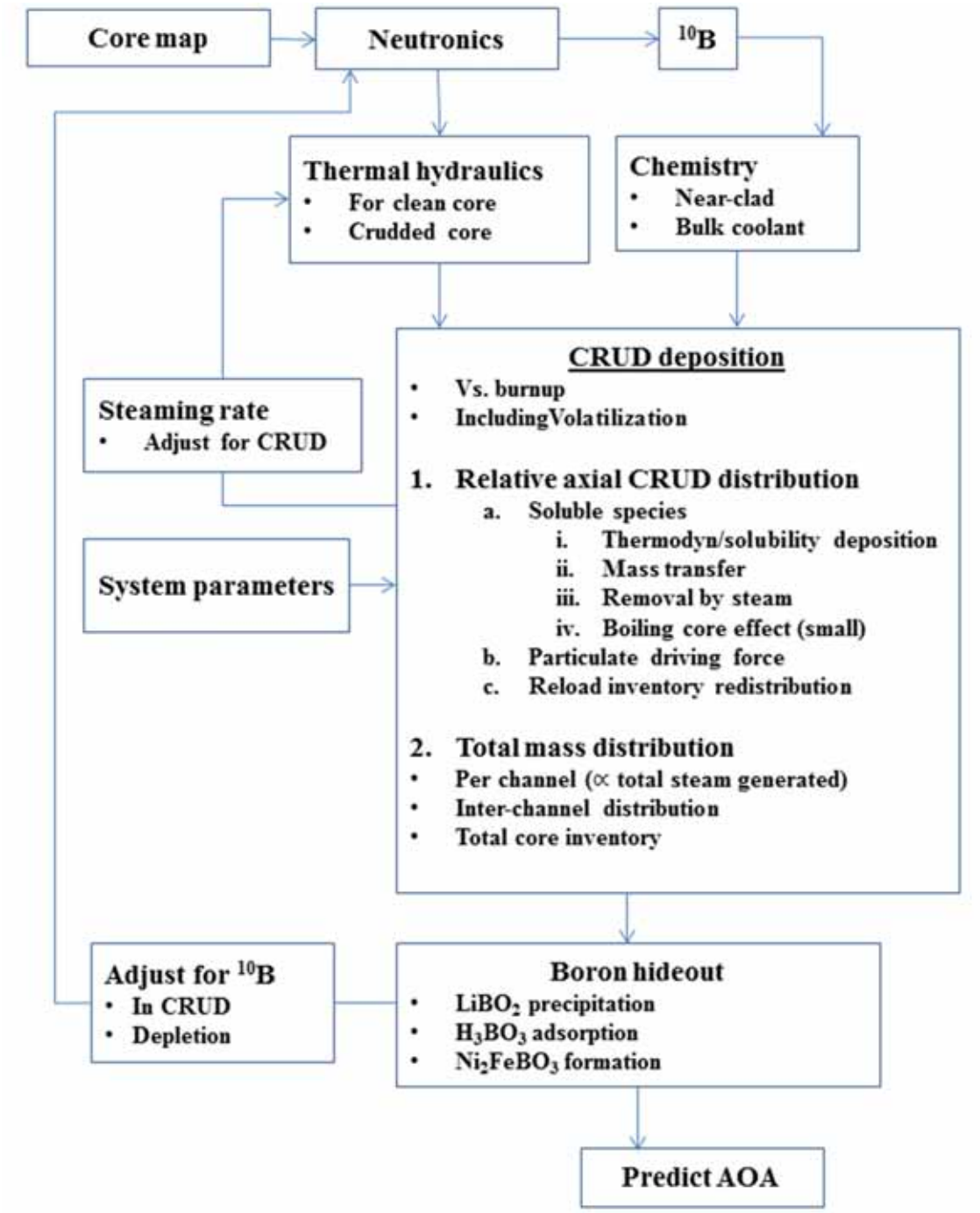

FIG. 98. Modeling boron hideout on PWR fuel.

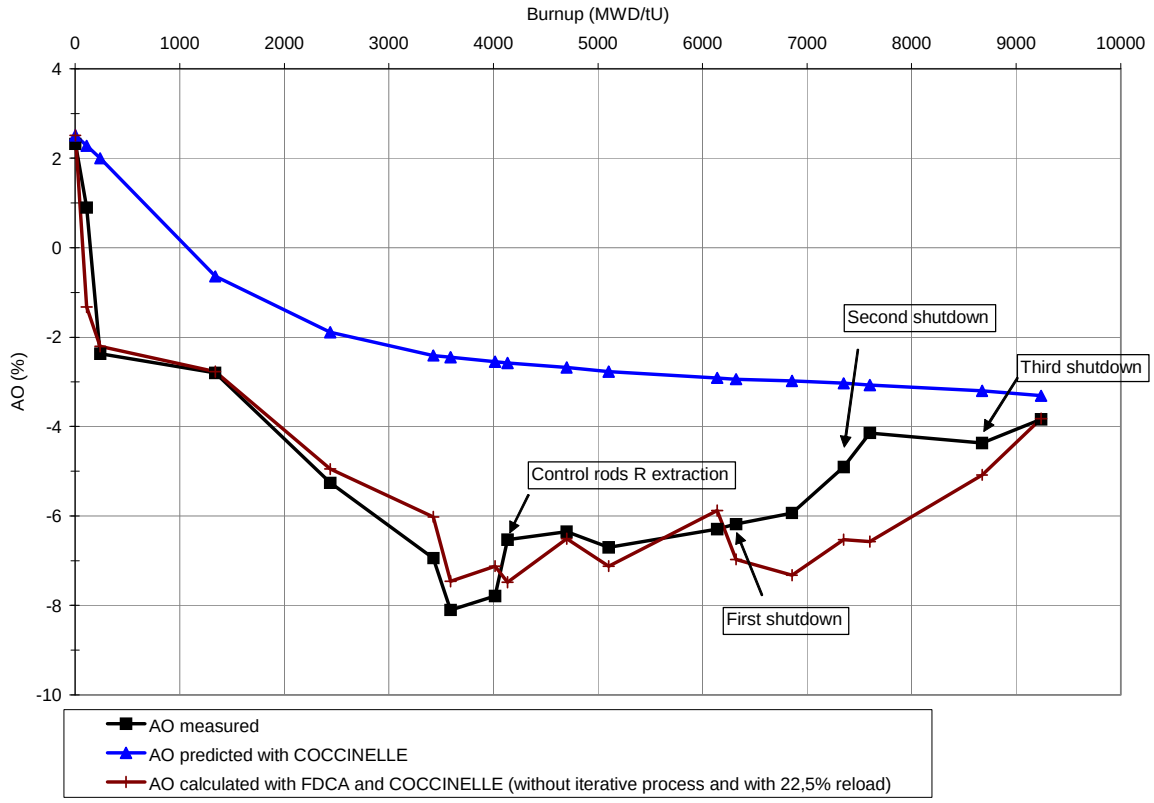

FIG. 99. Calculated axial offset compared with measured data.

A co-sponsored experimental program has been performed to verify the influence of water chemistry on the CIPS phenomenon has been developed in view of the interaction between water chemistry, core behaviour and fuel performance [111]. The main purpose of the experiment has been to identify the boron-containing species that are deposited in a thick crud layer under sub-cooled boiling and various water chemistry conditions (pH, Ni concentration). These parameters have been postulated to be important in the initiation of the CIPS phenomenon.

Generally speaking the scraped crud samples consisted of submicron particles dominated by iron- and nickel- containing oxides. Under scanning transmission electron microscopy (STEM) one could easily identify that most of the submicron- and nano-particles were nickel ferrite ($Ni_xFe_{3-x}O_4$) and nickel oxide (NiO). There were also some crystalline particles which contained a higher fraction of nickel than that of $NiFe_2O_4$

At all axial positions the inner layers of the crud from all tests appeared to be relatively dense while the outer layers looked porous. Electron dispersive spectroscopy measurements confirmed that the crud inner layers were denser and rich in nickel while the crud outer layers were more porous and contained a higher fraction of iron. Fig. 100 shows the crud total boron concentration as a function of crud total nickel concentration in all tests performed in phase 3 where the parameters such as boron and lithium concentrations as well as exposure duration were varied. It can be seen that crud boron concentration increases linearly with nickel concentration in the range of the crud nickel concentration variation in the different tests. This is in agreement with the time-of-flight secondary ion mass spectrometry (ToF-SIMS) results that boron concentrates in the inner dense layer of the crud where nickel also concentrates. Since a linear correlation is found in the tests performed under different experimental conditions (different pH or exposure duration), the crud density or nickel concentration appears to be a deciding factor for boron deposition. In other words, the boron deposition in crud due to the effect of pH or exposure duration cannot be compared if the pre-crud layers are different in their nickel concentrations or perhaps volume densities.

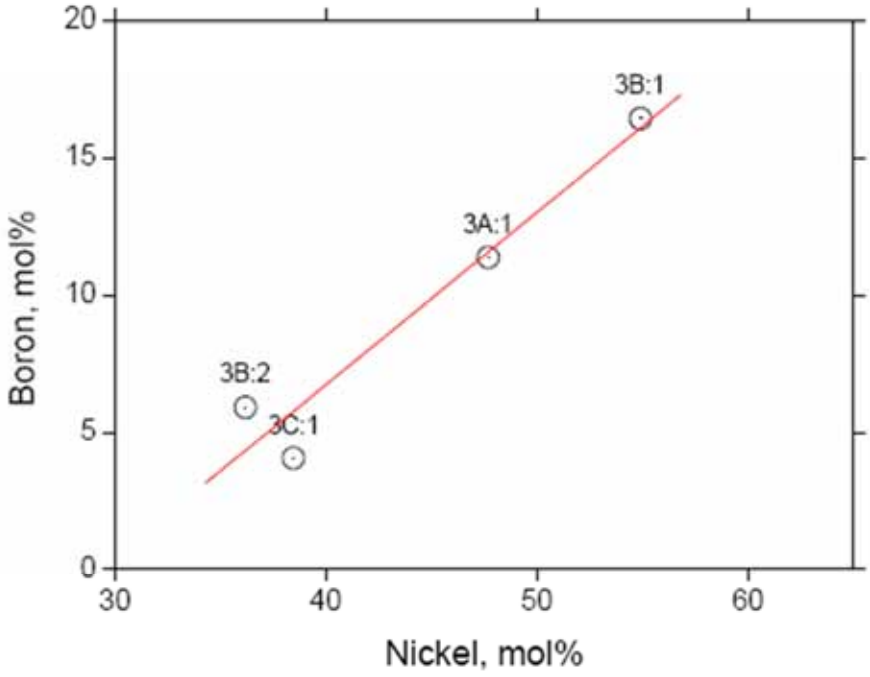

FIG. 100. The correlation between boron and nickelconcentrations in the crud formed in the different tests of phase 3.

From the results and experimental conditions of the present work the following conclusions were drawn:

- A considerable amount of boron is found to deposit in the crud layers in all tests under different pH, exposure duration and crud thickness in Phase 3.
- For all the tests performed at high pH the presence of $Li_2B_4O_7$ has been confirmed using electron diffraction technique in STEM.
- Boron deposition in the crud increases linearly with nickel concentration in crud in the range of approx. 36–55 mol% (Li, B, Ni and Fe are included) at different pH, exposure duration and crud thickness.
- Boron deposits in the inner dense crud layer which is also rich in nickel oxide.
- At high pH, lithium deposition increases with iron concentration in crud while at the low pH it decreases with iron concentration.

To study the effect of pH (or other parameters) on boron deposition under different test batches it is essential that the pre-crud layers for different test batch are made strictly identical (e.g. with the same nickel concentration).

7.1.4. Thermodynamic modelling of PWR coolant

A PWR thermodynamic database has been developed to calculate Ni, Fe, Co and Zn solubility from their oxides and ferrites [112]. The calculations have highlighted the limited experimental oxide solubility data available, particularly at high temperatures, and the considerable variation between different measurements. These uncertainties are compounded by uncertainties in the thermodynamic data for the ferrites, and the effects of changes in stoichiometry. Future work will be aimed at including radiolytic reactions in the database. The main conclusions are:

- The two data sets for Fe_3O_4 solubility diverge at high pH. The reason for the discrepancy is not known. A model based on Baes and Sweeton's [113] data appears to give better agreement with ferrite solubility measurements.
- There are discrepancies in the ZnO solubility data, particularly at low pH. Again, the reasons are not clear.
- Only a single set of data is available for CoO solubility up to 250°C. Care should be taken if the data are extrapolated to higher temperatures.

The model predicts that $NiFe_2O_4$ does not dissolve congruently, but that Ni or NiO is formed and this limits the nickel solubility. The calculated Ni and Fe solubilities are in reasonable agreement with experimental data.

Measurements of $CoFe_2O_4$ indicate that it dissolves congruently giving a Fe/Co solution ratio of 2. The model predicts congruent dissolution below ~600 K, but underestimates the extent of solubility somewhat. Similar results are obtained for mixed Co-Ni ferrites.

$ZnFe_2O_4$ is predicted to be thermodynamically unstable with respect to decomposition to ZnO and Fe_3O_4 at PWR H_2 concentrations. However, an ideal solution treatment predicts that non-stoichiometric ferrites of the type $Zn_xFe_{(3-x)}O_4$ would be increasingly stable as "x" decreases. There are considerable variations in the data for zinc ferrite used by various authors.

The database has been used to calculate Fe and Ni solubilities in PWR coolant under a range of operating and shutdown conditions. The calculations predict small differences between the pH of minimum solubility and that of the zero temperature coefficient compared with an earlier analysis by Walker and Thornton [114]. This highlights uncertainties within the thermodynamic data, which will not be resolved without additional measurements.

Reactor measurements indicate that, in reactors with low Ni content in the SG alloys, the concentration of Ni in the coolant is limited by its availability in the surface oxide. In reactors with high-Ni alloys, the circulating Ni concentrations may be dominated by colloidal material. The calculated changes in Ni and Fe concentrations during the acid-reducing phase of shutdown are in reasonable agreement with measurements from Sizewell B.

7.1.5. Modelling CIPS phenomena in WWER-440 type reactors

The activity of deposits is known to be proportional to the amount of corrosion products circulating in the circuit; therefore all models of the mass transfer processes in the circuit include the change of corrosion products concentration and the corrosion rates in time, removing these products by various filters and deposition. Decontamination of the primary equipment due to inspection, repair and the needs of replacement work can lead to a local change of corrosion rate, which results in the increase of corrosion product concentration in the circuit and then to an increase of deposition on surfaces. If, due to incorrect water chemistry, conditions for corrosion product deposition in the core are created in parallel with increasing corrosion produced by the coolant, the hydraulic resistance of the reactor also grows, which results in the increase of the pressure drop dP at the reactor core [115]. Based on the data obtained at a WWER-440 NPP, a model was developed at VNIPIET with the aim of explaining the rise of pressure drop under a variety of conditions. The pH values, ammonia and hydrogen concentration were considered as key parameters of the water chemistry in this model [116]. The preliminary analysis showed that the dose rates from the equipment of the primary circuit are correlated inversely with the pressure drop.

The correlation between the average pressure drop growth and activity of ^{58}Co in the primary coolant is shown in Fig. 101.

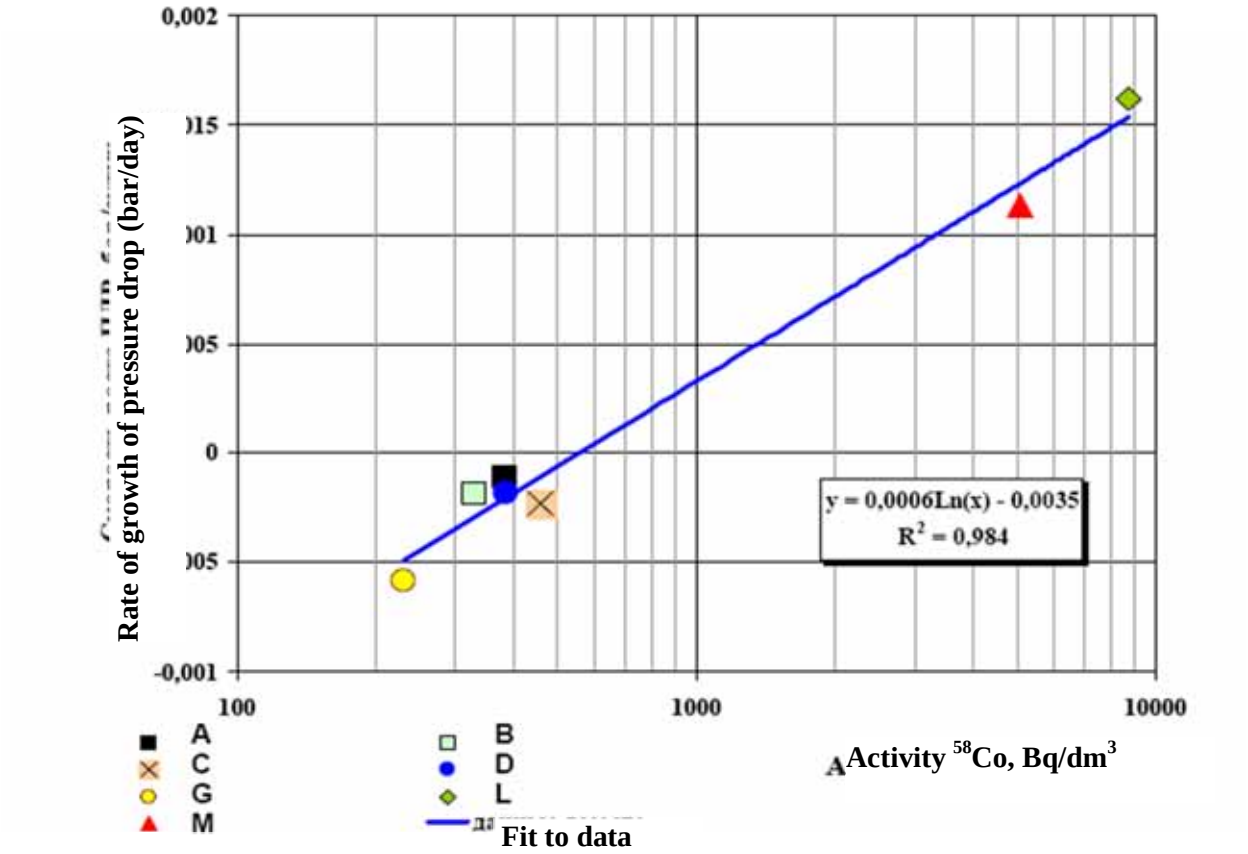

FIG. 101. Pressure drop as a function of activity of ^{58}Co in the coolant with $pH_{(300)}$ in the range 7.1–7.3. (A, B, C, D, G, L, M – identification letter of reactor block).

This correlation can be explained by the deposition of corrosion products in the circuit, mainly on the hotter surfaces (in-core) or on surfaces cooler than the coolant (the remainder of the circuit).

Each operating cycle can be characterized by several parameters: the pressure drop during a cycle, the pressure drop between the cycles and the mean value of the pressure drop during the cycles [117]. The rise of pressure drop between cycles is caused by the fact that loose corrosion products tend to move during start-up and adhere to the grids. Besides, the solubility of magnetite decreases sharply with the rise in temperature and is deposited in the circuit and under specific pH conditions, preferentially on hot surfaces. However, as well as the operational characteristics, these values depend on design features of the power unit and the length of its operation. The parameters that characterize the changes of pressure drop during the cycles are more reliable. VNIPIET developed a model of pressure drop changes during a cycle [118] which takes into consideration the follow main parameters:

- time of power unit operation under water chemistry with $pH_{(300)} < 6.8$ during cycle, days;
- ^{58}Co and ^{60}Co isotope activity ratio;
- thermodynamic data of solubility of magnetite and nickel ferrite in circuit.

$$\frac{\Delta\Delta P_C}{T_C} = a_0 + a_1 pH + a_2 \lg(A_{^{58}Co}) + a_3 \frac{A_{^{58}Co}}{A_{^{60}Co}}$$

The model is based on the following observations:

(a) The rise of the pressure drop at the beginning of the cycle is correlated with the low value of pH at start-up. An example of the change of pressure drop and $pH_{(300)}$ during cycles 19 of the Paks NPP is shown in Fig. 102. As can be seen in the figure, the rise of pressure drop occurs at a pH value below 6.8. When the $pH_{(300)}$ exceeds the value of 6.8, the pressure drop in the reactor is stabilized. The boundary values of pH are shown in the figure. These values are calculated for the case when the total content of alkali metals are in accordance with the standard and real concentrations of boric acid, ammonia and hydrogen and therefore the lines are uneven.

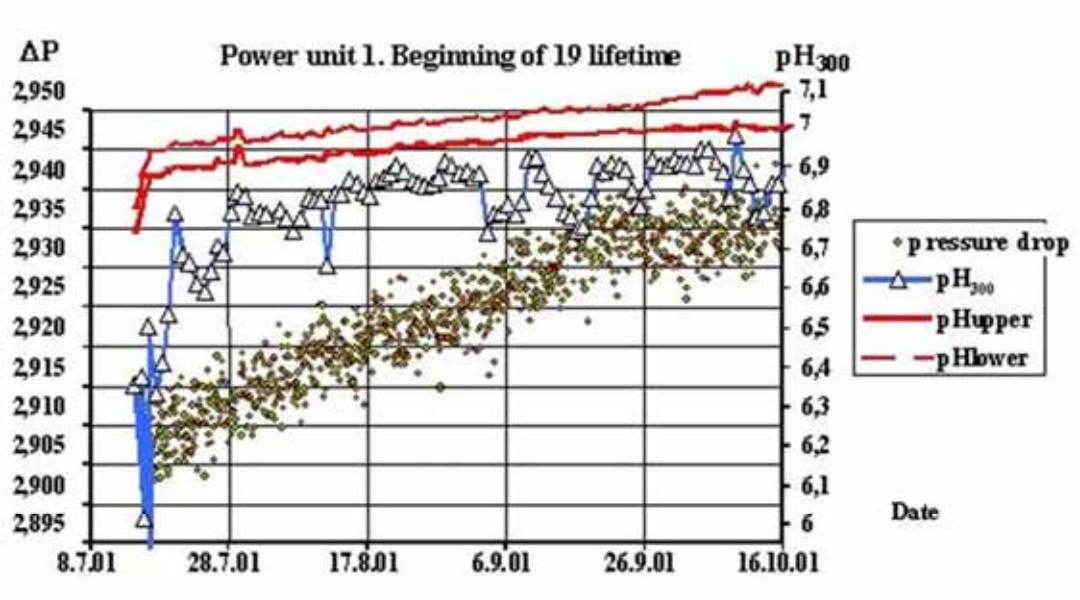

FIG. 102. Change of pressure drop and $pH_{(300)}$ at unit 1 of NPP Paks.

The data show that, during the first three months of the cycle, the pH was below the value specified in the standard. Another important feature is the necessity to maintain a constant value of $pH_{(300)}$, keeping it as stable as possible in order to minimize changes in the temperature gradient of solubility and thus solubility itself.

(b) The change of dP values for an average cycle is shown in Figure 103. The regression equations obtained are statistically significant. Before SG decontamination, classic deposits on FAs described by the termodynamic models can be seen (Figure 103a). After multiple SG decontamination, an increased release of corrosion products take place and the concentration of Fe, Ni and other corrosion products grows. The $pH_{(T)}$ dependence of CP behaviour changes and higher values of $pH_{(T)}$ lead to a decrease of the pressure drop during a cycle (Figure 103b).

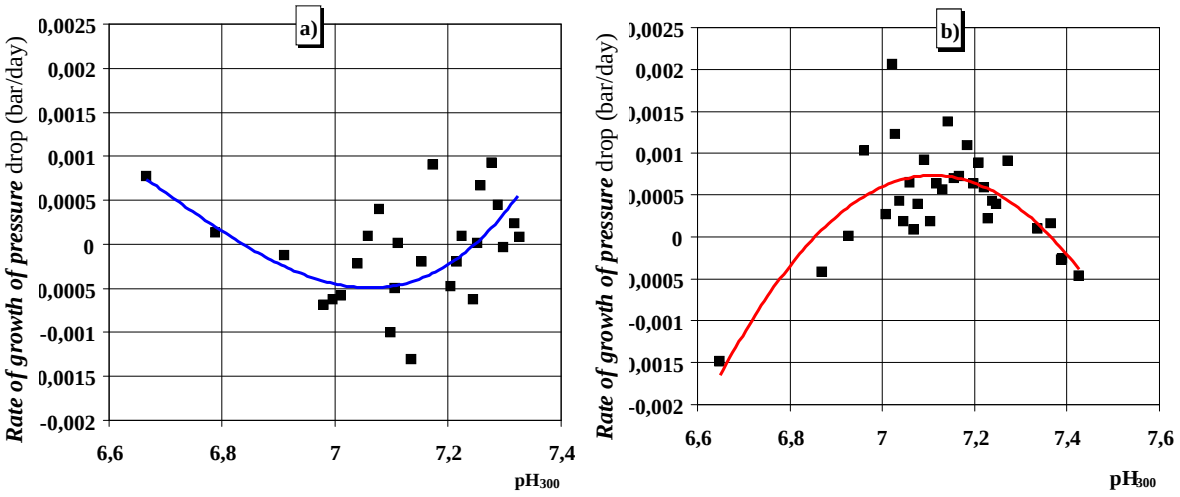

FIG. 103. Change of pressure drop during a cycle as a function of the mean value of $pH_{(300)}$ during the cycle before and after multiple SG decontamination (a –"classic" mass transfer, b – anomalous mass transfer).

(c) The $^{58}Co/^{60}Co$ activity ratio can be considered as a measure of the age of the corrosion products. During the first start-up of the reactor, this ratio is greatly in excess of 1, and only after 5–7 years of operation does it become stabilized at values below 1. The relationship between the number of decontaminated SGs after cycle(i-1) and the $^{58}Co/^{60}Co$ activity ratio is shown in Fig. 104. This can be explained by the fact that after decontamination following cycle(i-1), an additional quantity of corrosion product is generated which are deposited in the core and, after activation, it is re-distributed in the circuit.

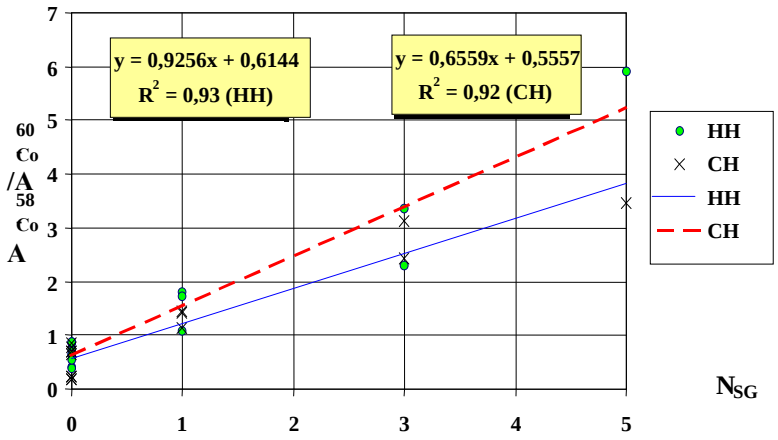

FIG. 104. $^{58}Co/^{60}Co$ activity ratio in cycle(i) depending on the number of SGs decontaminated during one preventive maintenance after cycle(i-1). HH – hot header, CH – cold header.

The results of VNIPIET model calculation [116], [119] are shown in Fig. 105. The pressure drop after decontamination of an assembled circuit without changing the technique of passivation can exceed 0.2 bar.

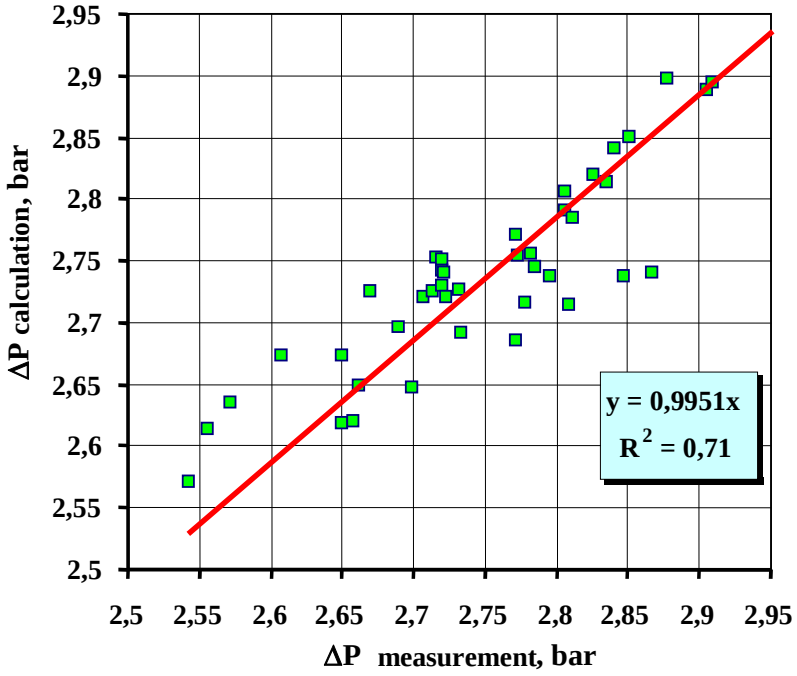

FIG. 105. Correlation between of the calculated and measured pressure drop values of several WWER-440 reactors.

With an increase in the core pressure drop, the surface temperature of the fuel also increases. Fig. 112 shows change of coolant temperature at the core exit after decontamination of three SGs in Loviisa-2 reactor. [115]

The number of affected fuel assemblies can be described by the function [119]:

$$N(FA) = f(dP^2 \times T_{eff})$$

where dP – the pressure drop, bar/day, T_{eff} – effective time of reactor operation.

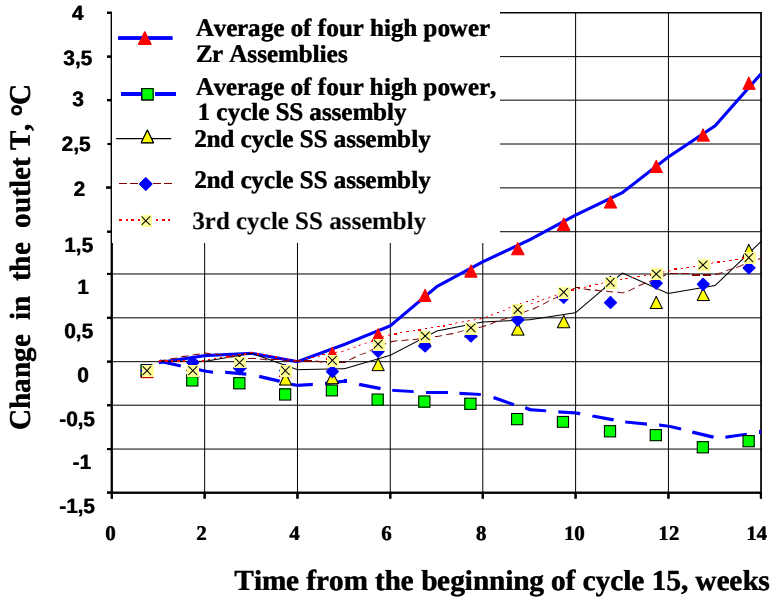

FIG. 106. Change of coolant temperature at the FA exit as a function of FA irradiation time.

7.1.6. WWER-1000 corrosion transport model

In 2003, another computer code COTRAN-M [120] was developed at the Kurchatov Institute in Moscow for the evaluation of radiation conditions in the vicinity of primary equipment in WWER-1000 units. For this purpose, it is necessary to have activity data on corrosion products originating during reactor operation. In order to obtain such data, the code contains modelling algorithms for the processes of generation, transport and accumulation of both active and inactive corrosion product species (^{58}Co, ^{60}Co, ^{54}Mn and ^{59}Fe) on the internal surfaces of the primary circuit with regard to the construction materials, water chemistry and the neutron flux during reactor operation. The following assumptions are made in the model:

- Oxide layer growth is determined by the corrosion resistance (behaviour) of each material which is described by a polynomial function.
- Oxides on the surface exist in a double layer structure – the internal layer is the product of corrosion of the base metal while the outer layer is created by deposition of corrosion products from the primary coolant.
- Corrosion product concentrations in the pores of oxide layer(s) correspond to saturation at a given temperature.
- Corrosion products are transported in both ionic and particulate form. Dimensions of ions and particles are part of input data.
- Transport processes are identical for activated and inactive species.
- Due to the absence of reliable data on the solubility of Co, Mn and Cr, their behaviour in the primary coolant is considered to be identical to Fe.

In the model, primary coolant is considered as a closed loop divided into segments. Each segment represents a separate primary component. Segments are characterised by several parameters – surface, hydraulic diameter, temperature of wall and fluid, mass flow and velocity. Hydraulic and temperature data for each segment are considered constant. In order to increase the accuracy of the calculation, reactor core and SG tubes are also divided to segments, each of them again with constant parameters. The fuel assembly is divided to 14 segments, 10 of them representing the fuel rods and the remaining 4 representing spacer grids. SG tubing is divided into 10 segments. The primary circuit is represented by the main flow through the reactor core, two by-pass circuits of ion-exchange and high-temperature filters and by-pass circuits through the pressurizer and the reactor core by-pass are considered.

For each segment, mass transport processes between fluid and wall and also between neighbouring segments are considered with the following processes assumed:

- Corrosion and corrosion release from the base material
- Precipitation and particles dissolution in the coolant
- Surface layer formed by crystallisation and deposition
- Dissolution and erosion of the surface layer
- Transport of both soluble and particulate forms by the coolant
- Neutron activation and radioactive decay
- Incorporation of activated products into both inner and outer oxide layer

Corrosion of base metal and corresponding oxide layer growth rates are determined by the parabolic law. Dissolution (corrosion release) of oxide layer and deposit takes place at those segments where equilibrium concentration in the coolant is lower than that in the oxide layer pores. In the reverse conditions, deposition and crystallisation takes place with the formation of an outer layer.

Corrosion product particles enter the coolant through erosion of the outer layer and are also formed from the crystallisation of supersaturated coolant. Such conditions exist in the segments where temperature is changed and the established equilibrium concentration of corrosion product in the coolant is higher than

the local thermodynamically saturated one. In the reverse conditions particles from the coolant will be dissolved.

Through turbulence in the coolant, particles can gain kinetic energy and penetrate the oxide layer to the surface of the material where they form deposit according to Beal's model.

In the core segments, both deposited and circulated corrosion products are activated by the neutron flux. Additionally, activation of the SS components in the core is assumed with transport of activated products through the oxide layer into the coolant (corrosion release mechanism).

Activated corrosion products enter the coolant by dissolution and erosion, through exactly the same processes as inactive corrosion products. Their transport from the core is with the coolant in both soluble and insoluble forms.

Activated corrosion products are then deposited by the processes of crystallisation and deposition. Incorporation of activated ions into crystalline structure also contributes to the activity accumulation. The driving force of this process is the concentration gradient between coolant and solution in the oxide layer pores.

In the model it is assumed that the technological parameters for particulate segments are constant during short time periods and are changed stepwise. With such an approach, the whole cycle can be divided into intervals, where unknown coefficients of differential equations can be considered as constant. In this way, the calculation reduces to the solution of differential equations with constant coefficients for periods with reactor operation with constant parameters. An exponential matrix method is used for solution of the equations. The solubility data necessary for calculation of mass-transfer coefficients are calculated from chemical equilibria, and activation coefficients in the neutron flux, decay constants and corrosion rates at given segment conditions are part of the input data set.

Validation and attestation of the model/computer code has been performed by the Russian Scientific-Technical Centre of Radiation Safety using operational data from NPP Zaporozhe.

8. SUMMARY AND RECOMMENDATIONS

8.1. Conclusions of the CRP

The following conconclusions were reached after the finalising of the CRP.

(1) For accurate prediction of activity transport, the corrosion rate and corrosion product release rate of plant materials must be measured under conditions duplicating those in a plant, e.g. same thermohydraulic conditions. High temperature water cooled loops may be used for these measurements.

(2) The trend toward longer fuel life means that the thermohydraulic conditions in various parts of the core may be quite different, with sub-cooled nucleate boiling possible toward the top of fuel channels containing freshly-loaded fuel, but not in other regions. In-core models to allow for the effect of boiling on activity transport must be written and added to the codes and more nodes must be added to allow for this change in surface heat flux with location.

(3) The role of particles versus dissolved species is still unclear. A more detailed understanding of the relationship between the various activity transport mechanisms is needed before the roles of the separate phases can be understood, modelled, and put into a code.

(4) Codes must allow for deposit removal with fuel in the refuelling process. Typically, refuelling of one-third of the core removes both nickel and ^{58}Co that would be released to the coolant during operation. This is especially important after the first fuel cycle when the codes predict the heaviest deposits of both elements incore.

(5) The identification of the actual oxide phases contributing to activity transport is essential for code improvement. The solubility of elements in substoichiometric nickel ferrite will be different than those same elements in nickel oxide or in magnetite. As well, the rate constant for crystal dissolution will be a strong function of oxide composition and if the composition changes with time of operation, then the rate constant will also change.

8.2. Current status of activity transport modelling

Current activity transport models seem too elaborate, given our current knowledge of the actual deposition and release processes on various system surfaces. Further, models are lacking good experimental data for verification/validation of some of the processes being modelled.

A step back towards simpler models based on limiting cases is suggested by the CRP in which the modelled processes have some basis for support by experimental data.

The first step in determining the dominant role of dissolved/particulate species in activity transport is suggested to be the creation of transport diagrams to provide a macroscopic model of elemental transport, e.g. for dissolved iron. Corrosion film dissolution and precipitation are suggested to dominate all other processes at a surface and the transport diagram identifies these surfaces around the primary circuit.

Fundamental data is needed for the electrical properties of metal oxides and transport properties in solution, although the work has not been accomplished yet. Further progress in modelling both corrosion product behaviour and the electrochemistry of corrosion are dependent on this data. It is not surprising, and it is appropriate, that the emphasis is in the area of modelling. The most daunting problems facing the industry are complex and draw on multiple disciplines of science. To consider thermally driven fuel corrosion in light water reactors (LWR) requires knowledge of: high temperature crud chemistry; transport properties in solution; zirconium oxide kinetics and electrochemistry; heat transfer properties of crud; and oxide formation. A complete understanding of the influence of all of the

factors may not be tractable, but only through a complete model of the problem is it possible to understand how all of the variables interact with each other to produce the observed corrosion.

In addition to fundamental data to support modelling for corrosion, radiation field control and fouling, it is anticipated that the industry will continue to seek to discover new inhibitors/methods to slow down or eliminate corrosion. It is hopeful that the models will shed some light on the desired properties of new chemistries. It will then be up to the industry to support some fundamental research programs to develop the high temperature chemistry data needed to identify and understand the role of inhibitors in the corrosion process. In parallel with this work, the industry should continue much of the fundamental work to understand the underlying materials degradation processes.

Considering the results of CRP, it might be easy to conclude that the slowdown of support for new science is simply due to the fact that the field has entered a phase of maturity. It is more likely that a period was reached where the technology caught up with the science and further advance will require new science. It is thought to be time for the industry to sit down again and work through a framework or roadmap to ensure that the science needs of the industry can be met by the research community.

8.3. Future requirements

An important requirement of future work to ensure a significant advance in understanding, control and modelling of activity transport, would be to understand the mechanisms which cause the following issues:

- deposit composition and thickness on the fuel,
- crud induced power shift (CIPS) and power limitation,
- fuel oxide growth and thickness,
- corrosion related fuel failure,
- crud induced localized corrosion (CILC),
- radioactivity build-up in the reactor coolant system (RCS).

It is believed to be useful to use the experience of the CRP and the present review to list and briefly describe the issues that need to be considered.

8.3.1. Reactor and core design

The first requirement would be to consider the effect of various reactor designs; PWR (all categories), BWR (all categories) and CANDU.

The identified materials that may have impact are the following:

- Fuel cladding material, with its influence on its corrosion resistance, the oxide film composition and thickness.
- Mixed cores, which represent a specific case with fuel comprising various types of cladding materials and in some cases different structure.
- Spacer material for which the material has been significantly modified.
- Inconel 600 or not: since the presence of this alloy does not allow operation at too high a pH and the alkaline reagent concentration for mitigating stress corrosion cracking. This pH limitation has a potential drawback on corrosion product release and deposition
- Ni content mainly in SG (high/intermediate/low). The nickel content has a direct influence on the composition and the solubility of the corrosion products in the various parts of the RCS, particularly on the fuel cladding surface.
- Use of stabilization elements since the presence of more resistant stabilized alloy does not require the same hydrogen concentration in the RCS. The hydrogen concentration has an impact on corrosion product solubility.
- The presence of a reactor pressure vessel (RPV) liner as it has a direct impact on the amount of released corrosion products to the reactor water.

8.3.2. Input data

The items listed have been identified as needing to be considered, but other parameters may be also be important.

- Reactor age has been identified a key parameter since the age of most of the operating plant is largely increasing with direct or indirect impact on the release of corrosion products from the components and the transport – deposition process on the fuel elements. Moreover, the design, including purification system, in old plants has not always been selected according to the high burn up fuel, which is used now in many of these plants.
- Fuel tramp contamination (manufacturing or previous fuel failure) has been shown to have a significant influence on CIPS although no firm explanation can be yet given (neutron adsorption on fuel tramp should be marginal as compared to boron neutron absorption, fuel tramp deposit thickness is marginal as compared to corrosion product thickness).
- Fuel duty as inferred from other parameters can be used as an input data for evaluation of CIPS and fuel failure occurrence.
- Neutron flux profile influences the oxide film growth mechanism as well as the chemistry condition in the downstream part of the fuel. This may have an impact on the corrosion product deposition processes.
- The fuel position in the core has been demonstrated to be correlated to the presence of CIPS and potentially on fuel failure, but has not been clearly explained
- Sub cooled boiling has obviously a key contribution to the risk of precipitating boron compounds in the deposits on the fuel surfaces.
- Radiochemistry results have a strong relation with the deposition of radioactive corrosion and fission products.
- Fuel cleaning is used to remove deposits from the fuel with an obvious direct impact on CIPS and fuel failure.
- RCS decontamination will be considered for the influence it may have on the material surface conditions which exist after decontamination and which may vary according to the final stage of the process. In some plants, a pressure drop has been seen and may be investigated for its potential relation to corrosion products deposition and resulting consequences.
- Corrosion product release from original/ replaced components (e.g. SG replacement) shall also be investigated for the influence it may have on the material surface conditions which exists after the repair and which may vary according to the application or not of passivation procedures.

8.3.3. Operating parameters

The characteristics of the fuel cycle have a direct influence on the neutron flux at various stages of fuel cycle. Then some operating particularities, such as load follow and transients could also contribute at impacting the CIPS. The following need to be considered:

- fuel enrichment and burn up,
- cycle length
- length of stretch out
- load follow
- transients
- fuel element cycle number

8.3.4. Chemistry parameters

The study of the chemical parameters will be most important since these are the main parameters which can be adjusted in order to mitigate or avoid radioactivity build-up, CIPS, fuel corrosion and failure:

- initial boron concentration, total boron and ^{10}B (use or not of enriched boric acid),
- concentration and type of alkaline reagent,
- pH control during cycle and the effect of history,
- Hydrogen concentration (via H_2, N_2H_4 or NH_3),
- O_2 and other oxidants: in BWR coolant O_2, in PWR make-up water,
- Impurity ingress (Si, ...),
- Key related events (e.g. CVCS operating mode),
- Zinc injection in PWRs,
- Zinc, noble metal chemical addition (NMCA), iron injections in BWRs.

8.3.5. Shutdown and passivation processes.

The shutdown process, with its corresponding chemistry, is the phase during which a large quantity of corrosion products is released from the material surfaces, due to the temperature decrease and solubility increase. Thus, the shutdown of the unit and associated purification process must be particularly considered and any practical and beneficial process identified.

Proper passivation of material surfaces, either for new plants or after main components replacement may drastically reduce the release of corrosion products during further operation of the unit with beneficial impact on radioactivity build up and potentially on CIPS. However, the drawback of the passivation is the lost generation time related to its application of a minimum duration. Thus, the optimum process and duration may be addressed.

REFERENCES

[1] WOHLBERG, C., KLEIMOLA, F.W., Factors which Affect Formation and Depostion of Transport Corrosion Products in High-temperature Recirculating Water Loops, Argonne National Laboratory report no. ANL-5195 (1953).

[2] VAVASOUR, G.R. (Ed.), Proceedings of the Tripartite Conference on Transport of Materials in Pressurized-Water Nuclear Systems, Atomic Energy of Canada Limited Report No. AECL-1265 (1961).

[3] MEDINA, L. (Ed.), Literature Survey for Activity Build-up on Reactor Primary System Components, Alco Products Inc., Report number APAE-25 (1958).

[4] STEINER, F.C., Primary Coolant Impurity Activation and Accessibility to Components in 53G/54G Lower Reactor Component, Knolls Atomic Power Laboratory, Report no. KAPL-M-SMS-45 (1956).

[5] PEMENT, F.W., Calculated Deposited Crud Activity in the PWR Primary System due to Corrosion of Core Materials, Westinghouse Atomic Power Division, Report no. WAPD-PWR-CP-2995 (1957).

[6] ALLSOP, H., BRIDEN, B.L., BURRILL, K.A., Proceedings of the International Symposium on Activity Transport in Water Cooled Nuclear Power Reactors, AECL report RC-1334 (1994).

[7] INTERNATIONAL ATOMIC ENERGY AGENCY, Coolant Technology of Water Cooled Reactors, IAEA TECDOC-667, Vol. 1–3 (1992).

[8] BENARD, J., MICHEL, A., PHILIBERT, J., TALBOT, J., Metallurgie generale, Masson et C^{ie} editeurs (1969).

[9] LACOMBE, P., LECOMTE, J., BERANGER, G., Les aciers inoxydables, Editions de la physique (1990).

[10] POTTER, E.C., MANN, G.M.W., Oxidation of mild steel in high-temperature aqueous systems, First International Conference on Metallic Corrosion, London (1962).

[11] HANNINEN, H.E., JAUHIAIEN, E., STARKMAN, T., Oxidation and decontamination mechanisms of stainless steels studied by electron spectroscopy, International Atomic Energy Agency, IAEA-SM-264/22 (1982).

[12] MIYAZAKI, S., OSHIMA, S.,OJIMA , Z., Characteristics of crud deposits on primary system surfaces, Proceedings of the JAIF International Conference on Water Chemistry in Nuclear Power Plants, Kashiwazaki (1988) 584–590.

[13] LISTER, D.H., DAVIDSON, R.D., Corrosion Product Release in Light Water Reactors, Final report EPRI NP-6512 Research Project 2008–1 (1989).

[14] PICK, M.E., The nature of PWR stainless steel and Inconel oxides in relation to decontamination in permanganate based (NP and AP) processes, Water Chemistry of Nuclear Reactors Systems 3, Proceedings of the British Nuclear Energy Society, Vol. 2, Bournemouth (1983).

[15] ALVAREZ, M.G., OLMEDO, A.M., VILLEGAS, M., Corrosion behavior of alloy 800 in high temperature aqueous solutions: long term autoclave studies, Journal of Nuclear Materials **229** (1996) 93–101.

[16] LISTER, D.H., Activity transport and corrosion processes in PWRs, Nuclear Energy **32** (2) (1993) 103–104.

[17] GARDEY, S., Etude de la corrosion generalisee des alliages 600, 690, 800 en milieu primaire, Contribution a la comprehension des mecanismes, These de doctorat de l'Universite Pierre et Marie Curie-Paris VI, Paris (1998).

[18] CASTLE, J.E., MASTERSON, G.H., The role of diffusion in the oxidation of mild steel in high temperature aqueous solutions, Corrosion Science **6** (1966) 93–104.

[19] ROBERTSON, J., MANNING, M.I., Criteria for formation of single layer, duplex, and breakaway scales on steels, Materials Science and Technology **4** (1988) 1064–1071.

[20] SOLOMON, Y., SHAW, R.A., ROESMER, J., BERGMANN, C.A., Crud effects and PWR reactor coolant chemistry: state of the art, Water Chemistry of Nuclear Reactors Systems 3, Proceedings of the British Nuclear Energy Society Vol. 2, Bournemouth, (1983).

[21] YOU, D., LAMBERT, J., FERON, D., Dissolution and solubility of cobalt and nickel ferrites in PWR primary conditions, 7th International Conference on Water Chemistry of Nuclear Reactors Systems, Bournemouth, (1996).
[22] KRITSKY, V.G., Water chemistry and corrosion of NPP structural materials, Sinto (1996).
[23] KRITSKY, V.G., ZAREMBO, V.I., PUCHKOV, L.V., SLOBODOV, A.A., Termodinamicheskaya model' povedeniya produktov korrozii kobal'ta v trakte AES s kipyaschim reaktorom, Atomnaya energiya **64**, Vol. 3, Moscow (1988) 223–225 [In Russian].
[24] RODLIFFE, R.S., POLLEY, M.V., THORNTON, E.W., Modelling the behavior of corrosion products in the primary heat transfer circuits of pressurized water reactors – A review of principles, Reactor water chemistry relevant to coolant-cladding interaction, International Atomic Energy Agency, IAEA-TECDOC-429 (1987).
[25] VESELKIN, A.P., SHAKH, O.Y., Effect of decontamination system on the buildup of active corrosion products in pressurized water reactors, Soviet Atomic Energy 20, Vol. 3 (1966) 273.
[26] YERAZUNIS, S., ALKIRE, S.E.H., SEIDEL, R.L., Mechanisms of Reactor System Activation, KAPL-M-SMS-98, Knolls Atomic Power Laboratory (1959).
[27] BONALUMI, R., OLIVI, A., A general method for studying the corrosion products buildup in the primary circuit of a reactor, Energia Nucleare **17** (5) (1970) 302.
[28] PATTISON, J., WALTON, G.N., The Distribution of Radioactive Materials in a Circuit, AERE-R-3661, Atomic Energy Research Establishment, Harwell (1961).
[29] WALTON, G.N., HESFORD, E., The migration of activated corrosion products in high-pressure water loops, Proc. of Conf. on Corrosion of Reactor Materials, Salzburg, Vol. 2, International Atomic Energy Agency, Vienna (1962) 547–556.
[30] WALTON, G.N., A method for estimating activity transport in pressurized water reactors from measurements in loops, Trans. Am. Nucl. Soc. **2** (1964) 180.
[31] NISHIMURA, T., KASAHARA, K., Improvement of crud behaviour evaluation code (ACE), Proceedings of 1998 JAIF International Conference on Water Chemistry in Nuclear Power Plants, Kashiwakazi (1998).
[32] KASAHARA, K., NISHIMURA, T., OSHIMA, S., Mathematical model of radioactive corrosion products transports for PWR plants, International Symposium of Activity Transport in Water Cooled Nuclear Reactor, Ottawa (1994).
[33] MIYAZAKI, S., OSHIMA, S., et al., Characteristics of crud deposits on primary system surfaces, 1991 JAIF International Conference on Water Chemistry in Nuclear Power Plants, Fukui (1991).
[34] BERGMANN, C.A., LANDERMAN, E.I., LORENTZ, D.R., WHYTE, D.D., Evaluation of cobalt sources in Westinghouse designed three- and four-loop plants, EPRI Report NP-2681, Palo Alto (1982).
[35] BEAL, S.K., Deposition of particles in turbulent flow on channel or pipe walls, Nuclear Science and Engineering **40** (1970).
[36] BEAL, S.K., The effect of erosion and deposition on sampling of entrained particles, Technical Report, WAPD-TM-1014, Bettis Atomic Power Lab, Pittsburgh (1972).
[37] KASAHARA, K., et al., Study of corrosion products behavior under PWR primary coolant condition, 1991 JAIF International Conference on Water Chemistry in Nuclear Power Plants, Fukui (1991).
[38] ABE, K., et al., Solubility measurement of crud and evaluation of optimum pH, 1988 JAIF International Conference on Water Chemistry in Nuclear Power Plants, Tokyo (1988).
[39] NISHIZAWA, E., et al., Thermodynamics evaluation of PWR crud chemical form, 1998 JAIF International Conference on Water Chemistry in Nuclear Power Plants, Kashiwazaki (1988).
[40] HISAMUNE, K., et al., Study on behaviour of activated corrosion products in PWR primary coolant system chemistry, Proceedings of Water Chemistry ’98, Japan (1998) 595–598.
[41] COBBLE, J.W., et al., High-temperature thermodynamic data for species in aqueous solution, EPRI NP-2400, Final Report San Diego State Univ., San Diego (1982).

[42] LEE, C.B., Modeling of Corrosion Product Transport in PWR Primary System, Ph.D. thesis, Massachusetts Institute of Technology, Massachusetts (1990).
[43] LEE, C.B., Evaluation of CRUDTRAN code to predict transport of corrosion products and radioactivity in the PWR primary coolant system, Proceeding of Water Chemistry in Nuclear Reactors Systems, Chimie2002, Avignon (2002).
[44] LEE, C.B., DRISCOLL, M.J., LINDSAY, W.T., JUNG, Y.H., CRUDTRAN: A computer code to predict corrosion product transport in the PWR primary coolant system, 1st RCM of IAEA CRP, Toronto, International Atomic Energy Agency, Vienna (1997).
[45] ZMITKO, M., Radioactivity transport modelling with DISER code – description and first calculation results, Proceedings of Second Research Coordination Meeting for the IAEA CRP on Activity Transport Modelling, International Atomic Energy Agency, Vienna (1998).
[46] ZMITKO, M., Investigation and modelling of activity transport in WWER primary systems, Proceedings of the International Symposium on Activity Transport in Water Cooled Nuclear Power Reactors, AECL report RC-1334 (1994).
[47] ZMITKO, M., Mathematical modelling of corrosion products transport under primary coolant conditions of VVERs and PWRs, PhD. thesis, Moscow Power Engineering Institute – Nuclear Research Institute Rez (1991).
[48] ZMITKO, M., Investigation and modelling of corrosion products mass and activity transport in VVER and PWR primary systems, Int. Conf. on Water Chemistry of Nuclear Reactor Systems 6, Bournemouth (1992).
[49] ZMITKO, M., Computer code DISER – A model of PWR corrosion products transport, NRI report No. 10319 (1994).
[50] ZMITKO, M., KYSELA, J., Analysis of the Loviisa primary circuit radiation fields, NRI report Z 59 (1995).
[51] ZMITKO, M., Modelling of corrosion products radioactivity transport in reactor primary systems by computer code DISER – IAEA co-ordinated research project, NRI report No. Z 647 (2001).
[52] DINOV, K., A model of crud particle/wall interaction and deposition in a pressurized water reactor primary system, Nucl.Technology **94** (1991) 281.
[53] GERASIMOV, V., Corrosion of reactor materials, Atomizdat, Moscow (1980). [In Russian].
[54] DINOV, K., KASAHARA, K., Thermodynamic study in support of pressurized water reactor specific reactor water chemistry, Nucl.Technology **115** (1996) 81.
[55] DOBREVSKI, I., DINOV, K., ZAHARIEVA, N., MENUT, P., Modeling of VVER light-water reactors activity buildup**,** 8th International Conference on Nuclear Engineering, , Baltimore, MD (2000).
[56] VENZ, H., DINOV, K., Effect of primary water chemistry on activity transport at unit 2 of Beznau PWR plant, JAIF 98, Proc. Intern. Conference, Kashiwazaki (1998).
[57] TARABELLI, D., ANTONI, S., IAEA Benchmark on Modeling on Radioactive Substances in Primary Circuit of Water Cooled Reactors, CEA report NT-SECA-LTC-165 (1998).
[58] TARABELLI, D., ANTONI, S., MENUT, P., Prediction of light-water reactor contamination using the PACTOLE code, 8th International Conference on Nuclear Engineering, Baltimore (2000) Paper ICONE-8094.
[59] BESLU, P., Mechanisms and driving forces in corrosion product transport and build-up., Specialist's Meeting on Influence of Power Reactor Water Chemistry on Fuel Cladding Reliability, San Maniato (1981).
[60] BESLU, P., FREJAVILLE, G., LALET, A., A computer code PACTOLE to predict activation and transport of corrosion products in a PWR, Proceedings of 1st Conference Water Chemistry of Nuclear Reactor Systems, BNES, London (1978).
[61] BESLU, P., ROBIN, J.C., LONG, A., PACTOLE: A computer code to predict the activation and transport of corrosion products in PWRs, International Symposium of Activity Transport in Water Cooled Nuclear Reactors, Ottawa (1994).

[62] COULET, F., Etude et modélisation de l'influence des matériaux sur la contamination du circuit primaire des réacteurs a eau pressurisée par les produits de corrosion, Thése, Institut National Polytechnique de Grenoble (1996).
[63] MARCHETTO, C., TARABELLI, D., YOU, D., ANDRIEU, C., LONG, A., ZEITOUN, D., PACTOLE V3: A new code version to predict corrosion product contamination, 8th Conference on Water Chemistry of Nuclear Reactor Systems (BNES), Bournemouth (2000).
[64] HORVATH, L.G., Development of a Corrosion Product Transport Code in the Primary Circuits of Nuclear Power Plants, VEIKI Report 93.92–077 (1991) [In Hungarian].
[65] CIVIN, V., A systemetic approach to the calculation of the high temperature pH and of solubility of magnetite, VEIKI Report 22.92–415–2 (22.92–408) (1988) [In Hungarian].
[66] BURRILL, K.A., An activity transport model for CANDU based on iron transport in the primary coolant, AECL-11805 (1998).
[67] BURRILL K.A., An activity transport model for CANDU based on iron transport in the primary coolant, AECL-11805 (1998).
[68] LISTER, D.H., The transport of radioactive corrosion products in high-temperature water, part II: the activation of isothermal steel surfaces, Nucl. Sci. Eng. **59** (1976) 406–426.
[69] BURRILL, K.A., Some aspects of water chemistry in the CANDU primary coolant circuit, 1998 Japanese Atomic Industrial Forum International Conference on Water Chemistry in Nuclear Power Plants, Kashawakazi (1998).
[70] KRITSKY, V.G., Models of Al-, Fe-, Cu- and Zr-alloys corrosion based on thermodynamic estimates of corrosion product solubilities in water coolants of nuclear power units, 1998 JAIF International Conference on Water Chemistry in Nuclear Power Plants, Water Chemistry, Kashawakazi (1998).
[71] ARBEAU, N., ALLSOP, H., CAMPBELL, R.H., LISTER, D.H., Kinetics of corrosion product release from carbon steel corroding in high-temperature, lithiated water, J.Corrosion. **54** (6) (1998).
[72] KRITSKY, V.G., SLOBODOV, A.A., ZAREMBO, V.I., et. al., Products of steels corrosion solubility in the conditions simulating various water chemistry modes of power units, J. Prikladn. Khimii, V. LXI, **12**, (1982) 2661–2667 [In Russian].
[73] MOROZOVA, N.K., et al., Carrying out and deposition of the products of reactor materials corrosion, Atomizdat, Moscow (1975) 280 [In Russian].
[74] MARGULOVA, T.H., et al., On the possibility of 08X18H10T steel abandoning in low-pressure heaters of single-circuit NPP, Teploenergetika **10** (1983) 65–66 [In Russian].
[75] KERREC, O., GARDEY, S., NOEL, D., RIQUELME, E., MIGUET, P., MASSOUD, J.P., Influence of initial surface state on the corrosion behaviour of nickel alloys in primary coolant medium, State of the art and state of practice of computerised corrosion information systems, EUROCORR'96, Nice (1996).
[76] KRITSKY, V.G., Water chemistry and corrosion of NPP structural materials, SINTO, S.-Pb, Moscow (1996).
[77] BECKER, F., RUF, R., Thermodynamic approach of corrosion product transport in water cooled reactors, Report at 2nd RCM of IAEA CRP on Modelling of Transport of Radioactive Substances in Primary Circuit of Water Cooled Reactors, International Atomic Energy Agency, Vienna (1998).
[78] ERIKSON G., HACK K., (Programmers), "ChemSage: SOLGASMIX-based advanced Gibbs-Energy minimiser", Distributors GTT Technologies, Herzogenrath, Germany.
[79] REDLICH, O., KISTER, A.T., Algebraic representation of thermodynamic properties and the classification of solutions, Industrial and Engineering Chemistry **40** (2) (1948) 345– 348.
[80] BECKER, F., Calculation of thermodynamic equilibria in the primary circuit of pressurised water reactors, Proc. of the Fifth Int. Symp. on Hydrothermal Reactions, Gatlinburg, TN (1997).
[81] BECKER, F., STELLWAG, B., Modelling and prediction of activity build up on system surfaces in light water reactors, EUROCORR'98, Utrecht (1998).

[82] BELOUSCHEK, P., et al., Modelling of transport and deposition of corrosion products in primary circuits, Proc. Int. Conf. On Water Chemistry of Nuclear Reactor Systems, Vol. 7, Bournemouth, British Nuclear Engineering Society, London, Vol. 1 (1996) 280–283.
[83] URQUIDI-MACDONALD, M., Importance of ECP in the prediction of radiation fields in PWR and VVER primary circuits: a comparison, Research report for IAEA CRP on Modelling of Transport of Radioactive Substances in Primary Circuit of Water Cooled Reactors, International Atomic Energy Agency, Vienna (2000).
[84] LISTER, D.H., The mechanisms of corrosion product transport and their investigation in high temperature water loops, Corrosion **35,** Vol. 3 (1979) 89–96.
[85] LISTER, D.H., WATSON, D.A., Proc. Int. Symp. Occupational Radiation Exposure in Nuclear Fuel Cycle Facilities, IAEA-SM-242/18, International Atomic Energy Agency, Los Angeles (1979).
[86] LISTER, D.H., Transport of radioactive corrosion products in high-temperature water. I. Recirculating loop experiments, Nucl. Sci. Eng. **58**, Vol. 2 (1975) 239–251; and Transport of radioactive corrosion products in high-temperature water. II. The activation of isothermal steel surfaces, Nucl. Sci. Eng. **59**, Vol. 4 (1976) 406–426.
[87] LISTER, D.H., KUSHNERIUK, S.A., CAMPBELL, R.H., The transport of radioactive corrosion products in high-temperature water, III, The interaction of dissolved cobalt with heated surfaces, Nuclear Sci. and Eng. **85** (1983) 221–232.
[88] MACDONALD, D.D., OWEN, D., The electrochemistry of iron in lM lithium hydroxide solution at 22° and 200°C, J. Electrochem. Soc. **120**, Vol. 3 (1973) 317–324.
[89] MACDONALD, D.D., URQUIDI-MACDONALD, M., Thin layer mixed potential model for the corrosion of high level nuclear waste canisters, Proc. 10th Intl. Congr. on Met. Corros., Oxford and IBH Publish Co., New Delhi (1987) 351; also published in Key Engineering Materials **35–36** (1991) 351.
[90] BERTUCH, A., MACDONALD, D.D., PANG, J., KRIKSUNOV, L.B., ARIOKA, K., Modelling the electrochemistry of the primary circuits of light water reactors, Corrosion'96, NACE paper 326 (1996) 1–15.
[91] YEH, T.K., MACDONALD, D.D., MOTTA, A.T., Modelling water chemistry, electrochemical corrosion potential and crack growth rate in boiling water reactor heat transport cicuits – part I: The DAMAGE-PREDICTOR algorithm, Nucl. Sci. and Eng. **121** (1995) 468–482.
[92] YEH, T.K., MACDONALD, D.D., MOTTA, A.T., Modelling water chemistry, electrochemical corrosion potential and crack growth rate in boiling water reactor heat transport cicuits – part II: Simulation of operating reactors, Nucl. Sci. and Eng. **123** (1996) 295–304.
[93] YEH, T.K., MACDONALD, D.D., MOTTA, A.T., Modelling water chemistry, electrochemical corrosion potential and crack growth rate in boiling water reactor heat transport cicuits – part III: Effect of reactor power level, Nucl. Sci. and Eng. **123** (1996) 305–316.
[94] ISHIGURE, K., TAKAGI, J., SHIRAISHI, H., Hydrogen injection in BWR and related radiation chemistry, Rad. Phys. Chem. **29** (1987) 195.
[95] IBE, E., NAGASE, M., SAKAGAMI, M., UCHIDA, S., Radiolytic environments in boiling water reactor cores, J. Nucl. Sci. and Tech. **24** (1987) 220.
[96] RUIZ, C.P., et al., Modeling Hydrogen Water Chemistry for BWR Applications, EPRI-NP-6386 Report, Electric Power Research Institute (1989).
[97] MARKANDEYA, S.G., et al, Development of computer code ANUCRUD for predicting the transport of corrosion product and radioactivity buil up in the primary HTS of PHWRs, Report at 3rd RCM of IAEA CRP on Modelling of Transport of Radioactive Substances in Primary Circuit of Water Cooled Reactors, Buenos Aires, International Atomic Energy Agency, Vienna (2000).
[98] NGUYEN, F., et al, First numerical simulations of contamination of the PWR primary circuit by activated corrosion products with the PACTOLE V3.0 code, Proceedings of International Conference on Water Chemistry of Nuclear Reactor Systems, San-Francisco (2004).

[99] DACQUAIT, F., et al., Simulations of corrosion product transfer with the PACTOLE V3.2 code, Proceedings of the International Conference of Water Chemistry Nuclear Reactor Systems, Berlin (2008).
[100] PARKHURST, D.L., APPELO, C.A.J., User's guide to PHREEQC (version 2) – A computer program for speciation, batch-reactions, one-dimensional transport, and inverse geochemical calculations, Water-Resource Investigations Report 99- 4259 (1999).
[101] BEAL, S.K., Deposition of particles in turbulent flow on channel or pipe walls, Nuclear science and engineering **40**, (1970) 1–11.
[102] MICHELL, S.J., Fluid and Particle Mechanics, Pergamon Press Ltd. (1970).
[103] PONTING, A.C., RODLIFFE, R.S., Intrinsic filtration and retarded deposition for the control of colloidal corrosion product deposition on PWR fuel, Water chemistry of nuclear reactor system, Proceedings of the BNES, Bournemouth (1983) 43–51.
[104] GIRARD, M., DACQUAIT, F., MARTEAU, H., LARAT, B., NGUYEN, F., GUINARD, L., VIALA C., The CIRENE loop: a tool to study ACP deposits and to validate the PACTOLE code, Proceedings of International Conference of Water Chemistry Nuclear Reactor Systems, Berlin (2008).
[105] BESLU, P., LEUTHROT, C., PACTOLE-PROFIP: two codes allowing prediction of the contamination of PWR primary circuits, Revue Générale Nucléaire (1990) 552–554.
[106] GÉNIN, J.B., et al., The OSCAR code package: A unique tool for simulating PWR contamination, Proceedings of the International Conference of Water Chemistry Nuclear Reactor Systems, Canada (2010) Paper 5.04.
[107] PLANCQUE, G., YOU, D., MERTENS, V., BLANCHARD, E., Experimental study and modelling of the corrosion product dissolution. Applications to PWR conditions (nominal operating and cold shutdowns conditions), Proceeding of the International Conference on Water Chemistry, Berlin (2008).
[108] GUZONAS, D., QIU, L., A predictive model for radionuclide deposition around the CANDU heat transport system, Proceedings of International Conference on Water Chemistry of Nuclear Reactor Systems, San-Francisco (2004).
[109] FRATTINI, P., et al, Axial offset anomaly: coupling PWR primary chemistry with core design, Proceedings of the VIIIth International Conference on Water Chemistry of Nuclear Reactor Systems, Bournemouth (2000).
[110] FRATTINI, P., et al, Modeling axial offset anomaly, Proceedings of International Conference on Water Chemistry of Nuclear Reactor Systems, San-Francisco (2004).
[111] DONCEL N., CHEN J., DESHON J., Water Chemistry Influence on AOA Phase 3 of the Spanish Experiment at Studsvik, Paper 1011, Proceedings of the 2007 International LWR Fuel Performance Meeting San Francisco, California, (2007).
[112] DICKINSON, E., SIMS, H.E., GARBETT, K., Thermodynamic modelling of PWR coolant, Proceedings of International Conference on Water Chemistry of Nuclear Reactor Systems, Avignon (2002).
[113] SWEETON, F.H., BAES, C.F., The solubility of magnetite and hydrolysis of ferrous ion in aqueous solutions at elevated temperatures, J Chem Thermodynamics **2** (1970) 479–500.
[114] WALKER, S.M., THORNTON, E.W., Reanalysis of oxide solubility data: results for nickel and cobalt substituted ferrites, CEGB Report TD/RPD/REP/1016 (1990).
[115] ROSENBERG R.J., TERÄSVIRTA R., HALIN M., SUKSI S. Investigation of iron deposits on fuel assemblies of the Loviisa 2 WWER-440 reactor. p.27-33,.Proceedings of the VIIth International Conference on Water Chemistry of Nuclear Reactor Systems, Bournemouth (1996).
[116] KRITSKII V.G., RODIONOV Yu.A., BEREZINA I.G. et. al., Predicting growth of deposits on fuel assemblies of WWER-440 Reactors, Thermal Engineering **56**, No. 5 (2009) 387–389.

[117] KERESZTÚRI, A., BOGATYR, S., MIKÓ, S., NEMES, I., Analyses for licensing of new fuel types at NPP Paks, Fifth International Conference on WWER Fuel Performance, Modelling and Experimental Support, Albena, Bulgaria (2003).
[118] KRITSKY V.G., Decontamination and post-decontamination water chemistry treatment. 3rd Research Co-ordination Meeting (RCM) on Optimisation of Water Chemistry to ensure Reliable Water Reactor Fuel Performance at High Burnup and in Aging Plant, (FUWAC), International Atomic Energy Agency Tecdoc (2011).
[119] BEREZINA, I.G., KRITSKY, V.G., RODIONOV, Y.A., Influence of corrosion product transport on fuel assembly reliability of NPP with WWER-440 reactors, 1st Research Co-ordination Meeting (RCM) on Optimisation of Water Chemistry to ensure Reliable Water Reactor Fuel Performance at High Burnup and in Ageing Plant (FUWAC), International Atomic Energy Agency, Vienna (2011).
[120] ZADONSKIY, N.V., Report on verification and justification of COTRAN-M model for calculation of corrosion product activity in the primary coolant of WWER-1000 reactor during operation, Report 32/1-38-404, RSC Kurchatov Institute, Moscow (2004).

LIST OF ABBREVIATIONS

ANN	artificial neural network
AOA	axial offset anomaly
BWR	boiling water reactor
CILC	crud induced localized corrosion
CIPS	crud induced power shifts
CL	cold leg
CP	corrosion products
CRP	coordinated research project
dP	delta pressure on the reactor core
ECP	electrochemical corrosion potential
FAC	flow accelerated corrosion
HL	hot leg
HTS	heat transport system
LWR	light water reactor
NPP	nuclear power plant
PCCL	PWR coolant chemistry loop
PHT	primary heat transport
PWR	pressurized water reactor
RCM	research coordinating meeting
RCS	reactor coolant system
RPV	reactor pressure vessel
SG	steam generator
SEM	scanning electron microscope
SS	stainless steel
STEM	scanning transmission electron microscopy
ToF SIMS	time-of-flight secondary ion mass spectrometry
TSE	thermodynamic stability effect
Vshe	Volts (standard hydrogen electrode)
VVER	water cooled - water moderated power reactor (acronym used in some figure captions)
WWER	water cooled - water moderated power reactor

CONTRIBUTORS TO DRAFTING AND REVIEW

S. Anthoni	CEA, France
K. Burrill	AECL, Canada
I. Dobrevski	INRNE, Bulgaria
L. Horvath	VEIKI, Hungary
K. Kasahara	MHI, Japan
J. Killeen	IAEA
V.G. Kritsky	VNIPIET, Russian Federation
C. B. Lee	KAERI, Republic of Korea
M. M^{c}Donald	PSU, USA.
P. Menut	IAEA
V. Onoufriev	IAEA
I. Smiesko	Slovenske Elekrarne, Slovak Republic
N. Zaharieva	INRNE, Bulgaria
M. Zmitko	NRI-Rez, Czech Republic

PARTICIPANTS IN THE COORDINATED RESEARCH PROJECT

PARTICIPANTS AND MEMBER STATES	DESIGNATED OFFICIAL ADDRESS
Argentina A.G. Maroto	Comisión Nacional de Energia Atómica Avda. del Libertador 8250 1429 Buenos Aires Tel.: 0054117547161 Fax.: 06541141547162 E-Mail: maroto@cnea.gov.ar
Bulgaria Ivan Dobrevsky	Institute for Nuclear Research and Nuclear Energy Bulgarian Academy of Sciences Blvd. Tzarigradsko Chaussee 72 Sofia 1784 Tel.: 0035929795000 (419) Fax.: 0035929753619 E-Mail: ivdobrevski@inrne.bas.bg
Canada K. A. Burrill	AECL Research Chalk River Laboratories Ontario K0J 1J0 Tel.: 001 613 584 3311 Fax.: 001 613 584 1220 E-Mail: burrilk@aecl.ca
Czech Rep. M. Zmitko	Nuclear Research Institute Rez plc. Reactor Services Division 25068 Husinec - Rez 130 Tel: 00420 2 6617 2453 Fax.: 00420 2 2094 0191 E-Mail: zmi@ujv.cz
Finland Magnus Halin	Imatran Voima Oy Loviisa Power Plant P.O.Box 23 FIN-07901 Loviisa Tel.: 00358195501 Fax.: 00358104554435 E-Mail: Magnus.Ha1in@ivo.fi

PARTICIPANTS AND MEMBER STATES	DESIGNATED OFFICIAL ADDRESS
France Serge Anthoni	Centre d'Etudes Nucleaires de Cadarache Commissariat a l'Energie Atomique Build. 219D, DTN/SMTM F-13108 Saint-Paul-lez-Durance Tel.: 0033 442 256109 Fax.: 0033 442 253553 E-Mail: serge.anthoni@cea.fr
Germany Fernando Roumiguiere	Siemens Nuclear Power GmbH Dept. SNP NW-C / Power Plant Chemistry Freyeslebenstr. 1, 91058 Erlangen Tel.: 0049 9131 187044 Fax.: 0049 9913 1187261 E-Mail: fernando.roumiguiere@erl11.siemens.de
Hungary Gâbor L. Horvath	Institute for Electric Power Research Co. P.O. Box 80 H-1251 Budapest Tel.: 003614578253 Fax.: 003614578253 E-Mail: Gabor.Horvath@jrc.it
India S.G. Markandeya	Bhabha Atomic Research Centre Reactor Safety Division Trombay, Mumbai 400085 Tel.: 0091225505050 or 5000 Fax.: 0091225505151 E-Mail: ccss@rnagnum.barc.ernet.in
Japan K. Kasahara	Nuclear Plant Engineering Department, Mitsubishi Heavy Industries Ltd. 1-297 Kitabukuro-cho Saitama 330 Omiya-city Te1.: 0081 78-672-3250 Fax.: 0081 78-672-3245 E-Mail:kazuo_kasahara@kind.kobe.mhi.co.jp
Korea, Rep. Chan Bock Lee	Reactor and Fuel Development Korea Atomic Energy Research Institute P.O. Box 105, Yusung Taejon, 305-600 Tel.: 0082 42 868 2257 Fax.: 0082 42 864 1089 E-Mail: cblee@kaeri.re.kr

PARTICIPANTS AND MEMBER STATES	DESIGNATED OFFICIAL ADDRESS
Russian Federation V. G. Kritsky	VNIPIET Dibunovskaya Street 55 197183 St. Petersburg Tel.: 007 812 430 18 93 Fax.: 007 812 430 15 64 E-Mail: kritski@vnipiet.spb.ru
Slovakia Ivan Smiesko	Slovenske Elektrarne a.s. Nuclear Power Plant Bohunice Department of Chemistry 919 31 Jaslovske Bohunice Tel.~ 00421 33 597 2275 Fax.: 00421 33 597 4756 E-Mail: smiesko.ivan@ebo.seas.sk
USA M. Urquidi-Macdonald	Dept. of Engrg. Science & Mathematics The Pennsylvania State University 203 C-EES Building University Park, PA-16802-4801 Tel: 001 814 863 4217 (in CA: 650 654 6638) Fax: 001 814 863 7967 (in CA: 650 802 8113) E-Mail: mumesm@engr.psu.edu

IAEA
International Atomic Energy Agency

Where to order IAEA publications

In the following countries IAEA publications may be purchased from the sources listed below, or from major local booksellers. Payment may be made in local currency or with UNESCO coupons.

AUSTRALIA
DA Information Services, 648 Whitehorse Road, MITCHAM 3132
Telephone: +61 3 9210 7777 • Fax: +61 3 9210 7788
Email: service@dadirect.com.au • Web site: http://www.dadirect.com.au

BELGIUM
Jean de Lannoy, avenue du Roi 202, B-1190 Brussels
Telephone: +32 2 538 43 08 • Fax: +32 2 538 08 41
Email: jean.de.lannoy@infoboard.be • Web site: http://www.jean-de-lannoy.be

CANADA
Bernan Associates, 4501 Forbes Blvd, Suite 200, Lanham, MD 20706-4346, USA
Telephone: 1-800-865-3457 • Fax: 1-800-865-3450
Email: customercare@bernan.com • Web site: http://www.bernan.com

Renouf Publishing Company Ltd., 1-5369 Canotek Rd., Ottawa, Ontario, K1J 9J3
Telephone: +613 745 2665 • Fax: +613 745 7660
Email: order.dept@renoufbooks.com • Web site: http://www.renoufbooks.com

CHINA
IAEA Publications in Chinese: China Nuclear Energy Industry Corporation, Translation Section, P.O. Box 2103, Beijing

CZECH REPUBLIC
Suweco CZ, S.R.O., Klecakova 347, 180 21 Praha 9
Telephone: +420 26603 5364 • Fax: +420 28482 1646
Email: nakup@suweco.cz • Web site: http://www.suweco.cz

FINLAND
Akateeminen Kirjakauppa, PO BOX 128 (Keskuskatu 1), FIN-00101 Helsinki
Telephone: +358 9 121 41 • Fax: +358 9 121 4450
Email: akatilaus@akateeminen.com • Web site: http://www.akateeminen.com

FRANCE
Form-Edit, 5, rue Janssen, P.O. Box 25, F-75921 Paris Cedex 19
Telephone: +33 1 42 01 49 49 • Fax: +33 1 42 01 90 90
Email: formedit@formedit.fr • Web site: http://www. formedit.fr

Lavoisier SAS, 145 rue de Provigny, 94236 Cachan Cedex
Telephone: + 33 1 47 40 67 02 • Fax +33 1 47 40 67 02
Email: romuald.verrier@lavoisier.fr • Web site: http://www.lavoisier.fr

GERMANY
UNO-Verlag, Vertriebs- und Verlags GmbH, Am Hofgarten 10, D-53113 Bonn
Telephone: + 49 228 94 90 20 • Fax: +49 228 94 90 20 or +49 228 94 90 222
Email: bestellung@uno-verlag.de • Web site: http://www.uno-verlag.de

HUNGARY
Librotrade Ltd., Book Import, P.O. Box 126, H-1656 Budapest
Telephone: +36 1 257 7777 • Fax: +36 1 257 7472 • Email: books@librotrade.hu

INDIA
Allied Publishers Group, 1st Floor, Dubash House, 15, J. N. Heredia Marg, Ballard Estate, Mumbai 400 001,
Telephone: +91 22 22617926/27 • Fax: +91 22 22617928
Email: alliedpl@vsnl.com • Web site: http://www.alliedpublishers.com

Bookwell, 2/72, Nirankari Colony, Delhi 110009
Telephone: +91 11 23268786, +91 11 23257264 • Fax: +91 11 23281315
Email: bookwell@vsnl.net

ITALY
Libreria Scientifica Dott. Lucio di Biasio “AEIOU”, Via Coronelli 6, I-20146 Milan
Telephone: +39 02 48 95 45 52 or 48 95 45 62 • Fax: +39 02 48 95 45 48
Email: info@libreriaaeiou.eu • Website: www.libreriaaeiou.eu

JAPAN
Maruzen Company, Ltd., 13-6 Nihonbashi, 3 chome, Chuo-ku, Tokyo 103-0027
Telephone: +81 3 3275 8582 • Fax: +81 3 3275 9072
Email: journal@maruzen.co.jp • Web site: http://www.maruzen.co.jp

REPUBLIC OF KOREA
KINS Inc., Information Business Dept. Samho Bldg. 2nd Floor, 275-1 Yang Jae-dong SeoCho-G, Seoul 137-130
Telephone: +02 589 1740 • Fax: +02 589 1746 • Web site: http://www.kins.re.kr

NETHERLANDS
De Lindeboom Internationale Publicaties B.V., M.A. de Ruyterstraat 20A, NL-7482 BZ Haaksbergen
Telephone: +31 (0) 53 5740004 • Fax: +31 (0) 53 5729296
Email: books@delindeboom.com • Web site: http://www.delindeboom.com

Martinus Nijhoff International, Koraalrood 50, P.O. Box 1853, 2700 CZ Zoetermeer
Telephone: +31 793 684 400 • Fax: +31 793 615 698
Email: info@nijhoff.nl • Web site: http://www.nijhoff.nl

Swets and Zeitlinger b.v., P.O. Box 830, 2160 SZ Lisse
Telephone: +31 252 435 111 • Fax: +31 252 415 888
Email: infoho@swets.nl • Web site: http://www.swets.nl

NEW ZEALAND
DA Information Services, 648 Whitehorse Road, MITCHAM 3132, Australia
Telephone: +61 3 9210 7777 • Fax: +61 3 9210 7788
Email: service@dadirect.com.au • Web site: http://www.dadirect.com.au

SLOVENIA
Cankarjeva Zalozba d.d., Kopitarjeva 2, SI-1512 Ljubljana
Telephone: +386 1 432 31 44 • Fax: +386 1 230 14 35
Email: import.books@cankarjeva-z.si • Web site: http://www.cankarjeva-z.si/uvoz

SPAIN
Díaz de Santos, S.A., c/ Juan Bravo, 3A, E-28006 Madrid
Telephone: +34 91 781 94 80 • Fax: +34 91 575 55 63
Email: compras@diazdesantos.es, carmela@diazdesantos.es, barcelona@diazdesantos.es, julio@diazdesantos.es
Web site: http://www.diazdesantos.es

UNITED KINGDOM
The Stationery Office Ltd, International Sales Agency, PO Box 29, Norwich, NR3 1 GN
Telephone (orders): +44 870 600 5552 • (enquiries): +44 207 873 8372 • Fax: +44 207 873 8203
Email (orders): book.orders@tso.co.uk • (enquiries): book.enquiries@tso.co.uk • Web site: http://www.tso.co.uk

On-line orders
DELTA Int. Book Wholesalers Ltd., 39 Alexandra Road, Addlestone, Surrey, KT15 2PQ
Email: info@profbooks.com • Web site: http://www.profbooks.com

Books on the Environment
Earthprint Ltd., P.O. Box 119, Stevenage SG1 4TP
Telephone: +44 1438748111 • Fax: +44 1438748844
Email: orders@earthprint.com • Web site: http://www.earthprint.com

UNITED NATIONS
Dept. I004, Room DC2-0853, First Avenue at 46th Street, New York, N.Y. 10017, USA
(UN) Telephone: +800 253-9646 or +212 963-8302 • Fax: +212 963-3489
Email: publications@un.org • Web site: http://www.un.org

UNITED STATES OF AMERICA
Bernan Associates, 4501 Forbes Blvd., Suite 200, Lanham, MD 20706-4346
Telephone: 1-800-865-3457 • Fax: 1-800-865-3450
Email: customercare@bernan.com · Web site: http://www.bernan.com

Renouf Publishing Company Ltd., 812 Proctor Ave., Ogdensburg, NY, 13669
Telephone: +888 551 7470 (toll-free) • Fax: +888 568 8546 (toll-free)
Email: order.dept@renoufbooks.com • Web site: http://www.renoufbooks.com

Orders and requests for information may also be addressed directly to:

Marketing and Sales Unit, International Atomic Energy Agency
Vienna International Centre, PO Box 100, 1400 Vienna, Austria
Telephone: +43 1 2600 22529 (or 22530) • Fax: +43 1 2600 29302
Email: sales.publications@iaea.org • Web site: http://www.iaea.org/books